GROWTH AND CHARACTERIZATION OF BN THIN FILMS DEPOSITED BY PACVD

A thesis for the degree of Ph.D.

Presented to

DUBLIN CITY UNIVERSITY

by

MD. ZIAUL KARIM, M. Sc.(EEE)

SCHOOL OF ELECTRONIC ENGINEERING
DUBLIN CITY UNIVERSITY

RESEARCH SUPERVISOR

DR. DAVID C. CAMERON

February, 1993.

TO

**THE DEAREST MEMBERS
OF SHAPBNIL LODGE**

**MUM, DAD
PIAS, LUCKY, SOHAIL & BIPLAB**

DECLARATION

I hereby certify that this material, which I now submit for the assessment on the programme of study leading to the award of Ph.D. is entirely my own work and has not been taken from the work of others save and to the extent that such work has been cited and acknowledged within the text of my work.

Signed:

Date: February 2, 1993.

ACKNOWLEDGEMENTS

GROWTH AND CHARACTERIZATION OF BN THIN FILMS DEPOSITED BY PACVD

MD. ZIAUL KARIM

ABSTRACT

Boron nitride has become the focus of a considerable amount of interest because of its properties which relate closely to those of carbon. In particular, the cubic boron nitride phase has extreme hardness, chemical inertness, high resistivity, thermal conductivity and transparency and resistance to oxidation up to 1600°C. The conventional methods of synthesis use highly toxic and inflammable source materials at high deposition temperature.

A hot filament activated PACVD technique was developed to deposit BN films under a wide range of conditions. The source material was borane-ammonia (BH_3-NH_3) which is a non-toxic crystalline solid, free of carbon and oxygen. Using this technique, mixed-phase boron nitride (BN) films, containing crystallites of the cubic phase embedded in a hexagonal matrix, were deposited at a substrate temperature of 350°C. These films showed good thermal and chemical stability with smooth surface topography.

A good correlation was obtained between the properties of the films and plasma diagnostics. With increasing rf power, the ratio of cubic to hexagonal phase, determined by infra-red spectra, was increased with a shift towards lower wave number. In the growing and phase stabilization of the cubic phase, ion bombardment plays an important role in forming the sp^3-microstructure of BN films. The ion-density and thus ion flux to the more negatively biased substrate was increased with rf power corresponding to an increase of N_2^+ species in the plasma, determined by OES. This increased ion-bombardment contributed in increasing the volume fraction of cubic phase in the film. For a specific substrate and filament temperature, if the deposition conditions are measured in terms of ion-bombardment, a sharp threshold value exists where the phase of the films changes from being hexagonal to being cubic. At a substrate temperature of 350°C, this threshold value was found to be 160 W of rf power. A substrate temperature of 300°C was necessary for enhancing the growth of cubic phase. The shift towards lower wave number at higher power was considered to be a transition to the cubic phase from the wurtzite phase of BN which grows under less highly activated conditions. Hydrogen free film was deposited at a temperature greater than 300°C and a rf power greater than 200 W.

The refractive index of the films increased with rf power which correlates with the increasing cBN content. The indices of mixed-phase films (1.8-2.3) are higher than those of hexagonal BN films (1.55-1.77).

Films were adherent to the Si substrates. There is a very close parallel between the film containing cubic phase and a higher level of compressive stresses in the film. It was observed that the stress crosses over from tensile to compressive from 100 W to 200 W and remains compressive at higher rf power. Hardness of the mixed-phase film measured by ultra-low load indentation showed an improvement compared to the substrate.

MIS structures consisting of Al/BN/n-Si showed normal behaviour with high negative charge density and a relatively low level of fast interface state density. The distribution of surface density showed a U-shaped variation with a minimum density of 1.75×10^{12} states/cm^2/eV. The dielectric constants of the film were in the range of 2.2-4.4. Mixed phase BN films showed a high resistivity ($>3 \times 10^{12}$ Ω-cm) and a high breakdown field and the I-V characteristics were essentially linear in the low voltage region.

A growth mechanism of BN films from borane-ammonia in this technique is also presented showing the effect of rf power, ion density in the plasma, substrate temperature and filament temperature in relation to the properties of the films.

CONTENTS

CHAPTER 2   METASTABLE GROWTH OF BORON NITRIDE

CHAPTER 4 GROWTH AND PHYSICAL CHARACTERIZATION OF BN THIN FILMS

CHAPTER 5 ELECTRONIC PROPERTIES OF MIXED-PHASE BN FILMS

CHAPTER 6 CONCLUSIONS

LIST OF ABBREVIATIONS

AES	Auger Electron Spectroscopy
ARE	Activated Reactive Evaporation
BN	Boron nitride
CVD	Chemical vapour deposition
cBN	cubic boron nitride
ECR	Electron cyclotron resonance
EPMA	Electron probe micro-analysis
FNS	First Negative system
hBN	hexagonal boron nitride
IR	Infra-red spectroscopy
LPPD	Low pressure plasma deposition
MIS	Metal insulator semiconductor
OES	Optical emission spectroscopy
PAM	Plasma aided manufacturing
PVD	Physical vapour deposition
PECVD	Plasma enhanced CVD
PACVD	Plasma assisted CVD (same as PECVD)
PCBN	Polycrystalline boron nitride
SEM	Scanning electron microscopy
SPS	Second Positive system
TEM	Transmission electron microscopy
UHV	Ultra high vacuum
XPS	X-ray photoelectron spectroscopy
XRD	X-ray diffraction
wBN	wurtzite boron nitride

LIST OF NOTATIONS

λ	wave length
Γ	Brillouin zone centre
ε	dielectric constant
ε_0	static dielectric constant
ε_∞	high frequency dielectric constant
ε_i	dielectric constant of the insulator
ε_s	dielectric constant of the semiconductor
n	refractive index
k	extinction coefficient
Z	atomic number
μ	permeability
E_g	band gap
σ	conductivity
σ_t	total stress
σ_i	intrinsic stress
σ_{th}	thermal stress
E_f	Young's modulus of the film
ν_f	Poisson's ratio of the film
ρ	electrical resistivity
$\mathcal{P}$	a state property
k	Boltzman constant
T	temperature
T_s	substrate temperature
T_F	filament temperature
T_m	melting point
L	inductance
R	resistance
h	Planck's constant
N_{ss}	surface state density
Q_{ss}	surface state charge

Q_s	surface charge
δ	deflection
C	capacitance
C_i	insulator capacitance
C_D	space charge capacitance
C_{fb}	flat-band capacitance
ϕ_{ms}	metal work function
ϕ_B	potential barrier
ψ_s	surface potential
V_{fb}	flat-band voltage
p	pressure
λ_D	debye length
L	inductance
q	electronic charge (1.67×10^{-19})
χ	semiconductor electron affinity
β	absorption coefficient
c	velocity of light

CHAPTER 1

INTRODUCTION

1.1   INTRODUCTION

The importance of materials for the evolution of human society is incalculable. This is hinted at by the way archaeologists divide early history into the stone, bronze and iron ages. In modern times we talk of the age of the silicon chip but such have been the advances this century that one could almost as easily talk about the age of plastics, advanced composites, optical fibres etc.

This thesis is concerned with another area of rapid progress in 20th century materials science. That is the production of ceramics at temperatures where they are thermodynamically unstable. Specifically, attempts at growing thin films of cubic phase boron nitride under conditions of low temperature and pressure will be described.

For this to be successful it is essential that the growth take place in a far from equilibrium environment. This consideration has led investigators to use glow discharge or plasma techniques.

The target application relates to surface engineering where boron nitride thin films may be used as an insulating layer or wear-resistant coatings. Potentially these films may be grown by any of the deposition processes used in surface engineering, especially plasma assisted techniques and may be useful as surface engineered materials.

The remainder of this chapter introduces surface engineering in general, Plasma-Aided Manufacturing (PAM) including various plasma deposition techniques. These sections will then be referred back to as a kind of reference source when specifics are discussed later on.

1.2   SURFACE ENGINEERING

Surface engineering may be defined as the modification or coating of the surface of a bulk material in order to impart a property to, or to tailor, this surface for a specific application. The surface material is the only part of any component which has to coexist with the external environment such as contacting surfaces and chemical attack. Surface technology deals with the methods for achieving these desired surface requirements and their behaviour in service.

The achievement of desirable surface properties involves either surface coating technology, in which coating serves that purpose or processes which modify the properties of the bulk material to meet the surface demands.

1.2.1 MODIFICATION

This thesis will be solely concerned with surface coating but for completeness a few words on surface modification is included here. This category can be further divided into two more. Firstly, there are those techniques in which the surface structure is changed by thermal or mechanical means such as induction hardening, flame hardening, laser hardening, electron beam hardening, spark hardening, chill casting of cast iron, and work hardening. These need no further elaboration since the names are explanatory and a short overview is the intention here. Secondly, there are those techniques in which both the surface composition and the structure are changed by diffusion or ion implantation such as carburising, carbonitriding, nitriding, boriding, chromising, aluminising, siliconising, sherardising, and ion implantation. These latter diffusion techniques (excluding ion implantation) can involve the workpiece being immersed in appropriate chemical solutions or being exposed to suitable gases or plasmas at elevated temperature for a period of time which varies depending on the method used. The purpose of these procedures is to improve certain properties such as wear, fatigue, corrosion and oxidation resistance. In the fabrication of integrated circuits such diffusion techniques are often used to deposit dopant into the semiconductor lattice. Ion implantation is not a diffusion but rather an ion beam method. This method will be discussed later.

1.2.2 COATINGS

Coatings are often categorised as being either thick or thin. Here only thin vacuum deposited coatings are of interest but a brief account of thick (>50 micron) layer deposition is given. Thermal or plasma spraying, welding and cladding are methods all of which produce thick coatings. Thermal flame spraying are among the most flexible deposition techniques available. The principle is to insert powder into either an oxyfuel or flame. The powder is then projected by the flame onto the piece to be coated. In this way coatings as diverse as alumina, tungsten carbide, MCrAlY, aluminium/polyester, stainless steel, copper etc can be deposited. Applications include resistance to wear and corrosion, abradable coatings for turbine blades, building up of worn or mismachined parts, thermal barrier coatings, high temperature superconductors, and biocompatible coatings such as hydroxyepitite. Thermally sprayed coatings have the disadvantage that they are porous and must often be fused afterwards. This limits their use somewhat since many substrates will not survive the fusing temperature which is typically around 800°C.

In the familiar fusion welding process, a hard wear resistant layer is deposited on a metallic substrate by fusing them together. The layer is usually an alloy. The heat generated by a gas, electric arc or plasma arc welding gun is used to melt the coating material, which is supplied in the form of powder, paste, rod, strip or wire. Advantages are simplicity and versatility. Disadvantages are lack of thickness control. Finally, cladding is a process in which a metallic foil or sheet is metallurgically bonded to a metallic substrate to produce a composite structure, and the bond is usually stronger than the weaker of the parent metals. Claddings are usually of the order of 1 mm or more in

thickness. Its strengths are that two materials can be bonded without disturbing the effect of cold work, dispersions, and precipitation hardening. The process inhibits the formation of brittle intermetallic compounds at the bond zone by contrast with thermal spraying and welding. Since cladding is with wrought material, questions concerning layer integrity do not arise. Lastly, bonding can be quickly achieved over large areas. A disadvantage is that coverage of complexly shaped parts is difficult.

Other techniques include atomised liquid spray, compressed air spray, electrostatic spray, spray pyrolysis, dipping, fluidised bed, spin-on, brush, roller, sol gel, electrochemical deposition, and chemical deposition. Of these electroplating is the most important being widely used throughout industry. Further details concerning these and other techniques may be found in ref. 1.

This work is concerned especially with the coatings deposited by plasma assisted processes or more generally vacuum processes. This area of manufacturing might be called as Plasma Aided Manufacturing (PAM). We will now illustrate the role of plasmas and PAM in the advancement of Surface Engineering.

1.3 PLASMA AIDED MANUFACTURING (PAM)

Plasma-Aided Manufacturing (PAM) has a direct impact in the world economy in virtually every aspect of high technology industry as well as many of the more traditional industries. Industries all over the world have made major inroads into the use of plasma coatings which have drastically improved their competitive position. If the potential of plasma coatings can be further developed both scientifically and technologically, it can make a significant contribution to the creation of markets worth billions of pounds and substantial increases in jobs.

PAM encompasses a vast range of industrial applications, from thin-film sputter deposition, plasma polymerization and microcircuit fabrication to welding, tool hardening, arc melting, synthesis of pure, ultrafine powders, plasma spraying, plasma sintering and microwave generation [2]. It is also a topic that is inherently cross-disciplinary. It is also a topic that is ripe for major "breakthroughs", which will be extremely important in preserving and increasing an industry's competitive position in the international marketplace.

The present and potential applications of plasma-aided manufacturing (PAM) include:

* Fabrication of semiconductor integrated circuits and other electronic devices
* Hardening of tools, dies, and industrial metals
* Production of biocompatible and packaging materials for pharmaceutical applications
* Anticorrosion and other coatings deposited on surfaces

3

* Production of new chemicals and materials
* Refining of metals
* Printing of polymer films
* Hazardous waste removal
* Welding
* Magnetic recording media
* Precise machining
* Lighting and displays
* Plasmas in electronic circuit and switchgear.

Estimates of the current potential markets for some of these are:

* £16 billion in semiconductor processing
* £24 billion in plasma electronics
* £1.5 billion in tool and die hardening
* Many billions in thin polymer films for recording and medical uses.

Estimates for some new and exciting markets are:

* £30 billion in wear resistant and corrosion protection
* £3 billion in high-performance ceramics
* Many billions in markets for waste removal, metal refining, packaging and pharmaceutical applications.

1.3.1 GLOW DISCHARGE PLASMAS

Around 1600, W. Gilbert made the observation that a conductor loses its charge when brought near to a flame. This is perhaps the first recorded instance of interest in conducting gases. Since then our understanding of plasmas has evolved considerably but is still incomplete. In this macroscopic overview we consider only low temperature glow discharge plasmas.

A significant degree of ionisation appears in a normal gas when the temperature (T) of the gas is raised to the extent that the first ionisation energy of the gaseous atoms is of the order of kT where k is Boltzman's constant. With still further increases in temperature the gas may ionise completely. Plasmas are loosely categorised according to the degree of ionisation of the gases of which they are composed as seen in Fig. 1.1 [6].

A simple glow discharge system, accompanied with drawings indicating the electric field, the space charge densities and the current densities is illustrated in Fig. 1.2 [157]. The diagram appears in a number of textbooks and a very brief account is included here as a contextual guide for the main subject matter.

A potential difference of sufficient magnitude to ignite the discharge is applied across the two electrodes. This causes an electron in the vicinity of the cathode to accelerate away from it while gaining energy all the time. Eventually the particle
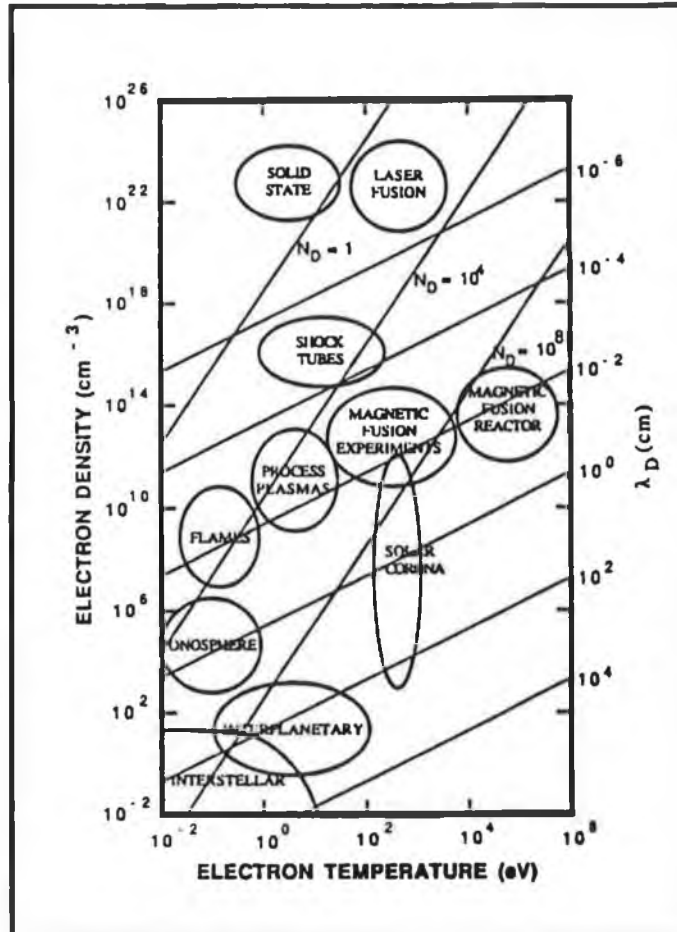
Fig. 1.1 : **Electron density and temperature ranges for a variety of natural and man-made plasmas. Lines of constant Debye length (λ_D) are shown, along with lines of constant number of electrons in a Debye sphere (N_D). The region labelled PROCESS PLASMAS delineates the parameter ranges for the plasmas used for thin fim deposition and etching [6].**
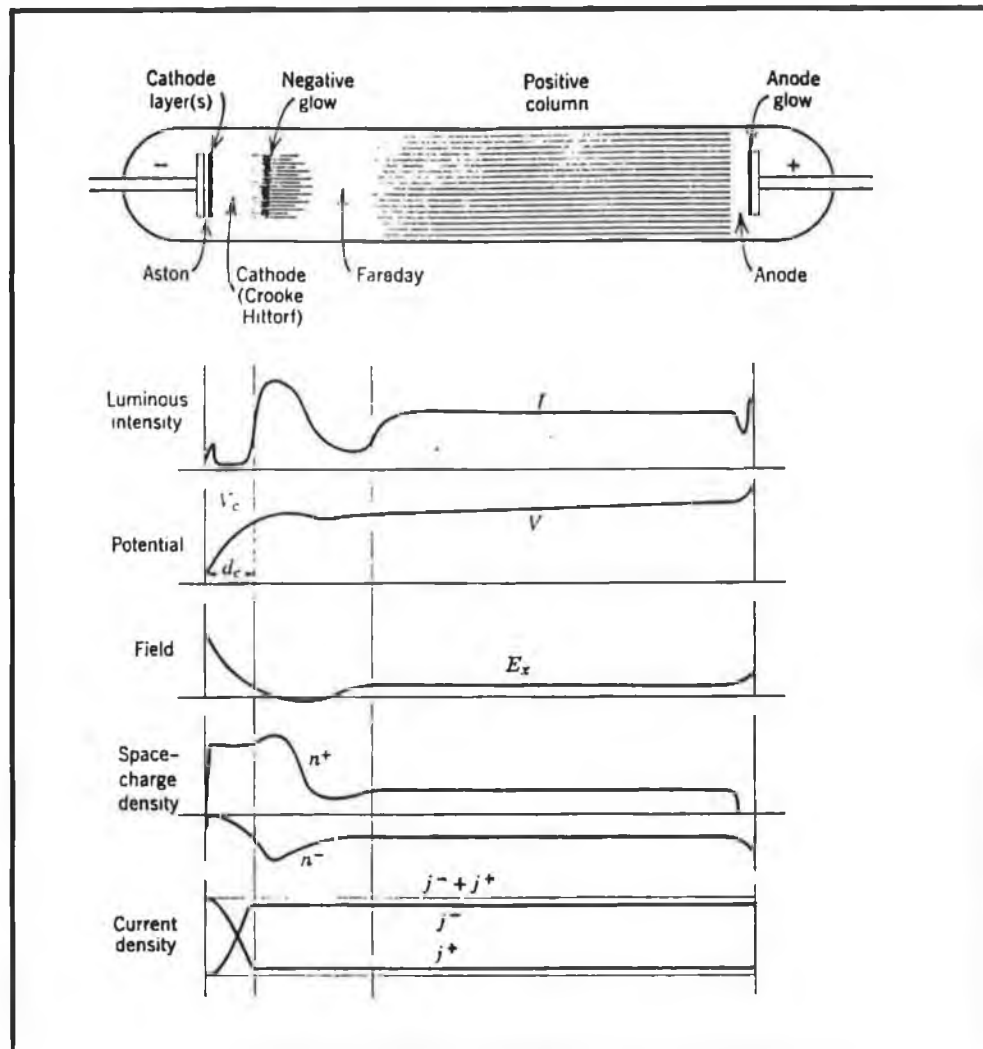
Fig. 1.2 : The normal glow discharge in neon in a 50 cm tube at 1 Torr. The luminous regions are shown shaded [157].

6

becomes energetic enough to cause ionisation, the resulting electrons go on to produce further ionisation and so an electron multiplication effect is initiated. Note also that many electrons undergo inelastic collisions and so lose energy. These slow electrons on arriving at the negative glow region have sufficient energy to excite, but not ionise, the gas atoms and this results in the glow being produced. As the distance from the cathode increases still further, the slow electrons have sufficiently low energy that recombination is possible. This process occurs in and beyond the negative glow. Thereafter, as the field rises, the likelihood of recombination decreases. So the Faraday dark space is created. Next the positive column is a region where the axial component of field is essentially constant and ionisation occurs from the random motion of the electrons (not the drift velocity). Electrons emerging from the positive column have low energy and enter a region where the electric field is increasing. They are accelerated towards the anode and after having crossed the anode dark space have sufficient energy to excite and ionise the gas in front of the electrode. This area is then referred to as the anode glow. The relevance of all this information to materials processing will be expressed in detail shortly. For the moment suffice it to observe that a substrate placed on the cathode will receive ion and neutral bombardment from the plasma. By this means a film can be built up. For example, a titanium tetrachloride/hydrogen plasma causes formation of a titanium film. It is also possible to cause atoms to be ejected from a negatively biased plate due to positive ion impact. This is called sputtering.

Though the plasma described above derives its energy from a direct current power supply, radio frequency discharges are also common. For reasons to be made clear it is important that a fairly high frequency be used. The 13.56 MHz frequency value is very often chosen because of regulations limiting radiative emissions on other channels.

The capacitively coupled r.f. glow is superficially similar to the d.c. glow. The big advantage from the materials processing point of view is that an insulating material (which would be placed on an electrode) can build up a negative bias on the surface and so it can be either sputtered, etched or have some material deposited onto it. The ion density is also higher. One disadvantage is the significantly greater complication involved in impedance matching the r.f. supply to the plasma. The general principle is now briefly described.

When a d.c. supply is used with an insulating substrate on the negative electrode, the plasma facing surface of the insulator initially goes to a negative potential but quickly increases to zero due to ions impacting on it. Thus any discharge will quickly be extinguished. Low frequency alternating current does not improve matters very much since the period is long compared with the time necessary to charge the insulator surface. Thus a series of short discharges occur at either electrode.

The solution is to use an r.f. power supply. At these frequencies the ions are no longer able to follow the temporal variations in applied potential. This is because of their relatively large size and consequently low mobility. So we can picture an oscillating electron cloud moving against a background of stationary ions. When the electron cloud moves towards one electrode a positive sheath is uncovered. This sheath has properties similar to its d.c. counterpart and so ions bombard the electrode. However the oscillation of the electrons marks a distinction between r.f. and d.c. glows. Electrons are not removed

at the anode and are lost only to the walls of the system. Furthermore in r.f. plasmas there is a volume ionisation due to electrons accelerated by the oscillating electric field. Both these last two mentioned effects contribute to the greater ionisation observed in the r.f. as opposed to the d.c. glow.

The discharge is capacitive and therefore the total number of ions and electrons to flow to a given electrode during an r.f. cycle must balance to zero. So a self-bias that is negative with respect to the plasma potential develops on a surface which is capacitively coupled to the discharge. A diagram which has become quite popular as an illustration of glow discharge behaviour is illustrated in Fig. 1.3. In Fig. 1.3a it is shown that larger currents are drawn when the electrode is biased positive relative to the plasma potential compared to when biased negatively. This is a consequence of the difference in electron and ion mobility values. Fig. 1.3b shows that in order to achieve zero net current flow a d.c. bias must develop on the electrode so that the average potential is negative relative to the plasma potential. So it can be seen that both electrodes are anodes for only a short time and cathodes most of the time and that mostly they are being bombarded with ions. This, of course, is what we want in order to enable thin film deposition.

It is possible to have an electrodeless discharge. This is achieved by wrapping an induction coil around the discharge chamber. See Fig. 1.4a. It can exist in two stages, a capacitively coupled electrostatic pre-discharge and an inductively coupled electromagnetic main discharge. Since the capacitive energy storage of the coil is small, the strong field between the coil turns can be easily compensated by small polarisation currents in the gas. The magnetic energy stored in the coil, which is much larger, remains untrapped until the coil current is raised to the point where the induced electric field can take over and maintain the discharge. This transition to the much more powerful inductive mode is usually accompanied by a strong increase in brightness. An equivalent circuit diagram is shown in Fig. 1.4b. It disregards the self-capacitance of the coil and considers the discharge to be an air cored transformer, where the gaseous turn of inductance L_2, and resistance R_2, are coupled to the primary circuit $L_1 R_1 C_1$ through the mutual inductance M.

To conclude this section, we say a few words regarding microwave discharges. In microwave frequency (typically 2.45 GHz), the direction of the electron changes very rapidly due to the low mass of the electron. Therefore, the electron will oscillate within the volume of the gas, if the container walls are far enough apart. It is this characteristic that makes the microwave discharges different from rf discharges. In the latter case, the change of direction of acceleration does not take place before the electron hits the wall. Thus it is possible to restrict the microwave plasma to a predetermined region away from substrate, avoiding bombardment on the films by plasma particles. As the energy transfer to the electrons is significantly greater than rf discharges, microwave discharges are very intensely ionised and the technique is electrodeless. Discharges can be initiated over a pressure range of sub-mtorr (upto 10^{-5} Torr) to several thousand torr. At pressures in the 1-100 mtorr range, it has been demonstrated that films of polycrystalline diamond can be grown. Substrate temperature for this kind of growth is in the region of 800°C. A schematic of a microwave apparatus suitable for diamond film production is given as Fig. 1.5a [1]. As shown in this fig., microwave power is introduced into the plasma chamber through a rectangular waveguide. In electron cyclotron resonance discharges, microwave

8
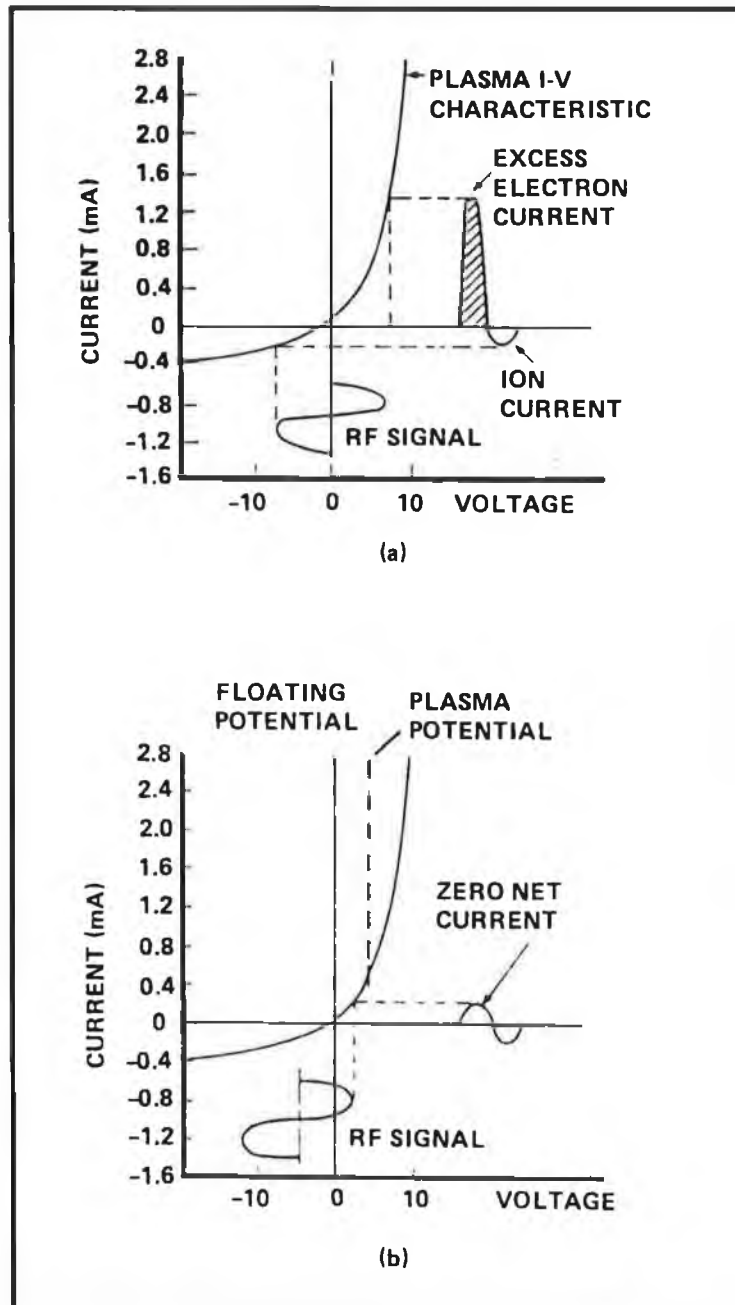
Fig. 1.3 : Schematic illustration of the development of a negative bias when an rf potential is capacitively coupled to a probe immersed in a plasma.

9
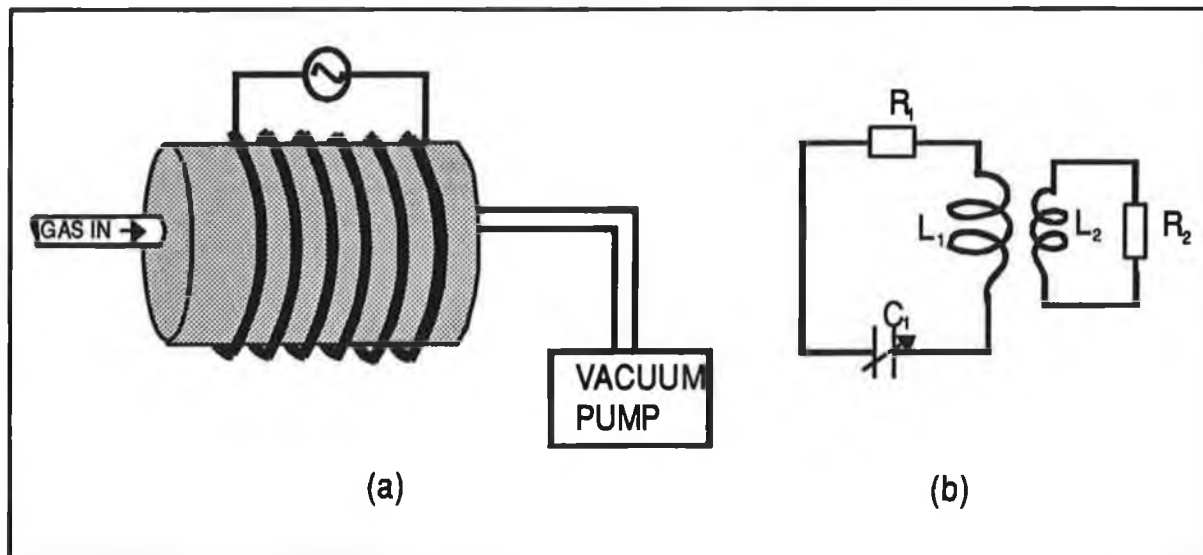
Fig. 1.4 Inductively coupled rf plasma formed within glass or quartz chamber,
a) Schematic diagram, b) Equivalent circuit.

energy is coupled to the natural resonant frequency of the electron gas in the presence of a static magnetic field. See Fig. 1.5b [6]. A disadvantage with microwave discharge technology is that currently it is only possible to ignite a dense discharge over a small cross-sectional area i.e. less than 5 cm^2.

1.3.2 PLASMA AND PLASMA-AIDED-MANUFACTURING

Industrial plasmas are often only partially ionized, and therefore also contain neutral particles and/or free radicals, in addition to the charged particles. They can be divided into two categories: thermal and nonequilibrium (glow-discharge) plasmas. Their basic difference is that the former tend to have ion and electron temperatures roughly equal, and they tend to be at higher operating pressure than the nonequilibrium types. Both of these plasmas are of major importance. The central unifying factor between them is the fact that measurement and characterization as well as theoretical modelling of the plasma are needed for process control and optimization for high quality. In many cases, the techniques are similar.

Plasmas used in industry encompass a wide range of processes which can often be classified as a function of operating pressure. Fig. 1.6 shows a number of such manufacturing techniques [2]. The vertical axis is the log of the operating pressure in

10

(a)

(b)
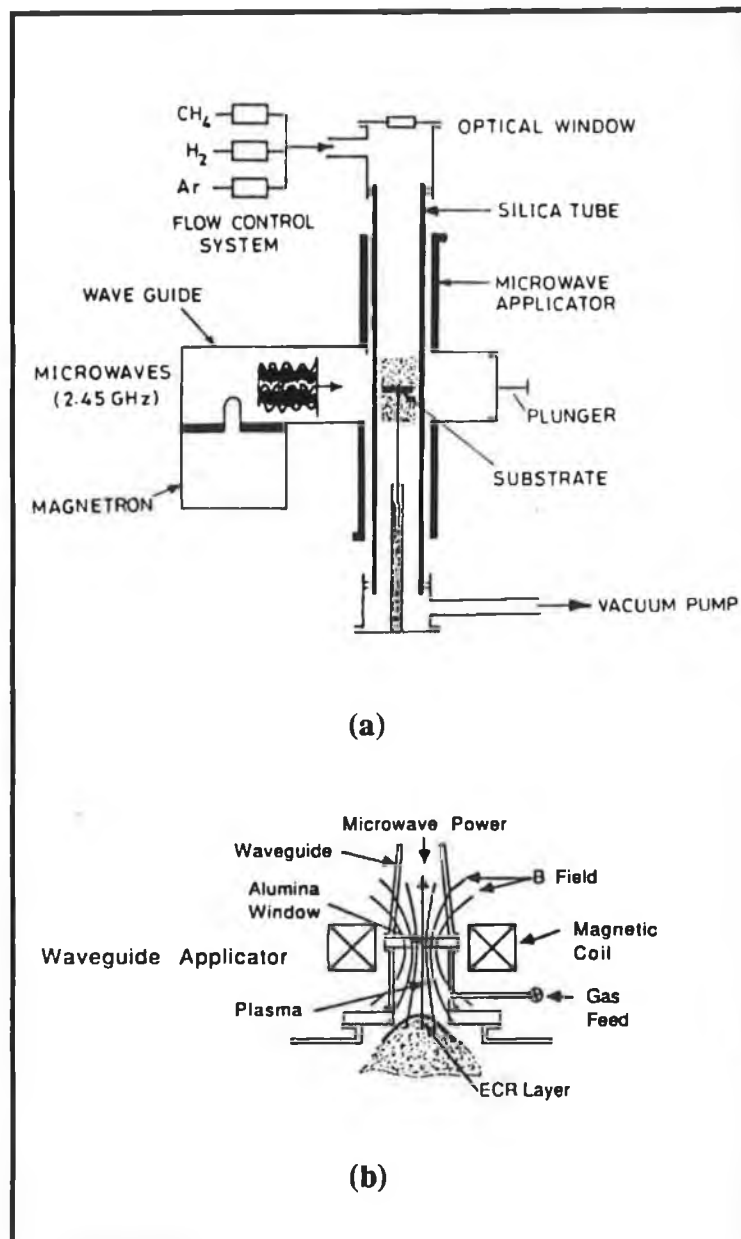
Fig. 1.5 : (a) Schematic diagram of microwave PECVD reactor system used for deposition of diamond coatings. (b) Schematic diagram of an electron cyclotron resonance (ECR) discharge [1,6].
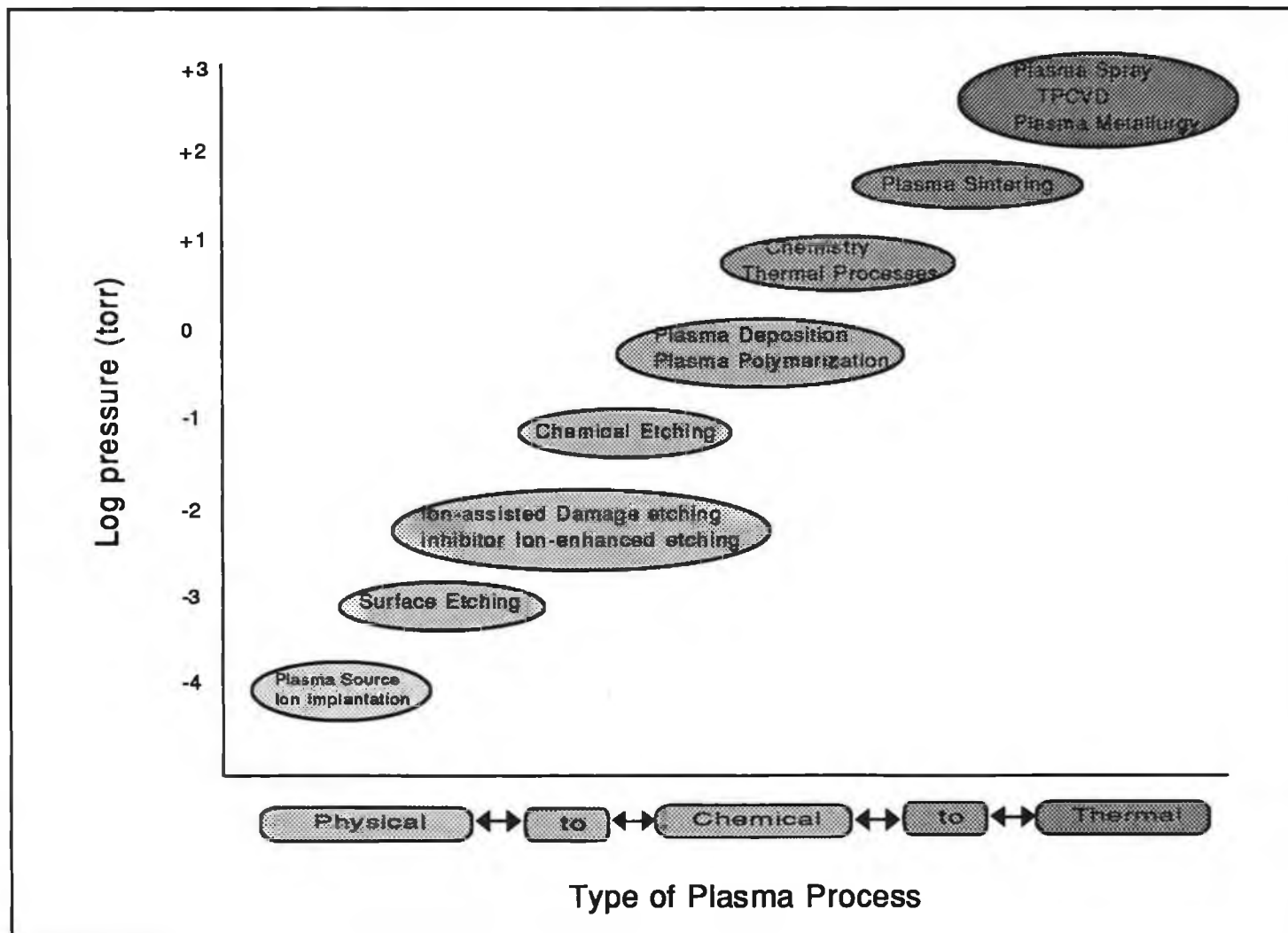
Fig. 1.6: Plasma processes arranged by operating pressure. As the pressure increases,the
of the process tends to move from physical to chemical to thermal in nature [2].

Torr, while the horizontal axis describes the general nature of the various processes. At low pressure, the collision frequency is low and the primary interactions are between charged particles and the material to be processed, so that the process is primarily physical in nature. As the pressure increases, collisions become more consequential and chemistry begins to play a more important role. As the pressure increases still more, and approaches 1 atm, the plasma begins to act more like a thermal or heat source, substituting in many cases for combustion. At these pressures (thermal plasmas), ion and electron temperatures are roughly equal and are of higher density than the low pressure (nonequilibrium plasma) types where electron tend to be hotter than ions.

Almost all applications of noneqilibrium plasma simultaneously involve four processes: sputtering, etching, polymerization, and surface modification, even though a particular piece of equipment might be designed to use only one of them; e.g., an etching device. Thermal plasma processing applications are concerned with the interaction of high-temperature plasmas with gaseous reactants or particulate matter. The later may be either injected into the plasma in the form of small particles (plasma decomposition and synthesis, plasma spraying, plasma reduction, etc.) or it may be exposed to the plasma in the form of bulk materials (melting and refining and other metallurgical applications). The goal of plasma aided manufacturing is to control the generation and flux of ions, electrons, and free radicals and/or larger particles incident on a surface so as to modify that surface, either by depositing material on the surface (deposition) or removing material (etching or sputtering), or imbedding particles (ion implantation).

The process is very complex. The plasma is used to activate a chain of chemical reactions and to deliver activation energy to a surface (substrate). The plasma contains electrons, positive and negative ions, neutral particles, and free radicals, all of which are often necessary for proper processing. Feedstock gases are flowed into the discharge where electron impacts dissociate and ionize the gas forming the free radicals and ions. These fragments further chemically react with the feedstock gases and other radicals as they diffuse and drift to the substrate. At the substrate, the radicals and ions adsorb, bond, sputter, or otherwise react to modify the substrate while products are released back into the plasma. The combination of neutral species adsorption and positive ion bombardment can result in surface chemical reactions. If the products of the surface reaction are volatile, they leave the surface and etching results. If the products of the surface reaction are involatile, a surface film grows (deposition). If the particles remain on or just below the surface, implantation results. Fig. 1.7 shows a stylized view of a plasma processing reactor with three types of processes occurring [2]. First, electron dissociation generates free radicals; second, the free radicals may recombine into other materials or back into the original components; and third, the free radicals and ions may travel to the surface, producing reactions there.

The film is therefore predominantly formed by the bonding of neutral radicals to the surface of the growing film. However, there is not necessarily a simple relationship between the chemical composition of the condensable radicals and the chemical composition of the film, because surface chemical reactions can take place between adsorbed species. Ions do not contribute measurably to the deposition process although the ionic bombardment during film growth can have a significant effect on the physical properties of the film. The fact that the species which contribute predominantly to film

13
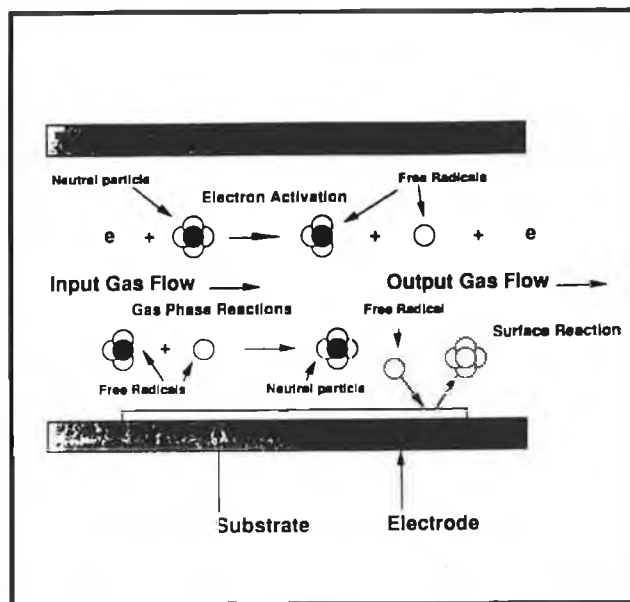
Fig. 1.7 : Reactions taking place in a plasma processing reactor [2].

growth are electrically neutral and have to find their way to the surface of the growing film by diffusion has important practical consequences. The diffusing radicals have a relatively low density and the plasma deposition process is therefore inherently materials inefficient. The deposition on a flat surface is isotropic in nature, i.e., the vapour at any point of a flat surface originates from a hemisphere with a radius of about the mean free path of the radicals. Step coverage of surface features depends on the size of the surface feature relative to the radical mean free path and is subject to electric field distortion. Furthermore, columnar structures and nodular film defects, resulting from self-shadowing or macroscopic shadowing during film growth, are prevalent defect patterns in plasma deposited films and indeed in most PVD coatings.

As neutral radicals are oblivious to the electric field, one expects that the mass transport during the plasma deposition process will be insensitive to the application of electrical biases to the electrodes. However, the film deposition rates on the cathode are generally higher than on the anode. Rather than indicative of a substantial ionic contribution to film growth, these asymmetries are associated with the asymmetric creation of the radicals in the discharge gap. Interesting differences in film growth rates and properties are observes in rf- and dc-excited reactors.

The implications of all this for plasma deposition processes are significant. In dc discharges, the condensable species are created relatively close to the cathode if the electron collision cross section with the gas is large, as is the case for silane, for example.

14

This causes a large difference between the deposition rates on the cathode and anode. In rf discharges these differences are smaller but still noticeable for asymmetric systems. Deposition rates in an rf-excited reactor are, for comparable operating conditions, generally smaller than the cathodic deposition rates in the same system when it is dc operated. This is attributable to the larger distance over which the radical species have to diffuse before they can bond to the surface of the growing film. Because the radicals are formed in the bulk of the rf plasma, the latter is more prone to the occurrence of gas-phase reactions involving these radicals (homogeneous reactions) than dc discharges. A more detailed discussion of homogeneous vs. heterogeneous reactions, which are reactions involving radicals at a surface, will be given in the next section in the context of operating parameters and reactor design.

There are many operating parameters (external process variables) such as gas flow rates, gas composition, pressure, electrical power and frequency, substrate temperature and reactor geometry. There are many process characteristics such as etch and/or deposition rates, spatial uniformity, selectivity, degree of anisotropy and sensitivity. In the past, this complexity has resulted in process techniques being developed empirically rather than on the basis of fundamental principles. One of the reasons for this situation is that the external process variables listed above cannot simply regulate the internal process variables which actually govern the process. These variables are the energies, densities and fluxes of electrons, ions, neutral gas molecules and free radicals produced in the plasma reactor as a function of position and time. Determining the relationship between the internal and external process variables may be a key to further advances in PAM. Fig. 1.8 shows this interdependence and complex nature of the plasma processing involved in PAM [187].

1.3.3 INDUSTRIAL NEEDS AND PROBLEMS CONCERNING PAM

Semiconductor electronics, which lies at the heart of virtually all modern manufacturing and high technology products, is an area in which PAM has become essential. In the manufacturing of integrated circuits, for example, so-called "dry" processing which uses plasmas and/or particle beams for microfabrication is replacing "wet" chemical processing. Dry processing is required because of the ever growing need for smaller and smaller separation between circuit elements. As critical device dimensions shrink to 1 µm and below, wet processing becomes impractical for many required processing steps owing to problems of surface tension, linewidth control, undercutting of mask images, contamination, and the inability to achieve high aspect ratio. Dry processing techniques such as plasma etching and ion milling overcome these difficulties. In addition, the smaller device dimensions are dictating a move toward more complex and difficult metallizations such as refractory metals and their silicides. These metallizations are best deposited by plasma or plasma-assisted techniques such as sputtering or plasma-assisted chemical vapour deposition (PACVD). Current estimates of the size of the market in semiconductor plasma processing world wide today approach £3.25 billion per year, and it is predicted that this will increase annually.

15

Coating
- composition
- internal stress
- temperature resistance
- stability
- phase distribution
- electric, mechanic and magnetic properties

Process
- phase distribution
- substrate temperature
- bias
- kind of process
- ionization grade
- electric and magnetic field
- gas and target material

Substrate
- composition
- kind of production
- roughness
- geometry
- phase distribution
- electric, mechanic and magnetic properties

Application
- corrosion
- adhesion
- diffusion
- abrasion
- surface crack
- oxidation

Fig. 1.8: Considerations in plasma coatings [187].

The high performance ceramic field is another area which is attracting increasing attention. Because plasma produced ceramic powders are extremely fine and pure, they lend themselves to pressureless sintering, resulting in superior material properties. In USA, the present market for high performance ceramics is about $5 billion per year. According to a report by the Long Term Credit Bank of Japan [3], high-performance ceramics will be among the three leaders (car electronics, office computers, high-temperature ceramics) in industry growth over the next 5 years. Japan has already begun to show results from their strong program. A significant growth in automobile engine parts will begin in the 1990's. It is expected that the ultimate goal-the "all-ceramic engine"- will require minimal or no cooling and will give unprecedented gas mileage. Preliminary work in fabrication these materials , using plasma sintering, has already begun. The new field of high temperature superconductors, which are, in fact ceramics themselves, can well be the beneficiary of plasma sintering in their manufacture.

Included in PAM are surface modification, plasma spraying, melting, thermal plasma synthesis, welding, and electrical discharge machining. In addition, plasma surface hardening, cleaning, nitriding, oxidizing, or other types of surface treatments preparatory to bonding or coating are major factors in today's technology. This is particularly true in high-technology areas where exotic or "difficult" materials such as ceramics, refractory metals, or composites must be processed.

The unique characteristics of plasmas (high effective temperatures, energetic particles, etc.) often offer the only practical means for such processing. Plasma spraying is already widely used for applying thick coatings of refractory materials and is one of the prime candidates for producing effective anticorrosion coatings [4].

The plasma environment also offers opportunities for the synthesis of materials that would be difficult or impossible to produce in conventional chemical reactors, and for simultaneously synthesizing and depositing materials in a usable form, eliminating many subsequent processing steps. Plasma polymerization offers such an example.Under suitable conditions, monomers introduced into a plasma environment can polymerize [4], often producing polymers having characteristics that are not found in conventional polymerization. Plasma processing is very well-suited to producing polymers in the thin film form which is required in many important applications such as coatings on other materials, multiple layers for magnetic recording tapes or disks, or "plastic" wrapping materials. Although it is not widely appreciated, the pound volume for magnetic recording media is considerably larger than that for micro-circuits. In the bio-medical area, coatings for biocompatible polymers will permit continued progress in the development of sophisticated prosthetic devices, implantable replacement parts, and tools for medical monitoring and diagnostics. The recent developments in producing diamond and diamond-like coatings are often the result of a plasma-deposition process as well. The same type of processing can be used to decompose materials; for example, hazardous wastes [5]. This is presently done by passing the waste material either in the form of a liquid spray or a fine powder through an arc plasma.

Plasma electronics covers the range from plasma displays to arc-switching devices used in the power generation and transmission industry. In addition to the need for further development of these and related devices, there is a great need for improved materials for

17

use in plasma environments. Deterioration of electrodes in arc devices, for example, as in power switchgear, is a constant and costly problem.

Analytical instrumentation and systems development based on plasma technology has become increasingly important, and there is now a substantial market for mass spectrometers, ion accelerators and implanters, sputter-deposition systems, ion-mills, plasma etchers, plasma torches, and thermal plasma reactors, as well as instrumentation for noninvasive diagnostics for plasma processes. Although much of this development has proceeded in an empirical, evolutionary manner, the manufacturers of instrumentation and plasma systems are now at the forefront of what is known about the generation, control, and behaviour of plasmas and plasma/materials interactions. Future progress in PAM will be greatly expedited if applications research is closely coupled with work on improved instrumentation, statistical methods, and manufacturing systems.

PAM is now at a critical point in its development . In order to put PAM on the firm base that will be required for future progress, it will be necessary to foster genuinely collaborative work among plasma scientists and engineers, statisticians, and industrial and manufacturing engineers from both universities and industry. Table 1.1 shows one view of the various types of complementary and cross-disciplinary activities that are needed [2].

1.3.4 PLASMA PROCESSES IN PAM

Nearly every problem in plasma-aided manufacturing requires a cross-disciplinary approach to develop and improve the manufacturing techniques and to ask and resolve the basic questions. In general, plasma-aided manufacturing is one or more steps in a manufacturing process, but not usually the entire process. Thus, all of these specific techniques must ultimately be integrated into systems in order that they can be utilized in industry. As a result, plasma-aided manufacturing involves not only the development of new techniques and precesses for manufacturing products, but their integration into a complete manufacturing system to produce these products.

1.3.4.1 Plasma modification of materials

This process is designed to improve the surface properties of materials without changing their bulk properties by implantation of specific ions into the materials. It is becoming economically attractive in Japan, Europe, and the US, and can be done on metals and alloys as well as semiconductors, ceramics, insulators and polymers. Some of the surface properties that can be modified by this process are: hardness, adhesion, corrosion, superconductivity, fatigue, friction, oxidation, resistivity, toughness, catalysis, wear, and dielectric properties.

In conventional ion implantation devices, an ion beam is extracted from a plasma source, accelerated to the desired energy, and then transported to the target. Typical beam currents are very small (in the microampere range) and the beam "footprint" area is less

18

Table 1.1

ENGINEERING AND SCIENCE IN PAM

PLASMA GENERATION

- **DISCHARGE KINETICS**

- **GAS PHASE PROCESSES**
  - ELECTRON ENERGY DISTRIBUTION

- **CROSS-SECTIONS FOR DISSOCIATION**
  - RADICAL/MOLECULE, ETC

- **MODELING**

- **PLASMA SOURCES**
  - ECR
  - MICROWAVE
  - RF
  - HOLLOW CATHODE
  - HELICON
  - MAGNETRON

PLASMA DIAGNOSTICS

- **DEVELOPMENT OR IMPLEMENTATION OF NEW METHODS**

- **EXPLOITATION OF PRESENT METHODS**

- **SPATIAL RESOLUTION**

- **UNIFORMITY**

- **FREE RADICAL CONCENTRATION**

SURFACE SCIENCE

- **UHV SURFACE STUDIES**
  - MOLECULE-SURFACE
  - RADICAL-SURFACE REACTIONS
  - SYSTEM WITH ENERGETIC BOMBARDMENT (IONS)
  - SURFACE DIFFUSION
  - RECOMBINATION OF RADICALS AT SURFACES.

- **ANALYSIS OF PLASMA-EXPOSED SURFACES**
  - ELECTIVITY MECHANISMS
  - BLOCKING LAYERS
  - CONTAMINATION

- **DAMAGE**

than 1 cm². In order to process large-scale targets and in order to avoid shadowing if the target is nonplanar, a combination of beam rastering and target rotation during the implementation is required.

In the plasma-source ion-implantation process, a dc discharge, the strongest electric field is in the cathode sheath, which accelerates positive ions to the cathode. If the pressure is kept low enough so that an arc discharge does not occur, positive ions can be accelerated to strike the cathode with energies of 100 keV or more. With these energies, ions can implant themselves in the cathode surface, which has important applications in improving tool hardness and lubricity. At lower energies, implantation can benefit the microelectronics industry.

The implantation process begins with the application of a pulsed, high-voltage, negative dc potential between the material to be implanted and the vacuum chamber wall. As the potential becomes more and more negative, the sheath moves into the plasma itself. As the sheath moves through the plasma, electrons are "reflected" from the plasma-sheath boundary and kept in the plasma. It should be pointed out that the plasma-sheath boundary does not move the ions as it travels into the plasma. Rather, since the ions are more massive, the boundary sweeps through the ions. When the ions find themselves on the other side of the boundary, they are affected by the electric field in the sheath, which tends to accelerate them to the cathode.

Currently, identification of the factors and their interactions which influence this process are poorly understood from the standpoint of the behaviour of the material which is implanted. To further advance this field, an understanding of how the bombarding particles interact with the base material and how to apply this knowledge to manufacturing techniques will be an opportunity for industry to further exploit this technology. Two aspects of this technique: (i) surface hardening and wear resistance, and (ii) corrosion and oxidation resistance are particularly important.

It has been conclusively demonstrated that ion implantation can beneficially modify the surface-sensitive mechanical properties of steels. Fatigue life has been extended by as much as a factor of 2, the coefficient of sliding resistance reduced by as much as a factor of 100, and the wear resistance increased by a significant amount. Most studies have concentrated on the use of nitrogen ions, but the use of C, B, Ti, and Mo ions have also shown promising results.

1.3.4.2 Plasma Etching and Microwave Processing for Microelectronics

Pattern transfer to a wafer by plasma etching has become an indispensable technique for fabricating semiconductor devices whose critical feature dimensions are less than 3 μm. Etching can be done with wet chemicals, such as acids. With plasma etching it is possible to etch faster in the direction perpendicular to the surface of the material than parallel to the surface, resulting in anisotropic etching. This allows finer features to be etched,

allowing many more transistors and diodes to be placed on a microchip. Anisotropic etching is the key to making smaller, faster, and cheaper chips. Plasma etching is a purely chemical process involving neutral atoms and/or free radicals which react with the surface. Reactive-ion-etching (RIE) is defined as plasma etching with required simultaneous energetic ion bombardment of the processed surface. In fact, the most important reason that RIE has replaced wet chemical etching in microfabrication technology is the ability of RIE to accomplish anisotropic etching. The following materials used in micro-fabrication readily lend themselves to plasma etching in that they form volatile compounds under proper conditions:

Silicon	Silicon dioxide
Silicon nitride	Photoresist
Polyamide	Aluminum
Tungsten	Titanium
Gallium arsenide	Indium phosphide.

The following materials do not readily form volatile compounds, at least at or near room temperature:

nickel

iron

copper

metals from groups I or II in the periodic Table.

In addition to the applications in microfabrication technology, the ability of RIE processing to eliminate the large quantities of liquid chemicals needed for wet processing is a decided advantage.

In the actual practice of plasma etching, it is required to monitor and control a wide variety of processing variables involving three major decision areas: 1) the electrode configurations for the plasma and the current, voltage, and frequency applied; 2) the reactant gas composition flow rate and pressure; and 3) the nature and kinetics of the surface reactions of the plasma-generated species. This inherent process flexibility provides a need for engineering statistics and manufacturing technology for operation and control. The emphasis here is in the identification of reactive species in the plasma and the characterization of the surface reactions which occur.

The basic need to improve plasma-etching techniques are: 1) to characterize in stages the gas-phase species present in a plasma using conditions appropriate for reactive ion etching; 2) to study the surface reactions which occur both on the photoresist covered and on the uncoated semiconductor surfaces; 3) to devices analytical diagnostic schemes to monitor and control a plasma-etching process leading to submicron minimum linewidth devices; 4) to utilize plasma modelling expertise to develop better understanding and control over the plasma-etching process; and 5) to increase yield, improve uniformity, and quality by using statistical methods of design and analysis for process optimization. These objectives can be accomplished by bringing a number of analytical techniques to bear on the plasma systems and by examining the etched image profiles. However, only with sufficient diagnostics and sensors can one hope to determine the importance of the internal

process variables, and that statistical techniques of experimental design and analysis can be used to reveal direct relations between the variables.

1.3.4.3 Plasma Deposition and Polymerization

A variety of plasma processes are currently used to deposit materials on surface. Several of them are described below. They are based on the fact that surrounding an electrode, a plasma sheath often develops. Such a sheath can have a considerable potential drop across it., which can be used to accelerate positive ions to the electrode. The impact of the ions on the electrodes can remove materials from the electrode or serve as an "activator", for free radicals that travel to the electrode.

1.3.4.3.1 Activated Reactive Evaporation & Ion Plating

We start this section by first considering straight evaporation. Typically this process is carried out at pressures between 10^{-5} and 10^{-6} torr. An electron beam source is used to heat the material to be evaporated though alternatives can be used. This is all illustrated in Fig. 1.9a [188].

Also illustrated in the same diagram is a chart indicating the spread of evaporant as it emerges from the ingot rod source. The atom flux is clearly much greater in the direct line of sight of the source than anywhere else. This often makes it necessary to complicate the arrangement in order to get acceptable uniformity of coating on the substrate surface. This end can be achieved in a number of ways. Most simply the pressure within the vacuum chamber can be increased to the extent that gas scattering becomes significant. This effectively increases the throwing power because of the multiple collisions the evaporant atoms must undergo before reaching the substrate. Another possibility is to move the substrates relative to the source. Alloy coatings may be deposited by using multiple sources.

Activated evaporation is the evaporation of a material in the presence of a plasma with the substrate floating, grounded or electrically biased. Reactive evaporation is the evaporation of a metal in the presence of a reactive gas to deposit a compound without the presence of a plasma. Activated reactive evaporation is the evaporation of a metal in the presence of a reactive gas and a plasma to deposit a refractory compound. The plasma is generated by a positively biased electrode when an electron beam evaporation source is used and by low energy electrons injected into the vapour phase from a thermionically heated filament when a resistance heating source is used. Variations on this process are illustrated in Fig. 1.9b [188]. A substrate bias can be used to attract positive ions from the plasma when the technique becomes akin to reactive ion plating. Using electron beam evaporation sources, the electric field may be generated by biasing the substrate positively instead of using a positively biased interspace electrode. This does not allow for the benefits of negative substrate bias however. Cubic boron nitride is one of many refractory coatings to have been deposited by this technique.
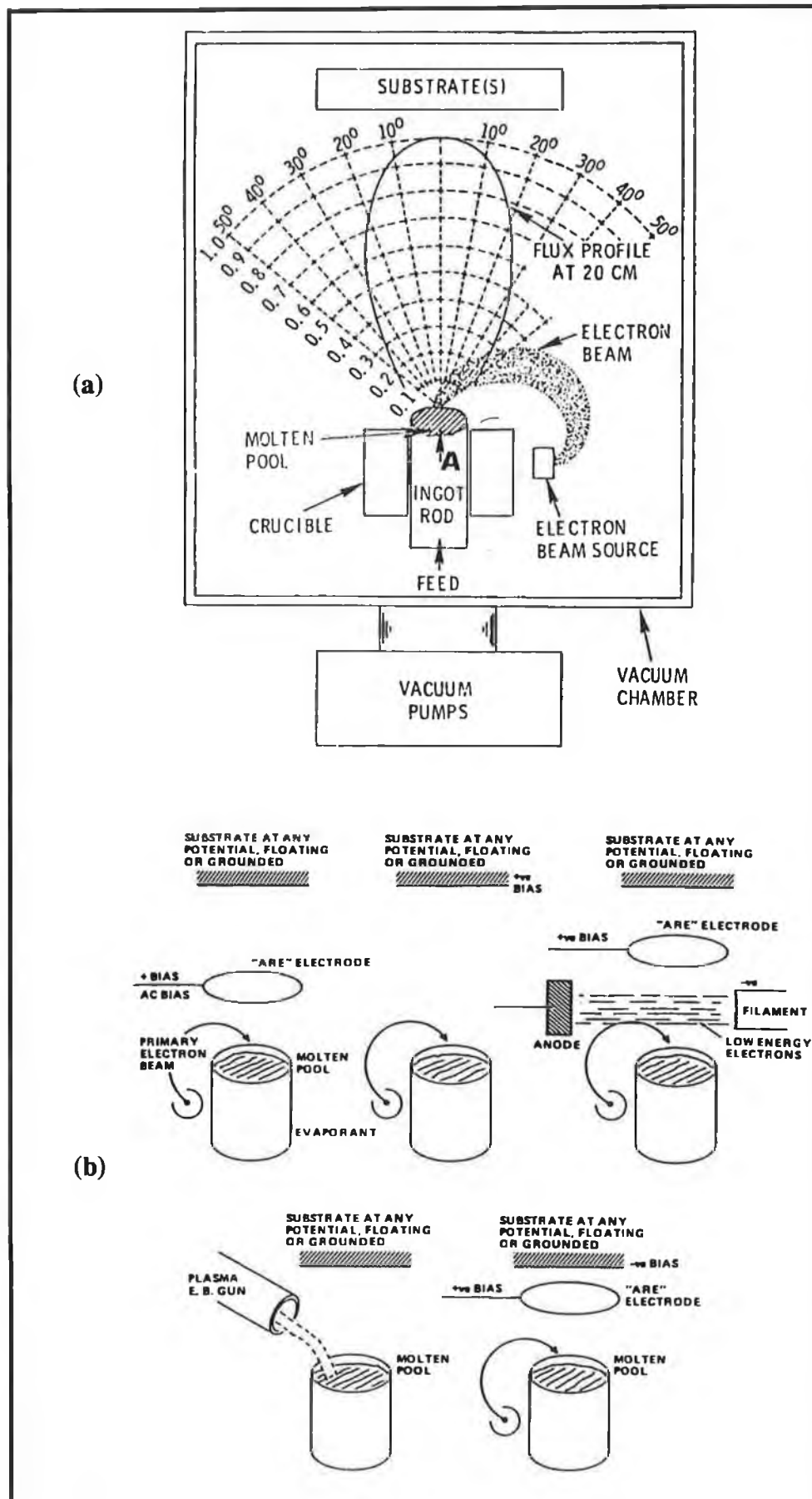
Fig. 1.9 : (a) Vacuum evaporation process using electron beam heating. (b) Basic
activated reactive evaporation (ARE) processes (from left - b1 to b5) [188].

Geometrically at least, the ion plating process is a simple one. A schematic is given in Fig. 1.10a [188]. The electrode potential may be in the 3 to 5 kV range. The coating source is started up and the coating material vapourised into the glow discharge and hence onto the sample. This large negative bias can cause problems if the samples are oddly shaped or have edges since the electric field will be different there. This leads to an irregular distribution of coating over the surface. Typically the source is a refractory boat or filament which supports the coating material. When a current is passed, this refractory heats up causing the lower melting point coating material to be evaporated. A variation on this which has the advantage of enabling refractories too to be evaporated is to use an electron beam source, such as is used in ARE, to heat the sample. One disadvantage with this arrangement is the necessity of a better vacuum for operation of the source. Such systems should have a conductance baffle to separate the electron beam area from the relatively high pressure plasma area. Other alternative set-ups are illustrated in Fig. 1.10b [188]. The use of a sputter source allows great flexibility as will be illustrated by the section on sputtering. It has the disadvantage that often the voltage on the sample electrode must be controlled in order that the rate of deposition exceed the rate of back sputtering. In chemical ion plating, a gas, typically a metalorganic for example $TiCl_4$, provides the coating material. In reactive ion plating, a reactive gas is introduced into the main chamber which then reacts with the coating source, for example nitrogen to form titanium nitride. The hollow cathode technique is also shown in Fig. 1.10b and details regarding this type of source can be found in ref. 6.

Variations on the ion-plating technique itself are common. A number of these are illustrated in Fig. 1.10c [188]. They centre around methods for enhancing the bombardment current at the sample which goal is achieved by increasing the plasma density. Increased ion bombardment is beneficial for production of high quality dense coatings.

1.3.4.3.2 Sputtering

Ions when striking the cathodes can produce a "collisional cascade," which may result in atoms being ejected from the cathode surface - sputtering. Sputtering "yields", the no. of atoms per incident ion , are functions of the input energy and the ion mass, as well as the target composition. The sputtered atoms can then deposit on the surface of a substrate material, producing a "thin film". A schematic diagram is shown in Fig. 1.11. The substrate is usually biased negatively to encourage ion bombardment on the growing coating.

The applied voltage which is required to drive the current through the system is a function of the system pressure. The rate of thin film formation on the substrate will depend on the amount of sputtering at the target; this in turn depends on the ion flux on the target and on the ion energy and hence on the voltage applied to the system, which then determines the sheath voltage at the target. The choice of the sputtering pressure and the implied choice of the V-I characteristics are important.

The actual sputtering gas is often not critical but in many cases it is required that the gas does not chemically react with the target, film, or substrate, so often inert gases

24
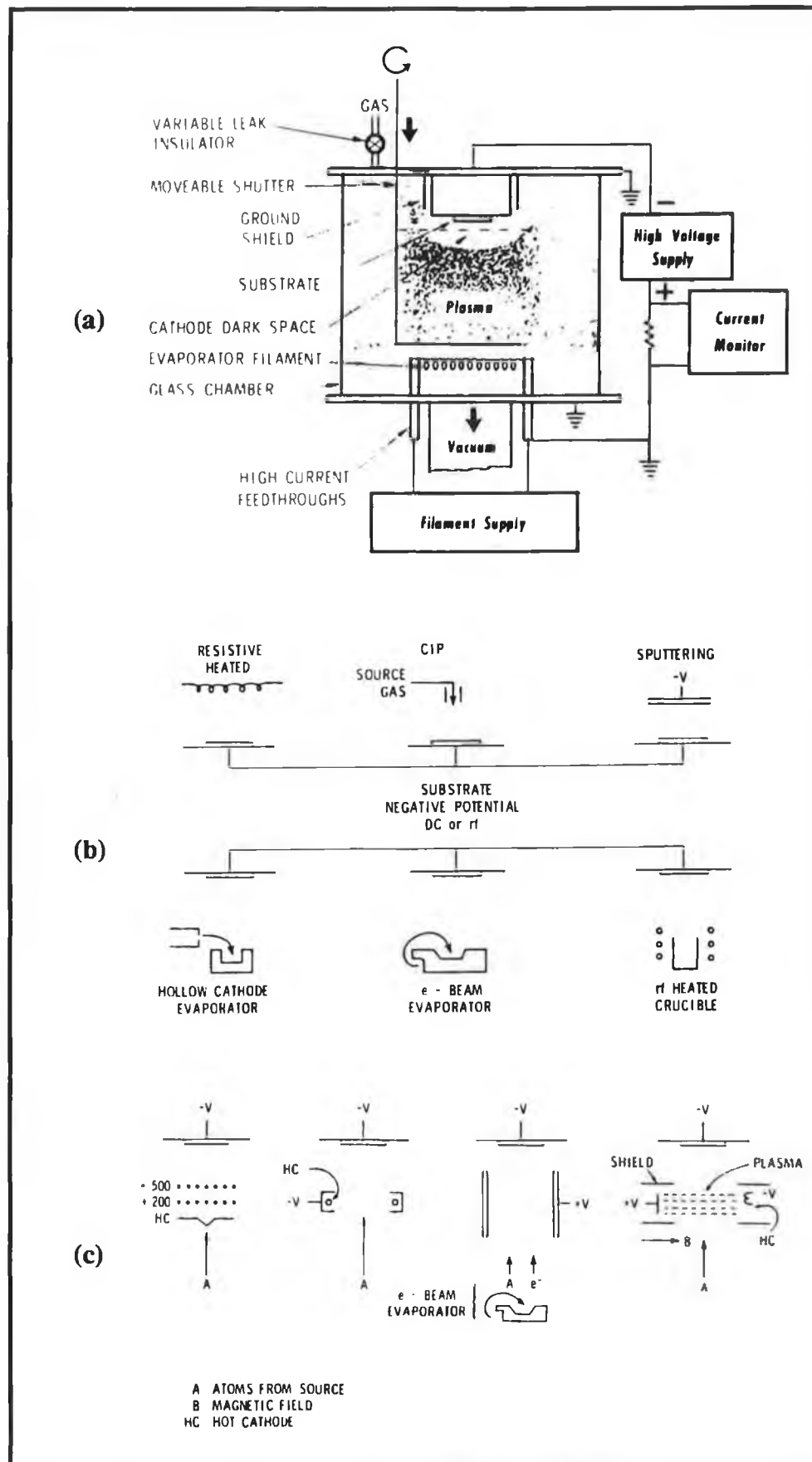
Fig. 1.10 : (a) Typical ion-plating system using a DC diode discharge. (b) Vapour sources for ion plating. (c) Methods of enhancing the ionization in an ion-plating system [188].
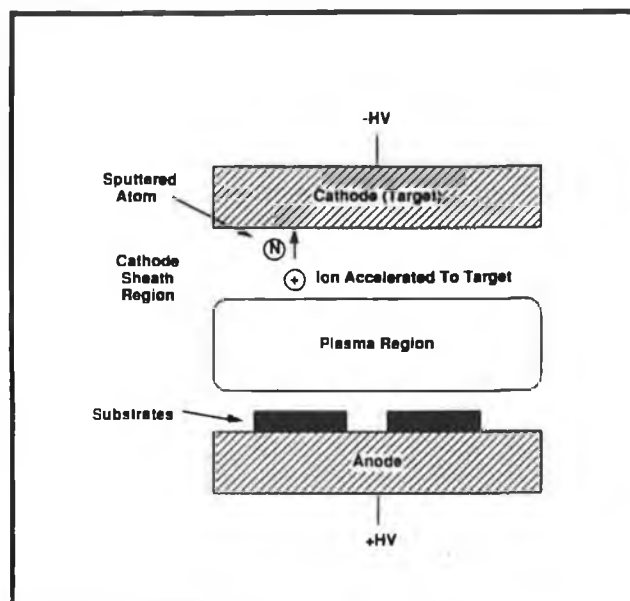
Fig. 1.11 :   **Plasma sputtering system [2].**

are used for sputtering. In addition, since sputtering gases may also become in trapped in the growing film, use of inert gases will not cause chemical reactions with the growing film.

Another important variant is where a reactant gas is introduced with the inert gas in order to form compound films. An example of such a system is where an argon\nitrogen gas mixture is used in conjunction with a titanium target to produce titanium nitride coatings. Compound targets can also be used in the production of complex coatings. Targets consisting of entirely separate materials may also be used if the materials are arranged in a geometrically appropriate way.

A serious problem with the "ordinary" sputtering as just described is that the growth rate is very low and this prevents it finding widespread application. This difficulty was overcome by Chapin [7] who introduced the concept of magnetron sputtering by using magnetic fields in conjunction with the electric field to force the electrons in the plasma to circulate in front of the target plate. This increases by one to two orders of magnitude the number of ions in the vicinity of the plate, hence the number of ions bombarding it and therefore the deposition rate which is of the order of 1 μm per minute. Ion densities are typically in the range 10^{11}-10^{12} cm^{-3}. A schematic illustrating a typical magnetic geometry and the principle involved is given as Fig. 1.12a. Note that while Chapin's original geometry was planar, cylindrical and other configurations are in common use. Moreover, while remarks in this section may be applicable to different

26

types of magnetron, they are specifically directed at the planar version. Both r.f. and reactive sputter modes are possible as well as d.c. however the r.f. technique suffers from the usual grounding and control problems which significantly add to system complexity. For this reason d.c. is the mode of choice where possible.

Yet another significant advance in sputtering technology came about when Window and Savvides [8] recognised that by increasing the flux from the outer magnet relative to the inner some of the field lines would not be absorbed in the centre magnet and would tend to head towards the substrate as shown in Fig. 1.12b. Electrons get trapped on these field lines and are more inclined to head towards the substrate than to go to the chamber walls. The increased electron concentration at the negatively biased substrate leads to increased ion bombardment which both theoretical and experimental evidence indicates gives denser coatings. Another possibility is to increase the strength of the inner magnet
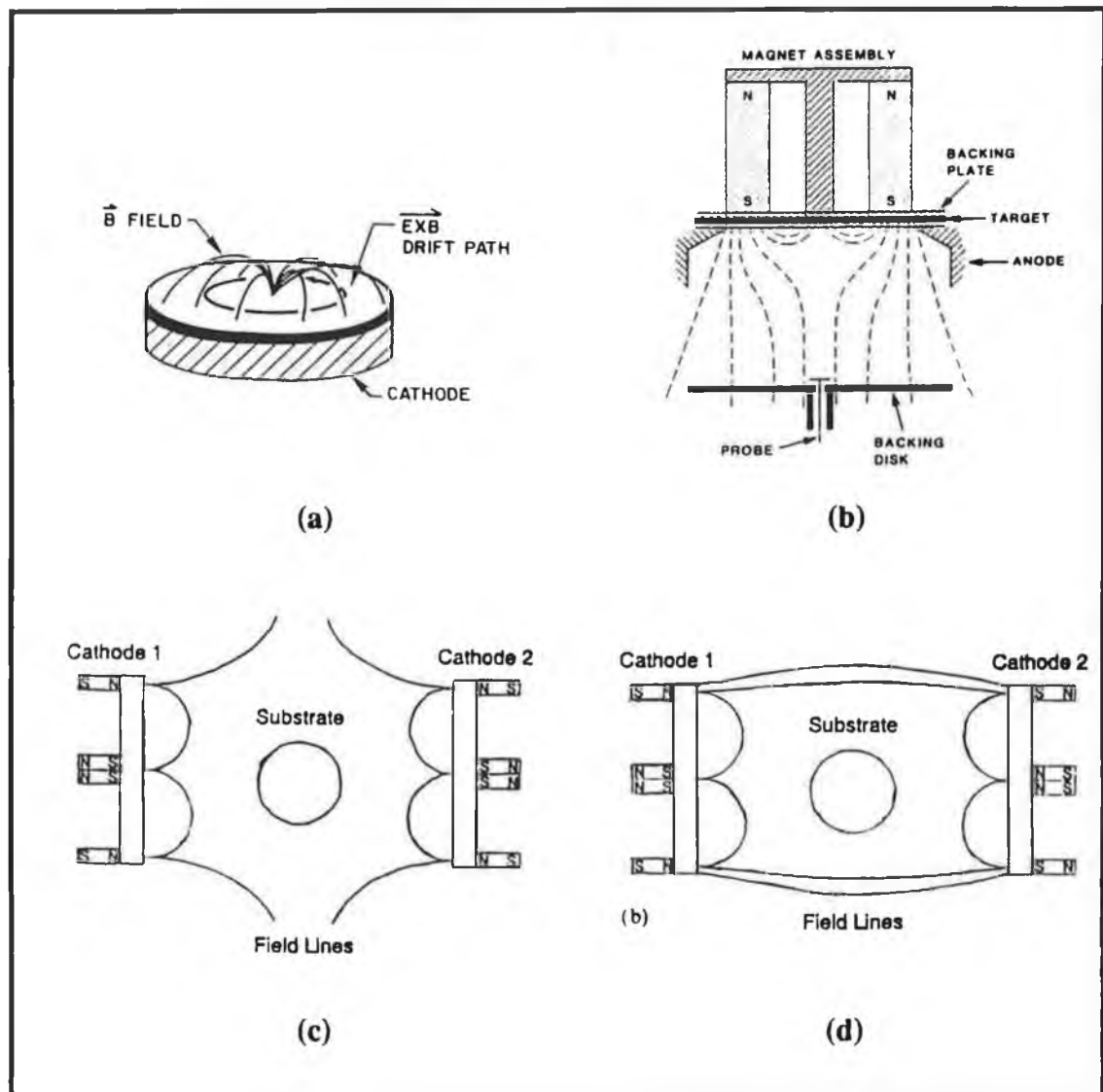
Fig 1.12 :   Shape of the magnetic field : (a) in a circular planar magnetron cathod, (b) in an unbalanced magnetron system, (c) in a mirrored magnetrons system, (d) in an opposed magnetrons system [6,8,189].

with respect to the outer. This may have some use where good target utilisation is required but is not much referred to in the literature and is of less importance than the first type. Collectively, these magnetrons in which there is no attempt to balance the flux passing from the inner to the outer magnet are known as unbalanced magnetrons. An unbalanced magnetron might typically operate at a pressure of about 1 mtorr, a voltage of 400 V and a current density of 20 amps/cm^{-2}.

Further improvements were made when it was realised that by placing two magnetrons in an opposed rather than in a mirrored configuration an electron trap was created between them which enhanced the degree of ionisation. See Fig. 1.12c and 1.12d [189]. Clearly this concept is expandable so that one could have 4,6,8,...magnetron systems if desired. It is not possible to get a closed field using an odd number of magnetrons.

Such a 4 magnetron sputtering system are employed in our laboratory to deposit titanium nitride and other refractory compounds.

1.3.4.3.3 Plasma Assisted Chemical Vapour Deposition (PACVD)

PACVD consists of the technique of forming solid deposits by initiating chemical reactions in a gas with an electric discharge. This technique is very similar to ion plating and any distinction would be very fine. However, the name PACVD is not generally used in a context where metal is being evaporated. Usually the materials one is trying to grow are aimed at the hard insulating, semiconductor or polymer areas. The plasma chemistry is almost invariably an important factor too whereas in ion plating this is less usually the case. Also an r.f. bias is more frequently used in PACVD and the bias is rarely as high as in ion plating. However this author would not quibble over the suggestion that chemical ion plating and PACVD are the same.

Though classified in this thesis as CVD, PACVD is really a hybrid PVD/CVD technique. PACVD will be described in a separate section as this work is devoted to this technique.

1.3.4.3.4 Plasma Polymerization

Plasma polymerization is very similar to PACVD. In many cases, the difference is that the later is concerned with the deposition of inorganic materials, and in the former, the deposition of organic materials which are often polymeric in nature. As an example, if an unsaturated fluorocarbon gas such as tetrafluroethylene is injected in a plasma, a Teflon-like film can be deposited on a substrate. The deposited polymer is often highly cross-linked and many high-quality films are formed which cannot be deposited by other means.

A polymer is normally built from a monomer precursor, but it can also be used to refer to a characteristic bonding structure of amorphous films. A polymer-like film differs from a glass by having less cross bonding of the major chemical components of the film, and instead, having a great deal of hydrogen or halogens saturating the dangling bonds.

28

Thus polymerization is often used to refer to the formation of polymer-like amorphous films even if no monomer exists. Some plasma polymers have been formed that appear to consist of linked monomers of the starting gas. Most commonly, however, the plasma decomposes the starting gas into fragments. These fragments either nucleate into a polymer film at the surface, or polymerize themselves into chains and clusters. The relative magnitude of gas or surface polymerization is sensitive to the power, pressure, and choice of starting material. Polymerization reactors are often quite different in construction from parallel-plate reactors used for deposition and etching.

1.3.4.4 Thermal Plasma Spraying, Synthesis, and Sintering

1.3.4.4.1 Plasma Spray

This process is of interest because of its ability to provide surface protection. Turbine blades of air-craft engines, for example, are protected by anticorrosion (super-alloys) and by thermal-barrier coatings (ceramics) applied primarily low-pressure plasma deposition (LPPD). In addition, LPPD is considered to be viable manufacturing technology for producing monolithic, nearest shape of metallic as well as ceramic materials. Rapid solidification, which is inherent to the plasma-spray process, may also produce desirable properties of coatings or monolithic bodies, because the process results in fine-grain structures and, in extreme cases (certain metallic alloys), in amorphous structures which reveal unusual properties in terms of strength and corrosion resistance.

Powder is heated to near or above its melting point in a plasma torch and is accelerated by a plasma gas stream toward a substrate. On impact, the powder forms a coating consisting of many layers of overlapping thin lenticular particles-"splats". Almost any material that can be melted without decomposing can be used to form the coating. As with most plasma processes, the variables include: type of gases, flow rates, anode design, power level, and the location in the plasma torch where the powder is injected.

Most powder used for plasma spray is between 5 and 60 µm in size. To achieve uniform heating and acceleration of a single component powder, as narrow a size distribution as possible is preferred. Fine powders are accelerated and heated more rapidly, but tend to lose momentum more rapidly when spraying at longer distances from the torch. This generally results in densed, but more highly stressed, coatings. Virtually all plasma coatings require a roughened substrate surface, often done with grit blusting.

In spite of considerable advances of the plasma-spray technology over the past 20 years, the plasma-spray process as such is still poorly understood. In particular, there are no well-defined correlations available between the plasma parameters of the spray torch and the properties and quality of the coatings produced.

1.3.4.4.2 Plasma Synthesis

Synthesis of materials, especially of refractory materials in thermal plasmas, is an emerging technology with the potential of providing ultrafine and ultrapure powders suitable for pressureless sintering. Development of this manufacturing technology has been

severely hampered by the lack of an engineering base which is necessary for developments on an industrial scale. Works need to be done to establish such a base.

1.3.4.4.3 Plasma Sintering

Plasma sintering is a new technology for the rapid sintering of ceramic materials, which are attracting increasing attention for a wide spectrum of uses, including structural, electronic, and biological applications. Thermal plasmas represent extremely strong and easily controllable heat sources for sintering, reducing the required processing time by orders of magnitude compared to conventional technologies. At the same time, rapid sintering may result in unique and desirable structures and properties of the sintered materials. For example, the auto industry and other manufacturers of internal-combustion engines expect that sintered materials will revolutionize engine technology, because engines made of these sintered materials will not need cooling like today's metallic engines.

A general requirement for developing plasma sintering into a viable technology is a thorough understanding of plasma heat transfer during the sintering process. A model for describing the heating transfer process is required over the entire range of potential operating pressures (10-1 atm).

1.4   CONSIDERATIONS IN PLASMA COATINGS.

It is evident from section 1.3, that for successful application of a PAM process and coatings, two requirements must be met. First, the process must be developed. For a new plasma process, much time and money can be saved if the understanding of how the plasma, chemistry, and surface reactions combine to produce a specific result is known from experience and/or predictive modelling. Second, the economic benefit must be well-understood before the process can be utilized if the maximum benefits are to be realized. For a particular coating-substrate system, it is of fundamental importance that the interrelationship between the coating-microstructure and its properties are understood.

The interest in this study is films of solids: metals, semiconductors, dielectrics, in which properties connected with a zone structure are combined with film peculiarities. Use of the term "film" usually means a three-dimensional structure with one geometrical parameter (thickness) that is much less than the other two. Films in the thickness interval 0.01-1 μm are generally called "thin" and those from 1 to 100 μm "thick". The thinner the film, the more its properties are determined by its surface.

Material selection for thin film coatings or layers depends on the criteria, most suitable for specific needs. Many fundamental relations between the position of film material components in the periodic table of the elements and the properties can be used to optimize these material selections. One should bear in mind that atomistically deposited materials often have unique mechanical properties which differ significantly from those
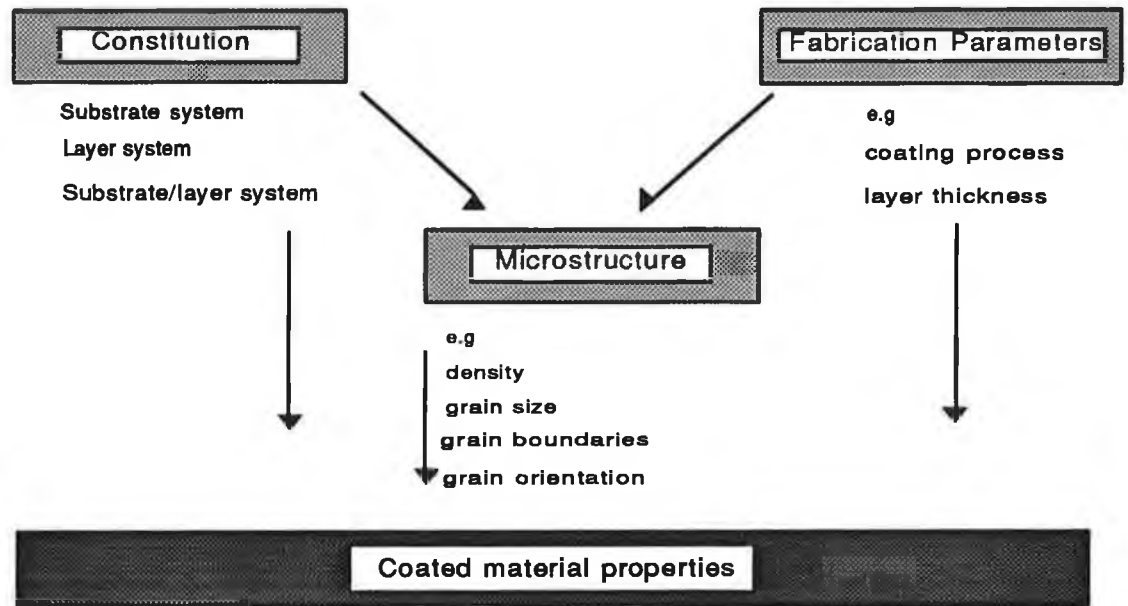
Fig. 1.13: Factors fixing coated materials properties [190].

of materials fabricated by melting solidification or sintering processes. These properties may be different because of unique microstructures, unique phase compositions, impurity incorporation and/or composition or phase gradients which may or may not be deliberate. It is difficult to obtain bulk properties in atomistically deposited materials because of the unique microstructures, graded properties and problems with compositional control. Problems with the material selection arise mainly because many desired properties such as good adherence at the substrate-film interface and no surface interactions, or good mechanical/electrical/optical properties cannot be obtained simultaneously. Fig. 1.13 [190] shows the main factors which determine plasma coating material properties. In this section, we will briefly describe some important considerations in plasma deposition of thin films, mostly related to our interests, e.g. PACVD.

1.4.1. EFFECT OF SUBSTRATE TEMPERATURE.

The effect of substrate temperature on the plasma deposited thin films were classified first by Movchan and Demchisin (M-D model) [9] (given in Fig. 1.14). MD identified three distinct structure zones as a function of the homologous temperature T/T_m (where T represents the substrate surface temperature and T_m is the melting point). The low temperature Zone 1 structure ($T/T_m < 0.25$-0.3) corresponds to low adatom mobility and

31
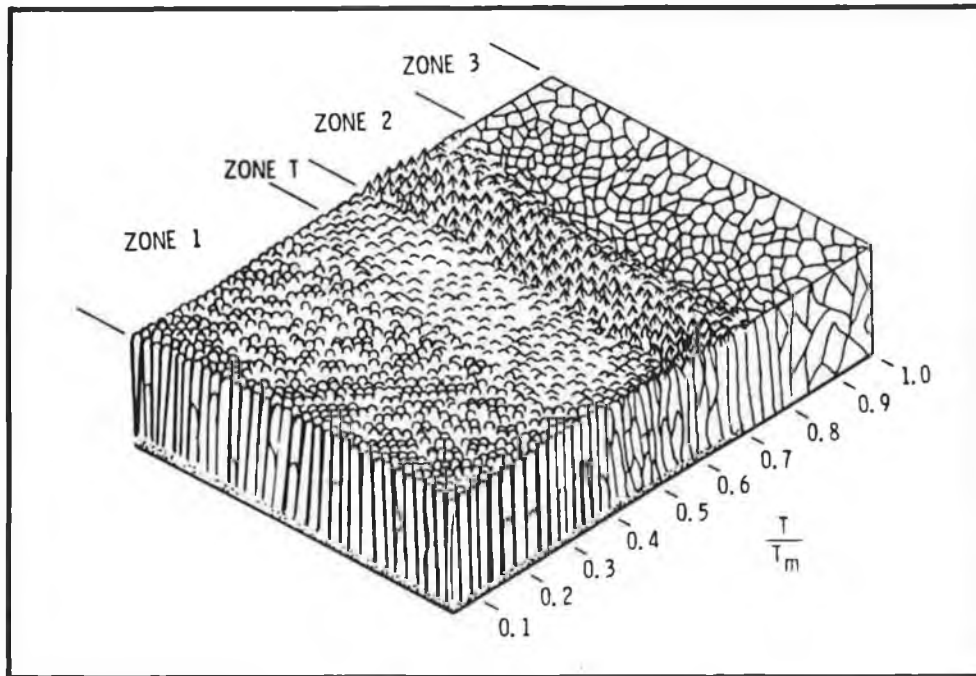
Fig. 1.14 : Movchan-Demchishin (M-D) diagram of structural zones in vacuum deposit as a function of the deposition temperature (T) and the melting point (T_m) of the deposit; Zone T described by Thornton [9,10].
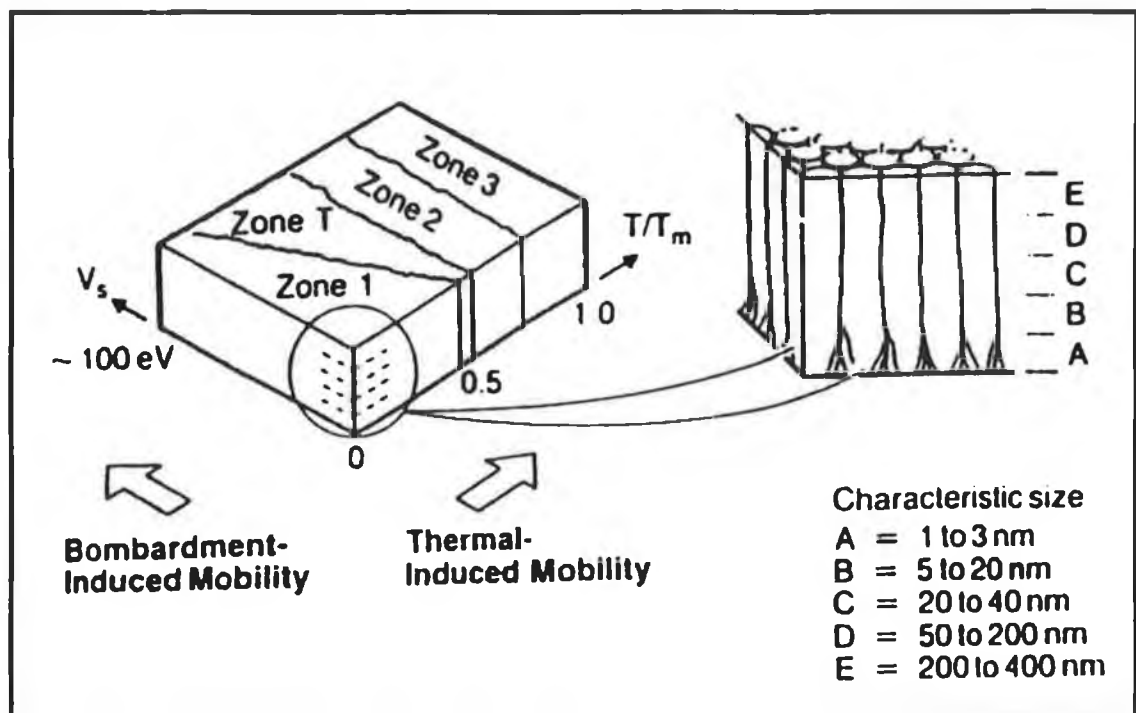
Fig. 1.15 : Revised Movchan-Demchisin (M-D) model showing the effect of substrate bias [11].

consists of tapered columns with domed tops. In Zone 2 ($0.3<T/T_m<0.5$), surface diffusion becomes important and the structure is of a straight columnar region and has a smooth surface topography. With increasing temperature ($T/T_m>0.5$), bulk diffusion becomes the dominant process and Zone 3 structure are characterized as being equiaxed in nature akin to recrystallized metals. Later work by Thornton [10] demonstrated that the presence of a sputtering gas could modify the MD model; a further region was identified called Zone T which consisted of poorly defined fibrous grains. Thornton also suggested that rough surfaces, high gas pressure, oblique adatom flux and reactive contaminant gases will tend to lower the T/T_m values for the zone boundaries.

It should be emphasized that all zones are not found in all deposition methods and deposits. For example, Zone T is not prominent in pure metals, but becomes more pronounced in complex alloys, compounds or in deposits produced at higher gas pressures. Zone 3 is not seen very often in materials with high melting points.

1.4.2 EFFECT OF SUBSTRATE BIAS

As an alternative to increasing deposition temperature, Zone 1 structures can be overcome by subjecting the growing films to bombardment by particles having sufficient energy so that the resultant momentum exchange causes coating atoms to fill the voided boundaries. Messier et al. [11] have suggested improvements to the M-D model [9] which account for the evolution of morphology with increasing film thickness and the effect of both thermal and bombardment induced mobility. In this idealized model all the distinct levels of physical structure column-void sizes are considered and assigned sub groups 1A, 1B, 1C, 1D and 1E as indicated in Fig. 1.15.

This model draws attention to the fact that ion bombardment promotes a dense structure of the Zone T type, but also that these atomic movements can have a thermal induced or bombardment induced origin. During ion bombardment it has shown that the void filling process involves a combination of forward sputtering of coating atoms into the void region, impact induced surface diffusion, and local heating such that recrystalization takes place during the growth and the underlying crystal structure is adopted. Clearly the application of a substrate bias during the deposition of a coating has a profound effect upon the growth and resultant microstructure of PVD films. The unbiased film shows an open columnar microstructure (Zone 1 type) whilst the biased film appears more dense, the individual columns being much less well defined (Zone T type).

1.4.3 IMPURITY INCORPORATION

The deliberate or unintentional incorporation of 'impurity' atoms into the depositing material may be important in several ways. The atoms may react in such a way as to cause renucleation and the destruction of the columnar microstructure, stabilize phases of the material, stabilize a fine grain structure, form second phase material or stabilize the intrinsic stresses in the film. Since a small amount of impurity material can have a large

effect on properties, it is not unexpected that there is appreciable variation in measured properties of deposited materials among various investigators.

Impurities may arise from a number of sources. In vacuum processes oxygen, nitrogen, hydrogen and carbon are common from residual gases, vacuum leaks and outgassing. In sputter deposition, the implantation of several atomic percent of the sputtering gas is not at all unusual, particularly when a substrate bias is used. In CVD, reaction products, carrier gases and unreacted or partially reacted source gases are commonly incorporated. Electrode deposited materials may contain hydrogen and co-deposited organic and inorganic additives.

1.4.4 STRESS IN FILMS

Virtually all metallic and compound films are in a state of stress. The total stress is composed of a thermal stress σ_{th} and a so-called intrinsic stress σ_i. The thermal stress is due to the differences in the thermal expansion coefficients of the coatings and the substrate materials. The intrinsic stress arises from the accumulating effect of crystallographic flaws which are incorporated into the film during deposition. While the intrinsic stress is a function of the deposition process, the thermal stress forms only when the film substrate combination cools down from the deposition temperature.

The internal stress σ_t can be expressed as follows:

$$\sigma_t = \sigma_{th} + \sigma_i$$

The thermal stress, σ_{th} can be expressed as:

$$\sigma_{th} = \frac{E_f}{(1 - v_f)} (\alpha_f - \alpha_s) \nabla T$$

where, E_f and v_f are the Young's modulus and Poisson's ratio of the film, respectively. α_f and α_s are thermal expansion coefficients of the film and the substrate, respectively. ∇T is the difference of deposition temperature and room temperature.

Intrinsic stresses are more complex in nature and can arise for a number of reasons:

(a)   Lattice mismatch between the substrate and film producing interfacial disorders.

(b)   Incorporation of impurities in the growing film which precludes the formation of a stress-free deposit.

(c)   Rapid film growth leading to the deposition of the kinetically more accessible rather than the thermodynamically more stable film.

34

(d)   Forward sputtering and ballistic recoil mixing (at high bias potential) leading to vacancy and interstitial sites.

Intrinsic stress may be affected by a number of plasma processing and growth parameters. Film deposition rate, angle of incidence, presence of residual gas, deposition temperature and gas incorporation affect the magnitude of stress in plasma deposited films as well as whether the stress is tensile or compressive.

From section 1.4.2, substrate bias promotes adatom mobility which leads to the favouring of type T microstructures over Type 1. However, the denser type T structures mean that high internal stresses can be supported, whereas for Zone 1 structures, where each column is an island surrounded by space, little or no stress can be supported since the weak columnar boundaries will not be able to transmit a stress.

The intrinsic stress in the film increases with layer thickness. The structure becomes less dense as it grows outwards. This tendency to move towards the more open Zone 1, Zone T type microstructures from the denser Zone 2 morphology is also accompanied by a reduction in the levels of internal stress due to an increased tendency for stress relaxation at the open columner boundaries.

1.4.5 ADHESION

One of the main reasons for the failure of hard wear resistant coatings during service conditions is the lack of sufficient adhesion. Adhesive strength is a function of the type of bonding across the interfacial zone. This bonding may be due to Van der Waals forces, ionic, covalent or metallic bonds. However, no predicative theory of chemical adhesion exists. A practical definition of adhesion states that the interfacial region does not fail under test conditions. The interface is of paramount importance both in the development of the adhesive bond and in the quality of the bond between film and substrate. The interface which forms is a function of the surface topography, level of contaminants, chemical reactivity of the film and substrate material in concert with the energetics of the deposition process.

Cleaning of the substrate prior to film deposition reduces the level of surface contamination which can be detrimental to good adhesion. The adhesion can also be improved by using substrates which are structurally similar to the coating material which will react with both the film and the substrate.

1.4.6 STRUCTURAL ANISOTROPY

Films grown by plasma deposition techniques commonly exhibit a strong preferred orientation. Normally, close packed planes tend to grow parallel to the substrate surface.

Zone 1, Zone T and Zone 2 microstructures are associated with the preferred orientation of the growing crystallites and it is the development of texture in films which has interesting consequences when it comes to understanding the inter-relationship between coating microstructures and properties. For example, it has been reported that PVD coatings are significantly harder when tested parallel to their growth direction compared with values derived from the other two orthogonal directions, whereas in contrast, coatings that exhibit a fine equiaxed grain structure (Zone 3 as produced by CVD) do not show hardness anisotrophy effect [12]. This texture is strongly dependent on the growth parameters, among which the substrate temperature is probably the most important. However, parameters such as deposition rate, gas pressure, substrate bias, and substrate surface structure, also affect the texture.

1.4.7 PROPERTIES OF THE FILMS

Process parameters such as deposition rate, pressure and ion bombardment can cause considerable changes in the microstructure and properties of the plasma-deposited coatings. For example, an increasing film hardness with increasing substrate temperatue is commonly observed for refractory compounds in contrast to the behaviour of metal films.

Usually, Zone T structure have high hardness and strength but very little ductility. Densely packed Zone 1 structures have the same hardness but little lateral strength. With Zones 2 and 3, the sizes of the columnar and equixed grains increase with T/T_m, the hardness and strength of simple metals decrease. In contrast to the simple metals, ceramic compound films tend to have lower than bulk hardness when deposited at low T/T_m but approach bulk values at high T/T_m.

Process parameters also affects the electronic and optical properties of the plasma-deposited films. Structure of the films depends on deposition parameters which in turn determines the dielectric constant, resistivity, refractive index etc. of the deposits.

1.4.8 STOICHIOMETRY OF FILMS

Deposition parameters of the plasma system affects the stoichiometry of the compound films. To control film stoichiometry many conditions must be met. In a sputtering system, the target itself must be homogenous. This is especially a problem with some alloys and mixtures in which constituents segregate out in patches. In other system, more volatile components of the film may be sputtered out by ion bombardment affecting the film stoichiometry. In depositing BN films by plasma system, obtaining a stoichiometric film, which affects its physical and other properties, is a major problem by both PVD and CVD methods [13].

1.4.9 DEFECTS IN THE FILMS

Let us consider the 'defects' found in plasma deposited materials. The first one is classified as a "spit", or small droplet ejected from the source materials or target materials and is incorporated into the coatings. A schematic diagram is shown in Fig. 1.16a. The composition of the droplet is different from that of the coating in the case of an alloy and can therefore be the site of corrosion initiation. Hence corrosion attack can proceed down the boundary of the substrate or undermine the coating. The "spit" may also fall out, leaving a pinhole behind which can act as a stress concentrator. Both spits and foreign particles on the substrate surface induce preferential growth of the deposit in that area. This region of preferential growth is termed as a 'flake', which is shown schematically in Fig. 1.16b.

1.5 LOW PRESSURE RF PLASMA ASSISTED CHEMICAL VAPOUR DEPOSITION.

Plasma assisted CVD (PACVD) also known as plasma or glow discharge deposition, refers to a particular thin film deposition technique in which molecular gases are decomposed into condensible radicals species under several distinct processes prior to being incorporated in the film. Electron impact first dissociates the molecular precursor gas, creating neutral and, to a lesser extent, charged radicals. Subsequently, these species are transported in the gas phase to the substrate. Finally their unsaturated bonds allow the radicals to be absorbed at the surface of the growing film. This condensation process may involve a temperature activated chemical reaction.

The use of sub-atmospheric pressure (0.1-1.0 Torr) result in higher gas diffusivity (inversely proportional to pressure) and of the increase of the boundary layer across which the reactants must diffuse (the layer is inversely proportional to the Reynold's number) which in turn results in an increase of the gas-phase mass transfer of reactants by more than an order of magnitude as the pressure is lowered from its atmospheric value to 1 Torr or lower. Therefore the rate determining step at low pressures is the chemical reaction rate at the surface, so that a uniform temperature leads to excellent uniformity of film thickness and composition. CVD processes, including PACVD, form coatings which closely follow substrate topography; this is the major advantage over PVD, which is essentially limited to the line of sight from coating source to substrates.

Radio frequency (RF) discharges are most common, since the deposition of insulation films destroys the conduction path necessary for dc or very low frequency discharges. Microwave discharges are also less common because of the complication of using resonant cavity structures.

In PACVD system, the reactants are dissociated, excited, and partially ionized by energetic plasma electrons, which have temperatures of 5000 to 20000 K. Thus the main advantage of plasma CVD over thermal CVD is the ability to deposit films at relatively

Nodular
growth flaw

Columnar structure

(a)

(b)
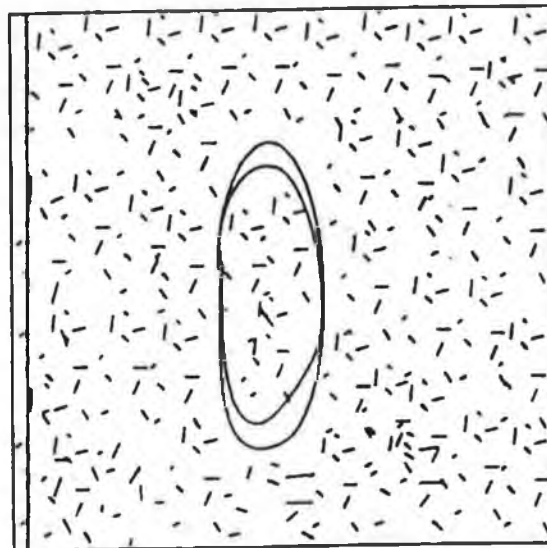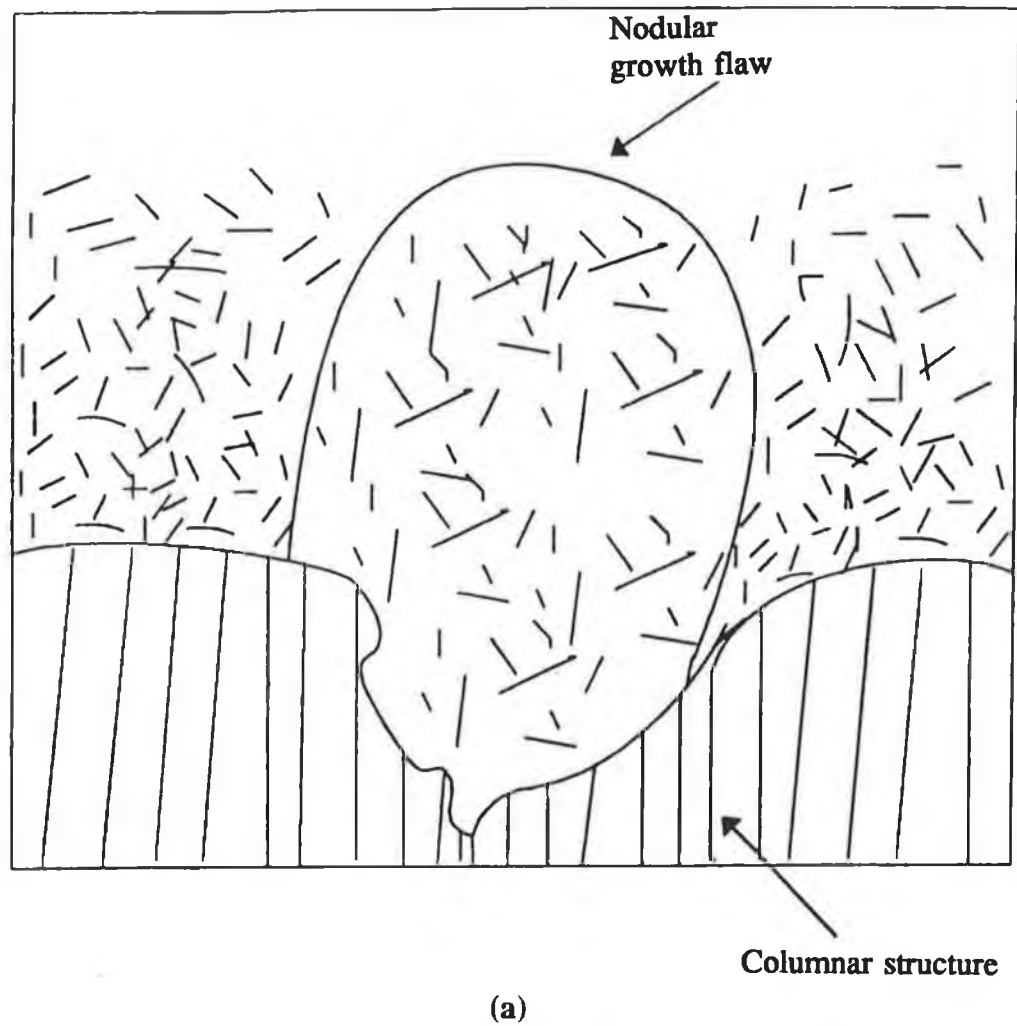
Fig. 1.16 : Schematic diagrams of (a) droplets (spit) defects, (b) flake defects
in the plasma coatings.

low substrate temperatures (typically less than 600°C vs more than 1000°C for CVD). Instead of requiring thermal energy, the energetic electrons in the plasma can activate almost any reactions among the reactants in the discharge. At the same time, the bulk of the gas and the substrates do not reach high temperatures because of the non-equilibrium nature of the glow discharge plasma.

Many of the gases or reactants used in PACVD are polyatomic molecules and many have low ionization potentials. Gases used for sputtering tend to be just the opposite, for example, argon. Also, the gas pressures are usually higher in PACVD (0.1 - 1 Torr) than in PVD (approximately 0.01 Torr), resulting in higher collision frequency and shorter mean free path for the electrons. As a result, electron energies are lower in PACVD and sensitive to the chemical nature of the gases and product gases, in the discharge.

For sputtering, the powered electrode is capacitively coupled and is purposely kept small so that a larger voltage develops across the sheath between the target and the plasma than at the sheath between the substrate and the plasma. On the other hand, most PACVD reactors have nearly equal powered and grounded surface areas. Therefore, large voltages develop across the sheath at the grounded surface. Floating, unpowered surfaces are closer to the plasma potential. In floating potential, where the substrate is generally 5-20 volts negative with respect to the enveloping plasma, the film forming surface is exposed to the effect of impacting low-energy electrons and ions which do not cause sputtering and/or implantation. Reactions such as recombination and excitation and de-excitation processes take place, which cause conversion of considerable quantities of energy into localized electronic and phonon states of the solid. This results in enhanced short-range diffusion, mixing and rearrangement of bonds and structural networks. Under a large negative bias of the substrate with respect to the surrounding plasma, the film forming surface is bombarded with energetic ions under impact energies in the order of 1000 eV or more, causing the generation of metastable high pressure structural phases (e.g. cBN films etc).

1.6   BACKGROUND OF THIS WORK

BN shows unique structural, mechanical, optical and electronic properties that make it ideal for a variety of industrial applications. The structure, properties and applications have been discussed elaborately in chapter 2 of this thesis. Here we will identify some of the fields where BN films have potentiality according to the salient features of the particular application.

Until recently, cBN was known and available exclusively as more or less bulky crystals: however the new techniques of low pressure synthesis now offer the possibilities of easily forming relatively extensive two dimensional thin films or sheets of this material.

1.6.1 RATIONALE FOR INVESTIGATING THIN FILMS OF BN

These thin film and coating technologies now employed to produce many types of materials can lead to important improvements of industrial applications in many fields. If integrated into the function of a system, the life time and more importantly technical performance of the resulting component, such as tools, electronic or optical device, etc, can be significantly increased. For many applications, the benefits obtained through thin films far exceed there manufacturing costs. Even if this costs are high, the resulting increase in performance of the components for their applications are justified by the highly competitive improvements in the products. Polycrystalline cubic boron nitride (PCBN) products currently have a well established market [14] . Their properties and performances under severe working conditions are generally considered to be outstanding and highly competitive in comparison to most ordinary wear resistant materials. The restrictions of PCBN material are as follows:

- Because of the complexity and inherent low volume of high pressure processing, the presently produced cutting tools are expensive.
- Fabrication of 3-D shapes is difficult and generally linked with time consuming, complex operations.
- Due to the high pressure technology applied, the products have definite upper size and shape limits, which cannot be exceeded without prohibitive cost increases .
- High pressure techniques are limited to certain source materials only, different varieties of sources are not feasible.
- cBN would enjoy much wider usage if it could be prepared in thin film form from a low pressure technology. The predicted advantages are :
    - a simple one step operation,
    - applicable simultaneously to a great number of substrates.
    - potential for evenly covering 3-D geometrical shapes, including the inner, surfaces of hollow products such as tubings, dies, nozzles, or even porous structures.
    - possible to use different varieties of source materials.
    - quality of thin films and process control may be possible (or have to be developed).
    - in the view of the rapid advances that have been made in very high speed digital and microwave integrated circuits development, there is a continuing need to deposit and characterize a variety of films (e.g. insulating, heat-spreading material, possible optical coating etc.) in order to meet the stringent requirements of the technology.
    - with the increasing restrictions imposed by legislation, the vacuum deposited processes are more environmentally friendly, i.e. free from pollution and safety hazards.

1.6.2 IDENTIFIED AREAS OF APPLICATION

After realizing the potentiality of BN thin films from low-pressure techniques, I will define now the specific requirements of some of the fields in which BN films could be

a candidate. In chapter 2 (and particularly in sections 2.8 and 2.9) the properties and potentialities of such films are described with respect to the requirements identified here.

For mechanical wear-resistant coatings, the requirements are superhardness (high Young's Modulus, rigidity etc.), high degree of chemical inertness and high thermal conductivity. In most of cases, polycrystallinity and lattice imperfections are acceptable. BN films exhibit those properties, moreover it shows excellent inertness to hot steel and resist oxidation up to high temperature.

The development of an improved and efficient thermal management system is becoming extremely important as density, integration, and performance level increase in VLSI devices. Recent trends toward micro-miniaturization and higher-and-higher packing densities have compounded the heat dissipation problems. The most desirable properties of heat spreading materials are high thermal conductivity and high electrical resistivity. High resistivity and high dielectric strength are required to reduce signal delays and to sustain a high electric field in high-frequency and high-power devices.

Halfway through 1990, Japan's Hitachi Ltd. surprised the semiconductor memory industry by announcing the first 64 M-bit dynamic RAM (DRAM) on a single silicon chip measuring 10 by 20 mm packing 140 million electronic components, shown in Fig. 1.17. A major problem they encounter was depositing a reliable dielectric film for the memory cell capacitor which had a large leakage current when the effective thickness was less than 3 nm. [15]. Oxide insulators are possibly unsuitable on III-V compound materials discussed in 2.8. The requirement on the dielectric is high dielectric constant and high band gap and very thin films, free of pin holes. BN films deposited by PACVD have the potentiality in this field pointed in section 2.8.

Ceramic materials are being used increasingly for machine elements in sliding or rolling contact. Monolithic ceramics continue to be of great interest for structural use in automobile and aerospace engines because of such properties as high-temperature strength, environmental resistance, and low density. However, the severity of operating conditions in engines has not favoured the use of bulk ceramics because of their high sensitivity microscopic flaws and catastrophic fracture behaviour. Thin ceramic films are widely used in a variety of applications in which materials in monolithic form are not suitable because of diverse and special requirements. Also, thin ceramic films serve a variety of purposes: providing resistance to abrasion, erosion, corrosion, wear, radiation damage, or high-temperature oxidation; reducing adhesion and friction; and providing lubrication [16]. BN is a promising ceramic material for those purposes.

Solid lubricants such as MoS_2 and WS_2 are currently used for vacuum instruments or for spacecraft [17]. Since the life expectancies of the most recently developed communication satellites are more than ten years under severe conditions, friction-reducing solid lubricants for communication satellite mechanism requiring long life and high reliability represent one important application BN films are one such candidate material mentioned in section 2.8.

X-ray lithography is a proximity lithographic technique to replicate patterns with feature dimensions of 0.5 µm or less, and is being investigated for the production of Ultra

41
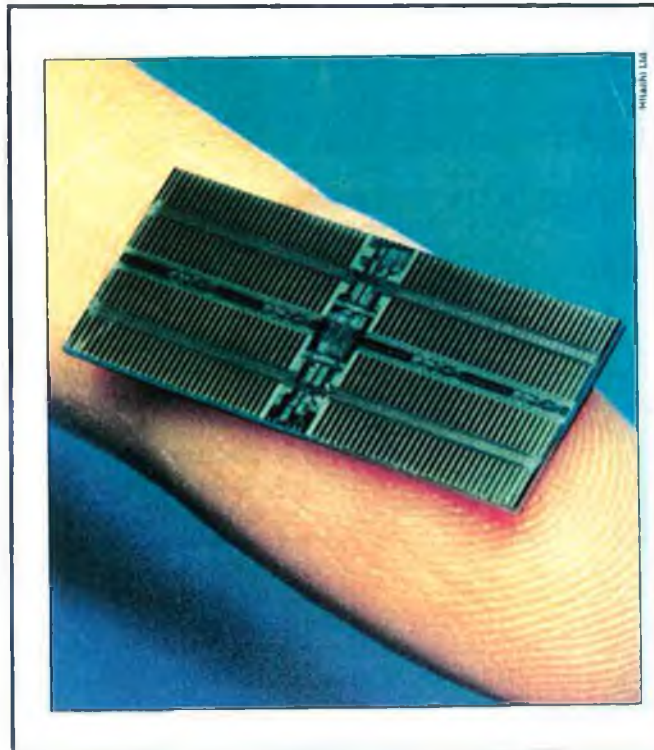
Fig. 1.17 :   The prototype 64 M-bit memory chip, made by Hitachi Ltd., holds
well over 100 components in its fingernail-size area.
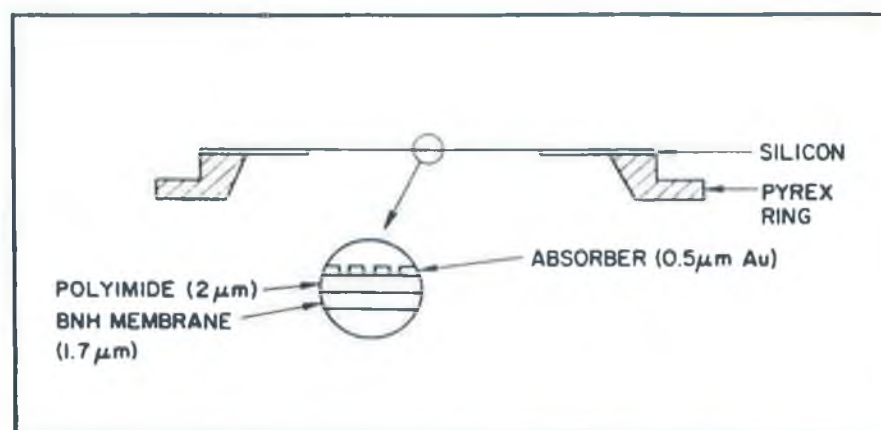
Fig. 1.18 :   X-ray lithography mask structure using BN thin films.

Large Scale Integrated circuit (ULSI) device. An x-ray mask consists of a thin film membrane which is held in tension by a supporting frame, and that supports the x-ray absorbed which makes up the circuit pattern. A cross section of a typical mask structure is shown in Fig. 1.18. The musk should be capable to meet the main requirements of the practical X-ray mask substrate, such as ease of formation technique, suitable mechanical properties, transparency and resistance to X-ray radiation, stability, optical transparency, etching resistivity and low defect density. BN films are most desirable for these requirements as showed in section 2.8.

1.7   OBJECTIVE OF THIS WORK

Realizing the substantial promise of cBN thin film and some of its superior preperties comparable to diamond, a low temperature plasma deposition of this film was investigated in this work.

The forecasted promise cBN holds and the success in growing diamond or diamond-like films revitalized the interest in cBN films worldwide for the last three years. At the commencement of this work, there was no report of growing cBN films by RF PACVD. Even in spite of a number of works with other techniques, there has been no report on the growth of cBN films from the vapour phase whose crystallinity is comparable to CVD diamond films. Very recently, some researchers from only Japan have reported the growth of pure cBN films with limited data on its properties.

In most of the cases, a high substrate temperature was employed (>500°C) in either PVD or CVD. Lowering of the deposition temperature is desirable for many of the substrate materials including steel and III-V compounds. The uniqueness of a plasma to create chemically reactive species at low temperature is due to the non-equilibrium nature of the plasma state whereby free atoms, radicals and molecules remain at only hundreds of degrees Kelvin. Compared to CVD or PVD, it is possible by PACVD to avoid heating and degradation of the substrate or the growing film.

Many of the source compounds employed have serious defects, including serious safety problems due to toxicity or highly inflammable nature of the source compounds. At the commencement of this work, there has been no report of growing BN films from non-toxic source materials either by PVD or CVD according to our knowledge.

This motivated us to grow cBN or mixed-phase BN films from a non-toxic source material by PACVD at low substrate temperatures.

The object of the present project is:

1) to design and develop mainly a radio-frequency (rf) Plasma Assisted Chemical Vapour Deposition apparatus capable of growing metastable cubic boron nitride (cBN) films.

2) to use a non-toxic source material in order to avoid commonly-used toxic boron source compounds. Borane-ammonia was used which is a non-toxic crystalline solid at room temperature but is volatile and can be decomposed by the electron energy. It is also an oxygen and carbon free compound which contains a stoichiometric ratio of boron and nitrogen.

3) to deposit cBN or mixed-phase BN films from this non-toxic material at low substrate temperature (around 350°C) using other activation sources, such as ion-bombardment during film deposition to form the high temperature, high pressure metastable phase and to remove the soft h-BN phase and thermal excitation of the source by hot filament.

The initial part of this thesis will concentrate on the details of BN material and their growth route including current status of the research. The subsequent chapter will deal with design and development both in the deposition equipment and in the method of deposition which allow desirable film formation at approximately 350°C. Structural and physical properties of the films will be investigated in chapter 4. Chapter 5 will concentrate on one of the primary goals of this work - insulating properties of the film and its potentiality in metal-insulator-semiconductor field-effect transistors (MISFETs). A short and long term outlook will be proposed in the final chapter.

CHAPTER 2

METASTABLE GROWTH

OF

BORON NITRIDE

2.1 INTRODUCTION

Scientists have long known that diamond is much more than a sparkling gemstone. Besides being the hardest material known to humanity, diamond scores high on almost all the categories of engineering properties such as thermal conductivity, electrical resistivity, dielectric constant and chemical inertness. The combination of these outstanding properties makes diamond very attractive as the engineering material of the last decade. The interest in diamond films was stimulated when Aisenberg and Chabot [18] reported the growth of an unusually hard phase of carbon using ion-beam deposition technique, subsequently confirmed by Spencer et al. [19]. The announcement of the growth of polycrystalline diamond films by Weissmantel from Eastern Europe [20], Spitsyn from Russia [21], Matsumoto from Japan [22] and Holland from U.K. [23] led to explosive growth of the field. In 1991, the total global revenues and research funding for companies and organizations involved in diamond coatings research, development, and commercia-lization was estimated to be $200 million with forcasted growth to more than $2 billion by the year 2000 [24].

Interest in diamond deposition and subsequent constraints diverted curiosity to growing cubic boron nitride (cBN) which is a sister-material to diamond. In general, boron nitride (BN) thin films have become the focus of a considerable amount of interest for the last three years because of their properties which closely relate to those of carbon. Boron and nitrogen being, in the periodic table, on each side of carbon, boron nitride is, thereby, iso-structural and iso-electronic with those of carbon: a hexagonal form similar to graphite and a cubic form analogous to diamond exist. They have somewhat similar properties to their carbon analogues e.g. hexagonal boron nitride (hBN) is soft while cBN has extreme hardness, chemical inertness, high resistivity, high thermal conductivity and transparency. With respect to diamond, cBN is a favourable superhard material that resists oxidation even at elevated temperatures up to about 1400 °C. BN exhibits an excellent inertness to hot steel surface under conditions where diamond is violently dissolved and therefore cannot be used. Thus, the low chemical reactivity of cBN with the iron group metals and its high thermostability, in particular in oxidizing conditions, make it a better candidate for surface engineered materials than diamond. The closeness of the properties of diamond and bulk cBN are given in Table 2.1.

Other than superior mechanical properties compared to diamond, cBN could be useful for electronic and optical coatings. The low atomic number combined with transparency and mechanical strength make BN potential for optical coating while the high resistivity, high dielectric strength and thermal conductivity along with the feasibility to dope the semiconducting cBN with both n and p type impurities makes cBN a strong competitor to diamond-based electronics.

Before going to preparation of BN films, the properties of bulk BN material will be explained for complete understanding.

Table 2.1   Comparison between the properties of Diamond and cBN

Properties	Diamond	cBN
Hardness (Kg mm^{-2})	7000-10000	7000-9000
Density (g cm^{-3})	3.51525	3.487
Crystal structure	cubic	cubic
Lattice constants (Å)	3.5678 (@ 298 K)	3.615 (@ 298 K)
Thermal conductivity (W cm^{-1} K^{-1})	20	13
Electrical resistivity (Ω-cm)	~10^{10}	10^{16}
Bulk modulus (GPa)	442	465
Thermal expansion coefficient (K^{-1})	1.7×10^{-6} (@ 293 K)	3.5×10^{-6} (@ 293 K)
Elastic modulii (c_{11} GPa)	1076 (@ 300 K)	712 (@ 300 K)
Refractive index	2.41 (@ 590 nm)	2.117 (@ 590 nm)
Static dielectric constant	5.66	7.1
Optical bandgap (eV)	5.48	6.4
Optical transmissivity	UV-VIS-IR	UV-VIS-IR
Oxidation in air (°C)	800	1600
Chemical reactivity	extremely low	extremely low

2.2   TYPES OF BN

Although there is an obvious difference between the B-N and C-C groupings because of the difference in the electronegativity between boron and nitrogen, BN is iso-electronic with carbon, and like carbon, its properties are highly dependent on the crystalline modifications under study.

BN is primarily found in hexagonal form, h-BN (also called g-BN or x-BN in some papers); cubic form, c-BN (also called zinc blend or z-BN mostly in Japan and sphalerite or β-BN in the CIS), and wurtzite type, w-BN (also called γ-BN) related to hexagonal diamond. Some derived varieties with a less-defined three-dimensional arrangement exist beside these phases: amorphous BN (a-BN), and turbostratic BN (t-BN).

2.3   CRYSTAL STRUCTURES OF BN

BN and other compounds formed by atoms from the first row of the Periodic Table behave differently than their counterparts in the later rows. The unusual properties are generally attributed to the very attractive nature of the electron-ion potentials of these atoms. BN exhibits solid phases similar to the phases of carbon but different from those of the other group IV or III-V solids. Hexagonal boron nitride (hBN) is the stable polymorph at standard temperature and pressure, whereas cubic boron nitride (cBN) is metastable. These two frequently occuring polymorphs are compared to the graphite and diamond forms of carbon, as stated before and to the wurtzite and zinc blende forms of zinc sulphide [25]. However, if carried too far, these analogies may actually hinder our understanding of the properties of this unique material.

Hexagonal BN has a layered structure, with B_3N_3 hexagons lying in the {0001} crystal plane and alternating B and N atoms aligned along the <0001> crystal axis [25]. Thus the hexagonal BN lattice, given in fig 2.1, consists of a stacking arrangement along the c-axis of planar layers of hexagonal rings, boron and nitrogen alternately occupying the corners. The stacking of the layers in h-BN, however, is different to that in ordinary graphite, with unlike atoms, in adjoining layers directly overlying each other while in graphite, only half of the carbon atoms in a layer are directly below the carbon atoms in the adjacent layer (fig. 2.2). The layer sequence in hBN is AaAa whereas that of graphite has an ABAB-stacking sequence [26]. The hBN structure consists of interlocking hexagonal boron and nitrogen sublattices displaced from each other by c/2. Boron and nitrogen atoms form six-membered rings with three boron atoms coordinated to nitrogen and three nitrogen atoms around each boron atom. The bimolecular unit cell (fig 2.3a) has the dimensions a=2.504 Å and c=6.661 Å. As well as three nitrogen atoms in the first coordination sphere each boron atom has six boron atoms as the next-nearest neighbours at a distance of 2.504 Å. The rings constitute planes piled up in the direction of the hexagonal axis with a boron atom over a nitrogen atom in the adjacent planes at a distance of 3.331 Å i.e. the B-N inter layer bond length is equal to 3.331 Å. The B-N intralayer bond length is equal to 1.446 Å. The space group of hexagonal modification is $P6_3/mmc$ (Schöenflies class: D_{6h}) [27]. The geometric relationship between the lattice constant a and a B_3N_3 hexagon is shown in fig 2.3b.

The bonding orbitals of both B and N atoms in h-BN are sp^2 hybrids, which may be thought of as arising from the resonance transfer of an electron from the N atom to the B atom, giving both atoms the electronic configuration of carbon in graphite. Thus the intralayer B-N bonds in h-BN are strongly covalent (sp^2) whereas the interlayer bonds are weak (van dar Waals type).

Hexagonal BN is highly anisotropic because of the large difference in B-N bond length parallel and perpendicular to the {0001} plane. Since the interlayer distance is fairly large, one can expect that in the non-crystalline state, these B-N bonds will break down, resulting in a two dimensional variant of the h-BN structure called turbostratic BN (t-BN) [25,27]. Turbostratic BN has a diffused structure of B and N networks which have 3-dimensional disorder and have lattice parameters somewhat longer than those of hBN.

47
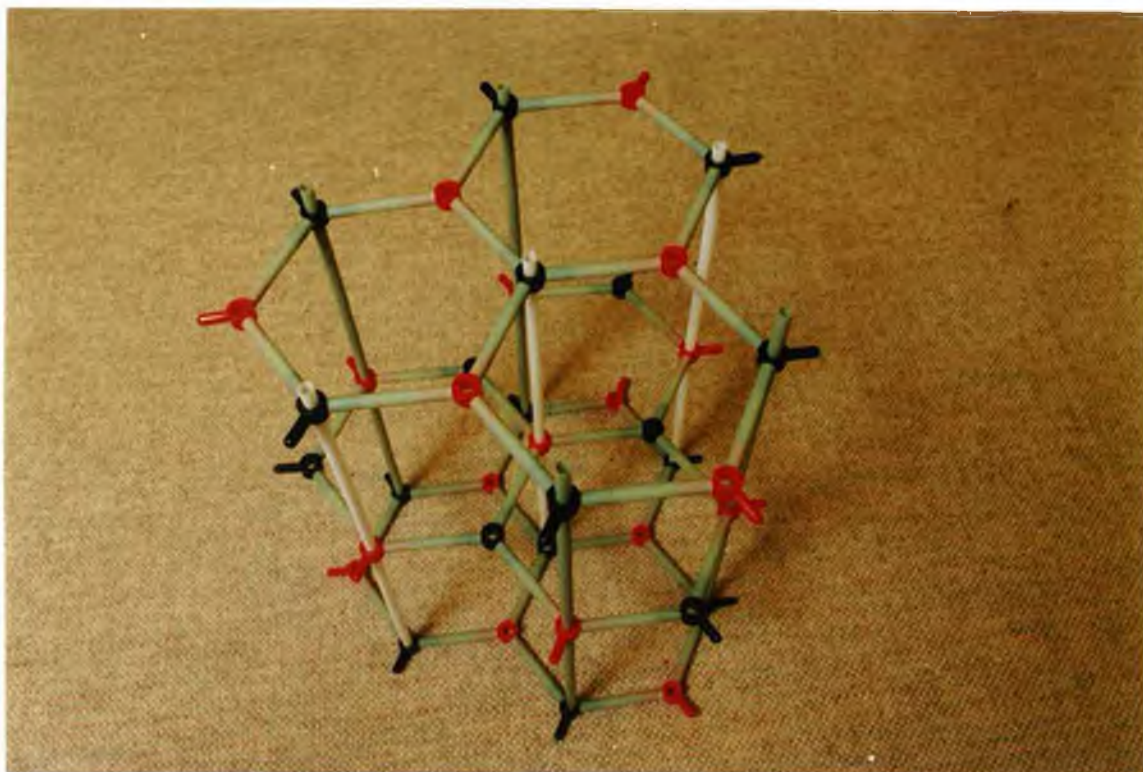
(a)
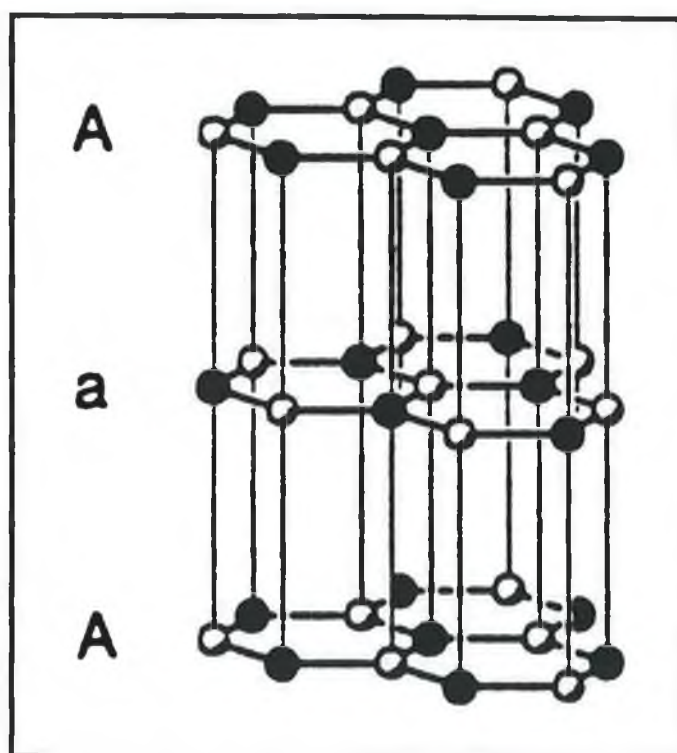
(b)

Fig. 2.1 : (a) photograph of crystal structure of hBN lattice, red for B and black for N atoms. (b) schematic diagram for crystal structure of hBN. ● for B and O for N atoms.
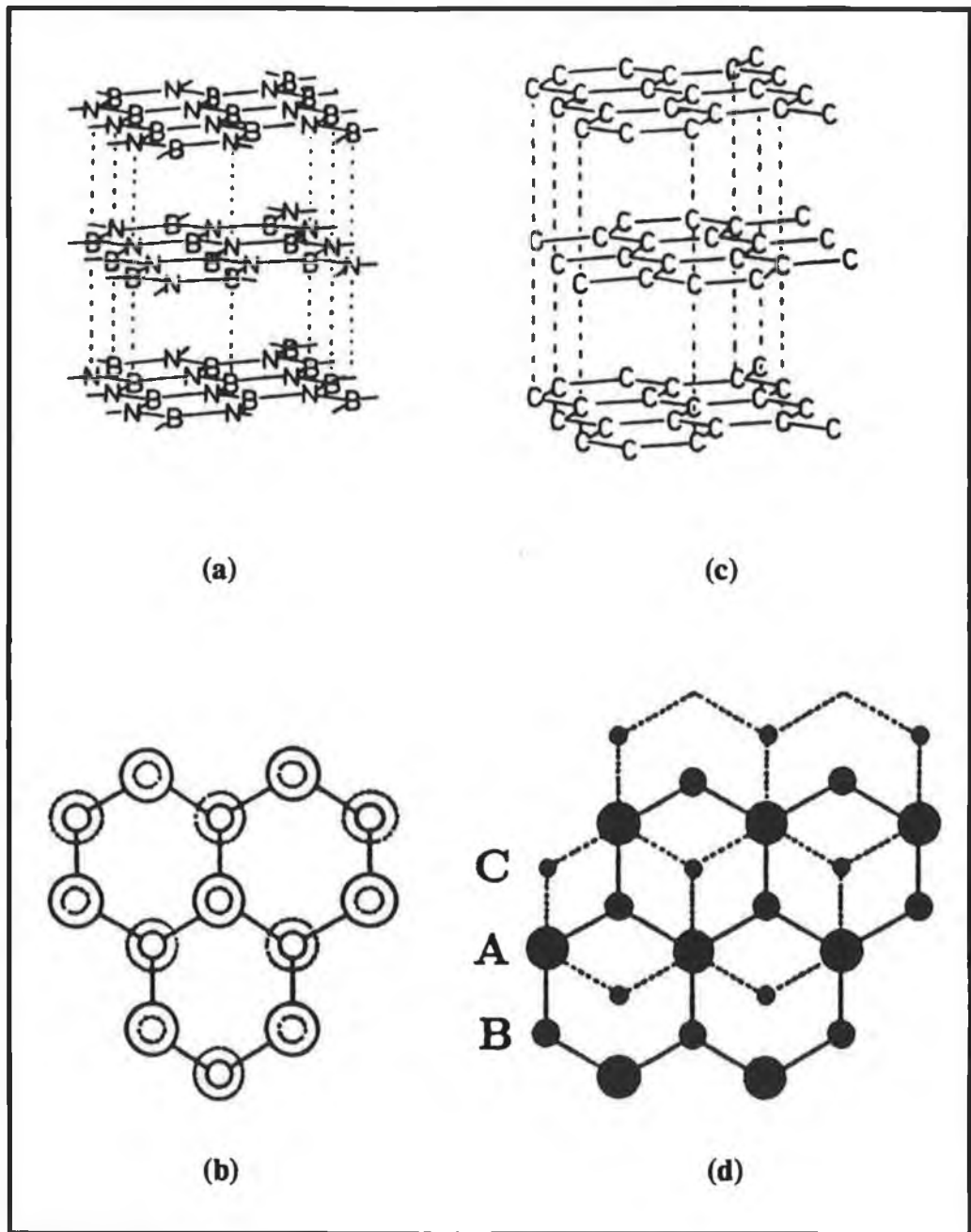
Fig. 2.2 : Comparison of hexagonal structures for BN and C. (a) crystal structure
of hBN. (b) (0001) surface structure of hBN. Boron and nitrogen atoms
are indicated by small and large circles, respectively. These atoms in the
top layer are indicated by solid circles and those in the bottom layer by
dashed circles. (c) crystal structure of graphite. (d) (0001) surface
structure of graphite. The top layer and the bottom layer are shown by
solid and dashed lines, respectively.
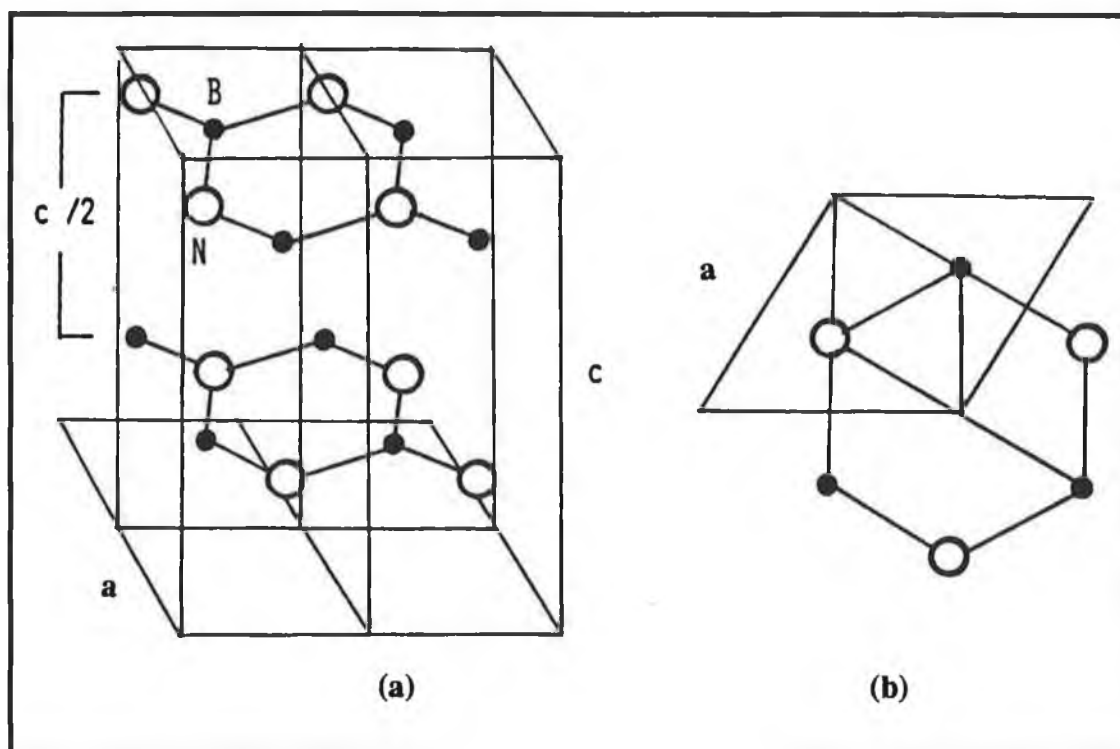
Fig. 2.3 : (a) the unit cell of hBN showing stacking of the B_3N_3 hexagons relative to the crystal axis. (b) a projection of the (0001) crystal plane showing a B_3N_3 hexagon relative to the lattice constant a.

The cBN structure consists of interlocking face-centered cubic sublattices displaced from one another along the cube body axis by a distance (a/4) <111> [25], where a=3.615 Å. It consists of cubically closest-packed layers of boron and nitrogen (fig. 2.4). Each boron atom is situated in the centre of a regular tetrahedron composed of four nitrogen atoms at its corner. Alternatively, each nitrogen atom is surrounded by four boron atoms at the corners of a tetrahedron. Atomic nearest neighbours in the tetrahedron and hexagonal structure are shown in figure 2.5. The B-N bond length in the c-BN structure is equal to 1.565 Å or $3^{1/2}$ (a/4). The unit cell of cBN is shown in fig 2.6. The bonding orbitals in c-BN are the tetrahedrally directed sp^3 hybrids as in cubic diamond and B-N bonds are strongly covalent. Due to this structural similarity, c-BN shares similar properties with diamond. The space group of cBN is $F4_3m$ (Schöenflies class: T_d) [27].

The interplanar spacing of hBN could be reduced by compression at high pressure, with a deformation of the hexagons leading to a hybridization change from sp^2 to sp^3 . Each (001) planar layer of the lattice splits into two planes, one contains boron atoms, and the other nitrogen atoms along the c-axis. The AaAa layer sequence is replaced by the abab sequence (alternate boron and nitrogen layers; a for boron layers and b for nitrogen
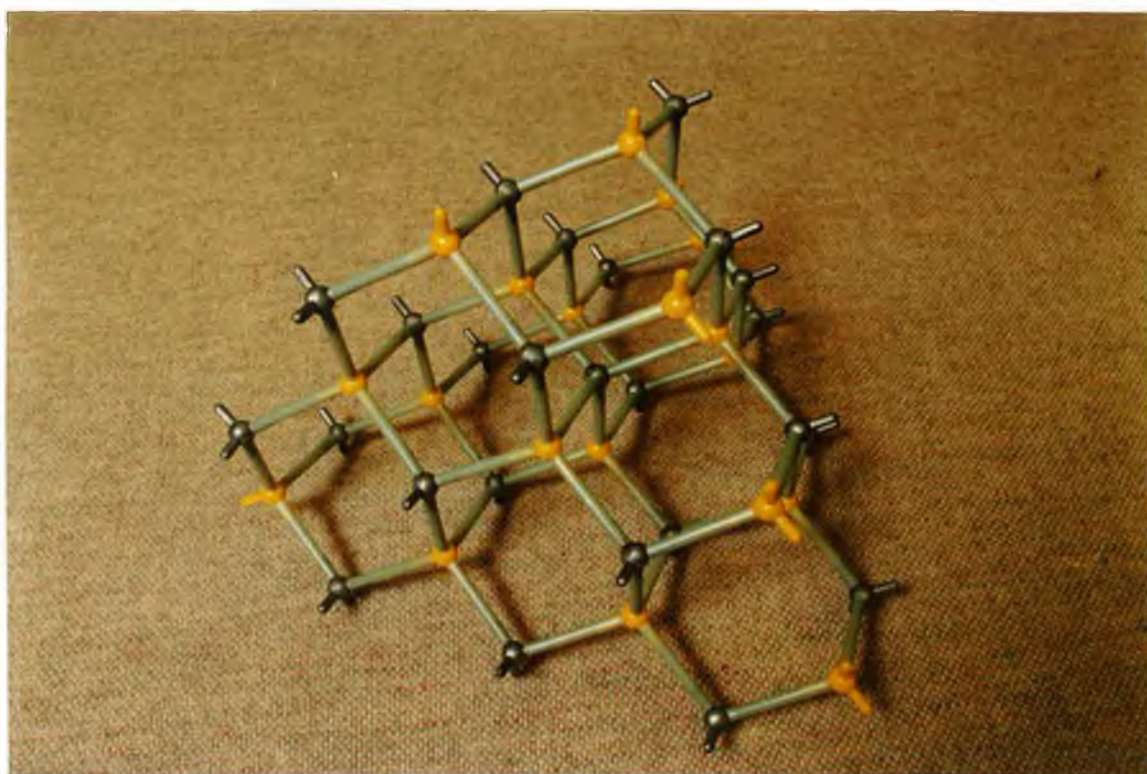
(a)
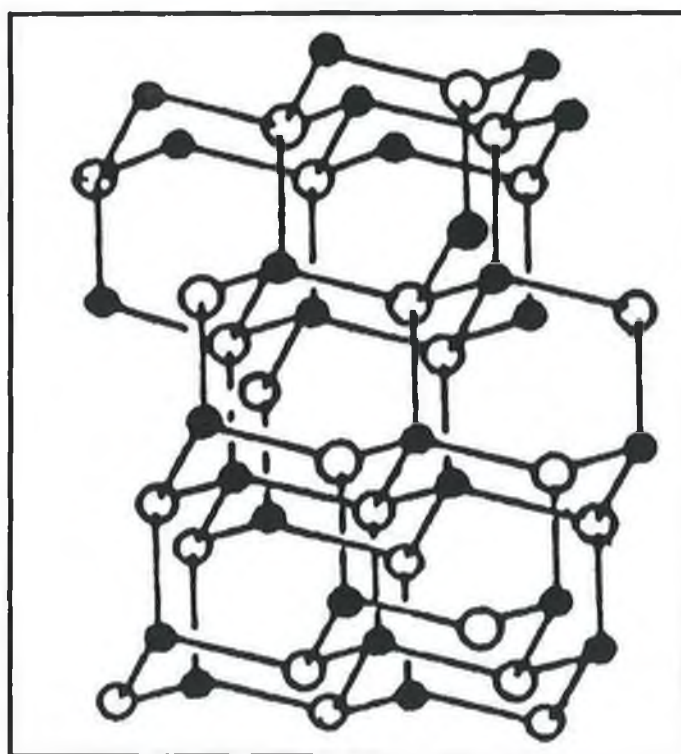
(b)

Fig. 2.4 : (a) photograph of crystal structure of cBN lattice, grey for B and yellow for N atoms. (b) schematic diagram for crystal structure of cBN. ● for B and O for N atoms.
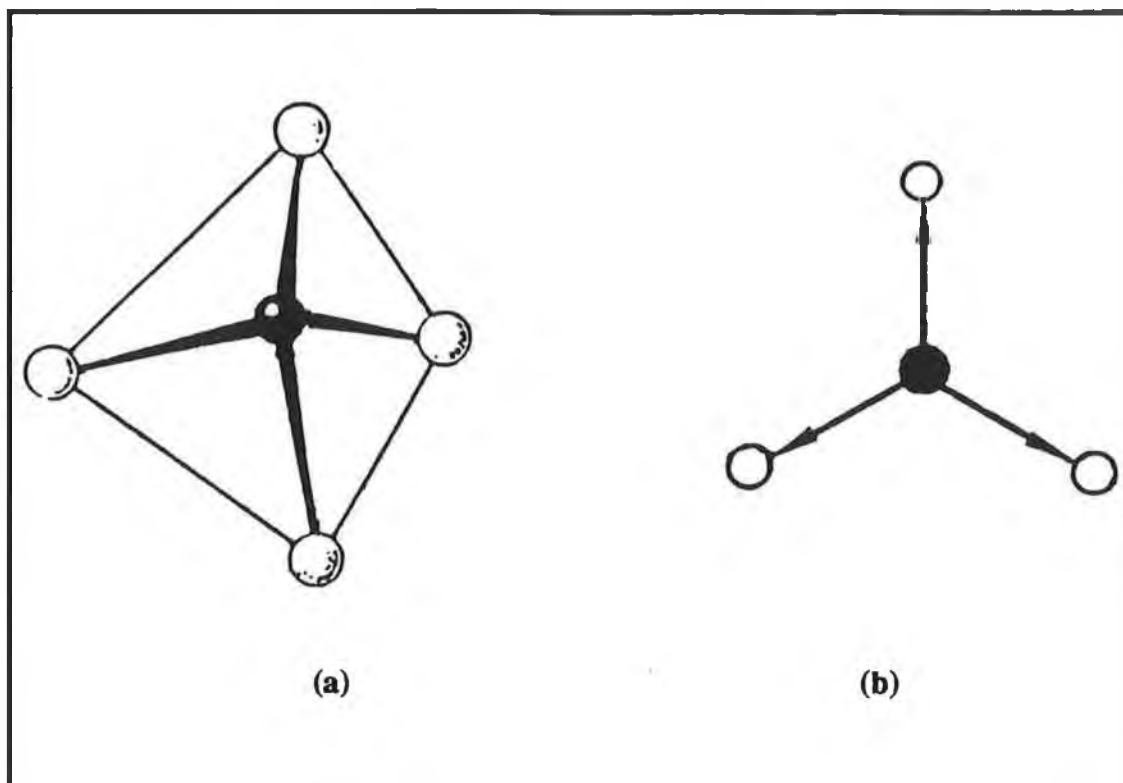
Fig. 2.5 : Atomic nearest neighbours in the (a) tetrahedron and (b) hexagonal structure.
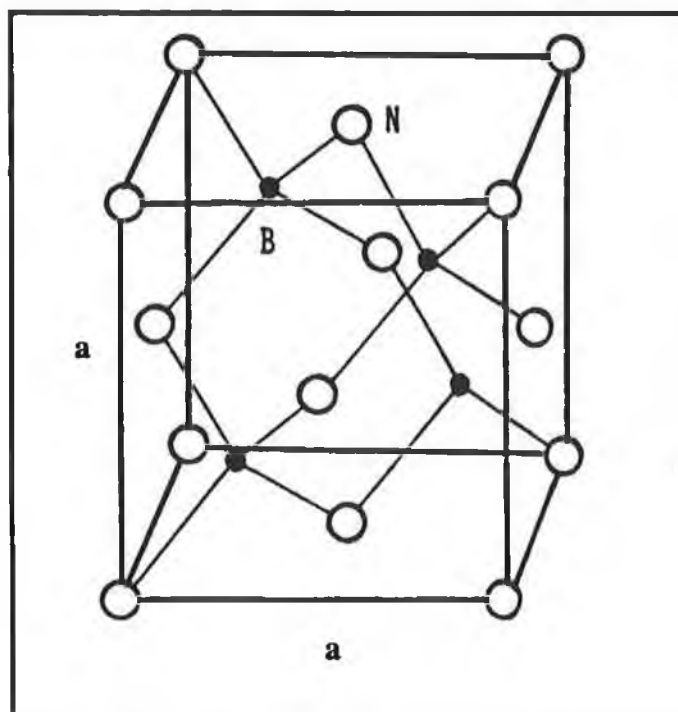
Fig. 2.6 : The cubic boron nitride unit cell. ● for B and O for N atoms.

layers) of the wurtzite lattice (fig 2.7) [28]. As in the cubic modification, boron and nitrogen atoms exhibit tetrahedral coordination in wurzite structure. This modification has a=2.56 Å and c=4.212 Å. This denser form of BN are analogous to hexagonal diamond, however the wurzite form of BN is described as being not thermodynamically stable. The space group is $P6_3mc$ (Schöenflies class: C_{6v}) [27]. The crystal structure data for BN is given in Table 2.2.

Table 2.2   Crystal structure data of BN [28-30]

	Cubic	Wurtzite	Hexagonal
Lattice constant (Å)	a= 3.615	a= 2.56 c= 4.212	a= 2.504 c= 6.661
Volume/molecule (Å³)	11.810	11.692	17.940
Density (g/cm³)	3.487	3.522	2.28
Space group	$F4_3m$ (T_d)	$P6_3mc$ (C_{6v})	$P6_3/mmc$ (D_{6h})
B-N distance (Å)	1.565	1.555	1.446 intralayer 3.330 interlayer
B-B or N-N distance (Å)	2.56	2.56	2.504 intralayer

Hexagonal structure can also exist with three-layered stacking sequence. This three layered form is similar to rhombohedral graphite; both have an ABC... stacking sequence (Fig. 2.8). Described in the hexagonal system the structure consists of (001) planes with the same atomic coordination in this plane as in the hexagonal modification, but the sequence of planes along the c-axis is different. The rhombohedral (r-BN) structure of space group R3m (Schöenflies class: C_{6v}) has lattice parameters a=2.504 Å and c=10.01 Å. The interatomic distances are the same in both modifications. It is structurally similar to rhombohedral β-graphite with sp² hybridized covalent bonds.

Amorphous BN consists of a random network of tetrahedrally coordinated atoms.

2.4   TRANSITION FROM THE LAYERED PHASES TO THE FOUR-FOLD PHASES

Cubic BN and hexagonal BN are both thermodynamically stable allotropes of BN, but only cBN is stable at high pressure and high temperature (HPHT), as shown in fig. 2.9. As mentioned, the most common form of layered BN at ambient pressure and temperature is the hexagonal phase(hBN). The rhombohedral layered form (rBN) can also be formed

(a)
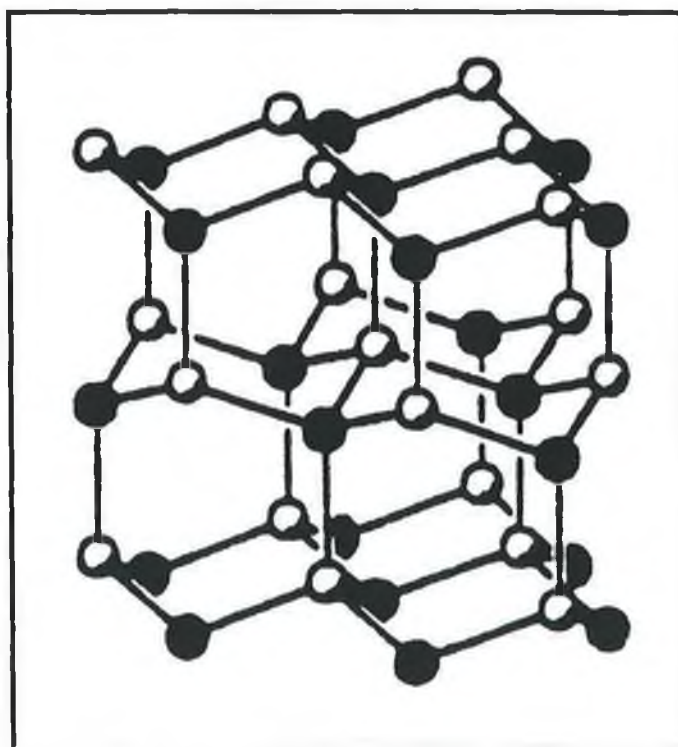
(b)

Fig. 2.7 : (a) Photograph of crystal structure of wBN lattice, black or red for B
and yellow for N atoms. (b) Schematic diagram for crystal structure of
hBN. ● for B and O for N atoms.
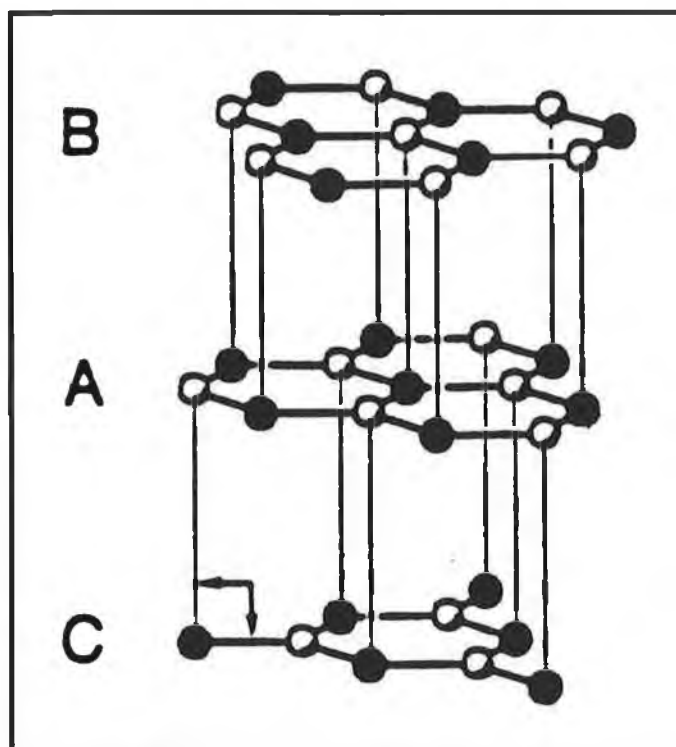
Fig. 2.8 : Schematic diagram for crystal structure of rBN. ● for B and O for N atoms.

at ambient pressure. While both dense phases, wBN and cBN, can be synthesized from hBN, the formation of wBN has been shown to require a lower temperature than the formation of cBN, mainly because of the closer structural relation between wBN and hBN than between cBN and hBN. Phase transformations between the three modifications in the thermodynamically stable region is shown in fig. 2.10.

However, under shock compression only wBN is produced from hBN and only cBN is produced from rBN which indicates that the initial stacking sequence plays an important role in the transformations. The geometrical relationships between the low density layered structures and the high density four-fold coordinated structures are shown in figs. 2.1, 2.4, 2.7 and 2.8.

Subsequently, molten-metal catalysts were developed and used for obtaining cBN from hBN at the industrial scale. Catalysts are added to h-BN in order to decrease the high activation energy barriers.

The synthesis procedure for the dense phases are relatively well established by these above methods and their production depends on the starting materials and
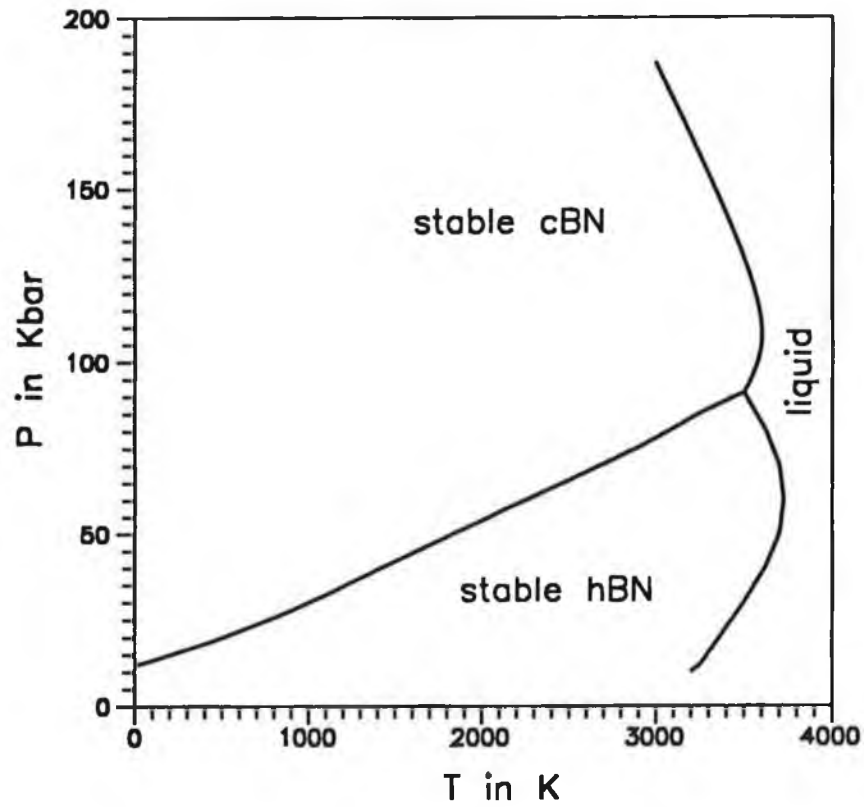
Fig. 2.9: The phase diagram of boron nitride.
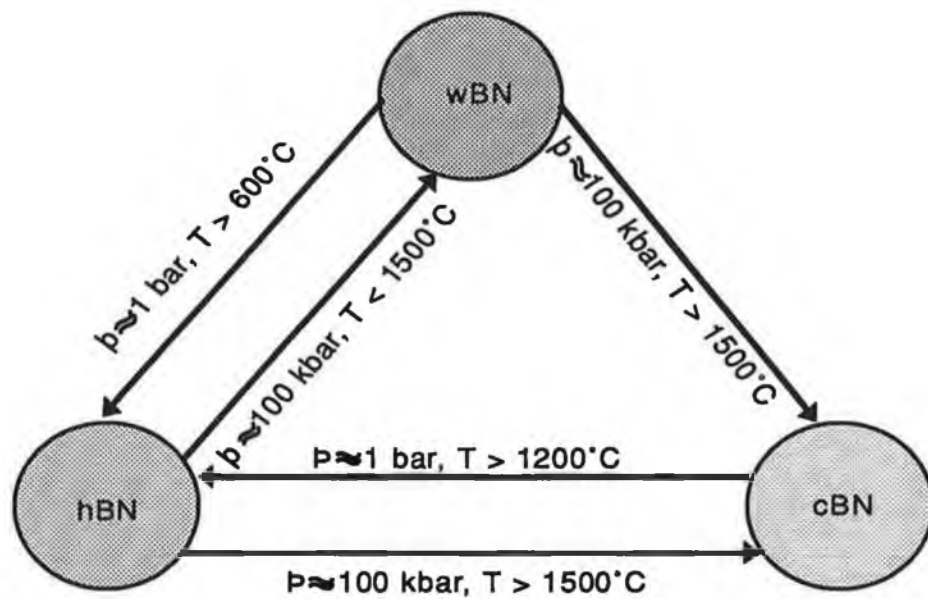
Fig. 2.10: BN phase transformations between the three modifications.

experimental conditions involved, such as pressure, temperature and presence of catalysts. An excellent review can be found in ref. [28]. Growth of the denser phase of BN under HPHT with or without catalysts is out of the scope of the present study, but the phenomenon involved in those transformation will be used to determine the growth mechanism of the more stable phases of BN in the metastable conditions in Chapter 6.

2.4.1. PROCESS MECHANISM AND STABLE ALLOTROPES

Though the dense phases are metastable under standard conditions, once formed by HPHT condition or shock compression, cBN is kinetically stable in a fashion similar to diamond. As mentioned, besides structural similarities, BN and C also manifests similarities in their electronic properties. Because of their similarities, we will often draw comparison between BN and C.

Quantitatively, the BN system requires smaller activation energies than the graphite → diamond transitions. The activation energy barrier heights for the transitions in BN are approximately 0.39 eV/pair while they are 0.66 eV/pair in the C system [26]. The smaller barrier is consistent with the fact that BN is less covalent and more ionic than C. The barrier height is mainly caused by the kinetic energy increase of the overlapping charges in the inter layer region and the Coulomb repulsion between the inplane σ bond charge and the inter layer charge. Both the kinetic energy and the Coulomb repulsion are weaker in BN because the bond charge is smaller in BN compared to C.

It was claimed [26] that cBN could be more stable than the layered phases. This trend can be rationalized as follows. The low coordination layered structure is usually preferred by materials which are capable of forming strong covalent bond. For example, carbon forms layered structures while silicon does not. The cohesive energy depends on both the strength and the number of bonds. However, strong bonds are usually associated with short bond distances which can accommodate only a few nearest neighbours because of pauli exclusion and electrostatic repulsion between bond charges, i.e. there is a trade off between the strength and the number of bonds. Even in the case of carbon, graphite is only slightly more stable than diamond, it is conceivable that the order of stability between the layered and four-fold phases would be reversed for the less covalent material such as BN.

In the static compression experiments, both wBN and cBN are produced from hBN [28], but only wBN is produced from hBN and only cBN is produced from rBN under shock compression [26]. This can be attributed to the fact that the hBN → cBN and the rBN → wBN transitions would have required a rearrangement of the BN layers. It is reasonable to expect that the activation barrier is higher and the reaction time is longer for these transitions. Under shock compression, there is not enough time for the kinetics for those transitions. Thus at low temperature or short reaction time, the product is wBN rather than cBN, because there is not enough kinetic energy to overcome the higher hBN → cBN barrier. However at higher temperature the hBN → cBN barrier can be overcome and the product is mainly cBN because it is more stable.

2.5   GROWTH UNDER METASTABLE CONDITIONS

Instead of synthesizing cBN in a thermodynamically stable regime, many scientists followed a different, unconventional route for producing cBN. This operating regime where hBN is thermodynamically stable and cBN is, in fact, metastable is characterized by low temperature (⟨1100°C) and low pressure (atmospheric to sub-atmospheric pressure). This process is generally termed as vapour deposition and using different type of sources (B containing gaseous feed or evaporation of powder or liquid source) and a reactive gas, products are grown as thin films on different substrates.

Well-crystallized diamond has been achieved by numerous vapour-deposition methods [31,32] and an increasing focus on the synthesis of well-crystallized cBN films has been seen in the past three years.

In spite of the substantial promise this materials hold, and the resources that have been committed worldwide, numerous experimental and theoretical problems remain. Much of this uncertainty is due to the metastability of diamond and cBN.

2.5.1   PHASES IN THIN FILMS

The individual microstructure of different phases of BN are discussed in section 2.2. Much work has been done to synthesize BN in thin film form. However it is difficult to obtain at will a specific phase. When it is deposited as a thin film by vapour deposition techniques of section 2.5, BN has the potential to form material with the hBN or cBN structures or possibly the wurtzite structure; or alternatively an amorphous structure having the corresponding local structure of these materials i.e. coplanar sp^2 or tetrahedral sp^3 bonding. Most of the films reported in the literature contain small regions of sp^3-bonded material embedded in a large matrix of sp^2-bonded material with no long range crystallographic order.

Thin film specimens rarely consist of parallel sided single crystals: usually they are a collection of small crystals with a distribution of size and orientation. Alternatively they show an amorphous microstructure without true crystalline region. Most of the applications of diamond and cBN have in common the need not only to grow large area single crystal or polycrystalline material, but to grow the material with a high degree of crystal perfection. Though many of the early reports of vapour phase cBN synthesis using either PVD or CVD, met with scepticism, the growth of well crystallized cBN has been reported very recently from mainly the researchers in Japan [33-39]. Thus an accurate assessment requires a much better understanding of the applicable chemistry and physics of the metastable condition.

2.5.2 PROCESS MECHANISMS AND METASTABILITY

Of interest then is the question of whether or not there is, in theory or in practice, a limit on the degree of crystal perfection possible, and this issue is complicated in the case of diamond and cBN by their well-known metastability relative to layered-phases (graphite or hBN respectively). The complication is of course that "annealing" techniques (i.e. zone refinement) used to improve crystal quality with stable phases become problematic with metastable phases, where transformation to the stable phase must be prevented while supplying sufficient energy for the migration of impurities and the elimination of defects. Hence, it becomes important to achieve the highest possible crystal perfection in synthesis, and this is, in practice, limited by the need also to achieve realistic deposition rates.

Diamond and cBN deposition and, parenthetically, the deposition of many other thin film materials, appears to contradict thermodynamic analysis as the expected or stable phase is often said to be graphite or hBN and not well crystallized diamond or cBN. It should be noted, however, that conventional (or equilibrium) thermodynamics sometimes called thermostatics, as usually understood is a special case where two assumptions are generally made. The first of these is the assumption of complete reversibility or equilibrium. Obviously, this is violated in all real material synthesis (including all vapour deposition) as it requires that the deposition or reaction rate be identically zero. The second of these assumptions is that the state of subdivision, i.e., the presence of surface and interfaces is neglected. In vapour deposited thin film and layers this means that, in calculating the free energy of the material, it is assumed that surface or interfacial contributions are negligible. In most cases, this leads to no particular difficulty and greatly simplifies the analysis; however, it can readily be appreciated that, in the preparation of very thin films ($\sim$10 Å) or superlattices and nanocomposites, this can lead to important errors in deciding which phase or phases might lead to the lowest free energy configurations. This is particularly true if one assumes, as might be reasonable for highly refractory materials such as diamond and cBN, that phase control is established at the growth surface and not in the bulk, i.e., the bulk transformation and reorganization can be ignored.

In the analysis of deposition processes, the more applicable theory is that of non-equilibrium, or irreversible thermodynamics, which reduce to the more familiar theory on the assumption of equilibrium. In this approach, the second law assumes primary importance, and it becomes a fundamental postulate, consistent with the second law, that all real processes are characterized by an entropy increase or the production of entropy in a local as well as a global sense. It was demonstrated that if the principle of microscopic reversibility [40] applies, any process with constant boundary conditions must tend to a steady state, a state in which the entropy production required by the second law is minimized.

Steady-state processes are characterized by constant thermodynamic potential and properties, i.e., there is no change with time of temperature, pressure, specific enthalpy or entropy, deposition rate, etc. Furthermore, if microscopic reversibility is assumed, then local equilibrium can also be assumed. The assumption of microscopic reversibility (or local equilibrium) ensures that various phenomenological laws, particularly those

59

governing transport, will hold e.g, Fick's law of diffusion, the Fourier heat theorem etc. As local entropy production is minimised, crystal "perfection" is maximized, and the maintenance of steady-state is important to the uniform and stable growth of relatively defect free materials. This offers a means of analyzing those systems where local equilibrium can be assumed and also provides a theoretical foundation for discriminating between different vapour-phase deposition techniques. The terms CVD and PVD are often used to characterize different vapour-phase methods, depending on whether the chemical reactions or purely physical phenomena are believed important to the deposition process. A more general thermodynamic differentiation can also be made on the basis of whether or not local equilibrium exists, with those methods, where it does exist being CVD, and those where it does not called PVD.

The phrases "far from equilibrium" or "near equilibrium" are necessarily vague, unless a specific experiment is defined for which calculations can be made. The fundamental condition for local equilibrium is that the variation in a state property, e.g., temperature, T, pressure, P or the chemical potential of the ith reactant of the product μ, must be small relative to its average value over the same volume [40]. That is

$$\frac{\delta P}{\langle P \rangle} \ll 1 \qquad (2.1)$$

sometimes described as equivalent to the approximation that $e^x = 1 + x$, where x is the ratio in Equ. (2.1).

Fortunately, an explicit expression for Eq. (2.1) exists for gas-phase process [40] and experimental parameters can be used to test this condition. For dilute gases, i.e., gas pressures of the order of an atmosphere or less;

$$\frac{\delta P}{\langle P \rangle} = \frac{\lambda |\nabla P|}{\langle P \rangle} \qquad (2.2)$$

where λ is the mean free path, ∇P is the gradient of P, and $\langle P \rangle$ is its average value, all in the region of interest. For a local temperature of 1273 K and a pressure of 50 Torr (0.0658 atm), the mean free path can be calculated from the kinetic theory of gases by the relation

$$\lambda = kT(p\pi\sigma^2\sqrt{2})^{-1} \qquad (2.3)$$

where σ is the effective molecular diameter and p is the pressure.

For H_2, λ equals 7.85×10^{-4} cm. For the thermal gradient inherent to the hot-filament CVD method, an upper limit for ∇T near the growth surface can be estimated by

$$\nabla T = (T_f - T_s)/d \qquad (2.4)$$

where filament of T_f=2273 K is located ~0.5 cm from a substrate of T_s=1273 K in a typical hot-filament CVD method. For the above, ∇T=2000 K/cm with T=1273 K giving a value for the ratio in Equ. (2.1) of $\approx 10^{-3}$ or much less than unity required.

Because the mean free path in gases at pressure greater than ~1 Torr is small, local equilibrium, along with microscopic reversibility for the relevant reactions, can be assumed. Thus local thermodynamic potentials can be defined and the principles of linear non-equilibrium thermodynamics applied to a properly defined local volume element, even in a system which, macroscopically, may be quite far from equilibrium. Parenthetically, this also gives rise to a thermodynamic differentiation between those processes often labelled PVD and those commonly referred to as CVD. For PVD processes carried out at low pressure where λ is very large or $|\nabla T| \approx T/\lambda$, local equilibrium (or microscopic reversibility) can no longer be assumed and analysis requires the use of variational techniques and the more general theory of non-linear equilibrium thermodynamics.

With the assumption that the local system of interest is the surface of the solid and its interactions with the gas phase species, and the processes occuring in the bulk can be ignored, it is argued in the case of diamond deposition that effective control of whether diamond or some other form of solid carbon is formed is primarily a function of growth temperature and the partial pressure of atomic hydrogen. In the case of cBN , this depends mainly on growth temperature, activation energy provided and ion bombardment on the substrate.

This suggests that if bulk organization of the solid does not occur or is inhibited, then phase control can be established and maintained at the growth surface. Furthermore, this approach argues that a detailed atomic model is not a prerequisite for deciding how to use low pressure vapour-phase techniques to deposit well-crystallized refractory phases, even though these phases might be metastable. This has obvious implications for the directions that might be pursued to prepare phases other than diamond and also argues that the preparation of relatively defect-free diamond and cBN for many electronic, electro-optical, and optical applications is not thermodynamically inconsistent. Thus, the principal challenge, as with many stable phase, is experimental in nature and there is no reason to suppose any fundamental theoretical limitations on either the amount or the quality of diamond or cBN that might be grown using vapour phase methods [41].

2.6   ENGINEERING PROPERTIES OF cBN.

In recent years, the properties of boron nitrides have been studied in great detail, both theoretically and experimentally. BN shows unique structural, mechanical, optical and electronic properties that make it ideal for a variety of industrial applications.

But the properties greatly depends on the crystal structure of BN and in some cases, vary widely from one phase to other phase. Other than the difference in properties in bulk BN, the properties again vary from bulk BN to the thin film BN grown from

vapour phase. Before going to vapour phase deposited thin film of BN, the selected properties will be summarized for the cubic and hexagonal phases of BN, as they are the two principal forms found in nature.

2.6.1 *PROPERTIES OF cBN*

Table 2.3 gives data on both the physical and the chemical properties of cBN.

As shown in Table 2.1, cBN has similar properties like diamond. Some of the fascinating properties of cBN, such as extreme hardness, high melting point, low dielectric constant, large band gap, etc, have many applications in modern microelectronic devices and its usefulness as a protective coating material. BN emerged as a very strong competitor with diamond and SiC as far as high-temperature applications are concerned.

2.6.1.1 Electronic properties of cBN

Cubic BN, the lightest of the III-V semiconductors with the zinc-blend structure, has the largest band gap.

This material is an indirect-gap insulator, in which the valence band maximum occurs at Γ (Brillouin zone centre) and the conduction band minimum is at X (the point of the first Brillouin zone surface at 4/mmm as symmetry). These valence and conduction bands are formed from the outermost filled 2s and partially filled 2p electrons shells of boron and nitrogen atoms [28]. The charge density is similar to those of typical III-V semiconducting materials and is strongly localized near the region close to the nitrogen atom [29]. With increasing pressure, the gap of cBN increases as in the case of diamond [26]. Table 2.4 is a summary of the principal properties of cBN and for case of comparison and to set the context of electrical/electronic applications of cBN, it also provides representative data for diamond, SiC, GaAs and silicon semiconductors.

2.6.2 *PROPERTIES OF hBN*

As discussed, the structure of h-BN is related to that of graphite, however, the physical properties of h-BN and graphite are not similar since hBN is non-absorbing at visible wavelengths and is electrically insulating, whereas graphite is almost metallic in properties. In fact, h-BN has a direct gap of 5.2 eV which makes it a good insulator. One of the main difference with cBN is, hBN is soft whereas cBN has extreme hardness. In many cases, hBN is itself a competitor with cBN. Table 2.5 gives physical and chemical properties of hBN while the electronic properties can be compared from Table 2.4.

TABLE 2.3: Chemical and physical properties of cBN [28,30,42]

Property	Value
Crystallographic	
Crystal structure	Cubic, Zinc blend Space group, $F4_3m$ (2 atoms $cell^{-1}$)
Lattice constant	$a = 3.615 \pm 0.001$ Å
B-B or N-N distance	2.56 Å
Ionic BN distance	1.565 Å
Density	3.487 ± 0.003 gcm^{-3}
Crystal habit	{111} first-order tetrahedra {111} second-order tetrahedra (truncated corner of the {111} form) Octahedra (sometimes truncated) flat platelets twinned on {111} irregular blocky forms.
Cleavage planes	six (110) cleavage planes.
Mechanical	
Hardness	7000-9000 kg mm^{-2}
Compressive strength	4.15-5.33 GPa
Compressibility	$(0.24\text{-}0.37) \times 10^{-11}$ m^2 N^{-1}
Optical and Electrical	
Colour	Some varieties of yellow (amber, honey), orange, black (B-doped), brown, deep blue (Be-doped)
Electrical resistivity	p-type (Be-doped, 10^2-10^4 Ω-cm, activation energy for conduction of 0.19-0.23 eV. n-type (B, S, Si doped) 10^3-10^7 Ω-cm, activation energy for conduction of 0.05-0.41 eV. Undoped, 10^{10}-10^{14} Ω-cm (298K),10^7 Ω-cm (773K).

Thermal

Thermal conductivity	13 W cm^{-1} K^{-1}
Debye temperature	1700 K
Melting point	>2973 °C
Linear thermal expansion	3.5x10^{-6} °C^{-1} (0-400°C)
	4.8x10^{-6} K^{-1} (700K)
	5.6x10^{-6} K^{-1} (1170K)
	5.8x10^{-6} K^{-1} (1430K)

Thermal stability

In air, oxygen stable to 1570-1670 K (B_2O_3 layer produced by slight oxidation protects against further oxidation).
No conversion to hBN at 1670 K
some conversion in nitrogen at 1798 K, 12h and under vacuum (10^{-7} Torr) between 1820 and 1870K.

Cubic to hexagonal transformation

P(Kbar) = 0.03 T (K) -10.3

Chemical Reactivity

Ni in 10^{-4} Torr vacuum; wets cBN at 1630 K Fe, Ni, Co in Ar: reaction with cBN starts at 1620-1670 K.
Al in 10^{-5} Torr vacuum, 1630K: wetting and reaction with cBN.
Fe and/or Ni based alloys containing Al: reaction with cBN at 1520-1570K.
Mo in 10^{-4} Torr vacuum: reaction with cBN at 1610K.
Acid and bases insoluble in usual acids
Soluble in molten alkalis: LiOH, NaOH, KOH, NaOH-Na_2CO_3 (used as etchants)
Soluble in molten nitrides: Li_3N, Mg_3N_2, Sr_3N_2, Ba_3N_2, Li_3BN_2
Soluble in ammonium borate at high pressure.

Thermodynamic

Enthalpy of formation	$\nabla H°_f$ (298 K) = -266.88 ± 2.2 KJ mol^{-1}
Enthalpy of hBN-cBN reaction	$\nabla H°_r$ (298 K) = -16.3 KJ mol^{-1}
Entropy of reaction	$\nabla S°_r$ (298 K) = -8.22 KJ mol^{-1}
Free energy of reaction	$\nabla G°_r$ (298 K) = -13.9 KJ mol^{-1}

Structural

Lattice energy	3420 Kcal mol^{-1}
Cohesive energy	12.2-14.2 eV (calculated)
	13.2 eV (experimental)
Bulk modulus	465 GPa (experimental)
	362-367 GPa (calculated)
Elastic modulii	c_{11} =712 GPa
	c_{12} =420 GPa
	c_{44} =450 GPa
Damping constant	0.038

Transport

TO mode frequency	1065 cm^{-1}
LO mode frequency	1340 cm^{-1}
centre frequency	1175 cm^{-1}

Energy gaps
  E_g(indirect)   6.4 eV (UV absorption)
  $(\Gamma_{15v} - X_{1c})$ 6.0-8.6 (calculated)
  E_g(indirect)   9.94-14.5 (calculated)
  $(\Gamma_{15v} - \Gamma_{1c})$
Effective masses
(in units of electron mass)
  electron   0.752
  heavy holes   0.375 ∥ [100]; 0.926 ∥ [111]
  light holes   0.150 ∥ [100]; 0.108 ∥ [111]

Static dielectric constant	ε_0 =7.1
High-frequency dielectric constant	ε_∞ =4.5
Refractive index	2.117

Table 2.4 Comparison of Semiconducting Properties.

Properties	cBN	hBN	diamond	β-SiC	GaAs	Si
Lattice constant (Å)	3.615	a=6.661 c=2.504	3.567	4.358	5.65	5.43
Thermal expansion (x10^{-6} /°C)	3.5	2.7($^{\parallel}$) 3.7($^{\perp}$)	1.1	4.7	5.9	2.6
Density (g cm^{-3})	3.487	2.28	3.515	3.216	-	2.328
Melting point (°C)	>2973	-	3800	2540	1238	1420
Bandgap (eV)	6.4	5.2	5.48	3.0	1.43	1.1
Carrier mobility (cm^{2}V^{-1}s^{-1})						
Electron	-	-	2200	400	8500	1500
Hole	-	-	1600	50	400	600
Dielectric Constant	7.1	5.06	5.66	9.7	12.5	11.8
Breakdown (x10^5 V cm^{-1})	~80	~80	100	40	60	3
Resistivity (Ω-cm)	10^{16}	10^{10}	10^{10}	150	10^8	10^3
Thermal conductivity (W cm^{-1} K^{-1})	13	-	20	5	0.46	1.5
Absorption edge (μm)	0.205	0.212	0.2	0.4	-	1.4
Refractive index	2.117	1.7	2.41	2.65	3.4	3.5
Hardness (Kg/mm^2)	9000	-	10000	3500	600	1000

Table 2.5: Chemical and Physical Properties of hBN [30,43]

Property	Value
Crystallographic	
Crystal structure	hexagonal
	Space group, P6$_3$/mmc
Lattice constant	a = 2.504 Å, c = 6.661 Å
B-B or N-N distance	2.504 Å (intralayer)
Ionic BN distance	1.446 Å (intralayer)
	3.330 Å (interlayer)
Density	2.27 g cm^{-3}
Crystal habit	planar, fused, six-membered rings stacked directly on top of each other, anisotropic properties.
Mechanical	
Hardness	low
Compressive strength	0.2067 GPa (298 K) $\parallel$ c
Bend strength	0.1034 GPa (298 k) $\perp$ c
Tensile strength	0.0413 GPa (298 K) $\perp$ c
Young's modulus	20.67 GPa (298 K) $\perp$ c
Flexural strength	103 MPa $\perp$ c
	10 MPa $\parallel$ c
Flexural modulus	24.8 GPa $\perp$ c
Electrical	
Colour	transparent when pure and defect free, opaque/white results from impurity and defect states in the electronic band gap.
Resistivity	3x10^7 Ω-cm $\perp$ c; 3x10^9 Ω-cm $\parallel$ c, resistivity decreases at high temperatures: 6x10^3 Ω-cm $\perp$ c at 1773 K; 3x10^5 Ω-cm $\parallel$c at 1773 K; material eventually becomes a semi-metal.
Thermal	
Thermal conductivity	62.7 W m^{-1} K^{-1} (298 K) $\perp$ c
	1.45 W m^{-1} K^{-1} (298 K) $\parallel$ c
	75.0 W m^{-1} K^{-1} (573 K) $\perp$ c
Debye temperature	598 K
Decomposition temperature	2600 K ± 100 K
Linear thermal expansion	3.24x10^{-6} K^{-1} $\perp$ c (298-531 K)
	81.0x10^{-6} K^{-1} $\parallel$ c (298-531 K)
Thermal stability	In air, oxygen stable to 1173 K, oxidation becomes significant at $\rangle$ 1273 K.

Property	Value
Chemical Reactivity	react with Al_2O_3 at 1700 °C and SiC at 800 °C; Al in 10^{-5} Torr vacuum, 1630 K; wetting and reaction. Insoluble in usual acids.
Thermodynamic	
Heat capacity	C_p (298 K) = 4.173 cal mol^{-1} K^{-1}
Entropy	S^o (298 K) = 3.536 cal mol^{-1} K^{-1}
Enthalpy of formation	∇H^{of} (298 K) = -60.3 Kcal mol^{-1}
Entropy of formation	∇S^{of} (298 K) = -20.62 cal mol^{-1}
Free energy of formation	∇G^{of} (298 K) = -54.15 Kcal mol^{-1}
Transport	
TO mode frequency out of plane in plane	770 cm^{-1} 1383 cm^{-1}
Energy gaps	5.2 eV (experimantal) 3.2-5.8 eV (calculated)
Static dielectric constant High-frequency dielectric constant	ε_o=5.06 $\parallel$ c and 6.85 $\perp$ c ε_∞=4.10 $\parallel$ c and 4.95 $\perp$ c
Refractive index	1.65

2.7   SELECTED APPLICATIONS OF BN

To identify the areas of applications of vapour-phase grown BN, there should be good understanding of the present state of the use of BN (both hBN and cBN) in different areas. In section 1.6.1, we gave a vivid picture of the reason behind using BN thin film instead of bulk BN or PCBN (polycrystalline cBN). The industrial usefulness of bulk BN and PCBN will be discussed in this section and the potential application of BN thin film will be detected in relation to the application discussed in this section. Only selected fields will be summarized here possibly leaving other area of applications. Again, BN thin films have shown potentiality in other different areas which are not related to this section. Though successful growth of BN thin film is still problematic and difficult, the potentiality of the films attracted a great deal of research for the last three years.

2.7.1 INDUSTRIAL AND POTENTIAL APPLICATIONS OF cBN

Cubic BN, comparable in hardness with diamond, is much harder than the conventional abrasive materials such as Al_2O_3, SiC and boron carbide. Thus the grinding performance with cBN wheels is considerably increased over the conventional SiC or Al_2O_3 wheels in grinding chilled cast irons, hardened and high speed steels.

A major application of cBN crystal is as a superabrasive, the crystals being bonded into wheels for grinding steels and superalloys. Another, growing application is for PCBN, which is used to make cutting tools.

PCBN is produced by compacting and sintering the individual crystals together to form a polycrystalline mass. Random orientation of the crystals provides uniformly high hardness and abrasion resistance in all directions. Again, a high-temperature, high pressure process is required, and catalysts and solvents are often used to enhance sintering. The resultant composite may have either a low or high cBN content, with either a ceramic or a metallic binder phase. Properties of these various PCBNs available depend primarily on the size of the cBN grains, the crystals and solvent used, the sintering method and the presence or absence of inert fillers. Wear resistance of PCBN tools is up to 50 times that of uncoated tungsten carbide tools and upto 25 times that of composite ceramic tools, but only about one-half that of diamond tools. The material combines a high degree of toughness with exceptional hot hardness. Unlike diamond, PCBN tools are chemically more stable when machining ferrous work pieces at high cutting temperature. Thermal conductivity is relatively high, heat being conducted away from the cutting edges faster than with carbide or conventional ceramic tools.

High thermal conductivity of cBN allows it to be used as a heat sink for semiconductor lasers, microwave devices etc. A pervasive problem in electronics packaging is quick and efficient dissipation of heat generated by the transistors on the integrated chips. Table 2.6 listed attributes of diamond, cBN, Beryllium oxide (the currently used material, but toxic) and aluminium nitride (one of the future candidates). Interestingly, diamond and cBN are the only material that posses the rare combination of high thermal conductivity and high electrical resistivity.

Cubic BN can be doped with silicon and beryllium in order to get n-type or p-type semiconductor respectively. These doped cBN crystals can be used to make p-n junction diodes which can work at high temperature because of the high thermal stability of cBN. Injection luminescence in the UV was absorbed from a cBN p-n junction made at high pressure [44]. This light emission occurs near the junction region only in certain conditions. The first p-n junction diode of cBN has recently been built [44].

The electronic application of cBN have only begun to be developed; there use should be increased considerably in the coming years. Because of the small size of the components required in electronic compounds, thin films are needed.

69

Table 2.6 Attributes of heat-spreading material

Attributes	Requirement	cBN	Diamond	BeO	AlN
Resistivity (Ω-cm)	High	10^{16}	10^{10}	10^{14}	10^{14}
Thermal Conductivity (W/cm-K)	High	13	20	3.7	3.2
Dielectric Constant	Low	7.1	5.66	6.9	8.8
Dielectric loss	Low	0.001	0.001	0.001	0.001
Dielectric strength (V/cm)	High	10^6	10^6	10^5	10^5
TE* match with chip material (Si)x10^{-6}/°C (0-400°C)	Good match	3.5	1.1	7.2	4.1

*Thermal expansion (TE) of Si is 3.5×10^{-6}/°C.

2.7.2 THE APPLICATIONS OF hBN

Although hBN has not attracted the attention given to SiC and Si_3N_4, it nonetheless has been used in a diverse collection of device- or process-enabling applications that take advantage of its high temperature shock stability, anisotropic thermal conductivity and electrical resistivity.

Perhaps the largest volume application for powdered hBN involves its use in high temperature crucible and evaporator boats that are employed in the semiconductor industry for containing Si and GaAs melts.

The powder also finds a large volume application as the raw material for the high-temperature, high-pressure conversion of hBN to cBN. The thermal conductivity and lack of wetting by many metals have led to applications of boron nitride in horizontal casters in the steel industry, mold-release agents for castings, casting nozzles, binders or fillers for organic polymers and resins, and insulation material for power transformers. The high

70

temperature lubrication properties of hBN have provided use in abrasive tools, liquid-metal processing, and motor oil compositions. The electrical properties have resulted in applications as electrode materials, electrode coatings, and semiconductor heat sinks. Boron nitride is noted to be partially transparent to infra red and microwave radiation, and the material has found some use as radar and infra red windows. There are some limitations, however, as a result of the intrinsic cut-off limit at short wavelengths and scattering resulting from sample anisotropy. Some CVD-prepared materials may allow for reduction of the latter problem. In the past few years, hBN has found increasing attention in advanced ceramic composite applications. Although they are widely utilized today, conventional oxides fail to meet many current and future materials technology needs. The dramatically increased demand for rugged ceramics has led to greater interest in non-oxide materials such as borides, carbides, nitrides, and silicides. One old commercially important non-oxide ceramic is boron nitride [43]. This deceptively simple material has enjoyed widespread use, particularly in a narrow range of traditional thermal/structural applications, but deficiencies in synthetic and processing methods have ultimately restricted its utilization in many advanced ceramic applications. Nonetheless, several unique bulk properties of BN has stimulated renewed interest in its chemistry and processing, and demands have appeared for fibres, coatings and foams that cannot be obtained by classical high-temperature powder preparative methods [43].

Although many ceramics are capable of surviving high-temperature environments such as many aerospace applications, most are intrinsically prone to brittle failure under stress. BN composites such as metal carbide- graphite and metal oxide (BeO, Al_2O_3)-BN composites, showed promise for specific thermal shock resistance. A number of other BN composites (Al_2O_3-BN, SiC-BN, AlN-BN, Si_3N_4-BN) have showed promising applications.

2.8   PROPERTIES OF BN FILMS

As discussed in section 2.4.1, BN films deposited by low pressure techniques may contain any of the phases or they can even have an amorphous structure. Moreover, as well as the two main crystalline forms, other structures in thin film have been identified and designated as iBN and aBN (ion assisted and amorphous BN respectively). So these films may not have the long range order of cBN crystal structure, but might have desirable characteristics, similar to bulk material, such as extreme hardness, high transparency (both at visible and infrared wave lengths), high electrical resistivity, low coefficient of friction, and chemical inertness. The advantages of film are already discussed in section 1.6.1.

Table 2.7 lists the properties of different BN films compiled from the literature. These values can be compared with that of table 2.3 and 2.5. In a couple of categories, these films do not quite measure up to those of bulk BN. For instance, the microhardness of cBN films (4000 Kg mm^{-2}) is approximately half of that of bulk cBN, still it is twice as hard as hard corundum (2085 Kg mm^{-2}) and harder than sapphire. A number of properties resemble that of bulk material, though film property varies with deposition techniques and parameters.

71

Up till now, however, attempts to synthesize cBN at low pressures have not been as successful as those to produce low-pressure diamond. Most of the semiconductor and optical industries needs high degree of crystal perfection to eliminate or minimize defect-related optical absorption, to maximize thermal conductivity, to ensure satisfactory carrier mobility, and to provide undoped material with the highest possible electrical resistivity and breakdown strength. Therefore, once appropriate low pressure synthesis methods are established, BN films and coatings should rapidly gain significant industrial importance.

Table 2.7 : Properties of different types of BN films [13,45-47]

Properties	cBN	hBN	iBN	aBN
Density ($g \ cm^{-3}$)	2.8-3.5	2.1-2.4	1.8-2.0	2.03
Microhardness (kg mm^{-2})	2000-5000	low	2000-3000	2000-3000
Resistivity (Ω-cm)	10^{10} -10^{14}	10^{9}-10^{14}	10^{10}-10^{14}	10^{9}-10^{10}
Refractive index	2.0 - 2.3	1.7 - 2.0	not known	~1.7
Optical gap (eV)	3.67 - 6.4	3.2 - 5.8	5.4 - 5.4	4.4 - 5.9
Visible & Infrared Transparency	High	Quite High	High	————
Chemical resistance	High	High	High	High
Dielectric constant	4.2 - 7.0	2.7 - 7.7 (orientation depended)	not known	3.5 - 6.5
Dielectric strength (V cm^{-1})	10^{6} - 10^{7}	$(5-7) \times 10^{6}$	not known	~10^{6}
crystal structure	cubic	hexagonal	amorphous with some evidence of microcrystallinity	amorphous with cBN in predominantly hBN or with a boron rich formation

The summaries provided in sections 2.6 and 2.8 are intended to illustrate the fascinating properties of bulk BN and BN thin films. In the following section, we will outline the wide array of applications BN films offer.

2.9   APPLICATIONS OF BN THIN FILMS

It is evident from the preceding sections that thin films of BN grown from vapour phase could be useful for mechanical, optical and electronic applications. Because of its similar properties with diamond, cBN films are candidate substitutes for most, if not all, the envisioned applications for diamond films.

There is a growing interest world-wide in cBN thin films and the reasons for this are almost varied as the reasons for the interest in diamond films. Cubic BN films' coatings have very high hardness and many potential uses in tribological and tooling applications where the reactivity of diamond with oxygen and ferrous metals renders it relatively unsuitable. Single crystallinity and a perfect crystal lattice are not primary requirements for wear and cutting application, this fact promises extraordinary possibilities of cBN or cBN-like films for cutting tools. They would be suited for applications such as the reduction of wear if it were possible to prepare films of BN with sufficient adhesion on metals.

Cubic BN represents, with SiC, one of the very few known high-temperature high-band-gap semiconductor materials, and, unlike diamond, can be passivated by an oxide layer. As shown in Table 2.4, hBN has also comparable electrical properties with cBN. BN displays multi band electro-, photo-,and cathode ray-luminescence. If crystalline thin film can be obtained with large carrier drift velocity, it can be a promising material for possible use in high power microwave applications. Good insulating properties occur with most of the BN films.

An interesting application of the BN films is as an insultor in a metal-insulator-semiconductor (MIS) memory diode and as high quality gate insulating films and passivation layers for MIS structures based on III-V compounds, such as GaAs. High temperature thermal oxidation processes, resulting in high quality dielectrics in silicon technologies, are not compatible with GaAs materials. At temperatures greater than 450^0C, dissociation of arsenic from the GaAs substrate occurs which degrades the semiconductors electrical characteristics. Additionally, temperature limitations exist with many compound semiconductors including InP where one of the components is very volatile. BN films is a suitable insulator for GaAs, because of the close match of the coefficient of thermal expansion of the two materials.

On Si, the attraction stems from the fact that the lattice mismatch between cBN and Si (100) lattices is only about 5% . A motivation for growing BN insulator on Si is the possibility that a higher degree of ordering at the crystalline insulator/Si interface may lead to semiconductor passivation superior to amorphous SiO_2 [48]. An electrical insulator with the high thermal conductivity of cBN may be superior to the other known epitaxial insulators. For example, the thermal expansion coefficient of cBN and Si are nearly identical over a wide range of temperature. This is, in contrast, with the large thermal expansion coefficients of the insulators CaF_2, SrF_2, and BaF_2, which can also been grown epitaxially on Si. Moreover, BN films show promise as dielectric materials for Si/insulator structures owing to their crystallochemical conformity with silicon.

Oxide insulators are possibly unsuitable for MIS structures on III-V compound materials such as GaAs since oxygen has strongly different reaction energies for the individual components so that the insulator-semiconductor transition does not become very sharp. Sometimes, SiO_2 insulating films turned out to have a large leakage current when the effective thickness is less than 10 nm [15]. Both from deposition temperature and thickness requirement, vapour deposited BN films have a good potentiality as a refractory dielectric films. Thus BN films could be introduced into semiconductor fabrication.

BN films are useful as a restricted area boron diffusion source which can be used to fabricate coplanar diodes using only one photo mask. BN films are also useful as chemically inert and electrical insulating layers to increase the stability of many types of devices (such as $Pd-BN-Si_3N_4-SiO_2-Si$ FETs for hydrogen detection) and as very thin insulating layers for tunnelling MIM structures.

As discussed in sections 1.6.2 and 2.6.1, BN thin films are valuable as a heat sink and heat spreading material in electronics packaging in VLSI circuits operating especially in high frequency which can replace the toxic and less readily worked beryllia.

In fact, cBN films may be better suited than diamond for electronic device applications, since cBN can be easily doped both n and p type whereas diamond cannot, and the heteroepitaxial growth of diamond thin films on substrates other than cBN has thus far been unsuccessful [49a].

Thin films of cBN could be useful for the fabrication of insulated conductors, capacitors and photo conductor. It is also useful for providing hard protective coatings for diodes, transistors and other monolithic devices. The inertness and resistance to wet chemicals helps in the use of BN films as a passivation coating. A film of about 100 nm (or thinner) could be used in integrated circuits as thin film varistors or voltage limiters. Moreover, owing to the large band-gap of cBN, it has potential for deep UV detectors and UV light-emitting devices because its high band gap and high resistivity would reduce the contribution, to photo-current due to thermal and background radiation, thereby making it possible to fabricate low-noise UV detectors. Like diamond, the external chemical and environmental stability of BN films together with their transparency in IR and UV make them ideal candidates for protective coating for IR and UV devices.

BN films could be used as a barrier to the incorporation of silicon in the GaAs melt during synthesis from elemental Ga and As in SiO_2 crucibles. The use of BN films may have application to gradient freeze (GF) growth of GaAs and other III-V crystal growth processes such as liquid encapsulated (LEC) growth when a solid pyrolytic BN crucible is normally used.

BN thin films could be used as possible optical baffle coatings for use in telescopes. Its high spectral emittance in the 8-12 μm window coupled with its demonstrated resistance to high energy pulsed electron radiation has made it an interesting candidate material. BN films has potential in using as a low-average Z (Z=6) refractory coating for use in plasma confinement systems. Low Z materials are preferred for use in this plasma environments because radiation losses from them produce less contamination and stability problems for the plasma. Also the controlled tensile film stress, the low

mass density and low atomic number make BN films' membranes ideal candidates for vacuum window applications with excellent transmission to soft radiation and electron beams.

Solid lubricant films are required for a variety of high precision, thermodynamically efficient engines (stirling, adiabatic diesel engines and gas turbine) in both terrestrial and space environments such as satellite mechanism bearings, gears,and splines. Although MoS_2 films are currently the material of choice, there still exists a need for materials with superior thermal stability and whose tribological properties are not degraded by air exposure. BN films are one such candidate material as discussed in 1.6.2.

BN films have been widely selected for use as a membrane material in x-ray lithography mask substrates. The requirement of the films are discussed in section 1.6.2. As discussed, x-ray lithography is widely believed to occupy an important future lithographic niche in the vicinity of 0.5 micron and below. It will be technically easier to achieve resolution and depth of focus with x-ray than with optical steppers in this lithographic system. It will be much less expensive to print large volume runners like dynamic RAMs, microprocessors, or CODECs with x-ray than with electron beam direct write. The main key point in order to manage such a precise lithographic technique is the x-ray mask substrate. The mask should be capable to meet the main requirements discussed in section 1.6.2. BN films are most desirable for these requirements: very low x-ray absorption coefficient (low atomic number material), controllable tension to achieve membrane flatness and mechanical strength, high Young modulus that provides the dimensional stability, adequate optical transparency required for alignment of mask to wafer during registration, thermal expansion coefficient close to that of the silicon frame to minimize the variation in tension, low defect density and chemical inertness which are advantageous throughout all phases of mask processing.

BN films can be used for thermal insulation, as a die-wash material and as a pressure transmission medium. BN films could be used in thin membrane based pressure transducers for sensing low pressure in the range 0-100 Torr. The change in the membrane defection exposed to pressure is sensed as capacitance variation of a capacitor formed by the membrane and a fixed plate.

As discussed 2.6.2, BN has been used in the fields of ceramic matrix composites. More recently [43], it has been shown that BN could be used as an interphase material. i.e. as a thin film between the ceramic fibre and the ceramic matrix, acting as a mechanical fuse to protect the former against the notch effect due to microcracking arising in the later. A BN film interphase has a mechanical behaviour similar to that of its carbon counterpart, with a much higher resistance to the environmental parameters (e.g. oxidizing agents).

The possibility relatively low temperature processes, for the deposition of BN thin films onto a variety of substrate materials has sparked investigation into utilizing this unique material in an ever widening variety of applications of commercial interest. Investigation on new methods of preparation of high quality BN should bring new possibilities for its applications.

2.10 PRESENT STATE OF ART IN BN THIN FILMS

In the midst of 1950s, drawing their brilliant inspiration from the layer structure of BN similar to that of carbon, Wentorf et. al. succeeded in the synthesis of BN with a diamond-like structure, namely, cubic BN (cBN) (called by them "borazon"), only two years [50] after that of the "man-made diamond" [51] under high pressure and high-temperature conditions. But difficulties were soon realized for the growth of large crystals at reasonable growth rates in both the diamond and cBN cases. Due to the above limitations, the wide range potential applications of them could not be realized and research on these unique materials soon lost the initial thrust.

However, it was not until early 1980s that the early 1970's report on ion beam deposition of i-carbon [17], which seems to have the bonding form of diamond (sp^3) but is essentially nanocrystalline, was followed by that of the corresponding "i-BN" by Wiessmental et. al. [52a,52b]. The unique properties of these films such as extreme chemical inertness and high hardness soon attracted a great deal of interest among some groups to produce these i-BN films [53-55]. These i-BN films were structurally different from tetrahedrally bonded cBN and they were amorphous in nature.

The synthesis of cBN thin films under low pressure was reported for the first time by Sokolowski [56a] using reactive pulse plasma CVD in 1979. Just at the same period, it was assured that highly crystalline diamond can be prepared by CVD using atomic hydrogen [20,21]. Even in spite of the number of works motivated by the realization of some superior properties of cBN thin films comparable to diamond, there has been no report, since the pioneering works by Sokolowski et. al. (56), on the growth of cBN from the vapour whose crystallinity is comparable to CVD diamond films

The forecast promise cBN holds and the success in growing diamond or diamond-like films revitalized the interest in cBN films worldwide for the last three years and very recently, some researchers from only Japan have reported the growth of pure authentic cBN films on mainly silicon substrates [33-39].

Realizing the substantial promise of cBN thin films, we started our work on cBN by PECVD at the end of 1989 when there was no report, as far as we know, of growing cBN or good quality cBN-like films deposited by PECVD in a RF plasma. Though in 1988, Chayahara reported growth of cBN film by electron cyclotron resonance plasma (not by RF plasma), but their film was grown at high substrate temperature (600°C) from toxic source materials and other than optical properties, thermal or mechanical stability of the films were not reported. At that time, there has been no report of BN films grown from non-toxic source material either by PVD or CVD according to our knowledge. This motivated us to grow cBN or cBN-like films from a non-toxic source by PACVD at low substrate temperatures.

After an extensive research worldwide for the last three years, numerous experimental and theoretical problems remain and success in synthesizing well-crystallized cBN films are discouraging compared to diamond films. Most of the reported films are

highly defective with many experiments showing nanocrystalline and pyrolytic (hexagonal) material present. Especially, researchers are facing considerable difficulties and different views in characterizing cBN films. In the following sections, we outline the wide array of approaches that have been used to prepare BN films. The films properties which can be obtained by the various techniques have been evaluated and the problem in characterizing these films have been cited. Identifying the current state of the art of the synthesis of BN films, we will address the limitations of the various deposition processes.

2.10.1 REVIEW OF PVD TECHNIQUES

2.10.1.1 Ion-assisted deposition (IAD)

Weissmantel [52a,52b] first recognized that ion deposition could be applicable to the production of cBN films. After the successful synthesis of diamond-like carbon films by IAD techniques, Weissmantel raised the question whether metastable BN films with properties close to those of cBN could be prepared by the same techniques. In 1980 and later years, Weissmantel and his group [52c-52f] reported the deposition of hard, transparent BN films with a range of properties and structure analogous to those of diamond-like carbon films. The following techniques were employed: (a) an ion plating process in which electron-beam-evaporated boron together with ionization of nitrogen, NH_3 or NH_3/Ar were involved to provide reactive ions (N_2^+, NH_2^+, H^+) with energies of 0.1-3 keV; (b) direct ion-beam-deposition (IBD), using a Kaufman source fed with borazine or other volatile compounds; (c) dual beam technique operated with a boron or BN target and nitrogen ion beams. They suggested that i-BN might be used instead of i-C, though their i-BN films contained tiny crystallites of hBN and cBN embedded in the amorphous phase [57].

Further evidence for cBN films was provided by Shanfield and Wolfson [53] whose ion plating method of i-BN from a borazine plasma goes back to the proposition by Weissmantel et al. [52]. Formation of BN films using an ion beam extracted from a borazine plasma has also been reported [54].

Using a method called ionization vapour deposition (IVD) or dynamic mixing method, Satou and Fujimoto and their group [55a,55b] were the first to provide clear evidence that cBN can be prepared by metastable film synthesis. Simultaneous 25-40 keV nitrogen ion irradiation onto evaporated boron was used to produce films with a composition ratio B/N=0.7-2.7. The pronounced implantation caused during film formation seems to be responsible for the observed formation of cBN crystallites. This group [55c] later prepared BN films using nitrogen molecular ions with much lower energy (2-25 keV) than in the previous case [55a,55b]. In the former cases, the microstructure of the films depended considerably on B-to-N ratio but in the later case, almost all of the films indicated the existence of cBN. Recently, some members of that group [55d-55g] prepared BN films using much lower energy nitrogen ions (200-1000 eV). They concluded that an ion beam in the low energy region is effective for forming the metastable cubic phase.

These results significantly differ in the low energy region (100-1500 eV) from that of a recent work of Sainty et al. [58]. Sainty et al. reported that all films were consistent with the presence of hBN with sub-stoichiometric films containing amorphous boron as the other constituent. For low energies (500 eV), stoichiometric films can be achieved, however at higher ion energies (1000 eV) there are considerable difficulties in achieving a stoichiometric film. No evidence could be found for cBN in their energy range (100-1500 eV), whereas Satou and Fujimoto et al. [55c-55g] reported cubic BN films with nitrogen to boron ratio as low as 0.4 and in the range 200-1000 eV. Using ion-beam-assisted deposition, Burat et al. [59], Carosella et al. [60] and Tetreault et al. [61] deposited hard and transparent BN films which had structural similarity with the film deposited by Sainty et al. [58].

Deposition of BN layers by IVD method were also reported by a number of workers using nitrogen ion energy of 1.2 keV [62], 4 keV [63], 30 keV [64], 100 keV [65] and 120 keV [66]. Elena et al. [65b] have found that the adhesion and cohesion of the BN films could be considerably enhanced by using ion beam deposition as opposed to rf magnetron sputtering. In [66], one of their important conclusions was that differential pumping was essential for the formation of quality BN films as water contamination appeared to cause the formation of boron oxynitrides as well as other softer boron based compounds. Using this IVD method, Namba [67] from Japan and Glazova et al. [68] from USSR claimed success in depositing cubic BN films.

In China, Zhou et al. [69] have prepared boron nitride films containing amorphous, hexagonal, cubic and their mixtures by ionized deposition from evaporated boron and nitrogen gas at low pressure. Recently Lin et al. [70] also from China have reported deposition of cBN films using a dual ion beam technique which employed a bombarding beam of 5-100 keV N^+ ions and a sputtering beam of 0.05-1.5 keV Ar^+ ions.

It was found by Miyoshi et al. [71a] that the hardness and adhesion of ion-beam deposited BN films depended on the metallic substrate. This group showed that ion beam deposited BN films on III-V semiconductors exhibited amorphous behavior [71b] and iBN film adhered to silicon and SiO_2 and formed a good quality film though it adhered poorly to GaAs and InP [71c]. Recently, Kester and Messier [72] and Wada and Yamashita [73] showed the effect of ion-bombardment and substrate temperature on the growth of iBN films.

A number of works on cBN films have been reported by Ikeda et al. [34] from Japan using arc-like plasma-enhanced reactive ion plating method. They showed that the internal stress of cBN films was greatly reduced by providing an iBN buffer layer between cBN and substrate.

2.10.1.2 RF sputtering

Using an rf sputtering technique, there are a few reports [74-80] involving deposition of BN films.

Rother et al. [74], Wiggins et al. [75] and Mitterer et al. [76] prepared layers which were reported to have a structure similar to that of hBN and in particular to the turbostratic variant of hBN. In their reports, BN films were deposited by rf sputtering of a hBN targets in an N_2 or N_2/Ar atmosphere. In ref. 76, both non-reactive and reactive rf sputtering were employed. It was evident from these reports that rf sputtering of an hBN target is not suitable for the deposition of hard, resistive and highly insulating BN films. Mitterer et al. attributed high hardness values (2000-2800 HV 0.02) of the BN films deposited non-reactively to the formation of boron-rich I-tetragonal boron nitride ($B_{48}B_2N_2$) in addition to hBN. These films had high internal stresses. They also found that inclusion of Ti or Al was not suitable for stabilizing the cubic or the wurtzitic structure of BN and they enhanced the formation of hBN. Contrary to these reports, Seidel et al. [77], Yoshida et al. [35] and Gissler et al. [78] reported the preparation of cubic BN films by rf non-reactive and/or reactive sputtering with negative substrate bias of less than 300 V, though their films exhibited high compressive stress which strongly reduces their adhesion to the substrate. Goranchev et al. [77c] investigated the influence of the gas pressure and the type of sputtering gas on the stresses of cBN films determined by bending beam method. They deposited 500 nm thick crystalline BN films at 60 mtorr without any destruction of the films. It was also found that the content of cubic phase and the adhesion of the films was strongly dependent on substrate bias and temperature [35,78].

2.10.1.3 Reactive evaporation (RE)

The process of reactive evaporation described by Beale [81] is reported to deposit up to 75 wt.% cBN films using electron-beam-evaporation of an alloy consisting of boron and portions of Al,Co,Ni or Mn in an NH_3 environment.

A process called activated reactive evaporation has been developed and used by Bunshah and his group [82]. Polycrystalline cBN films have been prepared at 450°C by evaporating boric acid in the presence of NH_3 plasma. They claim to have unequivocally demonstrated that the films contained the cubic phase.

Using this activated reactive evaporation process, Inagawa et al. [36] have also succeeded in depositing cBN films using a gas activation nozzle. They found that it was necessary to apply rf bias to the substrate to accelerate the formation of cubic phase and the adhesion of cBN films to the substrate was significantly improved by inserting SiN interlayers.

A cBN film with stoichiometric composition has been synthesized by Murakawa and his group [37] using a hot cathode plasma discharge within a parallel magnetic field in an activated reactive evaporation process, called by the authors the "magnetically enhanced plasma ion plating" method. They improved the adhesion of their film by providing a multilayer structure comprising a thin B layer, a gradually increasing B content BN layer and then a cBN one.

79

2.10.1.4 Laser Assisted Depositions

Using laser assisted deposition techniques [49,83-87], a variety of different structure of BN films have been deposited. Kessler et al. [83] have deposited wurtzite BN films using a Q-switched Nd glass laser. Murray et al. [84] used a frequency-doubled Q-switched Nd-YAG laser and Paul et al. [85] used a Q-switched ruby laser to deposit BN films yielding hexagonal structure.

Doll et al. [49] using a KrF excimer laser and Mineta et al. [86] using a high powered (200-1000 W) CO_2 laser have succeeded in depositing cBN films while the former authors have reported heteroepitaxial growth of cBN films on (001) faces of Si substrates.

2.10.1.5 Other PVD techniques

Lee and Poppa [88] made BN thin films by electron-beam-evaporation of boron onto NaCl at room temperature. The films retained a very stable amorphous structure upto 1050°C and began to deteriorate above this temperature.

Using a molecular beam epitaxy (MBE) method, Paisley et al. [89] reported growth of amorphous BN films with some evidence of microcrystallinity using a microwave electron cyclotron resonance plasma source of nitrogen ion and evaporated boron. They deposited BN/BGaN/GaN epitaxial films but their attempt to deposit cBN films using microwave plasma as a potential ion bombardment for the formation of cubic phase has not been successful.

Other than that, DeKoven et al. [90] have prepared hard BN layer by 100 keV nitrogen ion implantation onto B_4C surface.

2.10.2   REVIEW OF CVD TECHNIQUES

2.10.2.1 Chemical vapour deposition techniques

Films grown by chemical vapour deposition techniques are normally deposited using ammonia or nitrogen mixed with boranes or boron trichloride or they can even be deposited using single compounds such as trichloro-borazine ($B_3N_3Cl_3H_3$). Because of important industrial applications, BN thin films were produced by pyrolytic CVD [91-94], high temperature and/or high pressure CVD (1200-2000°C, 45-75 kbar) [44,50,95-101], molecular flow CVD [102] and hot filament activated CVD [103] as well as low temperature and/or low pressure CVD [104-112]. A number of source materials were described in ref. 113a.

Deposition of clear and vitreous BN films onto silicon and other substrates has been reported by some authors [104-107] from diborane (B_2H_6) and ammonia (NH_3) mixed with inert gas at 250-1250°C. A number of workers [95-97,108-112] reported synthesis of BN films from a mixture of boron halide and NH_3 at 250-1400°C. It was found that the nature of the substrate could greatly influence the degree of preferred orientation of the crystallites [111]. Whereas the films deposited at temperatures below 450°C are unstable in a moist atmosphere [109], transparent BN films are produced between 1000 and 1200°C.

Nakamura proposed a molecular flow CVD [102a] and metal organic CVD [102b] method for depositing BN films using NH_3 with decaborane ($B_{10}H_6$) and triethyl-boron respectively. BN thin films have also been prepared by the decomposition of hexachloro-borazine ($B_3N_3Cl_3$) [114] or polymeric cyanoborane ($CNBH_2)_n$ [115].

Using low pressure CVD (LPCVD) techniques [91-94,116-119], deposited BN films exhibit an increase in hydrogen content than those deposited by other techniques. Thus these films exhibit properties which differ from BN films deposited at higher temperatures [118]. Using these LPCVD techniques, BN films were deposited using B_2H_6 and NH_3 [117-119], BCl_3 and NH_3 [91,94] or a single compound as borazine [92a] or trichloro-borazole [116]. Most of these films can be described as amorphous hydrogenated BN (a:BN-H) films which are commonly used as a membrane material in x-ray lithography.

The CVD grown films are amorphous or of hexagonal structure and therefore do not exhibit any high hardness. Other film properties such as refractive index, absorption coefficient and dielectric constant are dependent on deposition temperature and the ratio of reactants.

2.10.2.2 Plasma assisted chemical vapour deposition techniques (PACVD)

Plasma assisted chemical vapour deposition techniques used for the synthesis of BN coatings involve decomposition/dissociation of boranes or organic/inorganic boron-based compounds in a plasma using dc, rf or microwave excitation.

A plasma assisted CVD technique for the deposition of BN was first used by Russo et al. [120]. Using BCl_3/N_2, they showed that production of BN in a PACVD system was higher than those predicted from thermodynamic processes. Using diborane and ammonia, Hyder and Yep [121] obtained polycrystalline hBN using a high temperature (>750°C) reactive plasma. With PACVD from B_2H_6, N_2 and/or NH_3, soft coatings of potential use as insulating films in microelectronics devices have been prepared [122-123]. Schmolla and Hartnagel [124] have described an organic PACVD (OPACVD) techniques to deposit high quality BN films from organic compounds like borane-dimethylamine or boran-triethylamin at low temperature. The BN coatings deposited from PACVD of BCl_3 and N_2/NH_3 [125-127] are mostly amorphous with small amounts of hBN.

81

Savel'ev and co-workers [128] and Kouvetakis and co-workers [129] studied the PACVD of amorphous BN films using borazine as a precursor. In the later work, they deposited mixtures of poorly crystalline hBN and cBN, but their films contain considerable amount of hydrogen.

The deposition of BN thin films was also performed from a mixture of diborane and other gases using an inductively coupled rf reactor [130] and a magnetically enhanced PACVD system [131]. Liepins et al. [132] conducted a low pressure nitrogen plasma treatment on the thin films grown from borane-ammonia (H_3B-NH_3) or its pyrolysis products in order to grow cBN films. They deposited hydrogenated BN films of composition BNH_5. The generation of pure BN as a film was not achieved by this technique though they later deposited cBN films by high pressure shock-compression synthesis method from borane-ammonia [133].

Ichinose and his group have reported the deposition of cBN films from diborane [38] as well as from various solids, i.e. borane-ammonia, boric acid or sodium borohydride [134] in H_2 or NH_3 plasma produced by rf induction thermally assisted with tungsten filment heating. It was found that tungsten filament heating greatly contributes to the formation of cBN as compared with the contribution of rf induction.

Kim et al. [113a] proposed decaborane ($B_{10}H_6$) as an alternative non-toxic source material for the deposition of BN films though no information was given regarding the structure or properties of the films. They later deposited BN films from borane clusters using a PACVD technique [113b]. Karim et al. [135] proposed borane-ammonia as a non-toxic source material to deposit cBN thin films though their films are likely to contain crystallites of cubic phases embedded in a mostly hexagonal matrix. The same kind of film was also obtained by Mendez et al. from BF_3, N_2 and H_2 gas mixtures [136]. Maya deposited BN films by PACVD from polymeric cyanoborane [137].

Chayahara and co-workers have published a number of papers on cBN [39a-39c]. They deposited cubic BN films from B_2H_6 and N_2 using two types of discharges with rf substrate bias: 1) rf discharge in a magnetic field and 2) microwave discharge at the electron cyclotron resonance (ECR) condition. They concluded that the formation of cBN needs a negative substrate self-bias and ion bombardment on the growing surface might be a prerequisite for the generation of the metastable phase of cBN. Okamoto et al. [39d-39i] from the same group have improved the adhesion of cBN films deposited by ECR plasma using a buffer layer consisting of B and BN_x between the Si substrate and cBN. They also observed that the adhesion of cBN films on diamond substrate is entirely satisfactory [39f]. Shapoval et al. [138] and Eddy Jr. et al. [139] recently reported the deposition of cBN films by employing an ECR-microwave plasma source. Using a microwave PACVD technique, Saitoh and Yarbrough [140] deposited cBN films using $NaBH_4$ in a gas mixture of NH_3 and H_2. Using the same technique, Weber et al. [141] deposited cBN films at 800°C from N-Trimethylborazine [$(CH_3-N-B-H)_3$].

Levy [142] reported the deposition of BN films useful as masks in x-ray lithography. Komatsu et al. deposited cBN films by using chemical vapour transport of B particles under a rf H_2-N_2 plasma [143].

2.10.2.3 Other CVD techniques

A modified version of thermal CVD has been used by Sokolowska et al. [144] to deposit cBN films. This technique termed as 'electron assisted CVD' involves the active role of electrons in the growth process of cBN layers from gas mixture of B_2H_6, H_2 and N_2. The significant feature of the method is the presence of thermionically emitted electrons in the reactive zone in the process of crystallization of cBN layers. They concluded that the presence of energetic electrons is an important process parameter for cBN crystallization.

Reactive pulse plasma deposition has been reported from Poland by Sokolowski et al. [56] as well as Szmidt et al. [145] and Sobczynska et al. [146] to form BN deposit with large fractions of cBN with a view to using the films in electronic applications (i.e. MIS/ISFET). They used a high energy pulsed plasma rather than a continuous discharge to avoid excessive substrate heating. But the presence of micro-inclusions of impurities of these films put severe limitations on their optical and electronic properties.

Komatsu et al. [147] have reported deposition of cBN crystallites from $BCl_3 + NH_3 + H_2 + Ar$ using laser-enhanced plasma CVD technique. Employing an inductively coupled high power rf plasma with simultaneous pulse laser irradiation onto the deposited film, they have grown cBN films heteroepitaxially on the (100) faces of a Si substrate.

2.10.3 LIMITATIONS OF CURRENT TECHNIQUES

PVD techniques have yielded the most promising results so far though the structure of some of the ion-assisted deposited films is predominantly amorphous but with small crystallites of cubic phase [52-71]. Successful deposition of cBN has been reported using ion-assisted [53-55,67-70,72-73], arc-like ion plating [34], rf sputtering [35,77-78], activated reactive evaporation [36-37,81-82] and laser-assisted [49,86] processes. Hard films with hardness in the range of 2000-4000 kg/mm^2 can be grown. A number of workers using PACVD techniques report success in forming the cubic phase of BN by employing rf discharges [38,129,134-136] or microwave discharges [39,139-141]. A vast majority of these films are a mixture of cBN and hBN phases, a better designation being cBN-like films. It appears that most researchers succeeded in the deposition of cBN films if the technique included the input of additional energy from energetic ions during the deposition process.

Other than that most of the films are amorphous or of hexagonal structure and therefore do not exhibit any high hardness. The deposited films comprise a broad family of materials with markedly different properties. Most of the film properties such as refractive index, absorption coefficient and dielectric constant are dependent on deposition temperature, the ratio of the reactants and other process paramateres, so the inherent limitations of the aforesaid processes are related to the coupling of the different process parameters controlling the growth and properties of the films.

Although cubic BN films have been deposited using variations of all the different techniques discussed above, the practical applications of cBN technology are not yet realized due to one or more of the following reasons: (1) use of toxic and hazardous starting materials. Many of the so far used source compounds have serious drawbacks, including serious safety problems due to the toxicity and/or highly inflammable nature of the source compounds (113a); (2) requirement of high substrate temperatures, making them unsuitable for heat treated metals; (3) degradation of film properties owing to unwanted trapped gas and microinhomogeneities; (4) a high mechanical stress with poor adhesion to the substrates; (5) difficulty in nucleating cubic phase on various substrates; (6) inability of the present processes to deposit films at reasonable rates with desired properties such as high hardness, optical transparency, smooth surface topography etc. and (7) necessity to incorporate phase stabilizer element in the cBN films which would be undesirable in electronic applications.

Deposition techniques currently used for the synthesis of BN films are compared in terms of the above considerations to highlight their respective limitations in Table 2.8. Table 2.9 lists a comparative study of the currently used rf PACVD system to deposit BN films.

2.10.4 REQUIRED PROCESS MODIFICATIONS

In order to realize the industrial applications discussed earlier, it is necessary to develop a suitable process capable of synthesizing cBN films with the following combinations of desired properties. They are (i) high hardness, (ii) smooth surface topograghy, (iii) optical transmission in UV and IR, (iv) high thermal conductivity, (v) high electrical resistivity. Moreover for successful industrial production, the process should have the following attributes: (a) suitable starting materials which have the properties of easy handling, availability and low cost, (b) capability of depositing BN films at reasonably high rates, (c) capability of coating large as well as complex shapes, (d) low heat of formation and low energy of film producing particles, (e) flexibility and control of the properties of the film as per the specific requirements for given applications.

TABLE 2.8 Comparison of various deposition techniques for synthesis of BN films

Techniques	Type and quality of films	Advantages	Limitations	Ref. nos.
PVD techniques:				
1. ion-assisted deposition	smooth,transparent hard amorphous films with some crystalline structure;growth of cBN films reported.	low substrate temperature, simple process, adherent films, very good operational control.	significant content of C & O₂, usable only for small area substrate, structure depends on B/N ratio.	52-55, 57-72.
2. RF sputtering	similar to hBN,but with -ve substrate bias, deposition of cBN film reported.	low substrate temperature, good operational control.	low deposition rate,texture of films strongly dependent on deposition parameters, high stress in the films.	35, 73-80.
3. Activated reactive evaporation	transparent cubic BN films.	simple, deposition rate reasonable.	expensive,usable only for small area substrate.	36-37, 81-82.
4. Laser assisted deposition	good quality hBN and cBN film deposition reported.	good quality hBN films useful for electronic applications,epitaxial growth of cBN on Si possible.	high power laser is needed for cBN films, usable for small area substrates.	49, 83-87.
5. Molecular beam epitaxy	amorphous, limited data available to comment.	useful for graded GaN-BN layer.	high substrate temperature, low growth rate, C & O₂ content.	89.
CVD Techniques:				
1. Thermal CVD	clear,vitreous, transparent, smooth films, amorphous/hexagonal.	inexpensive, easy to operate.	toxic source materials, high substrate temperature.	98-115.
2. Low Pressure CVD	hydrogenated amorphous BN films, rough surface topography.	cleaner process, good insulating properties.	toxic source materials, high deposition temperature.	91-94, 116-119.
3. Plasma assisted CVD	transparent films, mostly amorphous /hexagonal; deposition of cBN reported using high substrate bias.	cleaner process,easier to control & optimise, good insulating and electrical properties.	mostly toxic source materials, high substrate temperature or bias needed for hard films,difficult to scale up, optimization of film properties yet to be demonstrated.	38, 120-137, 147.

Techniques	Type and quality of films	Advantages	Limitations	Ref. nos.
4. Microwave/ ECR CVD	mixture of hBN and cBN films; cBN films deposited with substrate bias.	easier to operate, cBN phase more easily attainable.	expensive, difficult to scale up, suitable for small area substrates.	39, 138-141.
5. Pulse plasma CVD	high resis- tive,transparent cBN films.	low substrate temperature possible, good adherent films.	toxic source materials,difficult to scale up, film purity insufficient.	56, 145-146.
6. Electron assisted CVD	cubic BN films.	inexpensive, simple and easy to operate.	toxic source materials, high deposition temperature, damage due to corona discharge.	144.

2.11 IDENTIFICATION OF BN STRUCTURES

Significant progress has been made recently in the experimental techniques for synthesizing cBN films using various types of physical vapour deposition (PVD) and chemical vapour deposition (CVD). All these attempts were successful in producing polycrystalline films of cBN, although predominantly of a mixed phase nature with both cubic and hexagonal phases present.

When deposited as a thin film, boron nitride has the potential to form material with the hBN or cBN structures or possibly the wurtzite structure, or alternately films may contain crystallites of hBN and cBN embedded in the amorphous phases. These two frequently occurring polymorphs are distinguished from each other by large differences in optical, mechanical, electrical and chemical behavior.

The identification of the BN structures can be determined by more or less reliable methods: by x-ray diffraction [34,54-55,65,78,86] or electron diffraction [34-35,37,52b,54-55,77,82,136,140,147-148], but also through the optical properties of the deposited material by infrared (IR), Raman and UV transmission, refractive index and optical band gap measurements [34-39,54-55,70,72-73,77,86,129,134-141,143,147], by electron energy loss spectroscopy (EELS) [52d,148], Auger transition [149,150], nuclear magnetic resonance (NMR) analysis [151] or through other electrical and physical properties.

Physical properties like hardness or density and electronic properties are not unambiguous identifiers of BN phases. X-ray photoelectron spectroscopy seems to have a poor sensitivity to the coordination number in BN. X-ray diffraction may not be a good tool for investigating BN thin films because both B and N atoms are poor X-ray scatterers. Films of mixed phase constituents contain no long range crystallographic order and hence yield diffuse diffraction patterns. Also, with small film thickness (<1 μm), diffraction peak intensities from the BN film are very low.

Electron diffraction (ED) patterns, typically selected area diffraction from transmission electron microscopy (TEM) studies do show evidence of cBN and hBN quite clearly. Lattice constants determined from ED can be used as 'finger prints' of the microstructure in order to provide supporting evidence for the identification of phases. But the identification of the films on the basis of the electron diffraction pattern may become complicated owing to the possibility of preferred orientation in the films which is likely to change relative intensities of their diffraction lines.

A measurement of IR absorption spectra gives a useful information on the film structure, because each phase of boron nitride gives different absorption spectra. IR reflectance measurements show that cBN has a zone-center transverse optical (TO) mode frequency of about 1050 cm^{-1} and a zone-center longitudinal optical (LO) mode frequency of about 1340 cm^{-1}. The IR spectrum of thin films of cBN will therefore show a single absorption maximum at 1050 cm^{-1} if single phonon processes are dominant. The hBN phase results in a distinct and strong, asymmetrical band near 1365 cm^{-1}, which is attributed to B-N bond stretching (in-plane vibration), and a weaker, sharper band near 780 cm^{-1}, which is attributed to B-N-B bond bending (out-of-plane vibration). On the basis of the two quite distinct IR absorption spectra for cBN and hBN, useful microstructural conclusions can be drawn.

Most researchers have obtained good agreement between electron diffraction patterns and IR spectra [34-35,37-38,52d,55,73,86,143,147,148], though in some other works [65,77,82], even if similar electron or X-ray diffraction patterns indicating the formation of cBN phase were obtained, IR spectra did not always give the absorption peak due to the cBN phase. However, the presence of a c-BN peak at near 1050 cm^{-1} is always backed up by other methods which indicate that the presence of IR peaks corresponding to cBN and hBN phases can be considered as a means of microstructural identification. Nevertheless accurate identification of the BN film structure should be confirmed with other methods in addition to cBN reststrahlen band [148]. A definition of 'authentic' cBN can be found in ref. 151.

Table 2.9: Outlines of different rf PACVD techniques used for BN films

Reactants	RF Power	Substrates & its temperature °C	Characterisation Techniques	Summaries of film properties	Ref. no.
$B_2H_6 + NH_3$	4 W	Si, graphite or BN; 700-1000	Reflection Electron diffraction, TED, EMPA, IR, Electronic measurements	hexagonal film, ε=2.7-7.7, ρ=2x10^9 Ω-cm, good insulating properties.	121
$B_2H_6 + NH_3$	1-40 W	p-Si, n-GaAs & SiO$_2$; 300	AES, XRD, Raman, IR, UV, Electronic measurements	Hexagonal Films, n=1.75, E_g=5.0 eV, ε=6.5, breakdown strength 3x10^6 V/cm, film properties strongly depends on NH$_3$ to B$_2$H$_6$ ratio.	122
$BH_3.N(C_2H_5)_3$/ $BH_3.NH(CH_3)_2$ /Ar/NH$_3$	double plasma 150/15	290-600	IR, XPS, Electron diffraction and electronic measurements	hexagonal films, ε=3.7, breakdown field 3x10^6 V/cm, good insulating films, presence of O & C in films.	124
$BH_3.N(C_2H_5)_3$/ $BH_3.NH(CH_3)_2$ /NH$_3$	50 W	n-InP 300	XPS, Ellipsometry, Electronic measurements	hexagonal films, n=1.6-1.71, ε=4-5.2, ρ=10^{11}-10^{12} Ω-cm, breakdown field 3x10^6 V/cm, presence of O & C.	125a
$BH_3.NH(CH_3)_2$ /NH$_3$	50 W	n-InP & Si, 320	XPS, Ellipsometry, IR, UV & Electronic measurements	hexagonal films, n=1.68-1.73, E_g=5.8-5.9 eV, ε=3.5, interface state density=(2-6)x10^{11} /cm^2-eV, ρ=(1-5)x10^{13} Ω-cm, presence of O, C & H.	125b
BCl$_3$/NH$_3$/Ar		Die steel & graphite 550-620	SEM & XRD	amorphous coatings with small hBN, deposition rate depends on pressure & substrate temp., presence of Cl$_2$.	127

Table 2.9 (continued)

borazine & H_2	100 W/cm^2	Si 475-550	AES, ESCA, XPS, IR, RBS, EMPA & TEM	Films of poorly crystalline hBN & cBN; presence of H_2 in the films, stoichiometric film & better quality than CVD BN films.	128,129
$B_2H_6 + NH_3$	10-50 W magnetic field	200-400	FTIR, AES, XPS, Ellipsometry & UV	Hexagonal films, ε=4.0-4.8, n=1.7-2.8, E_g=5.6-5.8 eV; no effect of applied weak field on film property.	131
$B_2H_6 + NH_3$	100 W with filament	Si 800	IR, TEM & SEM	pure cBN films, strongly depends on filament temp., cBN obtained at >1600°C; nothing given on mechanical characterisation and adhesion.	38
BH_3-NH_3 or H_3BO_3 or $NABH_4$ & NH_3 or H_2	100-200 W with filament	Si 800	IR & Photoemmission Spectroscopy	Film growth at >1500°C filament temp., mixture of hBN & cBN, no adhesion data, <1500°C filament, no peaks in IR is surprising.	134
B/H_2/N_2	3.5 KV x1.22 A 4 MHz	n-Si	AES, TED, XRD, IR	Films of cBN & hBN mixture, polycrystalline film, no other properties given.	143
BCl_3/NH_3/Ar /H_2	2-3 kW+ laser irradiated	Si 500-900	TED, TEM, SEM, AES & IR	films with 10 nm size crystallites, mixture of hBN & cBN (claimed pure cBN), no other properties.	147
BF_2/N_2/H_2	75 W	Si, glass, NaCl, KBr & KCl 300	SEM, XRD, Ellipsometry, UV	Films of mixture of hBN & cBN (or wBN), n=1.52-1.77, poor adhesion, E_g=5.0-5.6 eV	136

CHAPTER 3

DEVELOPMENT

OF

A PACVD SYSTEM

3.1 INTRODUCTION

As cBN crystalline material exists in equilibrium only at temperatures above 2000K and pressures above 12 GPa, the formation of cBN thin films is very difficult under more favourable conditions. It appears from chapter 2 that for successful deposition of cBN thin films from any deposition techniques either PVD or CVD, the technique must include the input of additional energy from energetic ions during the deposition process. The growth of hard BN films requires ion bombardment during the deposition to form the high temperature, high pressure metastable phase and to remove the soft hBN phase. As PVD techniques have yielded the most promising results before the commencing of this work, designing a PACVD system incorporating the "so-called" additional energy inputs was not straight forward. As the whole cBN deposition system was designed and made in our laboratory, it was gradually developed and improved time to time according to the problem faced and to deliver more excitation into the system when previous technique failed. But the basic idea behind the design was that in PACVD technique, the ion-acceleration towards the substrate is due to negative self-bias of the substrate by the plasma electrons, by the r.f. driven voltage swings of the plasma potential and in some cases, externally applied voltage.

As mentioned, the conventional source compounds used in the literature, at least at the commencing of this work, have serious defects, including serious safety problems due to the toxicity and/or highly inflammable nature of the source compounds. This work was also motivated to explore a non-toxic source material to deposit hard phase of BN thin film. Low temperature requirement for the deposition of most of the electronic base materials and some of the cutting tools (e.g. steel) should also be maintained in our deposition system for BN thin films. Our primary target was to deposit BN films at 350°C.

Judging all the constraints for a PACVD system, we designed and developed a PACVD experimental technique in our microelectronic laboratory to deposit BN thin films from a nontoxic material at low temperature with a view to possible use of these films primarily in electronic materials and eventually as mechanical wear-resistant coatings.

3.2 EXPERIMENTAL SYSTEM

A simple low temperature system was developed initially in our laboratory without any commercial equipment to understand the PACVD system and to monitor the growth of BN films with respect to different plasma excitation and other deposition parameters. In the next step, this low-temperature system was modified to incorporate moderate temperature growth and to include some activation energy sources.

To avoid some practical difficulties faced during the course of the experiment, we modified our modest temperature system to get the final system in this work. Here we will give an account of all these systems.

3.2.1 LOW TEMPERATURE SYSTEM

The experimental system used initially is shown in fig. 3.1. It consisted of a pyrex glass bell-jar type chamber with an associated pumping system. The diameter of the tube at the reactant side was 3 inches and that at the substrate side was 6 inches.

The plasma was generated by using a 13.56 MHz r.f. generator coupled inductively or capacitively with the system. Further, to minimize surface damage by highly energetic particles, the substrate holder was placed downstream of the plasma zone corresponding to an indirect PACVD process.

Substrates were placed onto a heatable, optionally biased or grounded stainless steel support plate. The substrate was not water cooled.

The chamber was evacuated by a two-stage rotary pump (Edwards; 47 litre min^{-1}). The lowest possible value of pressure produced was less than 8×10^{-2} mbar and was monitored by a Pirani gauge calibrated for nitrogen gas.

Commercially available (Alfa Products) borane-ammonia (BH_3-NH_3) was used as a non-toxic source material to deposit BN films. This reactant was evaporated either inside or outside the plasma chamber. Inside the plasma chamber, the reactant was evaporated by using a resistance-heating system from a BN crucible. At high r.f. power, the reactant was evaporated outside the reaction chamber and was introduced in the chamber by using nitrogen as a carrier gas. The gas flow was monitored by the flow meters (Brooks Instruments, R-2-15-AAA).

All the feed-throughs in this system were made of PTFE (polytetrafluoroethylene). The temperature of the substrate holder as well as reactant holder was measured by a Chromel-Alumel K-type thermocouple attached to a digital microprocessor indicator.

3.2.2 FILM GROWTH

The chamber was evacuated to a pressure of 8×10^{-2} mbar and flushed with nitrogen gas for about 2 minutes. The chamber was re-evacuated to 8×10^{-2} mbar. After another flush with nitrogen, the base-pressure of 8×10^{-2} mbar was attained.

The reactant, borane-ammonia, was eveporated and introduced into the r.f. plasma chamber with the carrier nitrogen gas. The working pressure was maintained constant at 0.7 mbar when the nitrogen flow rate was 6.5 standard cm^3 min^{-1}. Then BN films were deposited for a desired time.
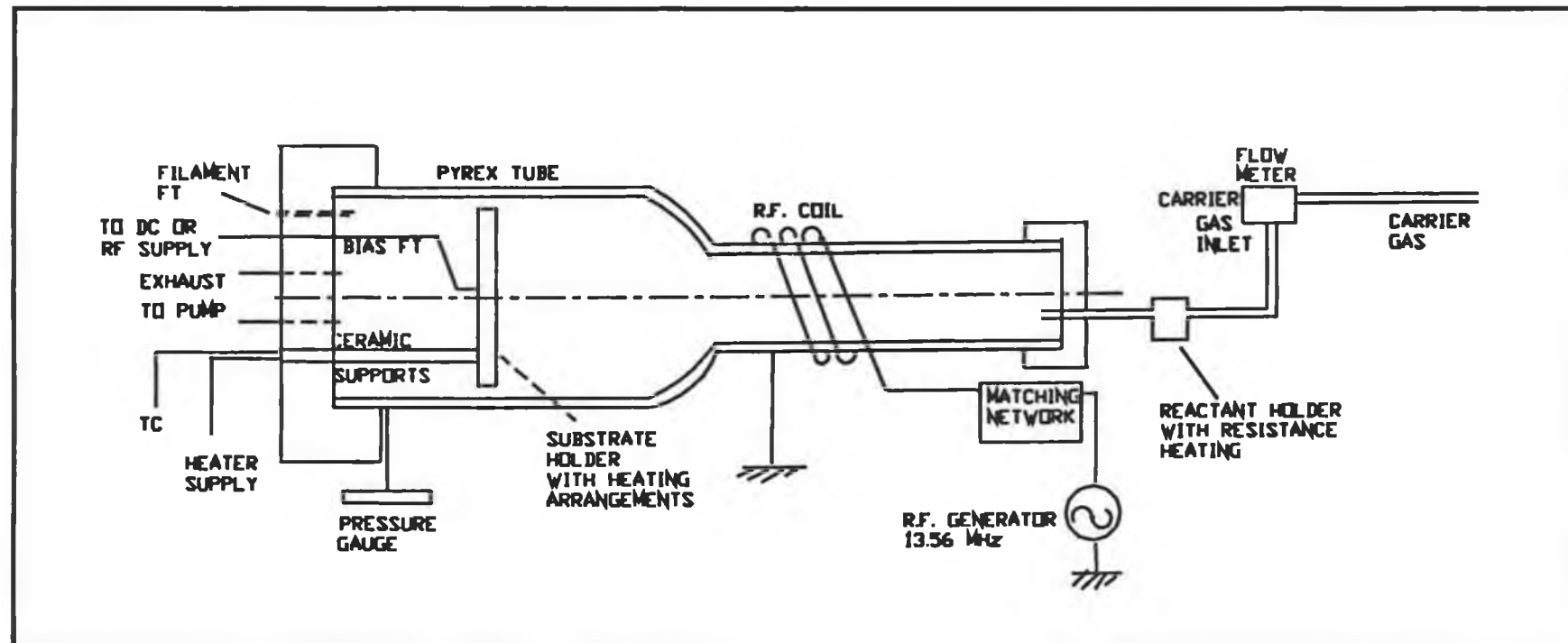
91

Fig. 3.1 : Schematic diagram of the low-temperature deposition system for BN thin films.

The film deposition was carried out with three types of plasma excitation: inductively coupled plasma with or without dc substrate bias and capacitively coupled plasma. In an inductively coupled system, the r.f. coil was coupled to the r.f. generator through an impedance matching network which will be detailed in section 3.5.1. The substrate was floated, or biased by connection to a dc supply. In the capacitively coupled system, the r.f. generator was connected to the substrate through a matching network and a blocking capacitor. In this system, the capacitor was a 1000 pF ceramic one. For the inductively coupled system, the r.f. power was varied from 0-200 W. For the dc excitation, the negative dc bias was varied from 0-400 V while the r.f. power was kept constant at 20 W. In the capacitively coupled excitation, the negative dc self-bias was varied from 0-900 V, measured directly from the RFX-600 rf generator (Advanced Energy). The deposition conditions are summarized in Table 3.1.

Table 3.1: Deposition conditions for the low-temperature system

Reactant	Borane-ammonia (BH_3-NH_3)
Carrier gas	Nitrogen (N_2)
N_2 flow rate (sccm)	6.5
Working pressure (mbar)	0.7
R.F. power (W)	0-200
Self-bias voltage (V)	0-900 (negative)
d.c. bias (V)	0-400 (negative)
Substrate temperature (°C)	48-180
Deposition time (min)	45-60
Film thickness (μm)	≈0.5-1.5

3.2.3 LIMITATIONS OF THE LOW TEMPERATURE SYSTEM

The results of the structure of BN film with respect to deposition parameters will be given in chapter 4. Only the general limitations we faced are stated as follows:

1. As we are using a Pyrex glass chamber it was not feasible to go to high deposition temperature. The highest substrate temperature for the inductively coupled system was 115°C at a r.f. power of 200W and the highest temperature for the capacitively coupled system was 150°C corresponding to -900V substrate bias.

2. The pressure monitoring through Pirani Gauge was troublesome for r.f. interactions.

3. It is difficult to get a low base pressure using the rotary pump of swept volume 47 litre per min. Low base pressure was needed to get low oxygen content of the films.

4. We faced problems in evaporating borane-ammonia. When evaporating inside the chamber, it was difficult to control the temperature of the BN crucible. The heater was heated without control by r.f. self-heating at high r.f. power. When evaporating outside the chamber, the gas supply system was warmed to about 40-50°C with heating tape in order to prevent condensation of the reactant on the way to chamber. But portions of the glass tube were difficult to heat and condensation occurs in that portion which goes through the feed through.

5. The PTFE feed through for r.f. power input was not capable of handling high temperature and high power situation in which case it showed cracking.

6. The smooth control of the flow of gas is difficult to obtain by flow-meters.

The technical limitations of the system are discussed in chapter 4. In short it was concluded that it was not found possible to deposit a good quality BN films in this system and further studies should be pursued to modify this system to accommodate more activation energy in this system [135a].

3.2.4 MODERATE TEMPERATURE SYSTEM

The experimental system shown in fig. 3.1 was modified to go up to a moderate substrate temperature, 350°C which is a suitable deposition temperature for most of the substrates such as GaAs, InP and high speed steel.

With a view to achieving deposition temperature, our moderate temperature system consisted of a quartz chamber and the substrate holder material was made up of 316 stainless steel.

To have ease of control on different deposition parameters, we further modified this system to get our final system for the deposition of BN films.

3.2.5 FINAL DEPOSITION SYSTEM.

The experimental system shown in fig. 3.2 was a modification of the system shown in fig. 3.1. Fig. 3.3 shows the photograph of the BN deposition system in our laboratory. Filament activation is the main feature of this system. In addition to that, smooth control of different deposition parameters and high-temperature handling capacity are the other

94

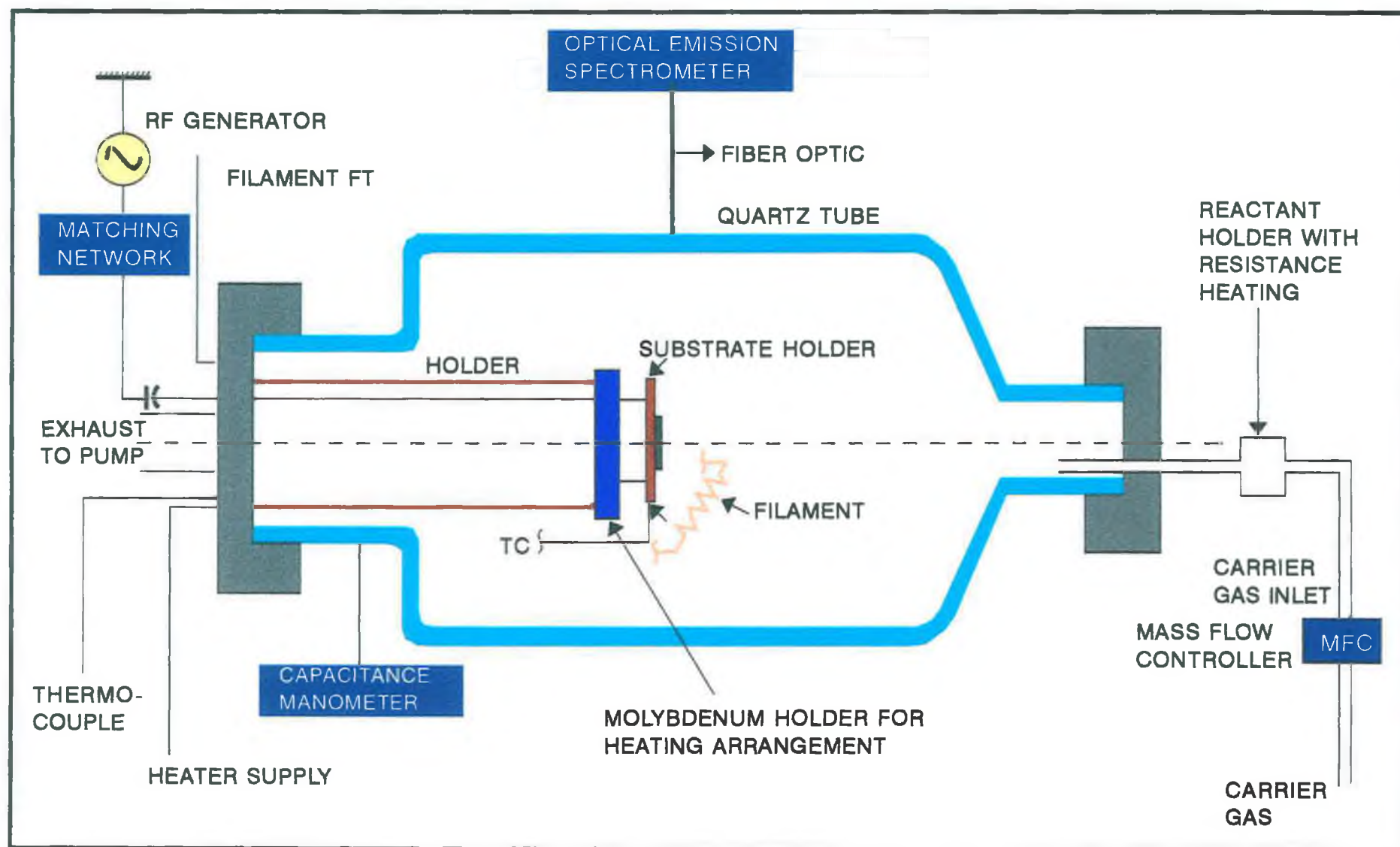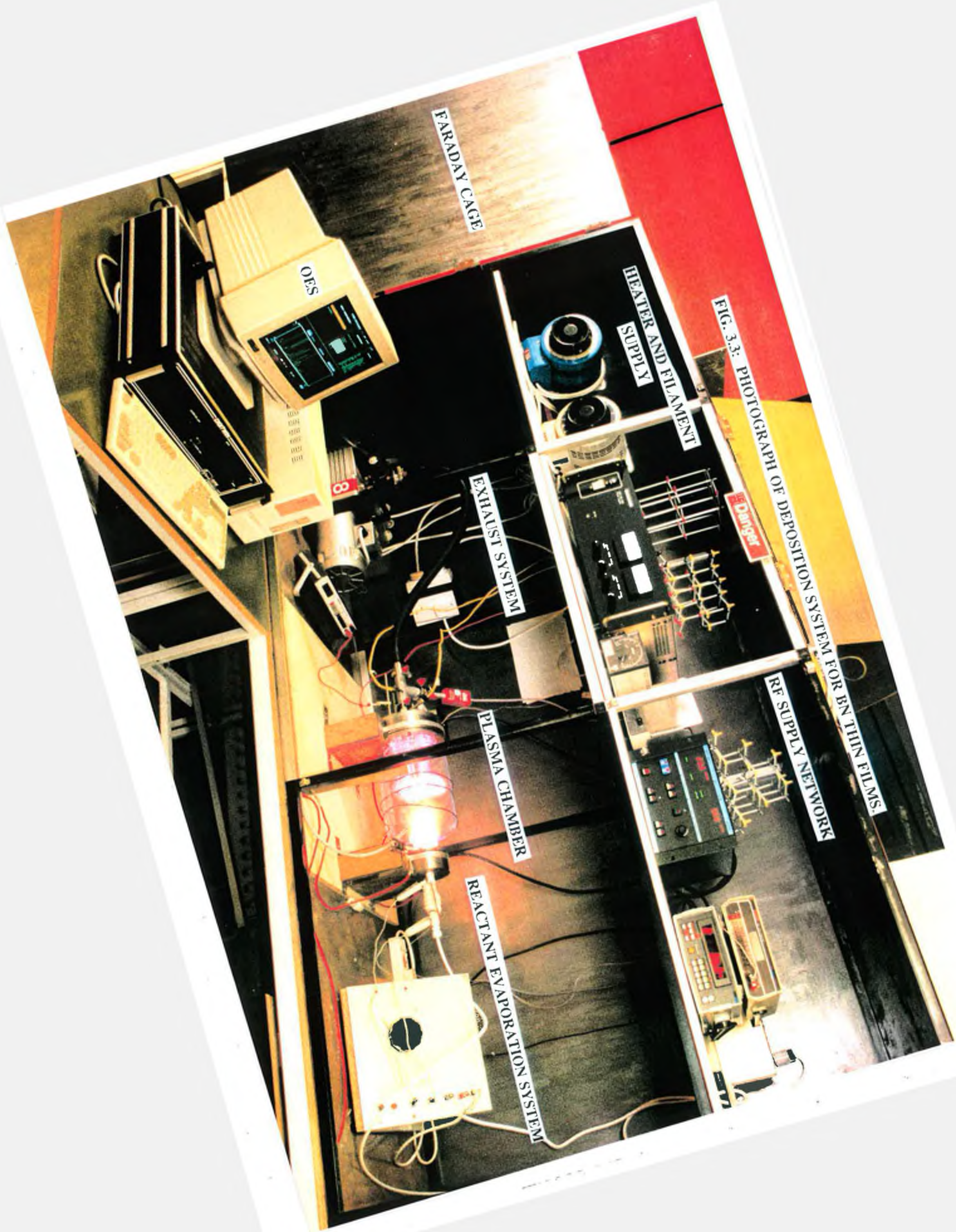Fig. 3.2 : Schematic diagram of final system for BN film deposition.

FIG. 3.3: PHOTOGRAPH OF DEPOSITION SYSTEM FOR BN THIN FILMS.

FARADAY CAGE

OES

HEATER AND FILAMENT SUPPLY

EXHAUST SYSTEM

PLASMA CHAMBER

RF SUPPLY NETWORK

REACTANT EVAPORATION SYSTEM

Danger

advantages of this system. We will describe this deposition system elaborately in the following sections.

3.2.5.1 Gas supply system

This system consists of reactant evaporation and introduction of this evaporant into the reaction chamber.

This PACVD system has provision for using three gases connected to the inlet. If needed, they are mixed together before entry into the chamber. They consisted of a reactive gas e.g. nitrogen N_2, a catalyst gas to prevent oxidation of the heating element e.g. hydrogen H_2 and a pre-etch gas e.g. argon. The reactor gas (99.99%) is admitted via a 1 metre long 'teflon' tube. The flow of the gases is controlled by electronic mass flow controllers (Tylan general FC280SA). The controller for N_2 gas is 0-100 sccm full scale calibrated with dry N_2. The controller for H_2 gas is 0-20 sccm full scale calibrated with N_2. The pressure in the chamber is maintained at a chosen value smoothly by means of a flow control unit (Tylan General, RO-28) on the gas admittance line. The admittance of all the gases are controlled by extra needle valves in addition to the solenoid valve control on the flow control unit.

The gas entry tube ended in the reactant evaporation unit. In this final system, the reactant evaporation unit consists of a glass vaporisation cell and a stainless steel tube entrance. The reactant, borane-ammonia (BH_3-NH_3), which will be described separately in section 3.3, is evaporated outside the plasma chamber in the vaporisation cell by using nitrogen as a carrier gas. The stainless steel reactant supply tube was warmed to about 40-50°C by r.f. self heating.

3.2.5.2 Plasma chamber

The r.f. plasma is generated in a quartz chamber of diameter 20 cm with two end plates of stainless steel. The smaller plate of diameter 75 mm holds the gas inlet steel feed through and the bigger plate of diameter 150 mm has 8 different-purpose ports. Inside the chamber, it holds the powered electrode with substrate and its associated heating assembly.

The bigger end plate houses feedthroughs for different purposes. The central port was 1" in diameter for the exhaust to the rotary pump. After the failure of PTFE feedthroughs to hold high r.f. power conductor in the previous system, a stainless-steel feedthrough was used to feed the power directly to the electrode plate. Usually stainless steel rod which is screwed to the electrode carried the r.f. power to the electrode plate of 75 mmx75 mm square. Symmetrically about the centre were five other PTFE feedthroughs, four of which supply ac current to heating coil and filament and fifth feedthrough is used to ground the heating assembly support plate. The other port was used for thermocouple feedthroughs. The chamber contains quite a number of O-ring seals.

There is an extra port on smaller end plate for optical emission spectroscopy (OES) window. But as OES studies were done directly holding the optical fibre port in different places of quartz wall, this port was blocked off with a blanking plug.

The heating coils, made of tantalum wire, were assembled in a molybdenum support plate. The wire was fed through high temperature ceramic tubing in parallel lines. The powered electrode plate which is also substrate holder was separated by 6 mm from the heating assembly due to a capacitive interactions between them (discussed in section 3.4). Substrate are clamped against this plate which can be stainless steel or molybdenum depending on the deposition temperature requirements. The substrate and heating assembly holders are electrically isolated from the end plate which is usually floated.

The electrode is usually capacitively driven with 100-400 watts of r.f. power at a frequency of 13.56 MHz generated by AE RFX-600. The smaller end plate are well-grounded, constituting an asymmetric arrangement. The r.f. power is coupled to the electrode plate through an impedance matching network with a blocking capacitor of parallel plate type to handle the high voltage condition.

A straight filament is situated very near to the substrate (~3 cm). The filament temperature was varied from 1300 to 1800°C (approximate values) determined by the current temperature relationship of an ideal tungsten filament [152].

3.2.5.3 Exhaust system

The chamber was evacuated by a two-stage rotary pump (Edwards; 158 litre min^{-1}). The base pressure attained was 6 mTorr (7.8x10^{-3}mbar) and was monitored with a capacitance manometer rated for full scale operation to 10 Torr. Such range has proved suitable for the r.f. plasma CVD system and allows the versatility of high pressure measurement. The manometer was located at the exhaust end of the chamber. Vacuum General 80-6A pressure display module was used to read the chamber pressure digitally in conjunction with Vacuum General CMLA transducer.

For long time use, a nitrogen gas stream was maintained to avoid hydrocarbon backstreaming from the pump oil.

The temperature of the substrate holder as well as the reactant holder was measured with a chromel-Alumel K-type thermocouple attached to a digital microprocessor indicator or millivoltmeter.

The pressure of the chamber was controlled by the total inlet gas flow rate and the variation of pressure for the present geometry of the cleaned chamber is shown in fig. 3.4

The plasma chamber with associated supply and monitoring system are fully rack mounted in an ergonomically convenient arrangement within a RF/EMI shielded Faraday box made of steel sheet to reduce r.f. interactions in surrounding labs.
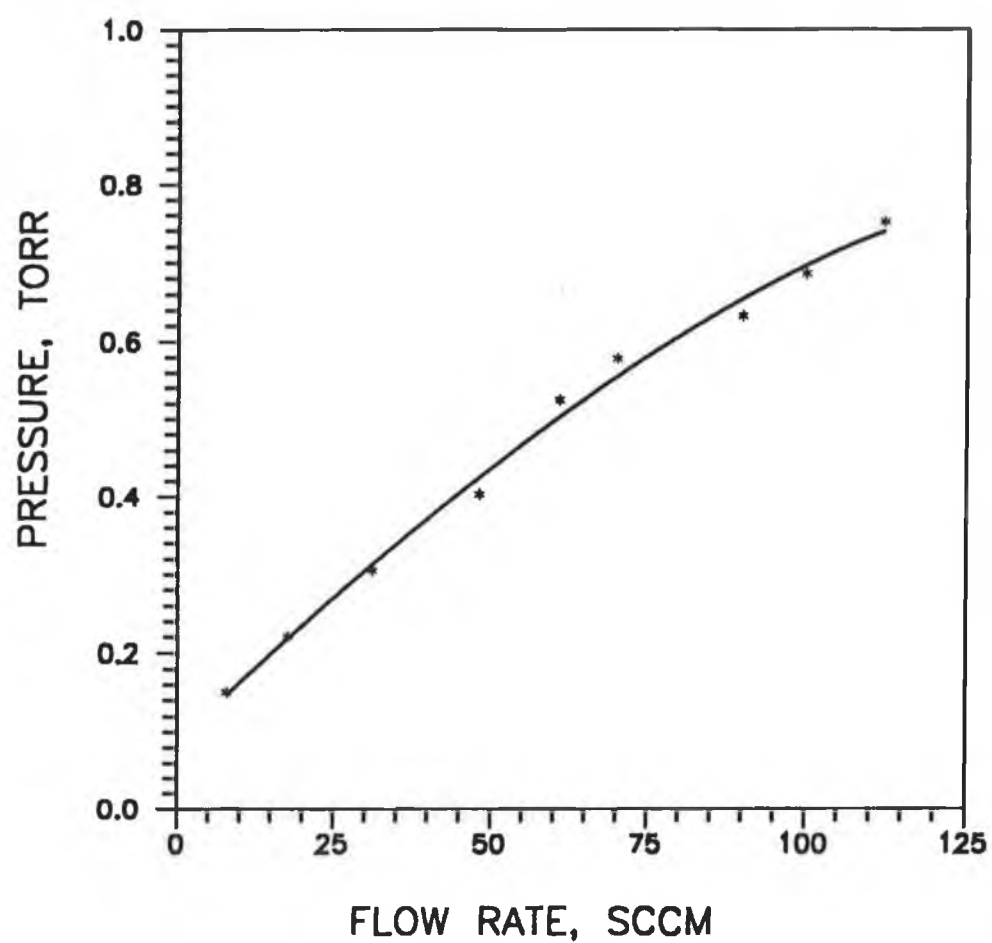
Fig. 3.4: Pressure of the final system as a
function of N_2 flow rate. The base
pressure is 6 mTorr.

Fig. 3.5 shows gas supply and reactant evaporation system, plasma chamber and exhaust system of the BN deposition apparatus.

3.3 REACTANT : BORANE-AMMONIA (BH₃-NH₃)

As a goal to produce pure BN films from a nontoxic source material, the reactant should have two properties: (1) It should be less thermodynamically stable so that the electron energy is sufficient to break the molecular bonds and (2) It should be free of impurities like oxygen, carbon etc. in order to deposit carbon free stable boron nitride films.

At the commencing of this work and even till now BN films are deposited mostly from toxic and/or highly inflammable materials like diborane, boron trichloride., boron triflouride, borazine etc. Nontoxic materials such as boric acid or boron di- or tri-ethylamine contains impurity materials such as oxygen or carbon.

Oxygen is very detrimental to the BN films and the films deposited from organic - boron compounds contains carbon impurity if deposited under 800°C . Other sources used are based on chlorinated six-membered B-N rings (e.g. hexa chloro-borazine). These precursors contain preformed boron-nitrogen bonds , but also have strong boron-chlorine bonds so that high deposition temperatures are required. There is also the problem of corrosive chlorine and chloride byproducts released by these reactions from all chlorine-boron compounds.

A potential source processing the boron-nitrogen stoichiometry and lacking strong halogen bonds or impurities is the adduct borane-ammonia, which has only hydrogen as a potential impurity that can be removed easily at low substrate temperatures.

For this reason, we proposed borane-ammonia as a nontoxic source material for the growth of cBN films in order to avoid serious safety problems as well as having the two properties mentioned above, compared to other known nontoxic source material, decaborane ($B_{10}H_{14}$), Ammonia boron was thought to be more volatile (melting point is much higher in the case of decaborane 170°C) and to be easier to decompose by the plasma energy.

3.3.1 PROPERTIES OF BORANE-AMMONIA (BH₃-NH₃)

Borane-ammonia is an air-stable white crystalline solid of density 0.74 gm/cm³ at room temperature. It is commercially available (Alpha product) powder of m.p. 112-114 °C. This low molecular weight compound starts decomposing at 70 °C.

Borane-ammonia was first synthesized and characterized by Shore and Parry [153], though most of its properties are still unknown [139].
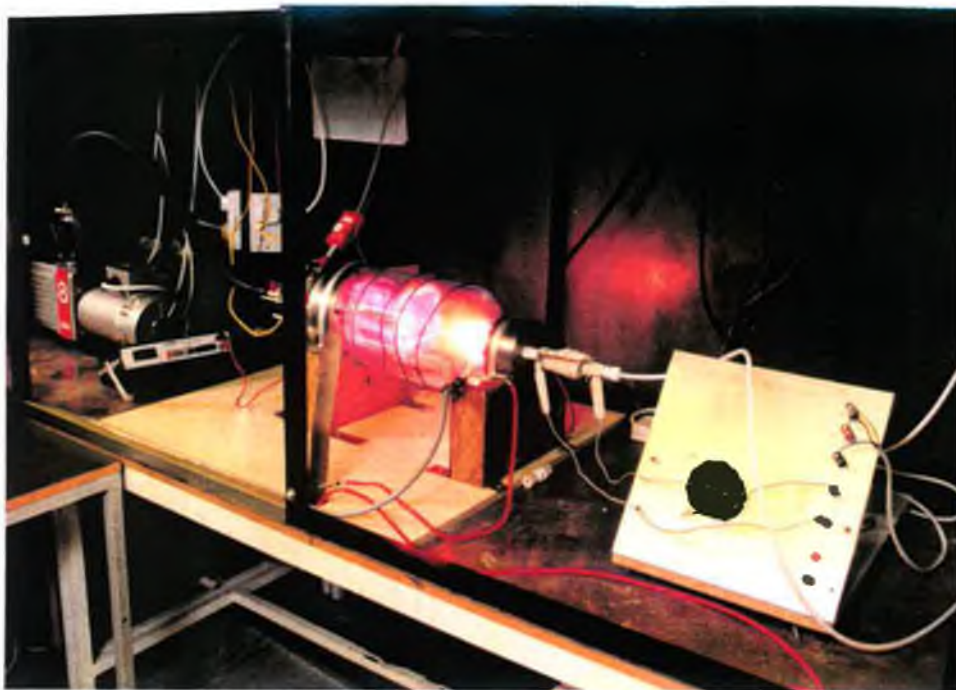
Fig. 3.5: Photograph showing gas supply system including mass flow controllers, reactant evaporation cell, plasma chamber, and rotary pump for the BN deposition system.

Numerous boron compounds being notorious examples of electron-deficiency, a useful classification of boron chemistry may start from distinguishing between classically and non-classically bonded boron atoms. In this context, the attributes "classical" and "non-classical" mean that the two-centre-two-electron approximation either describes the skeleton bonding situation sufficiently well or does not, respectively. The general distinction between a molecular and a solid-state structure may be superimposed, establishing four classes of compounds: classical molecular species (e.g. triethylborane, ether-trifloro-borane, etc) and classical solid-state species (e.g. boron oxide etc), on the one hand and non classical molecular species (e.g. diborane, dicarbodecaborane etc) and non-classical solid state species (e.g. elementary borane, calcium hexaboride etc.).

The diversity of traditional boron-nitrogen chemistry is dominated by classical molecules. The basic types are represented by amino-borane, $X_2B=NR_2$, and amine-boranes, X_3B-NR_3. A composition of average BN and CC bond length and force constants (fig. 3.6) demonstrates the weakest bond in single bond class.

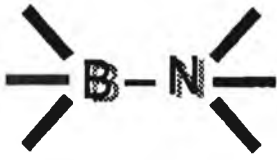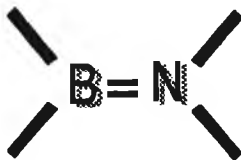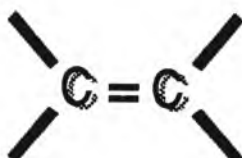|				
BOND LENGTH	158	140	124	pm
FORCE CONST.	3.7	7.5	13.0	N/cm
BOND LENGTH	154	133	118	pm
FORCE CONST.	4.5	9.4	15.7	N/cm

Fig. 3.6: Comparison of BN and CC bonds: bond length and force constant.

3.3.3 IR SPECTRA OF BH₃-NH₃ POWDER

The infra-red spectra of borane-ammmonia powder was taken by mixing a small amount of powder with KBr powder and by making platelets at high pressure. The infra-red spectra of such a sample is shown in fig. 3.7.

The peak at 3317 cm^{-1} was assigned to N-H or O-H band stretching. As the N-H peak is sharper than the O-H peak, the peak in fig. 3.7 might be due to overlapping peaks containing broad O-H peak and sharp N-H peak. Peak at 2338 cm^{-1} is due to B-H stretching. The peaks between 2000 and 1600 cm^{-1} could be due to any of N-H or O-H band bending. The peaks at 1381 and 781 cm^{-1} were assigned to in-plane and out-plane vibrations of B-N bonds respectively. But the peaks at 1165 and 1066 cm^{-1}, and 781 and 727 cm^{-1} occured possibly as a doublets. The bands due to certain boron-containing groups often appear as doublets, this being due to the presence of two naturally abundant isotopes of boron [154]. And it is unlikely to have a transverse optical mode vibration of cBN peak which occurs at around 1050 cm^{-1} in the borane-ammonia powder [154]. This two doublets could be due to B-O bond stretching and bending respectively with isotopic splitting present [154]. The doublet at 1165 and 1066 cm^{-1} could even be due to B-H in-plane deformation and the peak at 922 cm^{-1} could be B-H out-of-plane bending. In the later assumption, the later doublet could be due to B-N or N-H out-of-plane bending.

3.3.4 EVAPORATION BEHAVIOUR

At atmospheric pressure, borane-ammonia starts evaporating at just above 110°C. In the solid-state, H₃B-NH₃ is stable to at least 70°C. Even heating up to 200°C, the mass-loss is about 30%. If H₃B-NH₃ powder is heated instantly to 112°C or above, the solid starts boiling and sometimes evaporates with a blue flame.

At lower pressure, ammonia-borane starts evaporating at around 70°C extremely slowly and evaporation rate increases up to 100°C. Also at lower pressure if the temperature is increased instantly to 100°C, the solid starts boiling. This behavior was not well-understood, but we predict that this is due to any water constituent or due to vigorous hydrogen evolution. In ref. 132, it was found that the nitrogen was necessary to prevent rapid sublimation of H₃B-NH₃ and to facilitate its thermal decomposition. So to avoid sublimation and instant evaporation, we keep borane-ammonia at 40°C for about 15 minutes before evaporation in a nitrogen flow.

During experiment, H₃B-NH₃ powder is heated at 80 to 100°C for 1 to 2 hours. After evaporation, there remains a solid white residue which is usually corresponds to a weight loss of 30%. This residue is very difficult to evaporate avoiding boiling.
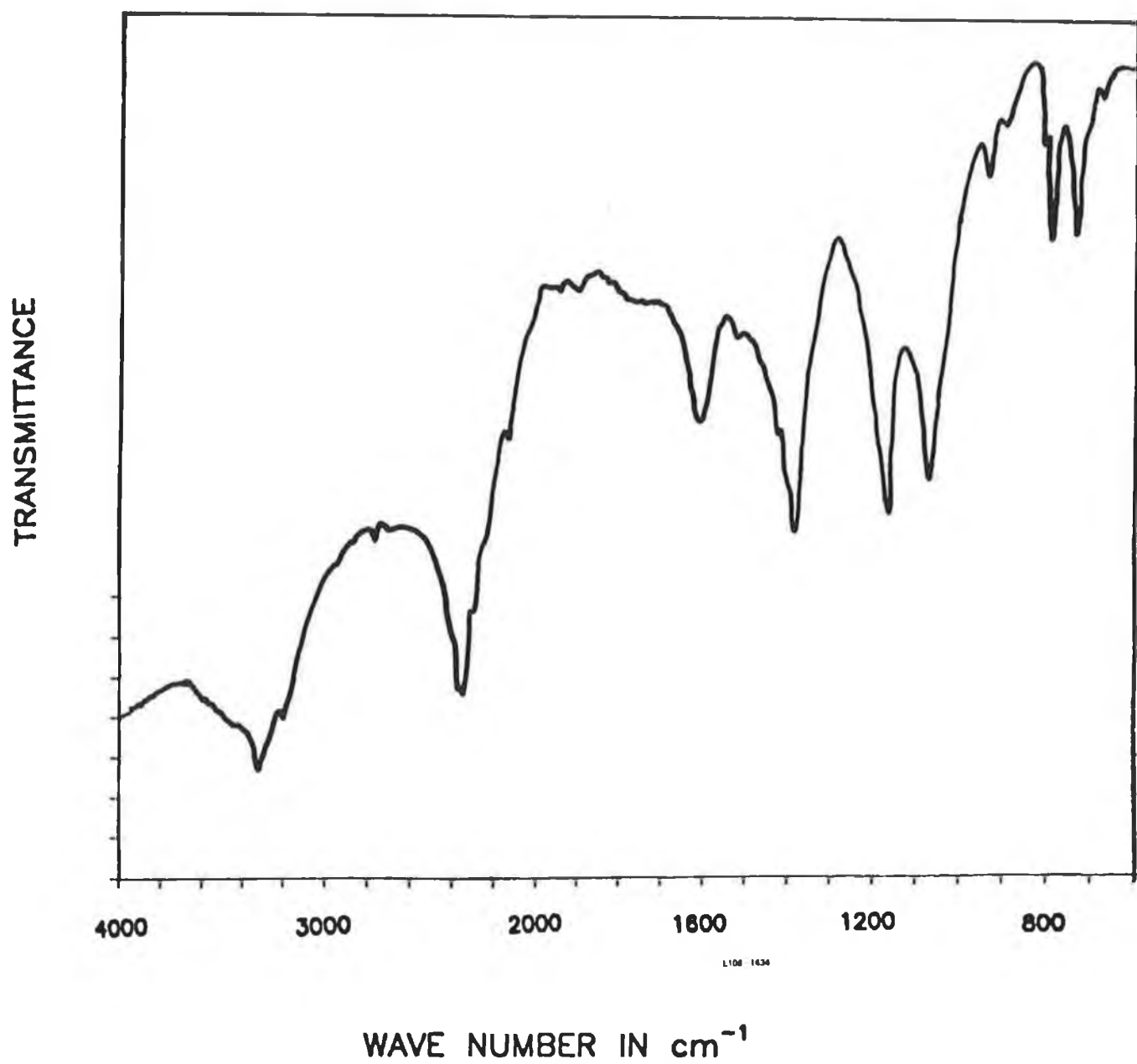
WAVE NUMBER IN cm^{-1}

Fig. 3.7: IR spectra of borane-ammonia (BH$_3$-NH$_3$) powder

3.3.5 GROWTH MECHANISM OF BN FILMS FROM BORANE-AMMONIA

The thermal pyrolysis of borane-ammonia is predicted with a two step reaction. In this two reaction steps [155], borane-ammonia undergoes thermally induced hydrogen loss. The first step involves hydrogen elimination in either an inter- or intra-molecular step shown in equation 3.1 and 3.2.

$$H_3N.BH_3 \rightarrow (1/x) (H_2N\text{-}BH_2)_x + H_2 \qquad (3.1)$$

$$2H_3N.BH_3 \rightarrow H_3N.BH_2\text{-}NH_2.BH_3 + H_2 \qquad (3.2)$$
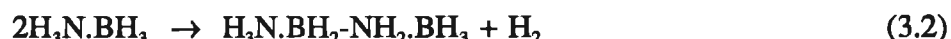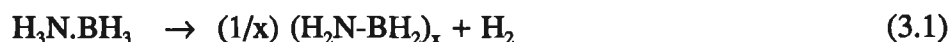
Amino-boranes such as would be produced in equation (3.1) are well known to associate, whereas the adduct produced in equation (3.2) could form extended B-N structure via further intermolecular H_2 elimination with additional $H_3N.BH_3$ molecules. In both cases, the ultimate result of this first stage of hydrogen loss is a material with BNH_4 composition. Earlier workers [156] have isolated and characterized several examples of such compounds including $(BNH_4)_2$ (cyclodiborazane), $(BNH_4)_3$ (cyclotriborazane), $(BNH_4)_5$ (cyclopenta-borazane) and polymeric $(BNH_4)_x$.

It is reasonable to suppose from this and other observations that $(BNH_4)_x$ materials may experience a second hydrogen loss shown in equation (3.3)

$$(1/x) (H_2N\text{-}BH_2)_x \rightarrow (1/x) (HNBH)_x + H_2 \qquad (3.3)$$
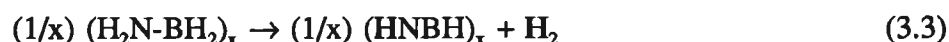
It was found [132] that low pressure nitrogen plasma treatment of $(BNH)_x$ films converts them to compositions approaching BN depending upon the length of the treatment time. Material that had been plasma treated for longer times or at high power densities was analyzed for the empirical formula of $BNH_{0.5}$ in that work.

However, the deposition of BN films cannot be explained by the pyrolysis mechanism only. These intermediate compounds are dominant species for deposition of BN films. This compounds are volatile and thought to be decomposed by the plasma electron energy. In view of this, the deposition might not occur on the substrate surface due to their volatility and only BN deposits on substrate. Again, if there is any deposition of intermediate species, removal of nitrogen-bonded hydrogen (bond strength 3.2 eV) and boron-bonded hydrogen (3.5 eV) will be performed by substrate temperature and ion-bombardment from the plasma.

Eitherway, this suggests that the adduct compounds contribute to deposit BN films, structure of which will be dependent on deposition parameters.

3.4 ROUTE TO FINAL SYSTEM

On the way of building a non-commercial deposition system in our laboratory, we have faced a number of problems and difficulties. To improve the system and to make it an efficient rig, we had to alter the system time to time and ultimately ended up with the final system for the deposition of BN films. In this section, we will give some of the difficulties solved which we think worth mentioning.

3.4.1 RF GROUNDING AND SHIELDING

When working with r.f. plasma, it is essential to appreciate the subtleties and difficulties associated with radio frequency design viz. different measurement can only be hampered by high level of r.f. noise, so that it is important to know how to minimize interference. After facing several problems with the r.f. interference both inside and outside the lab, we improved the grounding and shielding of our system. A few points about grounding and shielding of the r.f. system worthy of consideration are listed below.

3.4.1.1 Ac and dc grounding

The impedance of any length of conducting wire is

$$Z = R + j\omega L \qquad\qquad (3.4)$$

where R is the resistance given by

$$R = \frac{\rho l}{A} \qquad\qquad (3.5)$$

and L is the inductance of the wire. At low frequencies, Z is dominated by the resistance term and is small, whereas at high frequencies the inductive term may dominate. Thus in the real world there is a significant difference between the techniques used to provide a good dc ground and those used to provide a good ac ground. Apparent conductors may in fact represent quite large impedances at radio frequencies, at high frequencies the resistive term increases, due to skin-effect. Hence great care must be used when grounding r.f. systems.

In general, grounding wires must be of large surface area, and as short as possible; thus whenever possible, copper straps are normally used. A 8 ft x 4 ft copper sheet was used as a ground plate and unique grounding points are desirable, avoiding ground current loops. RF compatible connectors and r.f. co-axial cable was also used. Peculiar to r.f. systems, however, wire loops were avoided, since induced fluxes are proportional to the enclosed areas.

3.4.1.2 RF shielding

While significant number of r.f. problems are caused by improper grounding of r.f. power supplies used in the system, a plasma chamber is a type of oscillator and radiates r.f. energy if not shielded. As a result, radiation losses become significant at high radio frequencies. In the worst cases, this energy can cause noise in equipment at some distances from the source, often hundreds of feet or more away. Vacuum systems contain also vacuum pumps, solenoid valves, motors, power supplies and many other noise producers.

To avoid these noises, the following procedure was adopted in our system:

(1) RF filters were installed on the main-sockets of all equipments including r.f. power supplies. This greatly reduced noises in external circuitry, as there was considerable r.f. pick up on the grounds of the r.f. generator cables.
(2) The whole deposition system was surrounded by a Faraday cage - the classical "metallic barrier" against all sorts of electromagnetic fields because of stray airborne r.f. from the chamber. Its effectiveness depends on the selection of the shielding material and the geometry of its openings.

SELECTION OF MATERIAL FOR FARADAY CAGE

The idea behind r.f. shielding is that time-varying EMI fields induce currents in the shielding material. The induced current dissipate energy in two ways: I^2R losses in the shielding material and radiation losses as they re-radiate their own EM fields. The energy for both of these mechanisms is drawn from the impinging EMI fields - thus the EMI is weakened as it penetrates the shield.

More formally, the I^2R losses are referred to as absorption loss, and the re-radiation is called reflection loss. As it turns out, absorption loss is the primary shielding mechanism for H-fields, and reflection loss is the primary shielding mechanism for E-fields. Reflection loss, being a surface phenomenon, is pretty much independent of the thickness of the shielding material. Both loss mechanisms, however, are dependent on the frequency (ω) of the impinging EMI field, and on the permeability (μ) and conductivity (σ) of the shielding material. These loss mechanisms vary approximately as follows:

$$\text{reflection loss to an E-field (in dB)} \sim \log (\sigma/\omega\mu) \qquad (3.6)$$

$$\text{absorption loss to an H-field (in dB)} \sim t\sqrt{(\sigma\omega\mu)} \qquad (3.7)$$

where t=the thickness of the shielding material.

The first expression indicates that (1) E-field shielding is more effective if the shield material is highly conductive and less effective if the shield is ferromagnetic, and (2) that low-frequency fields are easier to block than high-frequency fields. Copper and

107

aluminium both have the same permeability, but copper is slightly more conductive , and so provides slightly greater reflection loss to an E-field. Steel is less effective for two reasons. First, it has a somewhat elevated permeability due to its iron content, and second, as tends to be the case with magnetic materials, it is less conductive.

On the other hand, according to the expression for absorption loss to an H-field, H-field shielding is more effective at higher frequencies and with shield materail that has both high conductivity and high permeability. In practise, however, selecting steel for its high permeability involves some compromise in conductivity.

Now in the near field, the EMI could be 90% H-field, in which case the reflection loss is irrelevant. It would be then advisable to beef up the absorption loss, at the expense of reflection loss, by choosing steel. A better conductor than steel might be less expensive, but it would also be ineffective.

The presence of seams, joints and holes in the physical structure of the enclosure has a big effect on the shielding. The shielding mechanisms are related to the induction of currents in the shield material, but the currents must be allowed to flow freely. If they have to detour arround slots and holes, the shield loses much of its effectiveness.

FARADAY CAGE IN OUR LAB

As the Faraday cage made up of aluminium did not work effectively, the present cage is made up of steel sheet. The effectiveness was proved to be satisfactory and little interference could be found in the adjacent laboratories. To avoid the effect of seams, joint and holes of our Faraday cage, all the walls are joined with copper.

The characteristic impedance of air is approximately 350 Ω, so that it is possible to match the output impedance of cables, etc. to this input impedance with resulting maximum power transfer. Clearly, this should be avoided, and is best done by using shielded cables with low characteristic impedance.

3.4.2 SUBSTRATE HEATING

As mentioned, to have wide range of substrate temperatures, we replaced our substrate material and chamber wall by molybdenum and quartz instead of 316 stainless steel and pyrex respectively. Tungsten wire was used to heat the substrate by means of resistance heating. But it was inconveniently found that after a few deposition, tungsten wire oxidizes easily and produces a black coating on ceramic tubes and surrounding places. So we used tantalum wire instead of tungsten to heat the substrate. Tantalum wire is also easy to bend and less brittle than tungsten wire.

3.4.3 CAPACITIVE INTERACTIONS

We have a major problem of capacitive coupling between the electrode plate and heating circuit when the heating coils were assembled inside the electrode in our moderate temperature system. Due to this coupling, substrate bias was found to be reduced considerably and matching of the r.f. power was affected by the amount of current flow in the heating coils. Though it was very difficult to point out the problem initially, we later found out the capacitive coupling between them that interferes with the r.f. power transferred through a stray or mutual capacitance of 12.6 pF.

We solved this problem by separating the electrode plate from the heating assembly holder by 6 mm and grounding the heating assembly holder. The schematic diagram of the substrate and heating arrangements is shown in fig. 3.8.
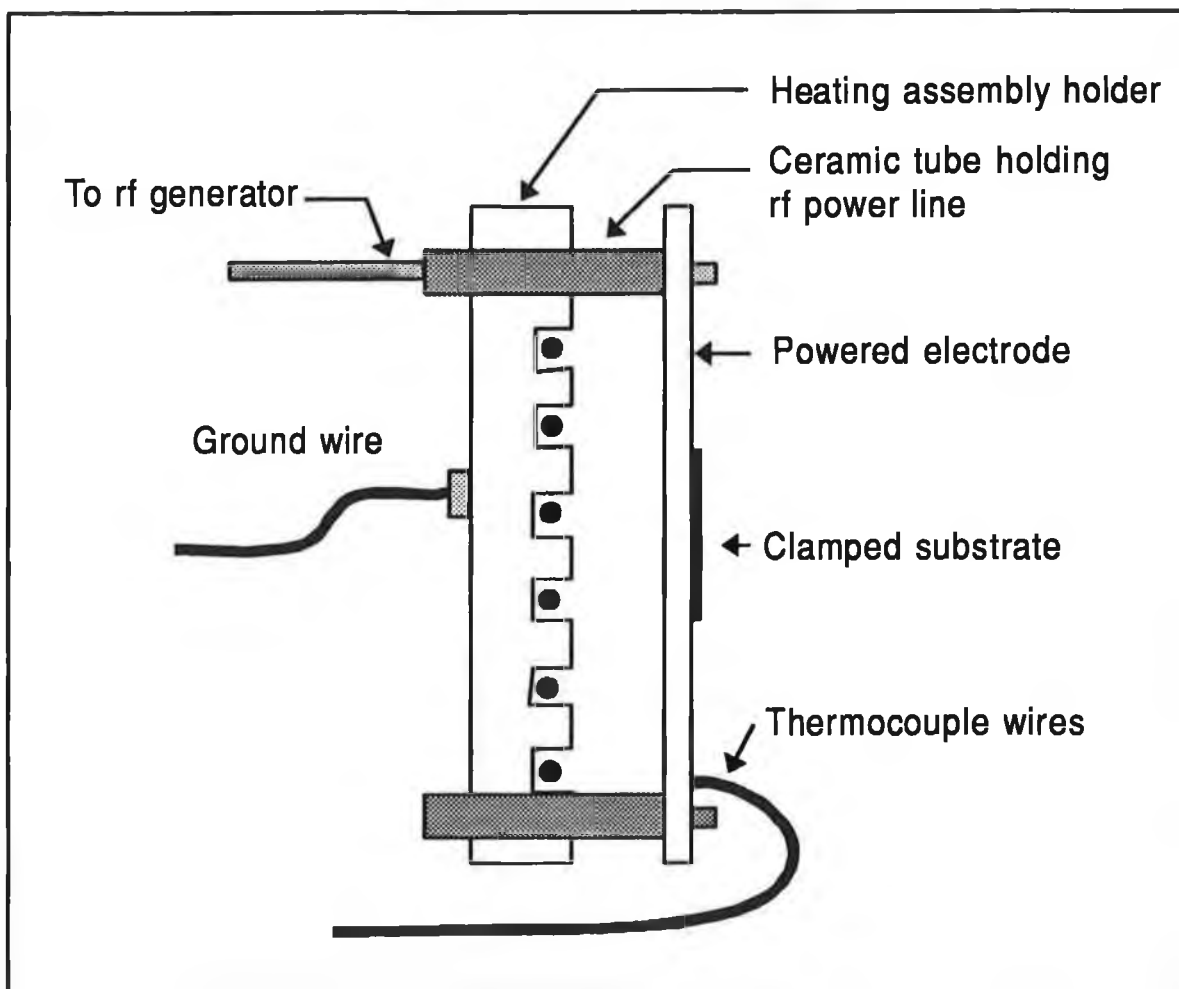
Fig. 3.8: Schematic diagram of the substrate and heating assembly holders in the final system.

3.4.4 EVAPORATION OF REACTANT

We faced difficulties to evaporate reactant, ammonia-borane evenly and it was also difficult to control the evaporation. Also sublimation and condensation of the reactant in the flow tube is a problem.

To avoid sublimation and condensation of the reactant, the gas supply system was warmed to 40-50°C by heating tape and the inlet tube was replaced by stainless steel tube to get r.f. self-heating. Also, reactant was heated to 40-50°C for at least 15 minutes prior to evaporation.

3.4.5 PRESSURE GAUGE

We used, at the beginning, a Pirani gauge to measure the pressure as reported in ref. [135a]. But it was difficult to measure pressure or gas flow accurately when r.f. is on as well as smooth control of gas flow and precise pressure measurement was difficult.

To have ease of control on these parameters, we replaced the whole gas supply system by a capacitance manometer and mass flow controllers.

3.4.6 HOLLOW CATHODE PLASMAS

There are always a hollow cathode plasma generated inside any hollow passage. In these passages, the plasmas are very dense and generate very high local temperature.

We avoided these hollow passages but the plasma generated inside the 4 mm reactant inlet tube was difficult to remove at higher r.f. power. Grounding the heating tape supply in one end removes this hollow plasma, though sometimes it is difficult to control.

3.5 FEATURES OF FINAL SYSTEM

As shown in fig 1.8 (deposition variables), there are many deposition variables which need to be controlled or monitored. Very many of these parameters have direct film characteristic relationships. A general rule of thumb used in the design was to monitor as much as possible and as accurately as possible. Close attention was paid to the practical considerations for r.f. plasma deposition systems and to possible future applications in the research laboratory. The reliability of the unit must be high for maintenance of quality. This means that the capacity of each component element should be stable and the reliability should be high. Considering all these considerations, this deposition system was designed in our micro-electronics lab. Some features of this system are worth mentioning in this section.

110

The r.f. generator alone is insufficient to ignite a plasma. It is necessary that a matching unit be placed between the generator and the driven electrode [157]. Matching units can be constructed in different ways, but the fundamental purpose is to match the output impedance of the generator to the input impedance of the load. When this occurs, according to the maximum power theorem, total power transfer is achieved; i.e. no power is reflected from the load back to the source. In dc systems, maximum power transfer is achieved when the load resistance equals the source resistance. In ac circuits, maximum power transfer occurs when the load impedance Z_1 is equal to the complex conjugate of the source impedance Z_s. Thus if $Z_s = R + jX$, then $Z_1 = R - jX$, for a matched system.

The primary function of the matching unit is to force the load impedance to look like the complex conjugate of the source impedance, and this is done by inserting the appropriate resistances and reactances between the two. Since we are dealing with reactances, which are frequency dependent, a perfect match is achievable at only one frequency. Hence variable reactances are employed in r.f. matching units.

There are many possible networks which could perform this task. The best known is probably the L network of an inductance and a capacitance. Matching units can also be constructed using transformers. For example, broadband transformers have been used to match the generator output to the plasma impedance at frequencies between 1 MHz and 5 MHz. Impedance matching can also be achieved using resonances, where the plasma is made to resonate with the matching element at a desired frequency. Modern processing systems include an automatic matching network, which tracks the plasma impedance as r.f. power or gas pressure is changed.

However, we employed a Π-network of L-C circuit to match the power. As in our system, the r.f. power can be coupled inductively or capacitively with the system, a wide range of values can be obtained with the all element variable Π-network. This Π-network is thus able to match in either inductively coupled power or capacitively coupled power.

Fig 3.9 shows the equivalent circuit for the r.f. generator, the plasma and a typical Π-matching network. X_c is a blocking capacitor. The plasma is represented in a simplified model of capacitor and resistor, $Z_p = R_p - jX_p$. The reactance term (X_p) is negative since we know the r.f. plasma impedance to consist mainly of a capacitive term [3.10]. Typically, the resistive part of the plasma impedance, R_p, ranges from a few ohms to tens of ohms, while the capacitive part, X_p ranges from a few tens of ohms to hundreds of ohms. In the actual matching unit used in all our 13.56 MHz plasma experiments, typically L ranges from 0.1 µH to 6.4 µH and C_1 ranges from 100 pF to 1000 pF and C_2 from 1 pF to 200 pF.

The impedance of the plasma depends on electrode area, electrode spacing, gas type, gas pressure and r.f. power. It may also be governed by the amplitude of the r.f. voltage, so that the discharge impedance may change over the r.f. cycle. The heating of
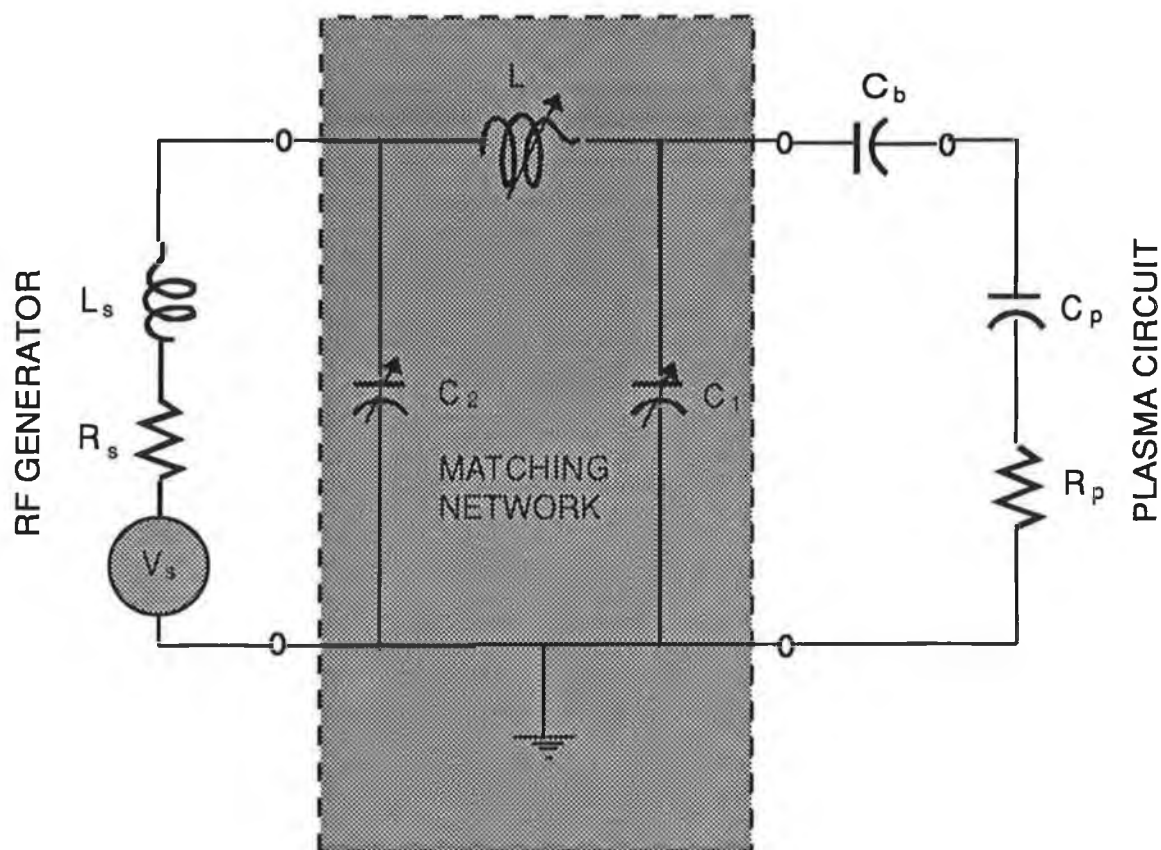
Fig. 3.9: Equivalent circuit for rf plasma system.

inductance coil due to r.f. is also a cause of change of matching. Thus a constant observation was done to match the reflected power during experiment.

3.5.2 FILAMENT ACTIVATION

After initial failure of getting a good cBN peak, a hot filament activation was incorporated into the system.

Generally, the feed gas is thermally activated by a filament made of a refractory metal selected from tungsten, tantalum, molybdenum, or rhenium and heated to 1600-2300°C. Tungsten filaments are a popular choice. The extreme temperatures at which the tungsten filament can be operated render it particularly suitable for these purposes. The hot filament enhances the dissociation of the feed gas as well as heating the substrate partially.

In our system, a straight tungsten filament was used 3 cm away from the substrate. The thermal activation process occurs at the surface of the hot filament placed in direct line-of-sight to the substrate where film growth takes place. Hot filament activation seems to be suitable because of the expected dissociation of the any of the products of equation (3.1), (3.2) and (3.3).

The temperature of the tungsten filament was measured by an approximate method described in [152] and also an accurate measurement of the temperature is problematic due to the possible BN coating on the filament as the growing film.

3.5.3 CAPACITANCE DIAPHRAGM GAUGES (CDG)

Capacitance diaphragm gauges (CDG) which were previously known as capacitance manometers, have become a ubiquitous part of the system used in the vacuum community because of their ease of use, compatibility with most gases, and potential accuracy and resolution. The CDG pressure measuring system provides rapid pressure determinations over a wide range with an accuracy and stability that is considered acceptable by a wide spectrum of users of vacuum technology and equipment.

This pressure measuring system consists of a pressure sensor, electrical circuitry to convert the physical reaction of the sensor into an electrical signal, and signal conditioning circuitry to process this signal into an output. The sensor is essentially a two-sided cavity, separated by a non-porous diaphragm. The operation of an modern CDG can be found in ref. 159. The long and short term stabilities are affected by such things as temperature variations, position and vibration.

Our CDG as described in section 3.2.5.3 is connected at the exhaust end of the system. CDG along with mass flow controllers gave a smooth control of the pressure.

3.5.4 FLEXIBILITY OF DESIGN

The flexibility in design of this vacuum coater permits the deposition of a range of thin films. The substrate holder can be biased with dc or r.f. potential allowing deposition of thin films onto conducting or non-conducting substrates. The thin films themselves can also be non-conducting, such as, silicon carbide, silicon dioxide, alumina, titania etc. when r.f. bias used. With r.f., potential applied to the substrate, ion-plating can be achieved. The deposition of conducting films onto insulating substrates and insulating films onto conducting substrates are possible.

The plasma can be generated using capacitively or inductively coupled systems. The case where ion bombardment on the growing film are necessary, the capacitive coupling would be suitable. To produce defect-free films, an inductively coupled plasma would be used. Moreover, as the substrate holder was placed always downstream of the plasma zone, the surface damage could be minimized while it is inductively coupled. As

the substrate temperature can be controlled easily, this system will be useful to deposit films for electronic purposes.

In this coater, films can be deposited from several gas mixtures (at present three inlet connections) or gas mixtures along with evaporation of chemical compounds e.g., this instrument could be used in this configuration to deposit diamond-like carbon films (DLC) from a gaseous mixture of methane/hydrogen or acetylene/hydrogen and/or argon. The deposition of compound films can be carried out in this apparatus. For example, B-C-N-H films can be deposited from B_2H_6, CH_4 and NH_3 gas mixtures. At the present system, even toxic gases can be used for film deposition.

Moreover, multilayered films can be deposited with some modifications.

3.6 FILM DEPOSITION

Prior to film growth, the substrates were cleaned by the usual techniques and clamped on the substrate holder for the deposition. This section describes the sample preparation and film deposition processes.

3.6.1 SUBSTRATES

Although the substrate is a mandatory part of any deposition system, without which the concept of films is lost, the substrate is often forgotten about or obliquely referred to. Specific application and film tests require different substrate materials which offer an acceptable compromise for the purpose on hand. Ideally, the substrate should provide only mechanical support, but not interact with the film except for sufficient adhesion. Main factors to be considered when choosing substrates would be their usefulness in a range of mechanical, optical, chemical and electrical tests on the films.

3.6.1.1 Choice of substrates

Silicon: As an intention to make metal-insulator-semiconductor structure, we primarily selected silicon as a substrate. It is also transparent to infra red light down to approximately 600 cm^{-1}. This allows the determination of BN bonding structure and whether bonding is sp^2 or sp^3 type, through infra-red spectroscopy.

The silicon substrates are cut into 25.4x25.4x0.5 mm size and n-type of orientation (100).

Steel: Steel substrate were chosen because it was ultimately hoped to be able to coat cutting tools. The samples were prepared from steel thin shim by cutting it 25.4x25.4x0.5mm size.

114

KBr: KBr were used as a substrate to confirm the c-BN IR peak. KBr platelets are prepared from KBr powder under pressure. Usually the size is 12.5 mm diameter of thickness 0.5 mm.

3.6.1.2 Substrate cleaning

Silicon: Mirror polished silicon wafers were etched by 40% diluted HF acid, washed in deionized water and dried in nitrogen blow. Then they were precleaned ultrasonically in an ethanol bath. They were dried in the nitrogen blow after washing in de-ionized water and held at the deposition temperature for at least 30 minutes under high vacuum to clean any residue and to get a uniform temperature over the substrates.

Steel: Steel platelets were continuously polished with silicon carbide paper, varying systematically in grit size from 320-4000 done in a Struers Tech's DAP type grinding and Polishing machine. The polishing residues were removed by ultrasonic agitation in ethanol bath at room temperature. After drying in nitrogen blow, the platelets were progressively polished on 6 µm and 3 µm diamond lapping wheels until the steel surface had a mirror finish. The polished samples were ultrasonically cleaned in ethanol bath after washes in 1,1,1 Trichloroethane. The dried samples were placed on the substrate holder and the chamber pumped to base pressure and backfilled with Ar gas to a pressure of 0.3 Torr. The sputter etching of the samples was accomplished by a 100 W r.f. power coupled capacitively to the substrate holder.

3.6.2 FILM GROWTH

The chamber was evacuated to a pressure of 7.8×10^{-3} mbar (6 mTorr) and flushed with nitrogen gas. The chamber was re-evacuated to 7.8×10^{-3} mbar (6 mTorr). The substrate was then heated to the deposition temperature 350°C and was held at 350°C for at least 30 min under vacuum to get a uniform temperature over the substrate. Then the filament was heated to required temperature and substrate temperature was adjusted to 350°C.

The reactant, BH_3-NH_3 was heated at 35°C for 10 min to evaporate its water content. After another flush, the base pressure 7.8×10^{-3} mbar (6 mTorr) was attained. The reactant was evaporated and introduced into the r.f. plasma reactor with the carrier nitrogen gas. The working pressure can be varied from 0.26 to 0.9 mbar by varying the flow of nitrogen from 18 sccm to 98 sccm. The gas supply system was warmed to about 40-50°C with heating tapes in order to prevent condensation of the reactant on the way to the chamber.

The film deposition was carried out with r.f. power of 100-400 W in all the experiments. The capacitive coupling gave rise to a negative self-bias on the substrate. Since the thermocouple is inserted in the sample holder with electrical insulation, the sample temperature will be somewhat higher than that recorded , though this was allowed

for with a correction factor. The deposition temperature of 350°C was attained again after turning on the plasma by varying current through the heating assembly. The filament temperature was varied from 1300 to 1600°C (approximate values) determined by current-temperature relationship of an ideal tungsten filament. The active system is shown in fig. 3.10. After every deposition, the heated substrate was cooled to room temperature in 80 sccm N_2 flow. The deposition conditions are summarized in Table 3.2.

Table 3.2 : Deposition conditions for the final system

Reactant	Borane-ammonia (BH$_3$-NH$_3$)
Carrier gas	Nitrogen (N$_2$)
N$_2$ flow rate (sccm)	18-100
Working pressure (mbar)	0.26-0.9
RF power (W)	100-400
Substrate temperature (°C)	350
Filament temperature (°C)	≈1300-1600
Deposition time (min)	45-90
Film thickness (nm)	100-300

3.7   SUMMARY

As mentioned for various semiconductor devices and cutting tools, it is important to cover the surfaces by suitable high-quality insulating films or by hard coatings (cBN or aBN has both the quality) under sometimes rather restricted deposition conditions. Also there are some important requirements for any BN deposition process or compound material semiconductors such as the quality of the resulting interface in spite of any volatility component present. Additionally the system needs to be flexible for any changes in deposition parameters. We designed our BN deposition system under the following constraints:

1) Only a low substrate temperature allowable,
2) Low heat of formation advisable,
3) The energy of the film producing particles must be small,
4) A non-toxic source material used, free from oxygen and carbon impurity,
5) A low-cost system utilizing very few commercial equipments.
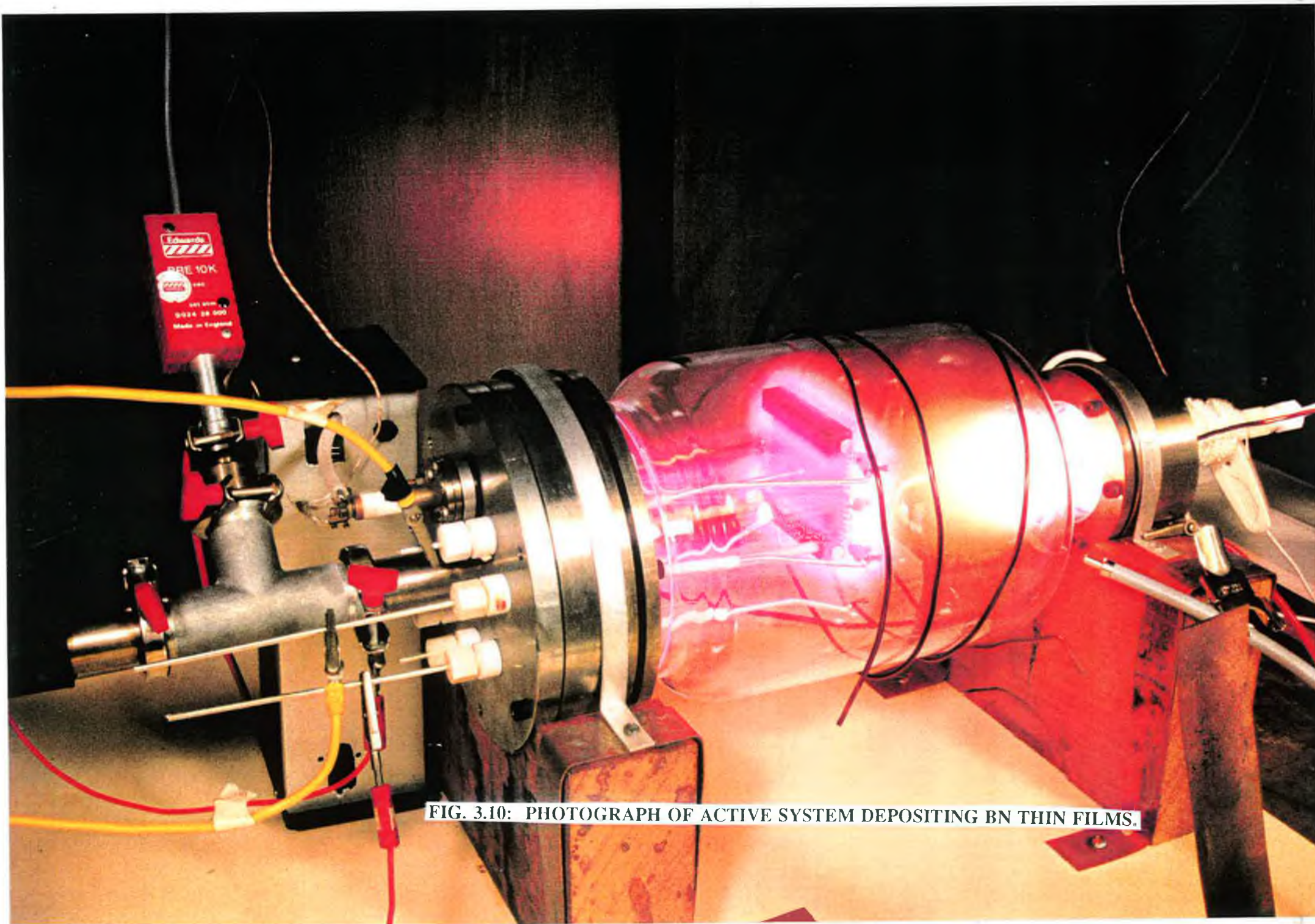
FIG. 3.10: PHOTOGRAPH OF ACTIVE SYSTEM DEPOSITING BN THIN FILMS.

To achieve the best BN film properties, a low hydrogen content in addition to an oxygen free film is essential. Oxygen content in the form of B_2O_3 has detrimental effect on the BN films and water contamination can occur in the hydrogen and oxygen content films. Water contamination appears to cause the formation of boron oxy-nitrides as well as other softer boron based compounds [66]. So the process parameters have to be optimized correspondingly. The following options are additionally available with our reactor:

(1) A change in the film characteristics during deposition with ion bombardment and/or filament activation.
(2) The possibility of using other suitable starting materials.
(3) The possibility of doping can be introduced.

Thus the present system could be used to enhance the required chemical reaction for the production of cBN films from borane-ammonia adduct by using low pressure plasma process which gives suitable electronically stimulated reactants under relatively low temperature conditions.

4.1 INTRODUCTION

In order to exploit the properties of BN, films of known and controllable physical, mechanical and electronic properties must be grown. These properties are strongly dependent on the deposition parameters, both large scale effects such as film thickness and uniformity and small scale effects such as crystal structures. As cBN films are difficult to grow under more favourable condition, the process parameters have to be optimised to get maximum cBN content in the deposited films. Varying different deposition parameters, a useful PACVD equipment to grow BN films from non-toxic borane-ammonia has been detailed in chapter 3 and this chapter details the different characterization techniques used to study the film properties under different growth conditions.

4.2 STUDY OF PLASMA BY OPTICAL EMISSION SPECTROSCOPY

Emission species played a very distinctive and important role in the development of analytical chemistry. Excitation of atomic species to produce characteristic emission spectra forms the fundamental basis of this technique.

4.2.1 PRINCIPLE OF EMISSION SPECTROSCOPY

Emission spectroscopy is based on the principle that excited atoms and ions emit radiation of a characteristic wavelength when electrons return to lower-energy orbitals. The electrons are regarded as existing in shells, or energy levels, at discrete distances from the nucleus. Under normal circumstances, the electrons are in their original shells, and the atom is said to be in the *ground state*. Excitation causes one or more electrons to be raised to higher energy levels, and the atom is then in an *excited state*.

When a gas or solid is atomized and partially ionized by plasma (or may be any other process), the electrons undergo transitions to higher energy levels. When an excited particle returns to a less excited plate, the emission wavelengths are determined by the difference in energy between the particular orbitals involved in the electron transition. The chain of events leading to emission is depicted in fig. 4.1. The transition of an atom from energy level E_2 to a lower energy level E_1 gives rise to a radiation quantum corresponding to the energy difference E_2-E_1 which can be expressed as

$$E_2\text{-}E_1 = hc/\lambda$$

λ is the wavelength usually expressed in nanometres (nm). These emitted quanta of energy originated from discrete transitions constitute the emission spectrum of the particular atom. As the electron configuration of each element is different from that of
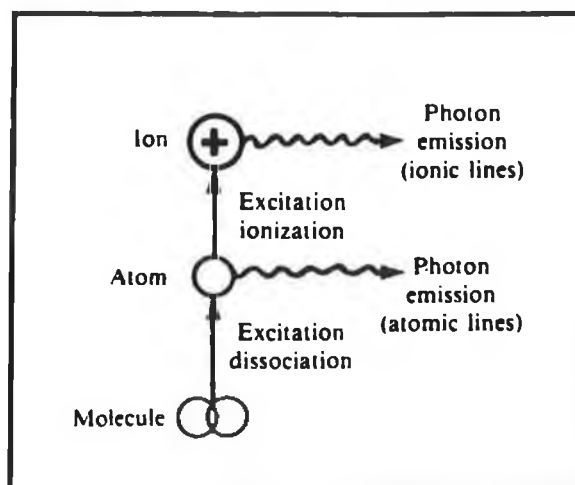
Fig. 4.1: The chain of events leading to emission.

other elements, its emission spectrum is also unique. In theory, if the electronic configuration of the elements are known, all the possible wavelengths can be calculated for each element but, in practice, wavelengths are determined experimentally and recorded in wavelength tables. Notation used for electronic transition is given in Appendix A.

4.2.2 EMISSION SPECTROSCOPY OF N_2

For the N_2 molecule, the lowest electronic configuration can be written as,

$$N_2 \ (Z = 14) = KK \ (\sigma_g 2s)^2 \ (\sigma_u 2s)^2 \ (\pi_u 2p)^4 \ (\sigma_g 2p)^2$$

Thus in the lowest state, both the $\pi_u 2p$ and $\sigma_g 2p$ orbitals are completely filled, and therefore the ground state is a $^1\Sigma_g^+$ state. The first excited electron configurations are KK $(\sigma_g 2s)^2 \ (\sigma_u 2s)^2 \ (\pi_u 2p)^4 \ (\sigma_g 2p)(\sigma_g 2p)$ and ... ... $(\pi_u 2p)^3 \ (\sigma_g 2p)^2 \ (\pi_g 2p)$. They account for the lowest observed excited states $^3\Pi_g$, $^1\Pi_g$, $^3\Sigma_u$ respectively. The second configuration, in addition, gives rise to the states $^1\Sigma_u^+$, $^1\Delta_u$, $^3\Delta_u$, $^1\Sigma_u^-$, $^3\Sigma_u^-$. Higher excited states are obtained by bringing the emission electron (taken from the $\sigma_g 2p$ or the $\pi_u 2p$ or the $\sigma_u 2s$ shells) to higher and higher orbitals.

The lowest electron configuration of N_2^+ can be written as

$$N_2^+ \ (Z = 13) = KK \ (\sigma_g 2s)^2 \ (\sigma_u 2s)^2 \ (\pi_u 2p)^4 \ (\sigma_g 2p)$$

The state $^2\Sigma_g^+$ is the ground state of the N_2^+ molecule. A third low-lying state $^2\Pi_u$ of N_2^+ is obtained by removing a $\pi_u 2p$ electron from N_2.

The energy level diagram of N_2 molecule is shown in fig. 4.2 [160,161]. Two ionization limits corresponding to the two states $^2\Sigma_g^+$ and $^2\Sigma_u^+$ of N_2^+ (at 125,666 and

120

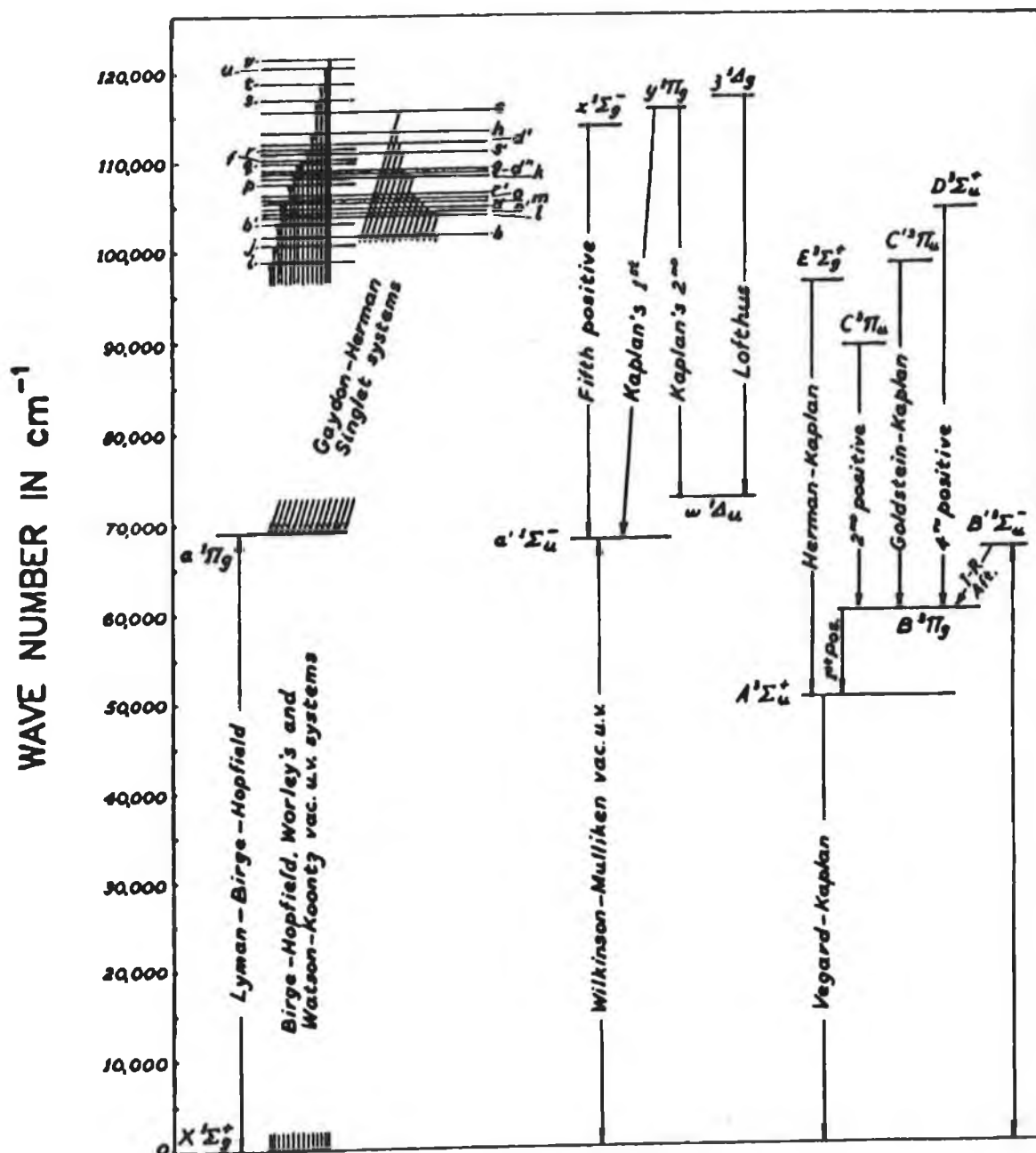**Fig. 4.2:** Energy level diagram of the N_2 molecule. Two ionization limits corresponding to the two states $^2\Sigma_g^+$ and $^2\Sigma_u^+$ of N_2^+ (at 125,666 and 151,232 cm^{-1}) are not shown in this figure [160,161].

151,232 cm^{-1} respectively) are not shown in the figure. Some levels of high energy are omitted to avoid overcrowding the lines.

4.2.3 EXPERIMENTAL SYSTEM

The essential components of an emission spectroscopic analytical system are, therefore, a source for excitation, a wavelength-dispersing unit, and an appropriate means for detecting and measuring the atomic spectral lines.

OES measurement were performed using an Optical Emission Spectrometer (DIGITWIN from Sofie Instrument). The detector has two changeable grids with 200-600 nm (UV) and 500-900 nm (VIS) range. The light emitted from the plasma was guided to the monochromator through the quartz wall by means of an optical quartz fibre.

The plasma emission intensities are measured directly from the spectrum by converting the height of the peak according to the gain of the system.

4.2.4 STUDY OF THE N$_2$ PLASMA

In order to get insight in the role of ion-bombardment of the growing film, we performed OES measurements at different rf powers with pure nitrogen plasmas applying the same deposition parameters. The light was sampled directly above the substrate holder in a dark room with no background light due to substrate or filament heating.

In a nitrogen discharge plasma, the First Positive System (FPS), attributed to the transition (B$^3\Pi_g$ - A$^3\Sigma_u^+$) and Second Positive System (SPS), attributed to the transition (C$^3\Pi_u$ - B$^3\Pi_g$) are the most readily developed, the second positive being the more easily measured in a plasma. Thus only the second positive system (SPS) due to nitrogen molecule is considered in our study which is in the 200-600 nm range of our spectrometer.

For N$_2^+$, First Negative System (FNS), attributed to (B$^2\Sigma_u^+$ - X$^2\Sigma_g^+$) occurs readily in a plasma at moderate pressure. The second negative system (SNS), due to the transition (C$^2\Sigma_u^+$ - X$^2\Sigma_g^+$) occured in 191-206 nm and the intensity is low, thus they are not considered in our study.

In SPS of N$_2$, the most prominent lines are 296.2, 316.4, 337.5, 353.5, 358, 375.5, 380.5, 399.4, 405.9 nm [161] which are all detected in all our discharges. In FNS of N$_2^+$, the two most prominent lines, 391.5 and 428.5 nm are considered. These lines have larger intensity than other lines in the same transitions. Other lines or systems are either weak or out of the range of our spectrometer.

The emission spectrum are taken at 10 W, 50 W, 100 W, 160 W, 200 W, 300 W and 400 W rf power coupled capacitively with the system and also with borane-ammonia

122

evaporation at 400 W. The plates of the spectrum at 10 W, 100 W, 160 W, 300 W and 400 W are given in plate nos. 1-5 and plate no. 6 represents the spectrum with BH_3-NH_3 evaporation. The amplitudes should be multiplied by the given factor corresponding to the gain of the system showed in each plate.

Table 4.1 tabulates the intensity of the peaks corresponding to characteristic wavelength attributed to either SPS of N_2 and FNS of N_2^+ at different rf power as well as other weak peaks.

4.2.6 DISCUSSIONS

No peaks due to the FNS of N_2^+ was observed 50 W rf power. The peaks due to SPS of N_2 were increasing with increasing rf power indicating a higher electron energy with the rf power. Up to 100 W, peaks due to FNS of N_2^+ are very weak. At 160 W, the plasma colour changes from pink to blue and a big peak attributed to FNS of N_2^+ at 391.5 nm appeared. A new peak also due to FNS of N_2^+ appeared at 428.5 at 160 W. Fig. 4.3 shows the colour of plasma at 100 W, 160 W and 400 W of rf power. With the colour change of the plasma at 160 W, the ion density is thought to be increased considerably at this stage.

With increased r.f. power, the intensity of all the peaks due to SPS of N_2 was increasing but after 100 W, the increase of FNS of N_2^+ was very sharp. At 400 W, the peak at 391.5 nm was increased by a factor of 25 times that of 100 W one whereas the most prominent peak due to SPS of N_2 was increased by a factor of 7.5. Fig. 4.4 showed the increase of the prominent peaks at 337.5 and 358 nm attributed to SPS of N_2 molecule and the prominent peaks at 391.4 and 428.5 nm attributed to FNS of N_2^+ with increasing power. This leads us to the conclusion that the additional power increases the ion density and, therefore, the ion flux onto the substrate also. This increased bombardment in turn leads to the formation of cubic phases in the BN films which will be discussed in 6.2.

Further OES measurements were carried out with addition of borane-ammonia vapour to the N_2 plasma. This leads to a slight decrease of the SPS peaks of N_2 but an increase of the peaks of FNS of N_2^+.

At lower rf power, there are five very weak peaks at 237.5, 249, 259, 272 and 283.3 nm. These peaks might be attributed due to γ system of NO ($A^2\Sigma^+$ - $X^2\Pi$) which is the most readily obtained. But these peaks disappears after 100 W. This is thought to be the high ionisation energy at higher rf power which decomposes NO into ions.

In our measurements, no emission due to boron species was detected. As the simple atom, boron, has only a few known spectral lines due to the transition $^3\Sigma_u^-$ - $^3\Sigma_g^-$, the peaks due to boron species are difficult to detect from the overcrowding lines of N_2 plasma. No emission due to NH at 336 nm or due to H_β at 486.13 nm and H_γ at 434.05 nm was detected. These peaks are hard to detect, if one keeps in mind that the flow ratio

(1)

(2)

(3)

Plate nos. 1-3: Optical emission spectra of N_2 plasma at 1) 10 W, 2) 100 W and 3) 160 W.

Plate nos. 4-6: Optical emission spectra of N_2 plasma at 4) 300 W, 5) 400 W and 6) 400W with Borane-ammonia evaporation.

Table 4.1 : Spectral Assignments for Emission from N_2 plasma

λ_{obs} (nm)	λ_{ref} (nm)	Species	Transition	Intensity x 10^{-5} (in arbitrary unit)							
				10 W	50 W	100 W	160 W	200 W	300 W	400 W	400 W & reactant
237.5	237.02	NO	$A^2\Sigma^+$ - $X^2\Pi$	2.8	1.325	0.85	0.0	0.0	0.0	0.0	0.0
249.0	249.34	NO	$B^2\Pi$ - $X^2\Pi$	3.75	1.475	1.35	1.3	1.3	0.0	0.0	0.0
259	259.57	NO	$A^2\Sigma^+$ - $X^2\Pi$	3.55	2.05	0.0	0.0	0.0	0.0	0.0	0.0
272	272.22	NO	$A^2\Sigma^+$ - $X^2\Pi$	2.175	0.0	0.0	0.0	0.0	0.0	0.0	0.0
296.2	296.2	SPS of N_2	$C^3\Pi_u$ - $B^3\Pi_g$	2.4	2.925	5.4	8.55	9.0	23.5	30.0	26.0
316.4	315.93	SPS of N_2	$C^3\Pi_u$ - $B^3\Pi_g$	7.625	11.775	16.05	25.2	35.7	82.5	112	106.0
337.5	337.13	SPS of N_2	$C^3\Pi_u$ - $B^3\Pi_g$	14.25	21.0	25.95	42.05	72.5	153.5	197.5	187.5
353.5	353.67	SPS of N_2	$C^3\Pi_u$ - $B^3\Pi_g$	3.525	5.25	7.55	13.65	18.3	46.5	55.5	52.0
358.0	357.69	SPS of N_2	$C^3\Pi_u$ - $B^3\Pi_g$	8.35	13.275	17.9	35.1	52.6	111	151	140.5
375.5	375.54	SPS of N_2	$C^3\Pi_u$ - $B^3\Pi_g$	1.7	4.025	3.2	8.2	10.0	24.5	36.0	22.0
380.5	380.49	SPS of N_2	$C^3\Pi_u$ - $B^3\Pi_g$	2.55	3.7	5.9	8.4	12.8	30.0	43.5	41.0
391.5	391.44	FNS of N_2^+	$B^2\Sigma^+_u$-$X^2\Sigma^+_g$	0.0	2.275	9.1	31.85	67.1	168.5	228.5	340.0
399.4	399.84	SPS of N_2	$C^3\Pi_u$ - $B^3\Pi_g$	1.075	1.875	2.5	3.5	5.6	6.5	22.5	20.0
405.9	405.94	SPS of N_2	$C^3\Pi_u$ - $B^3\Pi_g$	1.0	-	-	2.7	-	14.5	20.5	16.5
428.5	427.81	FNS of N_2^+	$B^2\Sigma^+_u$-$X^2\Sigma^+_g$	0.0	0.0	0.0	9.5	16.6	47.5	55.0	93.5

SPS: Second Positive System; FNS: First Negative System [161].

(1)
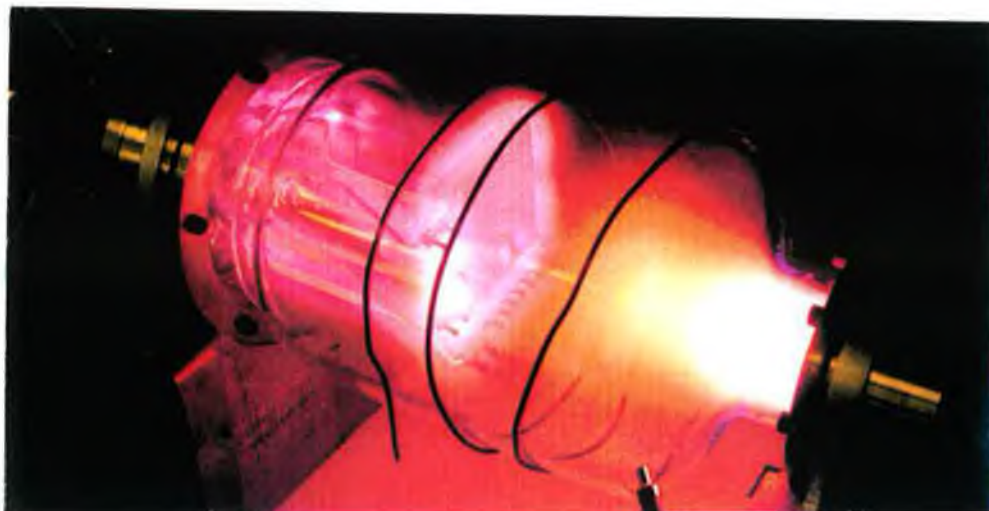
(2)

(3)

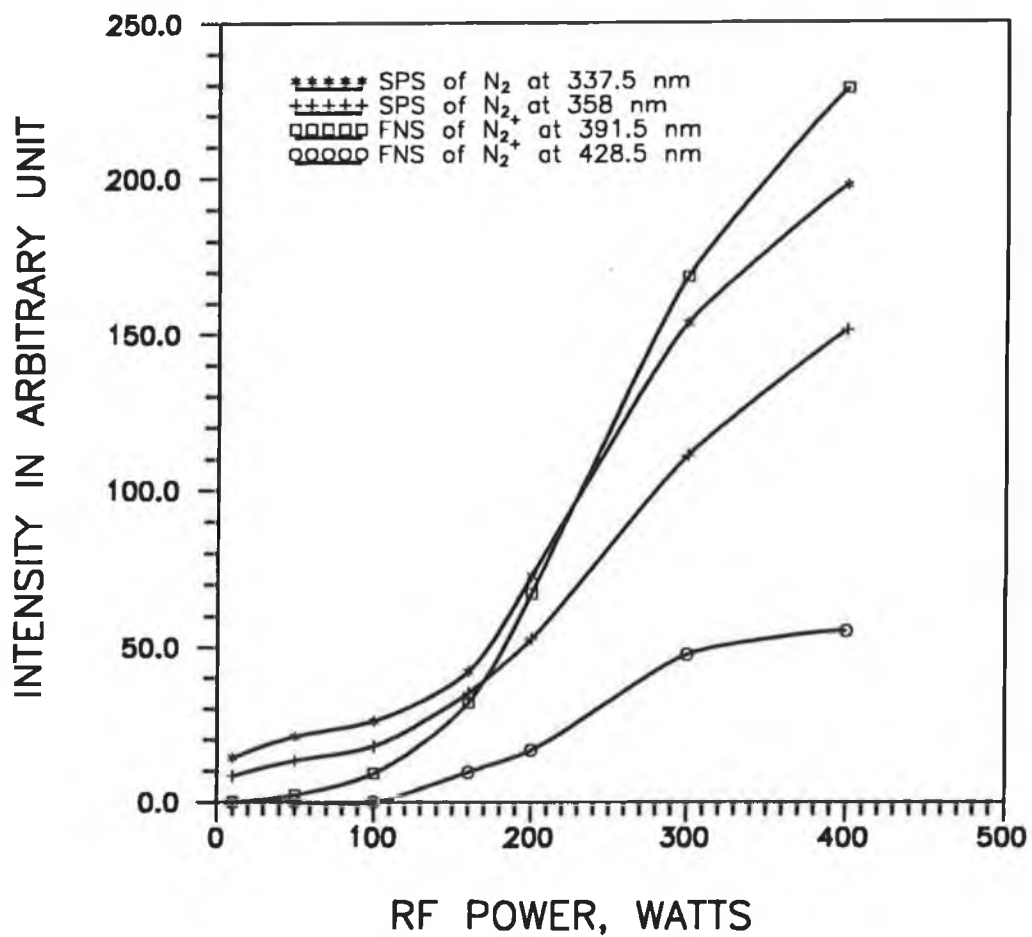Fig. 4.3: Plasma colour at a rf power of 1) 100 W, 2) 160 W and 3) 400 W.

Fig. 4.4:   Emission intensities of the second positive
system (SPS) of N_2 and of the first negative
system (FNS) of N_2^+ as a function of the rf
power coupled to the substrate.

of N_2 to borane-ammonia was approximately 1/1000. The peaks which are not obtained due to one or other reason are listed in Table 4.2.

Table 4.2: Spectral Assignments for the Species which are not found due to their low intensity or due to overcrowding of N_2 species.

λ_{ref} (nm)	Species	Transition
249.7	B	$^2P - {}^2S$
303.2	B^+	$^3D - {}^3P$
317.9	B^+	$^1P_1 - {}^1D_2$
329.3	B_2	$^3\Sigma_u^- - {}^3\Sigma_g^-$
332.4	B^+	$^3P_2 - {}^3D$
345.1	B^+	$^1P_1 - {}^1D_2$
412.2	B^+	$^3D - {}^3F$
419.5	B^+	$^1P_1 - {}^1S_0$
424.4	B^{++}	$^2P_0 - {}^2D$
447.2	B^+	$^3P_{2,1,0} - {}^3S_1$
343.97/346.7/349.6/ 359.9/362.6/380.3	BN	$A^3\Pi - X^3\Pi$
336.01	NH	$A^3\Pi - X^3\Sigma^-$
486.1	H_β	
434	H_γ	

A marked change in the optical constants of the film was also observed in ellipsometer measurements at the same conditions where OES showed a change in the ion density. Thus with OES, we were able to show qualitatively, that enhanced ion bombardment of the growing film at higher rf power is responsible for the formation of small amount of cBN in the films.

4.3   GENERAL PROPERTIES OF BN FILMS

BN films up to 300 nm thick were deposited directly onto silicon, KBr and steel substrates with controlled evaporation of borane-ammonia adduct in our final system. Films were grown with various combination of pressure, substrate temperature, filament temperature and rf power.

129

As the evaporation of borane-ammonia adduct was not even, the deposition rate was difficult to determine, but to be in the range of 20 Å/min.

Films consisted of a mixture of hexagonal and cubic phase, the ratio of which are dependent on the deposition parameters. But under appropriate growth condition, films are likely to contain crystallites of the cubic phase embedded in a hexagonal matrix.

The changes in colour and the surface roughness of the films at different conditions are observed. Some of the films showed multicolour strips due to thickness variation of the film over the substrate. But the smooth films showed a colour of brown, blue or amber. Most of the blue or some of the amber films are predominantly hexagonal in agreement with the deposition condition. Brown films or some of the amber films contains mixture of hexagonal and cubic structure.

Most of the films are not attacked by water. The best BN films were exposed to 40% dilute hydrochloric acid. There were no visible changes in the appearance of the films. But hydrogen contained films degraded in appearance after few days' exposure to atmospheric humidity.

Most of the films grown under desired condition of 350°C and at higher rf power (>200 W) adhered well to substrates, but adhesion of the films was strongly dependent on the cleanliness and smoothness of the substrates and also on substrate temperature.

The density of the films measured by gravimetric technique are in the range of 1.8 to 2.7 gm cm^{-3}. It is worth saying that thickness and weight of the films are measured very accurately by ellipsometry and microbalance techniques respectively.

The thermal stability of the films were determined by Thermogravimetric Analysis (TGA) carried out in a Stanton Redcroft TG 750/770 instrument. Hexagonal BN films and mixed-phase BN films containing both hexagonal and cubic phase were heated from 100°C to 1000°C at a rate of 15°C per min and cooled down in a N_2 dominant atmosphere. No weight loss or gain was observed for the samples showing that their thermal stability was excellent. However, a colour change was observed in the case of hBN films.

We will present the in depth study of the films mostly grown in our final system, but reference to the films grown in low-temperature system will also be given wherever necessary.

4.4　MICROSCOPIC STUDY OF THE FILMS

4.4.1　*OPTICAL MICROSCOPY*

Optical microscopy for topographic observation and other measurements was achieved using a Nikon Microscope (Nikon Optiphot). Observations of samples could be undertaken at magnifications of between x50 to x600 with an additional facility to record the images using a photomicrographic attachment. A micrometer eyepiece was used to measure dimensions down to 1 μm with a vernier resolution of 100 nm.

Optical microscopy was regularly used in initial observation of the films, topography studies, film thickness measurements and adhesion assessment. Any film cracking or stress relief was regularly observed by optical microscope. Fig 4.5(a) shows the stress relief of one of these BN films deposited on Si and fig. 4.5(b) shows the cracking of the film deposited on a moderately cleaned steel substrate.

Besides, the warping of the silicon strip before and after deposition during stress measurements was determined by optical microscope.

4.4.2　*SCANNING ELECTRON MICROSCOPE (SEM)*

Fine scale structural, topographic and dimensional measurements, beyond the scope of optical microscopy, were carried out using a Scanning Electron Microscope,

4.4.2.1　Principle of SEM

SEM is a popular method for the direct observation of surfaces because they offer better resolution and depth of field than optical microscope. The SEM has a magnification of 100,000x, a resolution of about 200-250 Å, and a depth of field at least 300 times or more that of the light microscope - all of which result in the characteristic photographs of dramatic three-dimensional quality.

The process principally involves the generation of a primary beam of electrons from an emission source which are then accelerated by a voltage of between 1-30 KeV and directed down the centre of an electron optical column consisting of two or three magnetic lenses. These lenses cause a fine electron beam to be focused onto the specimen surface. Scanning coils made to pass through the corresponding deflection coils of a CRT so as to produce a similar but larger raster on the viewing screen in a synchronous fashion.

Various phenomena occur at the surface of the sample including secondary electron emission [162] which in this case is used to form the image. There is a one-to-one
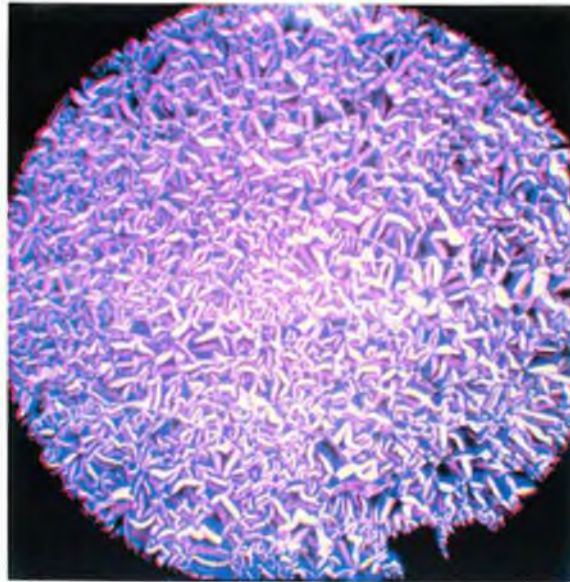
Fig. 4.5 (a): Optical photograph of stress relief pattern of a mixed phase BN films at the edge of the silicon substrate. This cracking depends on the cleanliness of the substrates.
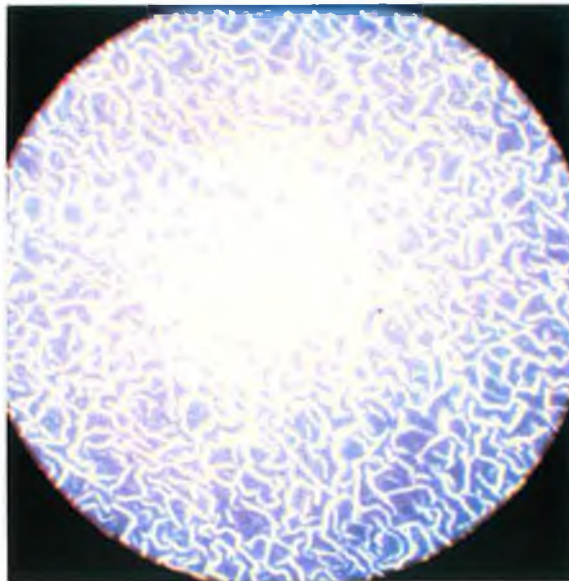

Fig. 4.5 (b): Optical photograph of stress relief pattern of mixed-phase BN films on steel substrates. This cracking strongly depends on cleanliness and roughness of the substrates.

correspondence between the number of secondary electrons collected from any particular point on the specimen surface and the brightness of the analogous point on the CRT screen. Consequently, an image of the surface is progressively built up on the screen. Some of the electrons are inelastically scattered by the K, L or N electrons shells in the atom losing their energy in the form of x-rays and it is these which are detected in energy dispersive x-ray analysis (EDX). The energy lost is characteristic of the scattering atom and intensity is used to establish the concentration of the element. EDX utilises a solid state detector to measure the X-ray radiation which is more sensitive to elements of higher atomic mass. ED analyzers have been used to detect elements above fluorine (atomic number 9). Problems are encountered when elements whose X-ray energies are too close together coexist in a sample. For example, in the low-Z region, the K lines of boron, carbon, nitrogen, and oxygen lie between 190 and 530 eV. Other factors limiting light-element detection are window thickness and electronic noise.

Wavelength diffractometers (WD) are also available as an accessory on some SEMs. In the WD method, a crystal of a known spacing d separates x-rays according to Bragg's law, $n\lambda = 2d\sin\theta$, so that at a diffraction angle of θ (collection angle of 2θ), x-rays of specific wavelengths are detected. To cover the whole range, the diffractometers are usually equipped with many crystals.

4.4.2.2   Operation and limitations

The morphology and topography were studied using a Leica-Cambridge S360 SEM and this also provided confirmation of measurements of thickness by ellipsometry.

A problem normally associated with thin layer is beam penetration through the film into the substrate, effectively rendering the film transparent to the detecting electron beam. This penetration can be minimized by selecting a lower beam acceleration voltage for analysis of the films and increasing the apparent film thickness by orienting the electron beam to a grazing angle with respect to the sample.

Since the probing beam of electrons is charged, insulating films of BN need to be provided with an artificially provided conducting path. A thin layer of sputter deposited gold approximately 100 Å thick is used to provide this path whilst maintaining the structural detail. The Au was deposited in a diode sputtering device. The sample temperature was < 50°C during Au deposition.

4.4.2.3   Study of the topography of the films

SEM photographs of most of the mixed-phase films showed a smooth and essentially featureless surface with an occasional nodule projecting above the surface. These nodules may be initiated when the rf power was momentarily turned off during the deposition to check substrate temperature and/or reactant temperature. When the rf power was momentarily turned off, it is likely that the evaporated reactant was deposited on the film as a nodular form. Such a film grown at 400 W rf power and a substrate temperature of

350°C and filament temperature of 1600°C (pressure 0.3 Torr) is shown in fig. 4.6(a) and (b). Most of the boron nitride films grown with rf power more than 200 W on properly cleaned Si substrates were found to be well adherent to the substrate.

Evidence of localized microporosity was noted in some of the films, grown under the same condition. This may be due to uneven evaporation of borane-ammonia reactant forming a very thin films which are bombarded with energetic ions. Such a film is shown in fig. 4.7 (a) and (b) for two different magnifications, but in most cases the structure appeared remarkably compact. Fig. 4.8 shows a film with rough surface containing microparticles of up to 250 nm in size. This is the case when borane-ammonia evaporated instantly during the deposition and deposited as a microparticles on the already grown BN films.

4.5   INFRA-RED STUDY OF THE FILMS

Intrinsic optical properties of a material are determined by three basic physical processes: free carriers, lattice vibrations, and electronic transitions. However, the dominant physical process depends on the material and the spectral region of interest. All materials have contributions to the complex index of refraction from electronic transitions. Metals and semiconductors are additionally influenced by free carrier effects. The strength of these effects depends on the carrier concentration; thus, they are very important in metals. Insulators and semiconductor also require the characterization of the lattice vibrations (or phonons) to understand their optical properties fully.

Infrared spectroscopy (IR) has been used for many years to obtain information about molecular structure. Its primary usage has been with gases, and with liquids or solids which are transparent to most of the wavelengths in the region of interest. Infrared radiation is an excellent probe of surface science where it is desirable to perturb the surface as gently as possible during a measurement. Most surface probes, i.e. electrons, ions, or UV photons cause desorption, rearrangement, or total destruction of the surface. Infrared radiation, on the other hand, only causes the molecules to vibrate with a slightly higher energy.

4.5.1   BASIC IDEA OF IR

A molecule or polyatomic ion absorbs energy in the infrared region of the electromagnetic spectrum causing transitions from lower to higher vibrational energy levels. Normal or fundamental vibrational frequencies correspond with transitions from the ground to the first excited state. If the absorbing species is considered as a harmonic oscillator, the selection rule obeyed for absorption is $\nabla v = +1$, where ∇v is the change in vibrational quantum number. As most molecules and ion are not perfect harmonic oscillators, this rule generally breaks down and transitions corresponding with $\nabla v = 2,3$, etc, are also observed. But their absorption intensity is much less than that of the corresponding fundamental band $(\nabla v = 1)$. When two or more fundamental vibrations are simultaneously excited,

134

Fig. 4.6(a): SEM micrograph of mixed-phase BN thin film showing smooth surface.

Fig. 4.6(b): SEM micrograph of fig. 4.6 (a) at higher magnification showing an occasional nodule.

Fig. 4.7(a): SEM micrograph of porous BN thin film on silicon.

Fig. 4.7(b): SEM micrograph of fig. 4.7 (a) at higher magnification showing microporosity of the film.
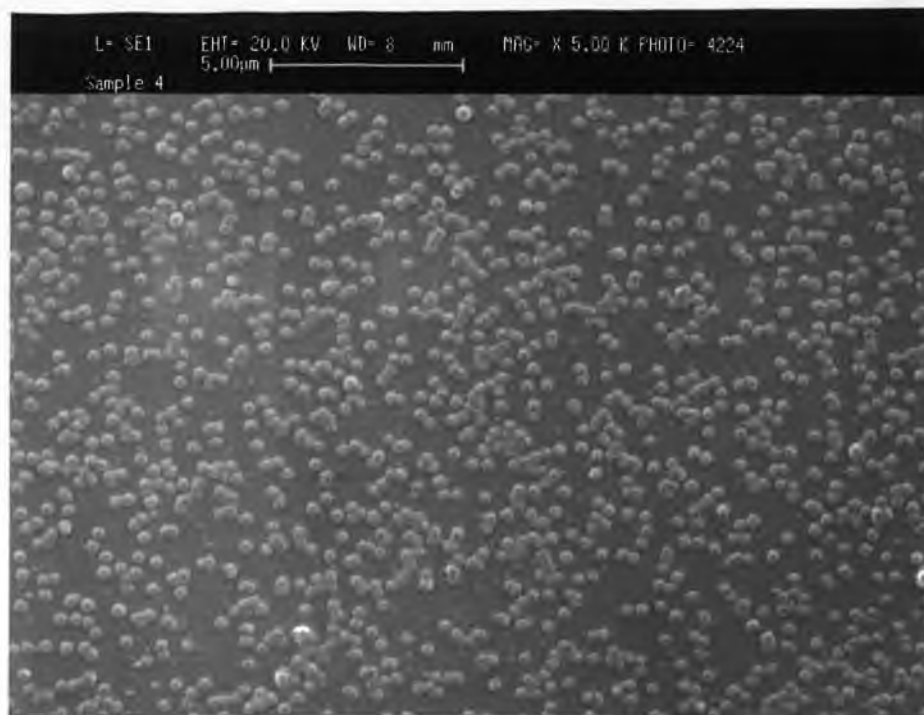
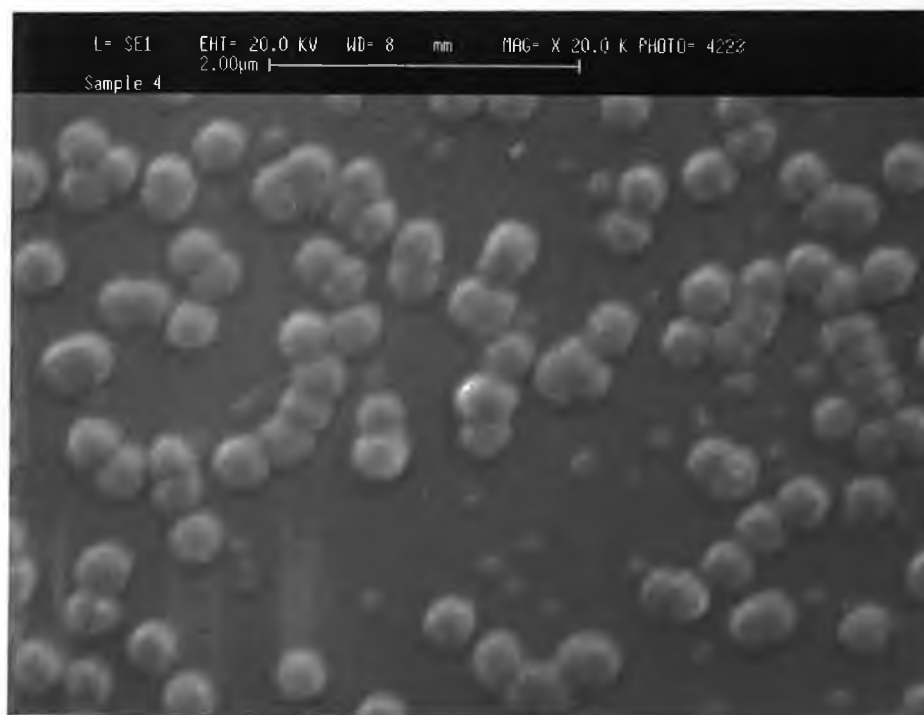Fig. 4.8(a): SEM micrograph of BN thin film with a rough surface.

Fig. 4.8(b): SEM micrograph of fig. 4.8 (a) at higher magnification showing microparticles of size 250 nm.

then combination band, for which the frequency is approximately the sum of the component frequencies, are observed.

The number of normal or fundamental vibrations possible in a polyatomic species can simply be expressed in the following way. The motion of each atom has three degrees of freedom, corresponding with movement in the x, y and z directions. For a molecule containing N atoms, there are 3N degrees of freedom. As three of these are associated with translatory movement and, in the case of non-linear molecules, three with rotation, the number of vibrations theoretically possible is (3N-6). For a linear polyatomic molecule, there are finite moments of inertia about the two axes perpendicular to the molecular axis and hence only two degrees of rotational freedom. The number vibrations possible in this case is (3N-5). Some of the fundamental vibrations are degenerate in many molecules and then the number of frequencies actually observed is smaller than indicated by this formulae.

Vibrations within a molecule are of different types, depending on the type of movement of the atoms. Thus there are 'stretching' vibrations, which caused bond lengths to alter, and there are 'deformation' vibrations which cause bond angles to change. Each vibration is not completely independent of moments occurring in the next of the molecule and will be affected to some extent by these. There is always some mixing of one vibration with others but it is often convenient to identify each vibration as predominantly of one type or the other.

Not all normal vibration are active in the vibrational spectrum. Those allowed are expressed by two important selection rules: (1) A vibrating molecule absorbs infrared radiation only if there is a change in dipole moment as it vibrates; (2) A vibration is active in the Raman Spectrum only when there is a change in the polarizability of the molecule associated with the vibration. The intensity of a band in the infra-red spectrum depends on the magnitude of the dipole moment change. The intensity of a Raman band is related to the polarizability of the vibrating atoms.

The complete vibrational analysis of a molecule must be based normally on its infrared and its Raman spectra because of the inactivity of some of the fundamental vibrations in one or other of these. An important special case is that of a molecule which has a centre of symmetry; then the rule of mutual exclusion is obeyed. In other words, the infrared and Raman spectra have no absorption bands in common. This can be a valuable aid in the determination of molecular symmetry, if an absorption band of the same frequency appears in both the Raman and Infrared spectra, it follows that the molecule has no centre of symmetry.

4.5.2 MICROSTRUCTURAL DETERMINATION BY IR

The lattice properties of materials can be used as 'fingerprints' of the microstructure in order to provide evidence for the identification of phases. The most convenient of these techniques is the measurement of the frequencies of particular modes of vibration of the lattice at the centre of Brillouin Zone as determined by infrared and Raman spectros-

copies. Compositional and structural evaluation can be made easily by use of infrared spectroscopy by comparing the intensities of various infrared absorption bands, one can determine relative amounts of various components or phases present in a sample.

In the case of transmitted spectra, the absorption band intensities are roughly proportional to the film thickness; ie. they obey Beer's law fairly well and are much better for quantitative determinations than are reflection spectra.

The transmitted intensity I is given by the equation [163],

$$I = I_0 \exp (-\beta x)$$

where, I_0 is the incident value,
β is the absorption coefficient of the absorption mode of interest,
x is the thickness of the film.
Thus, the absorbance is given by

$$A = \ln (I_0/I) = \beta x,$$

which is generally referred to as Beer's law. Thus the absorption coefficient will be proportional to the amount of bonds present at a particular wavelength and the thickness of the deposited film.

In the most simplest case, the IR spectrophotometer will contain a source of infrared radiation, an accessible sample compartment, a monochromator to disperse the radiation according to its wavelength, and a radiation detector.

4.5.3 VIBRATIONS DUE TO B-N BONDS

In ref. 164, the species of the normal modes of lattice vibrations for hBN lattice are given according to group theoretical considerations. An account of the notations used in IR and Raman spectroscopy are given in Appendix B. The irreducible representations for the normal modes near centre of the Brillouin Zone for hBN without inversion symmetry are

3	acoustical modes	$E' + A_2^{\sim}$
6	IR active and Raman active optical modes	$3E'$
3	IR active optical modes	$3A_2^{\sim}$

The irreducible representation for the normal modes near centre of the Brillouin Zone for hBN with inversion symmetry are

3	acoustical modes	$A_{2u} + E_{1u}$
3	infrared active optical modes	$A_{2u} + E_{1u}$
4	Raman active optical modes	$2E_{2g}$
2	inactive optical modes	$2B_{1g}$

In ref. 164, this second model with a symmetry centre fits their result best. In their infrared investigations, they have found two strong infrared-active zone-centre vibrational modes, The inplane transverse optical mode at 1367 cm^{-1} (strong) and out-of-plane transverse optical mode at 783 cm^{-1} (weak). The infrared transmission spectrum of hBN will therefore show two absorption maxima at 1367 cm^{-1} and 783 cm^{-1}.

Infrared reflectance measurements [165] show that cBN has a zone-centre transverse optical (TO) mode frequency of 1050 cm^{-1} and a zone-centre longitudinal optical mode frequency of 1340 cm^{-1}. The infrared transmission spectrum of thin films of cBN will therefore show a single absorption maximum at 1050 cm^{-1} if single phonon processes are dominant [166].

As mentioned in the literature, the TO mode of crystalline wurtzite BN appears at 1102 cm^{-1} [167]. Kessler et al. [83a] published also an IR spectrum of a wBN thin film with an absorption centred at 1100 cm^{-1}.

As discussed in section 2.11, on the basis of the two quite distinct IR absorption spectra for cBN and hBN, useful microstructural conclusions can be drawn.

4.5.4 QUANTITATIVE ANALYSIS

The films on Si or KBr were studied using IR spectrometry which was carried out on a Perkin-Elmer 983G spectrometer in the transmittance mode in the range 600-4000 cm^{-1}, using a bare silicon wafer as a reference where necessary. The silicon wafer was etched just before introducing it in the deposition chamber and then reference silicon was also etched just before IR study which was done immediately after each deposition.

The relative content of cubic to hexagonal phase was obtained by the intensity ratio of the IR absorption bands at ~ 1065 cm^{-1} and ~ 1365 cm^{-1} respectively, since the absorption intensity is a function of film thickness shown in Beer's law. This method was used in the literature [36,38,72,78].

The intensity was evaluated by the peak height common tangent base line method [163]. This method is shown in fig. 4.9. This method involved drawing a tangent line under the absorbance spectrum of the analysed band and selecting the two points of intersection of the common tangent line with the spectrum as the base line points. The measured peak height of the band was taken as the observed peak height minus the interpolated peak height on the tangent line at the position of the observed peak hight.

The intensity ratio of cBN and hBN, A_{cBN}/A_{hBN}, will be independent of the film thickness.
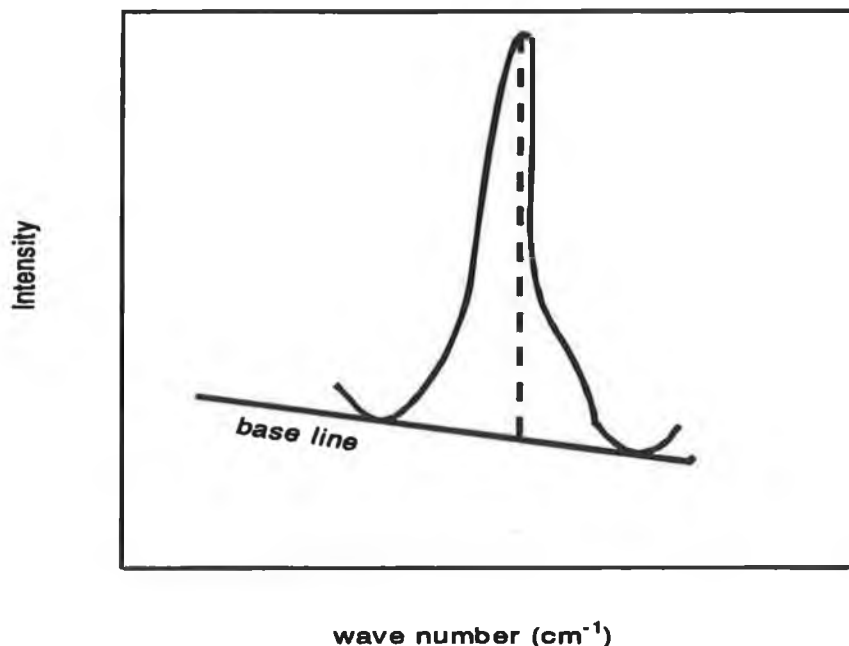
Fig. 4.9: Illustration of common tangent baseline method in spectral evaluation by peak height. The dotted line represents the intensity of the peak.

4.5.5 INITIAL RESULTS AT LOW TEMPERATURE SYSTEM

Under the growth condition described in section 3.2.2, the trend of the growth of the BN films under different conditions was studied and the conclusion drawn from this study has been used to develop the final system.

BN films up to 1.5 μm thick were deposited directly on silicon or KBr substrates with a deposition rate about 150 Å min^{-1}. The infrared spectrums of most of the films contain a strong absorption band at 1365 cm^{-1} , a medium or weak band at 1070 cm^{-1} and at 780 cm^{-1}.

4.5.5.1 Influence of inductively coupled rf power

Fig. 4.10(a) shows the intensity of the IR absorption band of BN films prepared by varying the rf power coupled inductively with the system. No cBN peak was detected when a rf power of less than 20 W was used. As the power was increased, the cBN peak intensity at 1070 cm^{-1} was increased and became sharper. Though the shape and intensity of the in-plane vibration of hBN phase did not exhibit any considerable change, the peak was shifted to a lower wave number from 1428 cm^{-1} at 20 W to 1365 cm^{-1} at 200 W.
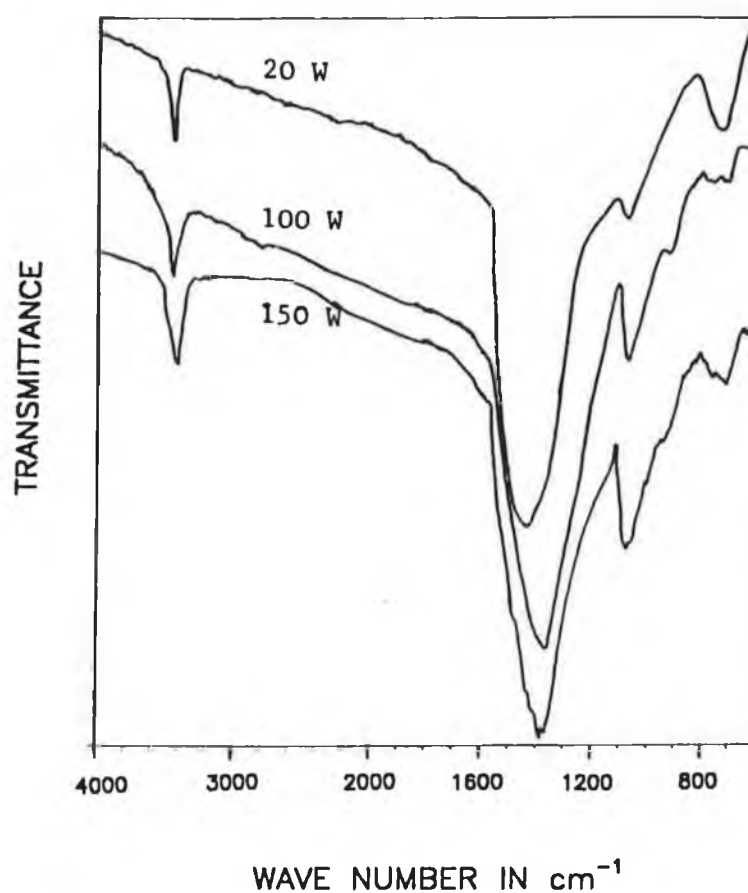
141

Fig. 4.10(a): **IR absorption spectra of BN films prepared by varying rf power coupled inductively with the low-temperature system.**
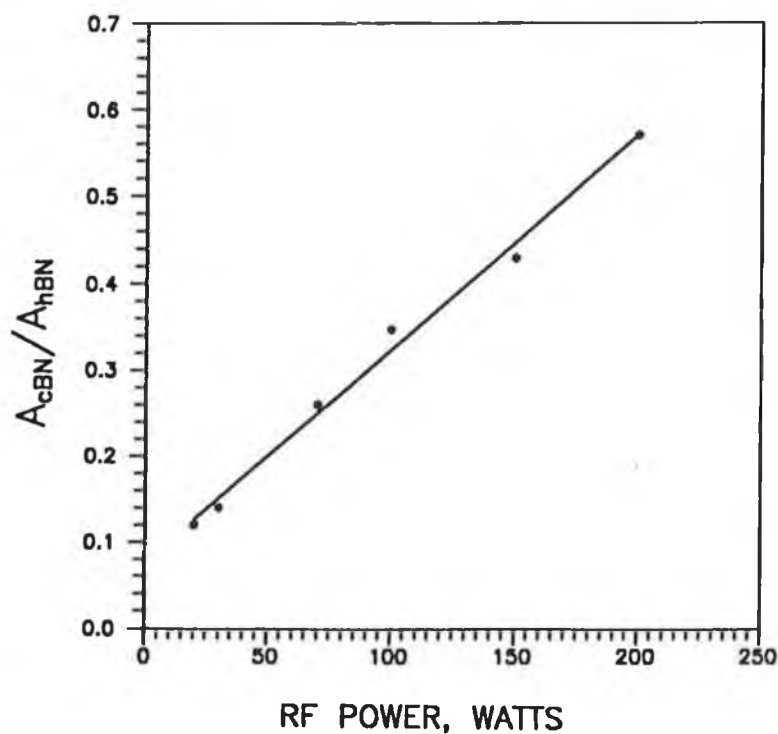

Fig. 4.10(b): **The intensity ratio of cubic to hexagonal phase of BN as a function of inductively coupled rf power.**

The out-of-plane vibrational peak was sharper at lower power than that at higher power and also it shifted to a lower wave number. This frequency shift indicates a weakened B-N bond and the broadening indicates an average decrease in the ordering of B and N atoms to form B-N bonds. The relative increase of cBN peak with respect to hBN peak is shown in fig. 4.10(b).

4.5.5.2 Influence of dc bias

Fig. 4.11(a) shows the IR absorption spectra of BN films deposited by varying the negative dc bias applied at the substrate while inductively coupled rf power was 20 W. The cubic BN peak at 1060 cm^{-1} showed increasing intensity and sharpness with the increasing bias, but the hexagonal peaks did not show any significant change in peak-shift or intensity. Due to high ionization of the plasma, it was not possible to go beyond 400 V. Fig. 4.11(b) shows the IR absorption ratio as a function of dc bias voltage.

4.5.5.3 Influence of capacitively coupled power

In the capacitively coupled system, no cBN peak could be detected at less than 70 V substrate bias. As the bias was increased up to 600 V, the cBN peak near 1070 cm^{-1} increased considerably. The film contained mixtures of hexagonal and cubic phases with a bigger hexagonal peak, as illustrated in fig. 4.12(a). After 600 V, cBN peak is more or less constant. The shape, intensity and peak-shift of the out-of-plane and in-plane vibrations of the hBN phase were found to be dependent on bias voltage. At low voltage, the in-plane vibrational peak was at 1363 cm^{-1} and was split. As the bias voltage was increased, it shifted to lower wave number (1278 cm^{-1} at 900 V), the intensity was decreased and the shape became more roundish. The out-of-plane vibrational peak was very sharp at low voltage. As the bias was increased, it also shifted to lower wave number, became broader and nearly disappeared after 600 V. The cBN peak exhibited no significant shift but became sharper at higher voltage. The IR absorption ratio of cBN and hBN is shown in fig. 4.12(b).

4.5.5.4 Hydrogen content of the films

A sharp, weak peak at 3430 cm^{-1} was also observed in all of our films. This peak is attributed to N-H stretching vibrations, since the N-H peak is sharper than the O-H peak (due to intermolecularly bonded O-H groups) which also occurs in this region [154]. This N-H vibration was found to be increased slightly with rf power and dc bias, but exhibited no significant change up to 500 V rf self-bias beyond which the sharp peak was found to be superimposed on a broad peak. It seems that films grown above 500 V might contain some O-H group. At low substrate rf bias, a very weak broad peak at 2519 cm^{-1}, characteristic of B-H stretching, was also observed, but it disappeared after a 300 V rf self-bias. No such peak was observed in the inductively coupled system.

143
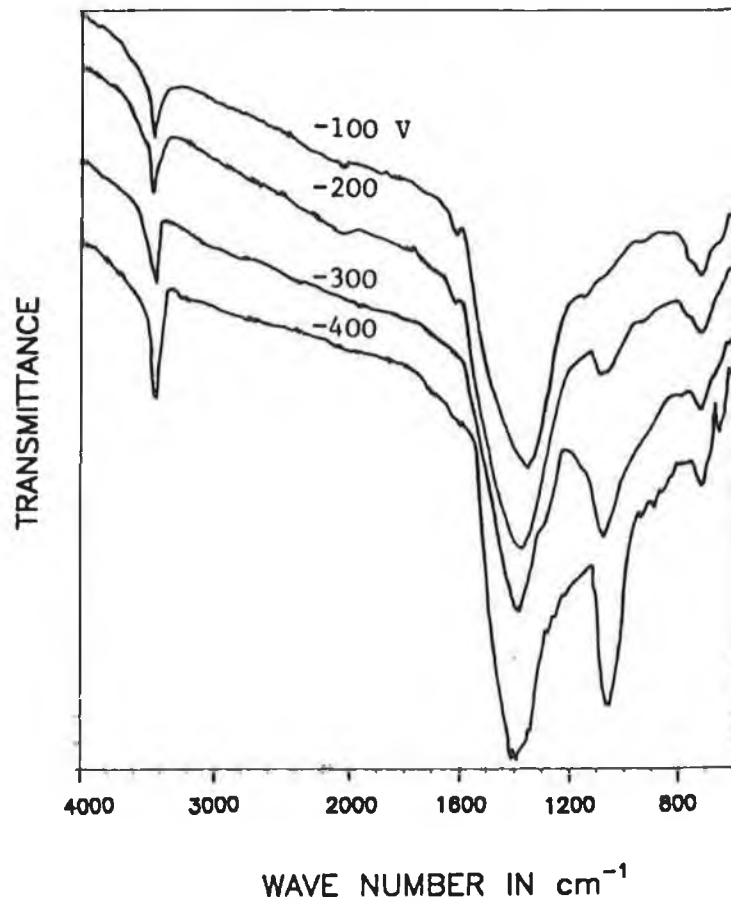
Fig. 4.11(a): IR absorption spectra of BN films prepared by varying the dc substrate bias (inductively coupled rf power 20 W).

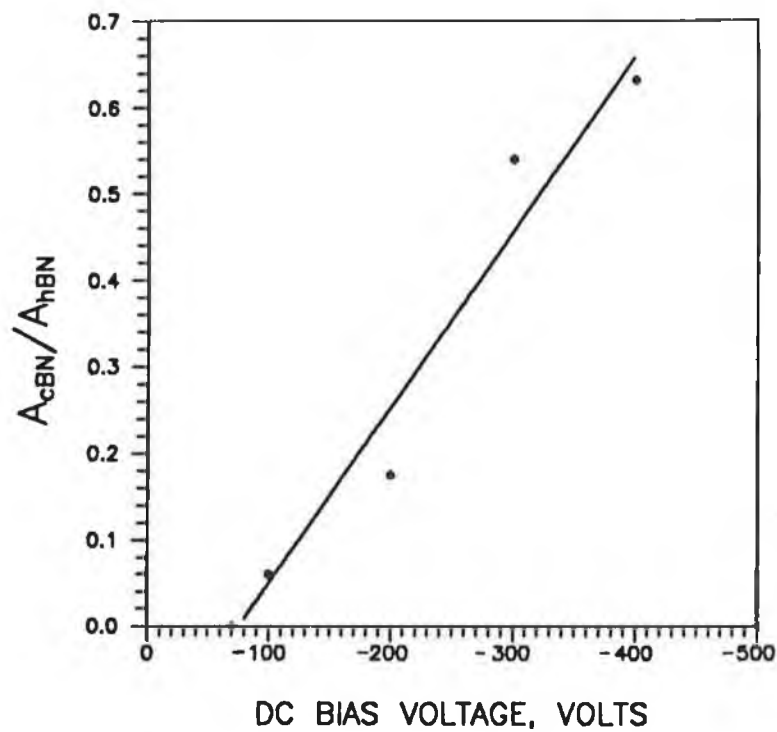**Fig. 4.11(b):** The intensity ratio of cubic to hexagonal phase of BN as a function of negative dc substrate bias.
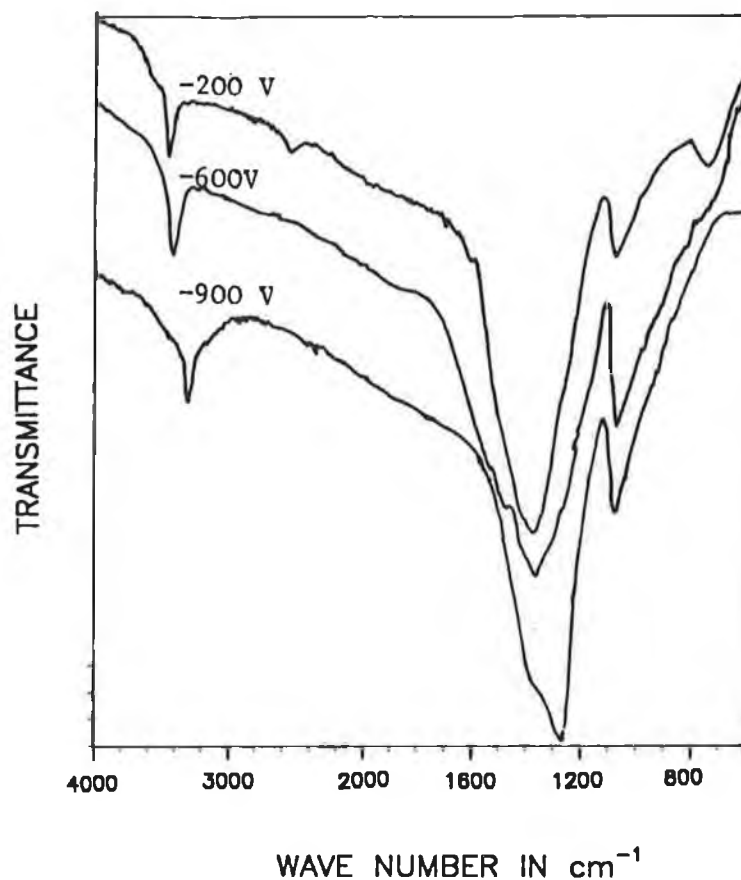
Fig. 4.12(a): IR absorption spectra of BN films prepared by varying the rf self-bias voltage at the substrate.
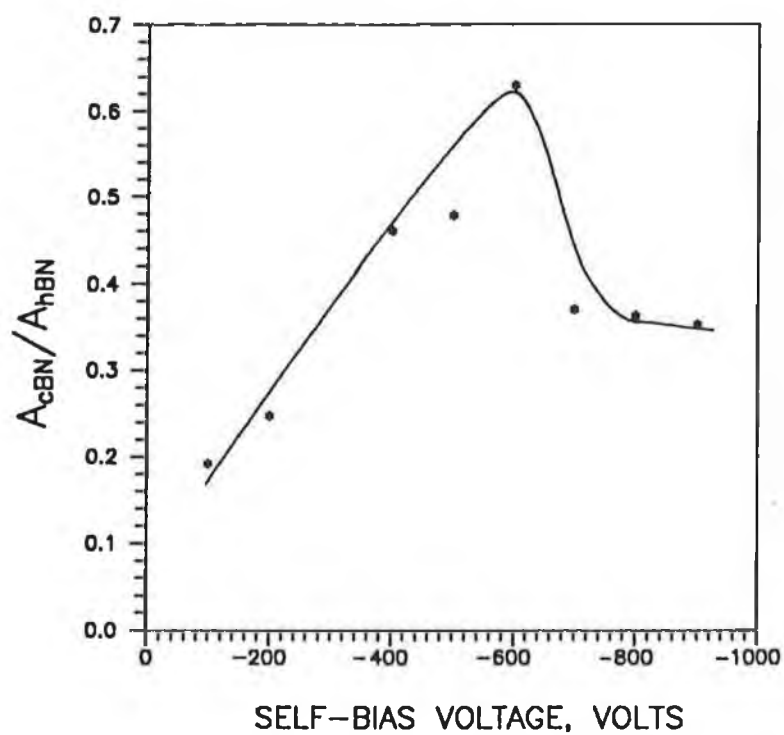

Fig. 4.12(b): The intensity ratio of cubic to hexagonal phase of BN as a function of negative self-bias voltage.

4.5.5.5 Discussions

As mentioned in section 3.2.1, the substrate of this system was not heated by external heating arrangements. Fig. 4.13 illustrates the influence of rf self-bias on the substrate temperature of the stainless steel substrate; the corresponding rf power is also shown. The self-bias was measured directly from the display of the rf generator. In both coupling systems, the substrate temperature was increased, though the highest temperature did not exceed 150°C. The highest temperature for the inductively coupled system was 115°C at a rf power of 200 W.

The adhesion of the films was strongly dependent on bias voltage and rf power. Films deposited at low bias and low rf power adhered well to the substrates. In contrast, the films, deposited on Si wafers using a high bias or a high power, tended to debond and break into minute fragments following to atmospheric environments. It is believed that a high residual stress in the films causes this result.

In all the systems above, the cBN content of the films was found to be increasing with the substrate bias voltage or with rf power. The is due to the increasing ion ion energy or ion density in the plasma. These facts showed that the ions accelerated by self bias to the substrate sputter selectively the hexagonal grains. The growth of the hexagonal phase was resisted. At the same time, the volume fraction of the cubic phase increased as shown in figs. 4.10(b), 4.11(b) and 4.12(b).

These films are likely to contain crystallites of the cubic phase embedded in a predominantly hexagonal matrix. Though dc bias showed a considerably bigger cBN peak compared to other system, it is not feasible to use dc bias as the films are insulating. Using only rf power or substrate bias, it was not found possible to deposit films which contained a good amount of cBN, though it was shown from this low-temperature system that the relative amount of cBN was directly dependent on rf power and substrate bias. The low substrate temperature and non-inclusion of any other particle energy source may not be sufficient to deposit hydrogen-free cBN predominant films in a PACVD system. The study shows that by a suitable choice of another activation source with moderate substrate temperature, the amount of cBN in the film could be maximized. From this conclusion, the final system was utilised to deposit BN films in a more favourable condition for cBN growth.

4.5.6 IR STUDY OF THE FILMS GROWN IN FINAL SYSTEM

Films were grown with various combinations of pressure, substrate temperature, rf power and filament temperature as well as different rf power coupling in our final system described in section 3.5.

At the same rf power, it was found that capacitively coupled system are more consistent of growing cBN containing films than inductively coupled system. Film adhesion and quality with respect to the hydrogen content of the film are better in the capacitively coupled system. It was also found that the reproducibility of the films produced in inductively coupled system was poor in contrast to the capacitively coupled
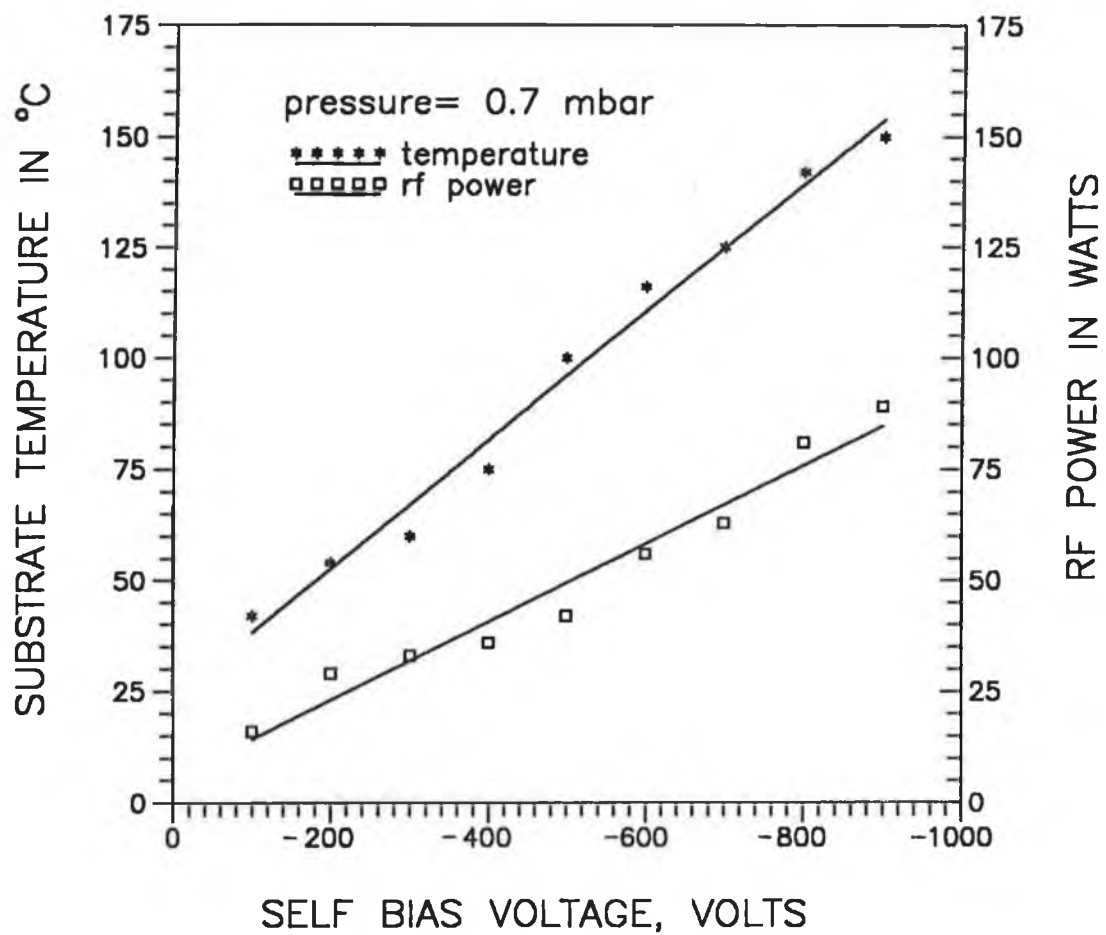
146

Fig. 4.13: The relation between the substrate temperature and rf power with the rf self bias voltage for the low-temperature system.

system. Thus the deposition parameters were varied to determine the condition of maximising the cubic phase of the BN films in only the capacitively coupled system.

The cBN content of the films strongly dependent on the deposition temperature, filament temperature and coupled rf power.

Without substrate temperature (the lowest substrate temperature was about 150°C with 400 W rf. power on) and without filament, the cBN peak is very small. As the substrate temperature was increased, an absorption band at nearly 1054 cm^{-1} was normally obtained after 250°C, though no functional relation could be determined between increasing substrate temperature and cBN content of the films. At lower rf power (<100 W), films are consistently hexagonal in nature with two absorption peaks at around 1380 cm^{-1} and at around 715 cm^{-1}, without any substrate temperature. The intensity ratio of cBN and hBN peaks of a number of films grown at 200 W rf power at different substrate temperatures are shown in fig. 4.14. The scattering of the values are apparent from this figure, but it is the threshold value which we are interested here. The films deposited from room temperature, meaning the substrate temperature was not turned on, to 200°C, the films contains a little amount of cubic phase, but films deposited after 250°C to 400°C shows an increase of the cBN content of the films, though maximum value obtained was around 0.3. While the percentage of the cubic phase increases with increased substrate temperature, the data are much more scattered, but it is apparent that there exists a threshold value of approximately 300°C below which films are mostly hexagonal. More-over, the adhesion of the films to the substrate was good and the peak at 3430 cm^{-1} attributed to N-H stretching vibrations disappeared in most of the cases after 300°C. For this reason, we kept our substrate temperature always at 350°C which is suitable for most substrates including high speed steel and GaAs.

With the filament, there was a considerable change in the shape of the cBN reststrahlen band in IR spectra. Less than 1400°C of filament temperature, little or no effect was found in the IR spectra of the films grown at 200 W rf power and at 250°C. Deposition rate, calculated roughly over a period of time increased slightly due to the presence of the filament. After 1400°C, the presence of the filament has a considerable effect on the cBN peak shape and height as shown in fig. 4.15. A value of 1600°C of the filament thus usually adopted in our experiments.

RF power has an important effect on the cBN content of the films. Less than 100 W rf power, and at 350°C, virtually no cBN peak could be detected. At 100 W, maxima in absorption appear near both the hexagonal and cubic vibrational frequencies, but the hexagonal in plane peak is stronger and wider than the tiny cBN peak. The hexagonal in-plane peak position varies widely from film to film ranging 1265 cm^{-1} to 1350 cm^{-1}. After 160 W, there is a sharp increase in the cBN reststrahlen band. Fig. 4.16(a) showed the IR spectra of the deposited films at 200 W, 300 W and 400 W respectively at a substrate temperature of 350°C and filament temperature of 1600°C; fig. 4.16(b) showed the intensity ratio of the cBN and hBN peaks with respect to the rf power.

As indicated in the IR spectra of fig. 4.16(a) the reststrahlen band related to sp^3 BN bonds is shifting from 1096 cm^{-1} at 100 W to 1054 cm^{-1} at 400 W (see fig. 4.16(c)), whereas the peak at around 1350 cm^{-1} shifts vary slightly at higher rf power with a
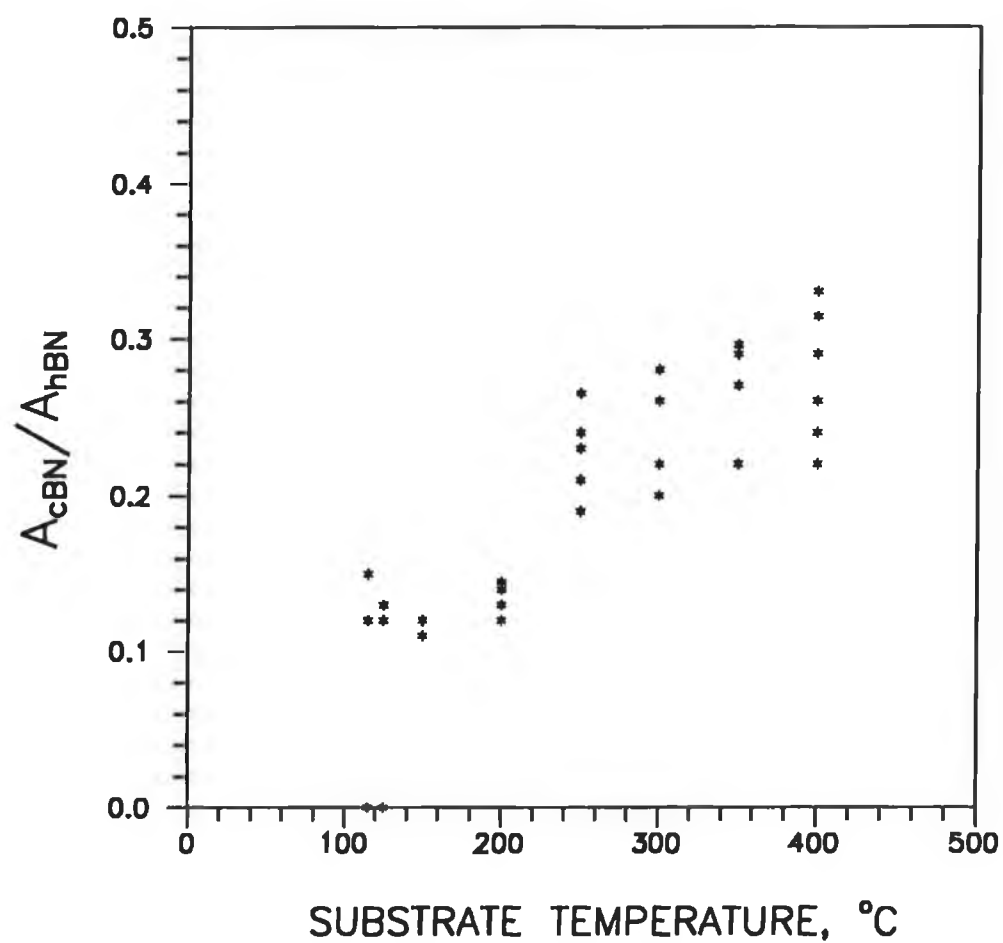
Fig. 4.14: The effect of substrate temperature on the intensity ratio of cubic to hexagonal phases in the BN films grown at 200 W power coupled to the substrate.

T_s=250°C, T_F=1400°C

T_s=350°C, T_F=1600°C

TRANSMITTANCE

4000   3000   2000   1600   1200   800

WAVE NUMBER IN cm^{-1}
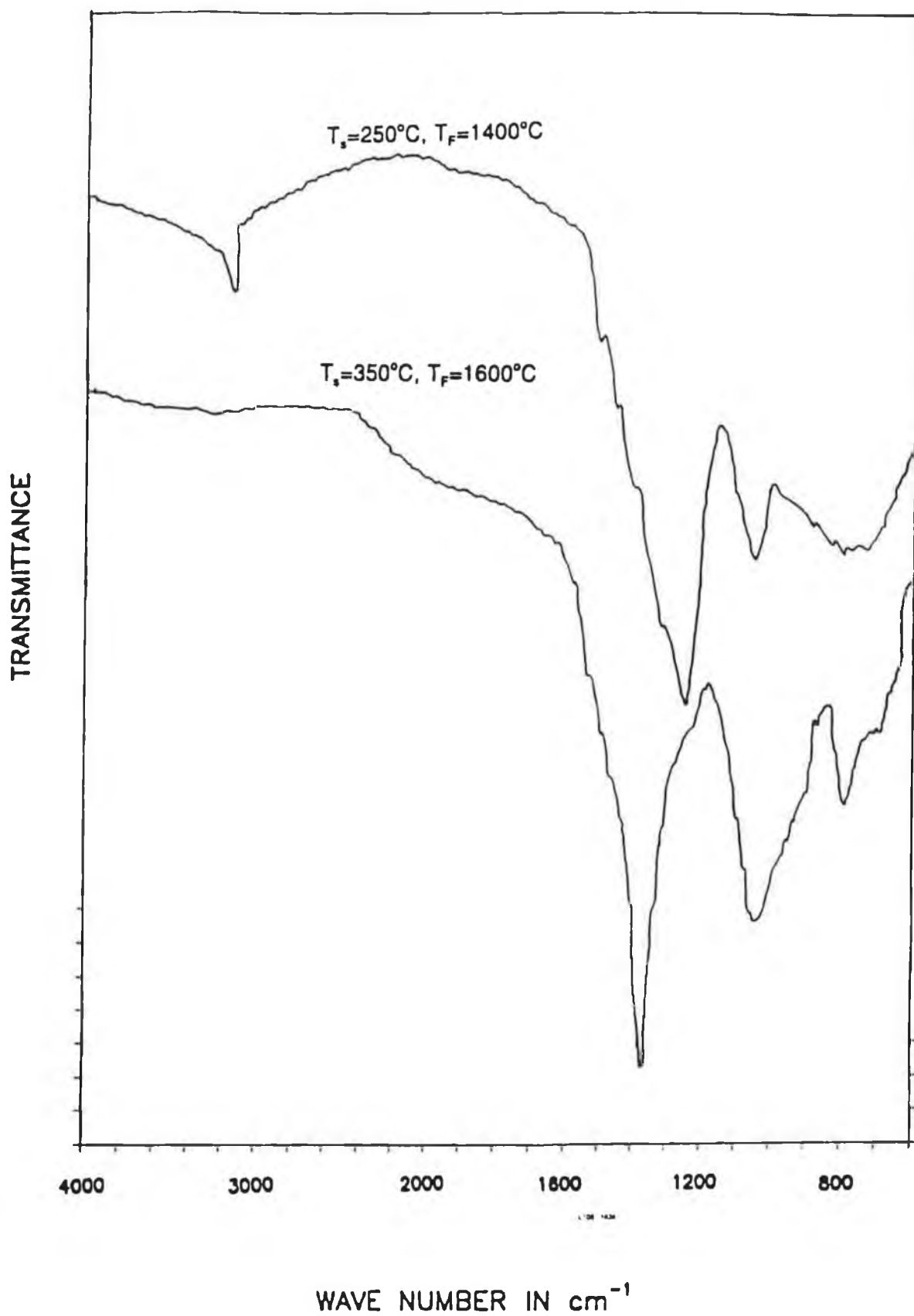
Fig. 4.15: IR absorption spectra of BN films showing variations due to substrate temperature (T_S) and filament temperature (T_F) using rf power of 400 W and total pressure of 0.3 Torr.

Fig. 4.16(a): IR absorption spectra of BN films prepared by varying rf power at substrate temperature of 350°C and filament temperature of 1600°C.

Fig. 4.16(b): The intensity ratio of cubic to hexagonal phases in BN films as a function of power coupled to the substrate.
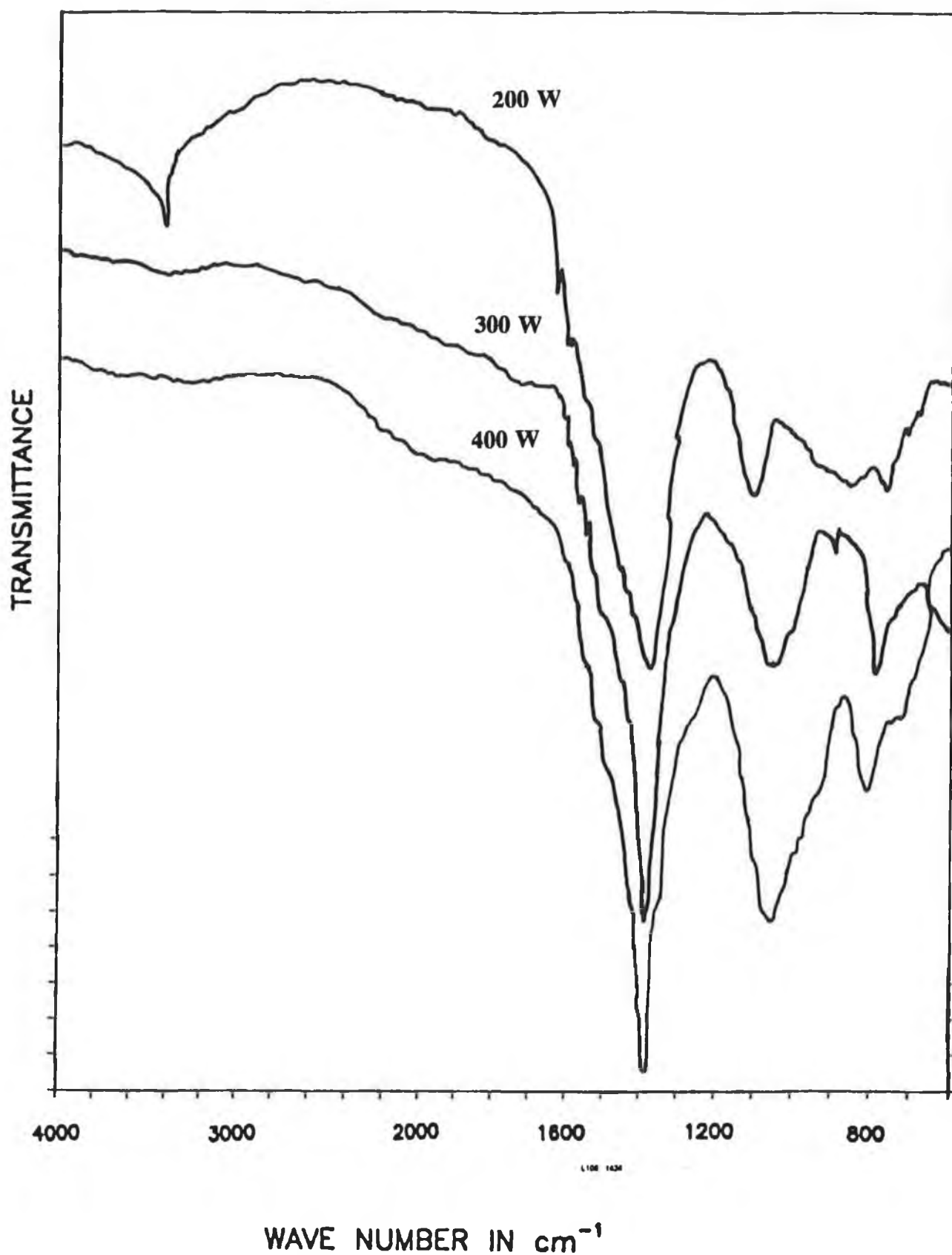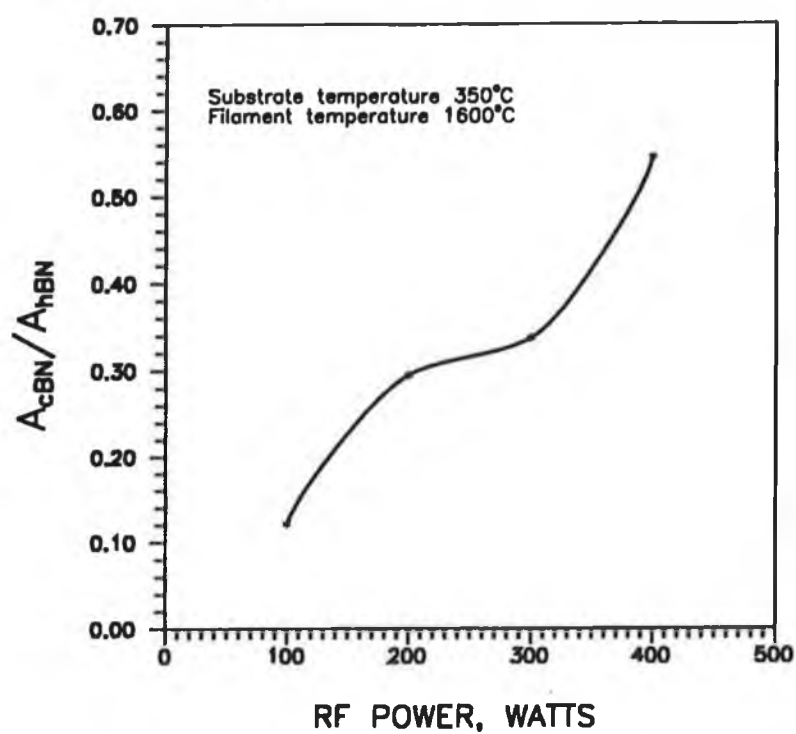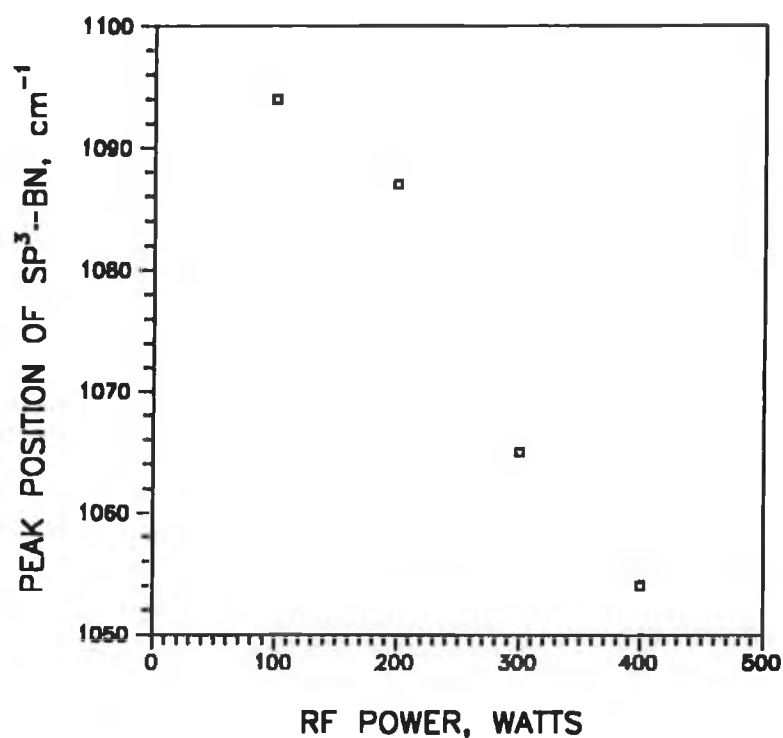

Fig. 4.16(c): The effect of rf power on the peak position of sp^3-BN in the films grown under substrate temperature of 350°C and filament temperature of 1600°C.

variation in the range of 1350 to 1357 cm^{-1}. But the shape changes considerably. The area under this peak at 100 W is higher than the area at higher power and it becomes narrower also at higher rf power.

At lower rf power, even at 350°C, there is likely to exist a peak at around 3220 cm^{-1}, attributed to N-H peak. At lower temperature, the B-H peak at around 2400 cm^{-1} usually exists, but at higher temperature and power greater then 200 W, the peak disappears. At 200 W, the appearance of the peak is inconsistent. No such peaks seemed to appear at higher rf powers. However some of the films showed appearance of N-H peak after exposure to the air for long time or the N-H peak containing films showed an increase in the height of the peak with time. Other peaks height were not changed.

4.5.7 DISCUSSIONS

The increase in cBN peak at higher rf power is due to increased ion bombardment on the growing film. This is due to two reasons: (1) with increasing rf power, the negative self-bias of the substrate was increasing as shown in fig. 4.17. The self-bias was measured by an oscilloscope connected to the substrate through a choke coil and a voltage divider. (2) the nitrogen ion volume was also increasing in the plasma as shown in fig. 4.4.

But the threshold value of rf power was thought to be 160 W where the plasma colour changes and a peak attributed to N$_2^+$ ions in the OES study occured. This increased ion bombardment is responsible in selective etching of the hexagonal phase and supply sufficient energy to cross the barrier height for the conversation of the stable phases to metastable cBN phase.

The shift of the sp^3 related IR bonds is thought to be due to two reasons:

(1) The band shift was also observed by other authors [34,37] and explained as an effect of internal stress. According to these reports, the film which was debonded from the Si substrates at the time of IR spectrum measurements showed a shift from 1100 cm^{-1} to 1050 cm^{-1} of the cBN reststrahlen band. At higher rf power, our film showed higher stress which does not comply with this stress reduction analogy. Besides, there was no shift observed between the film just after deposition and same film which are debonded from the substrate after atmospheric exposure.

(2) As mentioned in the literature, the TO mode of crystalline wBN appears at 1102 cm^{-1} [167]. Kesslar et al. [83a] published also an IR spectrum of a wBN thin film with an absorption centred at 1100 cm^{-1}. This leads to the suggestions that under not appropriate conditions for cBN growth, the wBN was formed in accordance with section 2.3 [hBN→wBN]. The formation of cBN occurs when we just supply enough energy at temperature greater than 300°C and rf power of 160 W. This phenomenon will be explained in section 6.2, when we explain the growth mechanism of the films.
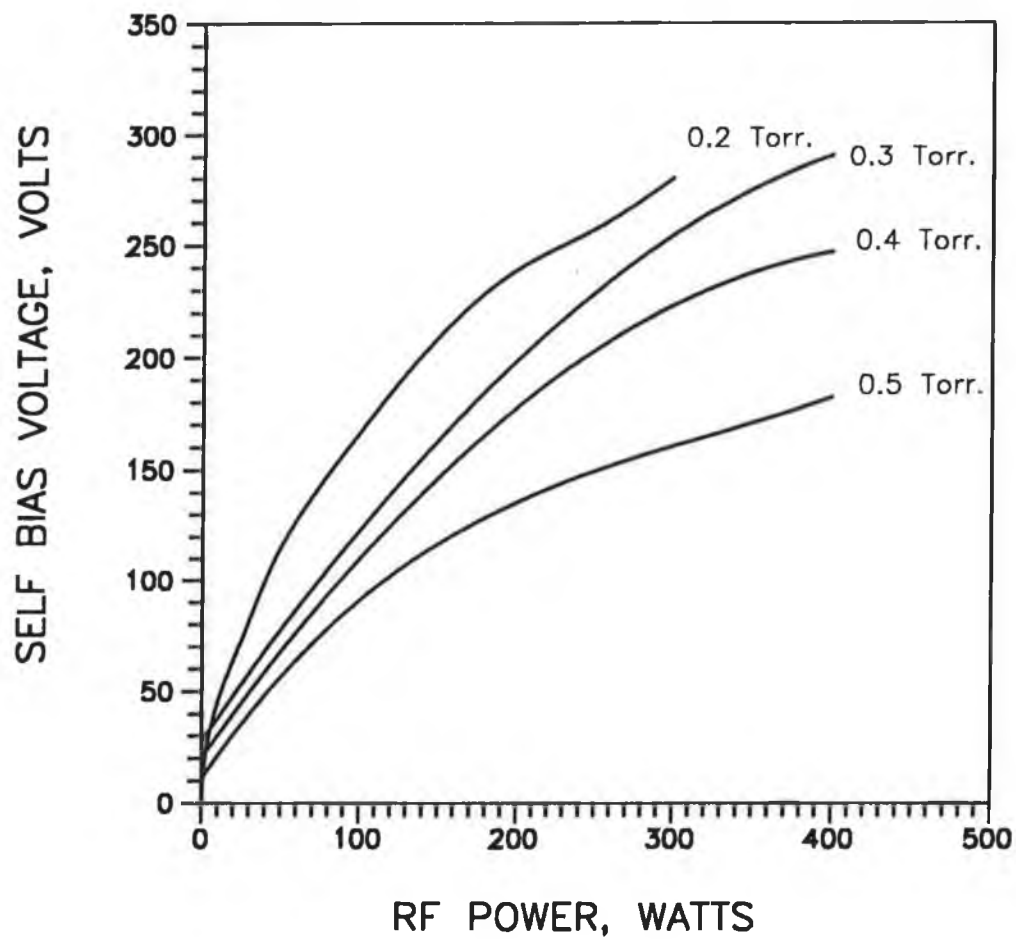
Fig. 4.17: Negative self-bias voltage of the substrate as a function of capacitively coupled rf power.

The sharper peak of hBN in-plane vibration at higher rf power may be due to more crystallized structure of the films compared to the amorphous state at lower rf power.

The hydrogen content of the film is very low at higher rf power and temperature. The strength of N-H and B-H bonds are 3.2 and 3.5 eV. At higher rf power, removal of nitrogen- and boron-bonded hydrogen could have occured giving hydrogen free films. The peak position of B-H bond at lower rf power was found to vary between 2330 and 2520 cm^{-1} for unknown reason.

4.5.8 SOURCES OF ERROR

The characteristic bonds of IR is an important tool to characterize BN films. but on Si, the cBN reststrahlen band is very close to the Si-O bond vibrational number 1103 cm^{-1}, which is typical for silicon dioxide film IR spectra. But this peak is very sharp compared to the broad peak due to cBN reststrahlen band.

Again, etching of Si wafers by HF acid just before deposition and etching of reference silicon just before characterization effectively remove Si-O peak. This is shown in fig. 4.18 where a hBN film at 50 W with no substrate or filament temperature was deposited on etched and unetched Si wafer. The sharpness of the Si-O band at 1110 cm^{-1} was apparent from the figure.

To identify the peak unambiguously, we deposited BN films on KBr substrates at 300 W and 200°C. The cBN peak at 1100 cm^{-1} can be seen in fig. 4.19. This confirms the presence of cBN peak at higher power.

Some of the hexagonal films showed absorption of in-plane vibrations as low as 1265 cm^{-1}, believed to be due to complete amorphous state [62].

4.6   ELLIPSOMETRY

Ellipsometry is a technique for the contact-less and non-destructive optical characterization of surface, specially measurement of thickness and refractive index of transparent thin films. It is based on the fact that a monochromatic electromagnetic wave changes its state of polarization if it strikes non-perpendicularly the interface between two dielectric media.

4.6.1 PRINCIPLE OF OPERATION

The reflection of an electromagnetic wave at and its transmission through the interface between two homogeneous media is described by Fresnel's equations [168].
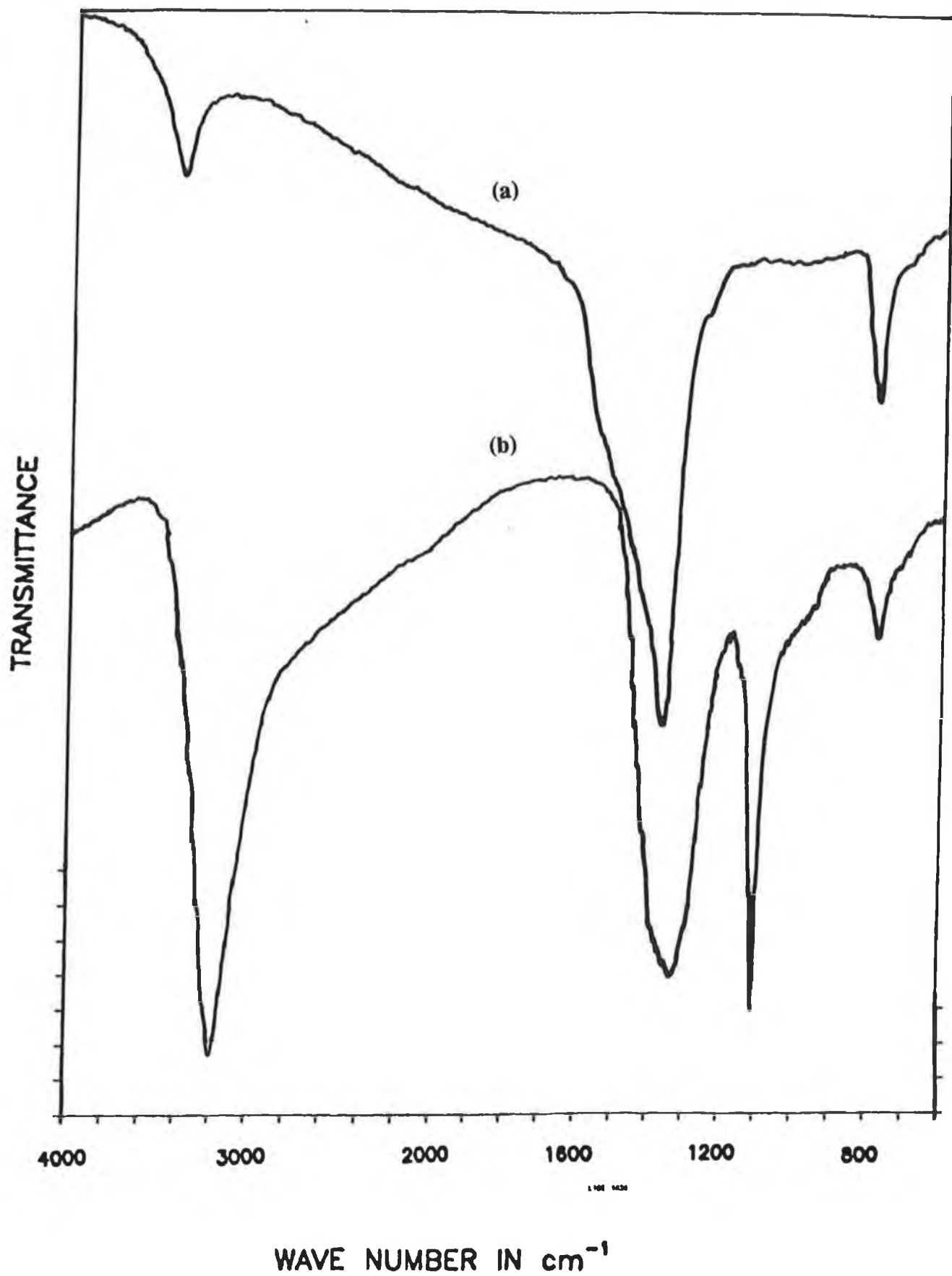
Fig. 4.18: IR absorption spectra of hBN films deposited on (a) etched and (b) unetched Si substrate.
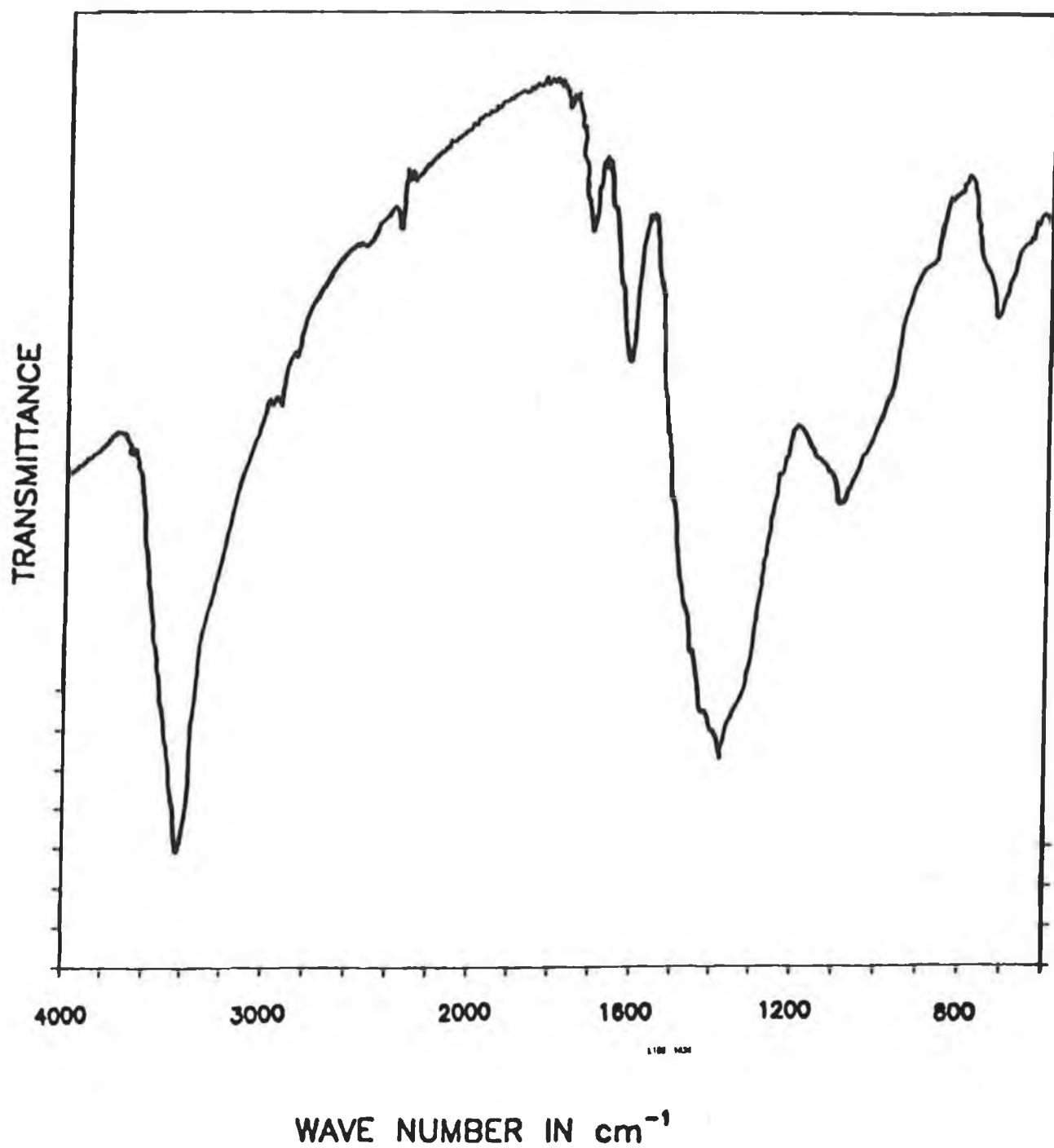
Fig. 4.19: IR spectra of BN films on KBr substrate showing a cBN peak.
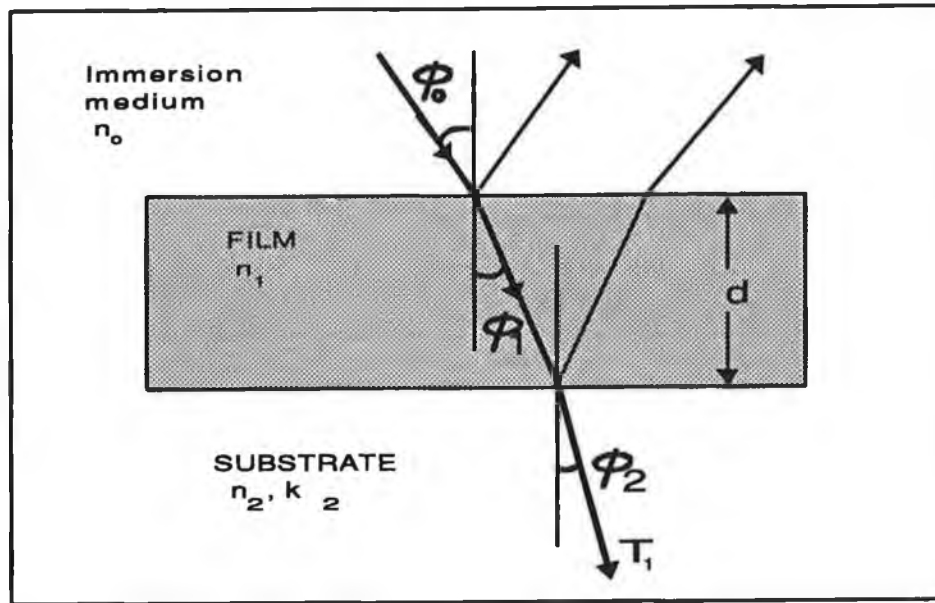
Fig. 4.20: Schematic diagram for two beam reflection and transmission
through a transparent film.

For the analysis of the system like in fig. 4.20, it is expedient to assume the
constituent wave to be polarized in parallel to the plane of incidence and perpendicular
to it respectively. In general, these parallel and perpendicular components are reflected
and transmitted to a different degree according to Fresnel's equations, resulting in
polarization dependent reflection and transmission coefficients respectively [168,169]. The
state of polarization of the wave is changed in this case. Ellipsometry entails the
quantitative analysis of such changes of the polarization, usually of an electromagnetic
wave within or near the visible part of the electromagnetic spectrum, and the interpretation
of the measured data with regard to the optical properties of the sample under
investigation.

The state of polarization is determined by the relative amplitude of the parallel (ρ_p)
and perpendicular (ρ_s) components of radiation and the phase difference between the two
components Δ_p-Δ_s, given by the following equation,

$$\tan\psi \ e^{i\Delta} = \frac{\rho_p}{\rho_s} \ e^{\Delta_p - \Delta_s}$$

For the system like in fig. 4.20, on reflection from a surface, bare or film covered,
the changes in the ratio of the two amplitude ρ_p/ρ_s and Δ_p-Δ_s are dependent upon optical
constants of the substrates n_2 and k_2, the angle of incidence φ_0, the optical constant of the

158

film n_1 and k_1 and the film thickness d. If the optical constants of the substrates are known and the film is non-absorbing (i.e. $k_1=0$), then the only unknowns in the equations describing the state of polarization [168,169] are the refractive index n_1 and the thickness d of the transparent films.

The parameters determined most frequently in technical applications of ellipsometry are the thickness and the refractive index of a thin dielectric or slightly absorbing film on a substrate with known properties. The refractive index of the film renders valuable information about the film composition and/or substrate, particularly for films in the thickness region of a few hundred nanometres or less, ellipsometry is the only technique which permits a reliable thickness measurement.

A Rudolph ellipsometer with a He-Ne laser (633 nm) incident at 70° was used to determine the film thickness and refractive index of our film on silicon.

4.6.2 STUDY OF THE FILMS

The refractive index of the films grown at 400 W and at a deposition temperature of 350°C and a filament temperature of 1600°C was 2.295. The value of refractive index with a good cBN reststrahlen peak in IR spectra did not show any value lower than 1.933. Values for the refractive index for cBN containing films are usually between 1.8-2.3 whereas the refractive index for the hBN films grown showed values in the range of 1.553-1.772. Run-to-run variations in the refractive index are usually within ±.05.

The variation of refractive index with plasma power is shown in fig. 4.21. After 200 W, the refractive index showed a sharp increase with rf power. This correlates with the increasing cBN content of the films as measured by the IR absorption peak.

It should be noted that the indices of the films with cBN content are substantially higher than those for hBN (1.7-1.8) [82c] and are close to the reported values of 2.0-2.3 for cBN [82c].

4.6.3 DISCUSSIONS

The dependence of refractive index on the power is reported widely in the literature. Targove and Macleod [170] reported a linear relationship between the refractive index of their LaF$_3$ films with ion-bombardment power. Hwango et al. [171] reported an increase of the refractive index and a decrease in the extinction coeffiecients of evaporated Ag and Al films with increasing momentum. Savvides and Window [172] reported an increase of refractive index of their a-C coatings with sputtering power.

As the refractive index showed very little increase with substrate temperature, the increase with rf power is directly related to the cBN content of the films. As the cBN content increased, the refractive index was increasing in agreement with ref. 136.
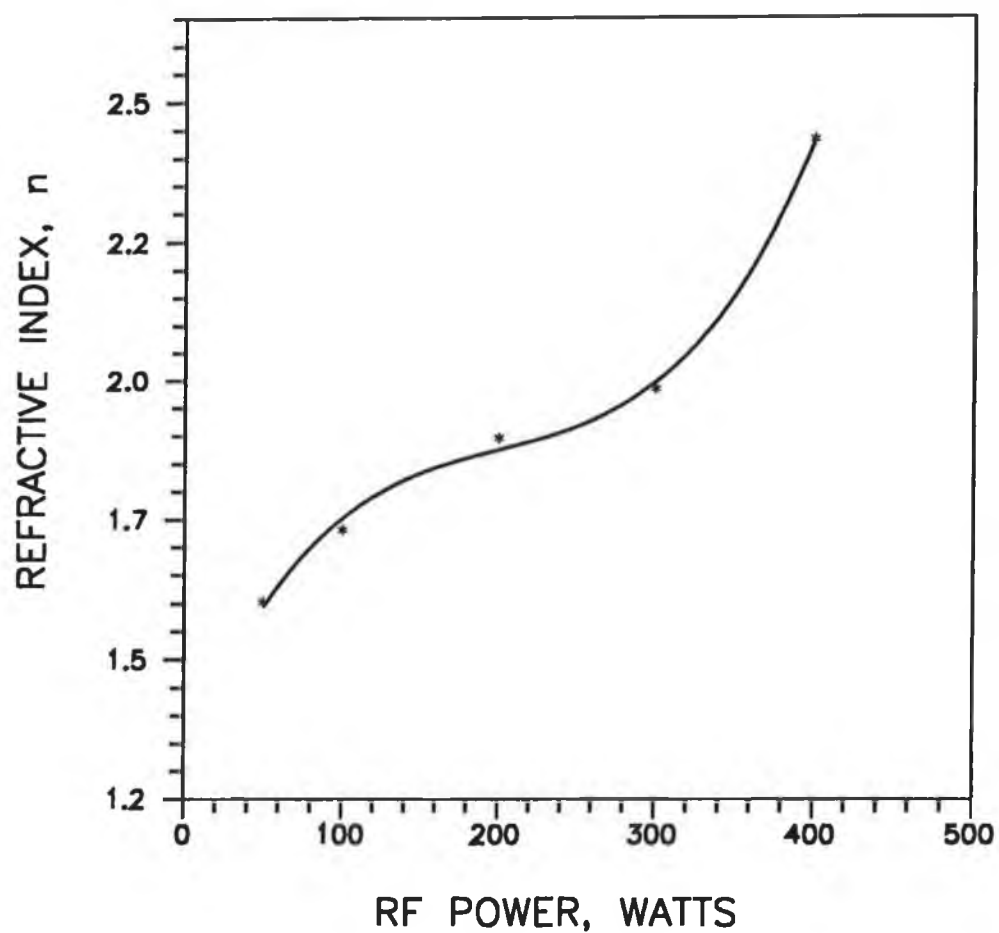
Fig. 4.21:   The effect of rf power on the refractive
index of the BN films grown at substrate
temperature of 350°C and filament
temperature of 1600°C.

4.7   STRESS OF THE FILMS

As explained in section 1.4.4, nearly all films, by whatever means they are produced, are found to be in a state of internal stress. The film would like to expand parallel to the surface under the compressive stress while it would like to contract, the stress is tensile. In the extreme cases, the interfacial shear stresses may exceed the adhesion strength of the coating-substrate interface and lead to cracking and delamination of the coating. However, compressive stresses are believed to increase coating hardness [173].

4.7.1   MEASUREMENT OF INTERNAL STRESS

Techniques used to measure internal stresses involve determination of the stresses by measuring the physical properties of the body that are affected by the presence of these stresses. The stress in the BN films are measured by the curvature method which is most commonly used.

If a coating is deposited in a stressed state on a thin substrate, the substrate will be bent by a measurable degree. A tensile stress will bend it so that the coated surface is concave, and a compressive stress will bend it so that the coating is convex. The deformation of the substrate is measured by observing the warping of the centre of a beam.

The internal stress of BN films was estimated by this bending beam method. When the films were deposited on one side of a thin substrate strip clamped at one end as shown in fig. 4.22(a), the film stress is calculated according to Stoney's equation [174].

$$\sigma = \frac{E_s d_s^2 \delta}{3(1-\nu_s)\, l^2 d_f}$$

Where, σ = film stress,
δ = deflection of the free end,
E_s = Young's modulus
ν_s = Poisson's ratio of the substrate,
d_s = substrate thickness,
d_f = film thickness, and
l = length of the substrate segment.

Since, the relation between δ and δ' is given by $\delta \approx 4\delta'$ $(l \ll \delta')$, the internal stress can be written as,

$$\sigma = \frac{4 E_s d_s^2 \delta'}{3(1-\nu_s)\, l^2 d_f}$$

Fig. 4.22(b) shows a schematic illustration of the measurement of the internal stress σ using a sensitive optical microscope technique. Films were deposited on 20mm x 6mm silicon strip of thickness d_s=0.055cm. The deflection was measured by optical

161

Fig. 4.22(a): Diagram for calculation of internal stress by bending beam method.
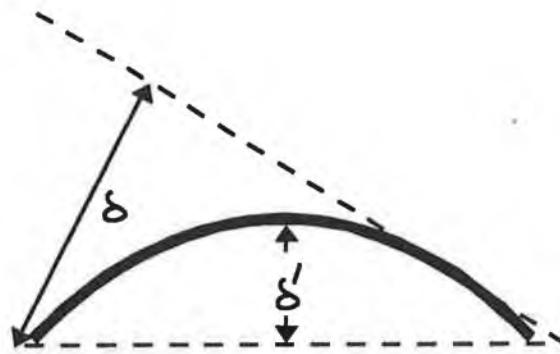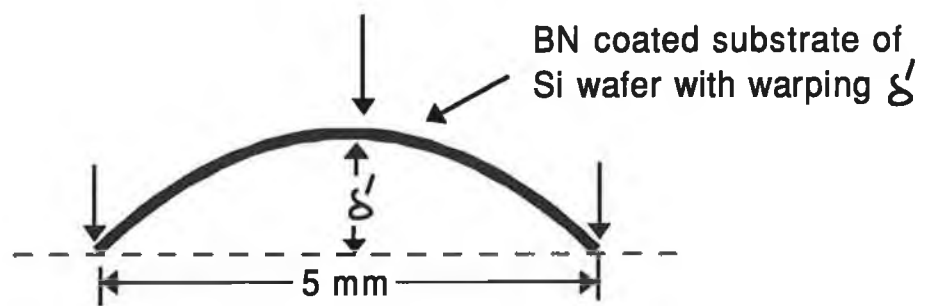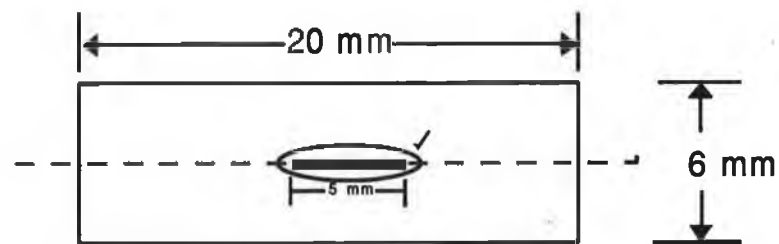

20 mm

6 mm

5 mm

BN coated substrate of
Si wafer with warping δ'

5 mm

Enlarged view of the √ portion.

Fig. 4.22(b): Schematic illustration of the measurement of the internal stress.

microscope on a 5mm length path in the middle of the substrate as shown in fig. 4.22(b). A 4" optically flat microscope slide was used to calibrate the system and initially an uncoated silicon wafer was evaluated to establish the internal curvature before deposition.

If the central deflection of BN deposited strip before and after deposition is known, the stress can be calculated from the above equation where E_s and υ_s of Si (100) substrate are 1.6 x 10^{12} dynes cm^{-2} and 0.33 respectively, d_s = 0.055 cm and l = 5mm. Thickness, d_f is measured by ellipsometric technique discussed before.

The internal film stress resulting from differences in the thermal expansion coefficients between BN films and silicon substrates was not considered here, because these differences are small enough to be considered negligible compared to the intrinsic stress in the film itself.

4.7.2 STRESS IN THE FILMS

The stress of the h-BN films grown at lower rf power ($\leq$100 W) was seen to be tensile. The average of this stress for 5 films at 100 W and 350°C is 1.67x10^{11} dynes/cm^2. But films grown at higher rf power are under compressive stress and seen to be increasing with rf power. The stress at 400 W rf power and 350°C was about 8.67x11^{12} dynes/cm^2.

The uncertainty in the stress measurement is ±10%. The data also shows large scatter at lower rf power. The scattering is thought to be due to thinness of the films. The experimental scatter is much smaller in the case of thicker films [118].

With increasing rf power, the stress crosses over from tensile to compressive from 100 W to 200 W and remains compressive up to 400 W, the maximum power investigated. Fig. 4.23 showed the variation of the film stress with rf power at a deposition temperature of 350°C.

The annealing of the film at 400°C at 10 mTorr for 15 minutes did not show any significant stress variation anyway.

4.7.3 DISCUSSIONS

High stress and poor adhesion of cBN thin films are common and widely reported [34,37]. Their films are under compressive stress. However, the origin of tensile stress of our films need to be explained. As it is difficult to explain this state of stress from only BN literature due to limited reports, we cite some examples of the behavior of metallic films.

Hoffman and Gaertner [175] thermally evaporated chromium films and bombarded them with inert gas ions. They found that the bombardment made the films go from tensile to compressive stress. Hwango et al. [171] evaporated Ag and Al films which were bombarded with Ar. They also found that the films become more compressive, and that
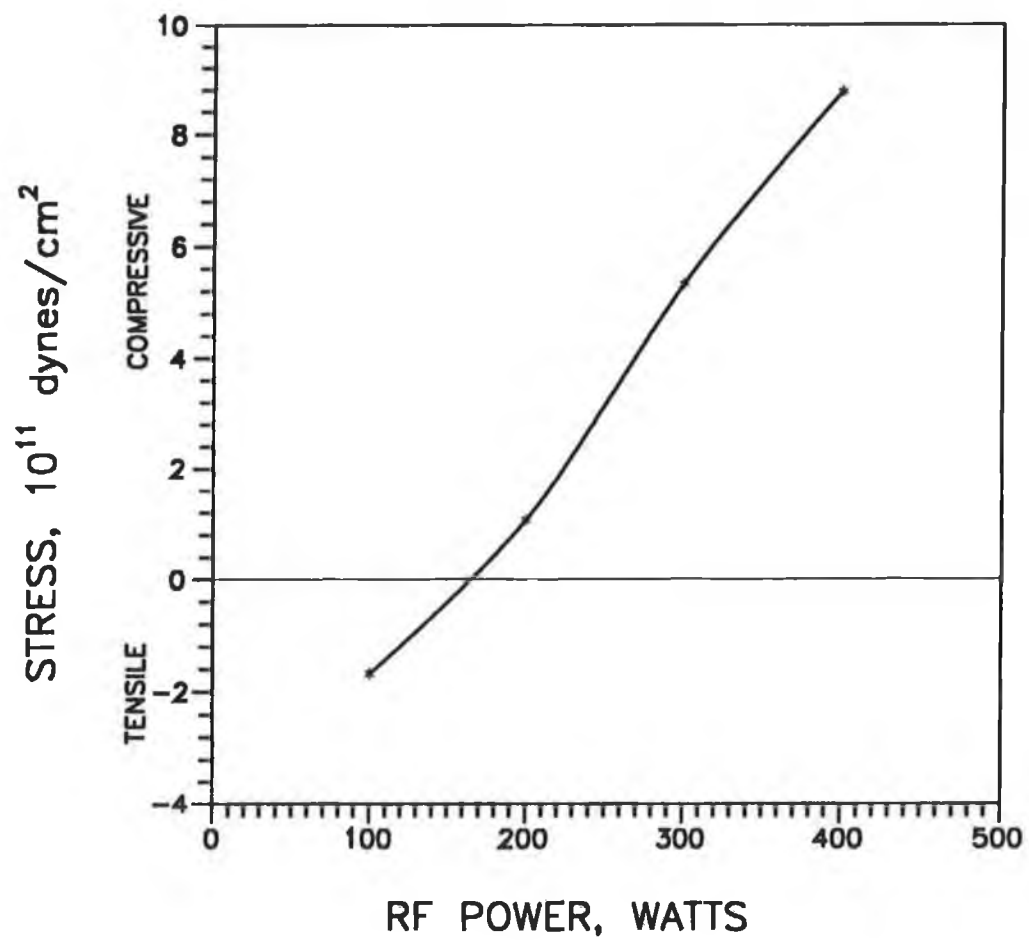
163

Fig. 4.23:   Effect of rf power on the stress of BN films

a threshold value of ion bombardment was required to make the stress in the Ag films go from tensile to compressive. Thus it has been found that films prepared with little or no bombardment are normally tensile [176] and ion bombardment leads to compressive stress in films [175].

This tensile stress of the films could be related to Zone structure model described in section 1.4. It has been shown in section 1.4.1 and 1.4.2 that films deposited under conditions of low adatom mobility (low deposition temperature relative to the melting point) or in the absence of energetic particle bombardment, generally develop a porous Zone 1 microstructure [10,11]. These films are usually under tensile stress due to attractive atomic forces acting across grain boundary or the voids pulling the film columns together. The tensile stress in the hBN films grown at lower rf power could be described from the above explanation.

Now the origin of intrinsic compressive stress is more or less established. The source of compressive stress are due to two reasons: (1) impurities generally produce compressive stress, (2) compressive stresses are produced by energetic particles striking the film [177]. Window et al. [178] investigated the effect of stress in a number of different refractory metal films deposited by ion-assisted deposition using an unbalanced magnetron. They interpreted their results as showing that bombardment led to compressive stress in the films. The compressive stress in turn, when it reached a certain level, led to a plastic flow in the films and a release of the stress. Because of this, they argued, the stress only increased with ion-bombardment up to certain point. Further increases in bombardment would not lead to increased stress due to the stress being relieved through the plastic flow of the material. They mention that the yield point where the plastic flow starts to occur would be very high for very hard materials such as TiN and diamond-like carbon film. This model may be used to explain the high stress seen in the mixed phase region and lack of it in the hexagonal region.

Hexagonal films were very smooth with good adhesion, while some cBN containing BN films were found to be cracked and peeled off when viewed under the optical microscope. Following the model of Window et al., it may be that the soft hexagonal region reaches a point of plasticity, relieving the intrinsic stress, while the cubic region never reaches that point. But the good adhesion of the mixed phase BN films may be due to the support the hexagonal region gives to the cubic region for stress relaxation.

This direct relationship of the stress and phase of the film is very interesting and the threshold value reported in Hwango et al. to make the stress go from tensile to compressive may be 160 W in our study.

4.8   NANOHARDNESS MEASUREMENTS

Hardness implies, in the simplest terms, resistance of a material to deformation and is usually measured by indenting a diamond stylus of know shape under load into the specimen and measuring the size of the resulting deformation. Common practice among workers in the coating field is to minimize the size of the indentation in an attempt to

insure that only the hardness of the coating is measured, i.e., there is no contribution to the measured hardness of the substrate.

Indentation microhardness measurements are a well-known and reliable test method frequently applied to coatings. The reproducibility is good, but when the ratio D/t of the indentation depth to the film thickness exceeds a critical value, the measured hardness H is influenced by the substrate material and is no longer a characteristic of the coating. The critical D/t ratio varies between approximately 0.07 and 0.2 where the most unfavourable case is that of a hard coating on a softer substrate, in most cases a value of 0.1 is adopted [179]. The critical value is not very distinct and, in fact, the measured hardness varies continuously with the indentation depth, the film thickness and the hardness of the film and the substrate.

The minimum load for commercial microhardness measurements is about 1g, and this may produce a depth of indentation of a few tengths of a micrometer, exceeding 10 to 20 percent of coating thicknesses on the order of a micrometer. At low loads, factors which could adversely affect the hardness measurement are loading variations, substrate support effect, penetration rates, dwell time of the indentor in the material, surface roughness, temperature and vibration. Dynamic indentation methods have thus been developed in an attempt to overcome these problems.

One way to overcome this difficulties and to measure the microhardness on thin coatings is to miniaturize further the measurement to an ultra-microhardness (nanohardness) test. As most of our films are of 100-200 nm thick, no attempt has been made to measure the hardness by microhardness techniques. The hardness of the films was performed using a Nanotest instrument manufactured by Micro Materials Ltd. The principle of this instrument has been discussed by Pollock et al. [180]. The Nanotest, unlike conventional hardness testers, produces continuous curves of load vs. indentation depth. When the depth is plotted for increasing and decreasing load, a hysteresis curve is produced the area of which represents the plastic work performed [Fig. 4.24].

4.8.1 DESCRIPTION OF NANOTEST INSTRUMENT

In the NanoTest Instrument, the position of the indenter is determined by a sensitive capacitive transducer. A coil and magnet assembly located at the top of the loading column is used to drive the indenter towards the sample. The force imposed on the column is controlled by varying the current in the coil. The loading column is suspended by frictionless pivots, and the motion is damped by airflow around the central plate of the capacitor, which is attached to the loading column. A schematic diagram is shown in fig. 4.25.

The indentor was a trigonal Berkovich pyramid with the same area to depth ratio as a Vickers diamond. The Berkovich indenter has a sharply pointed tip in comparison with the Vickers or Knoop indenters, which are four-sided pyramids that have a slight offset. A sharper tip is especially desirable for extremely thin coatings that require shallow indentations.
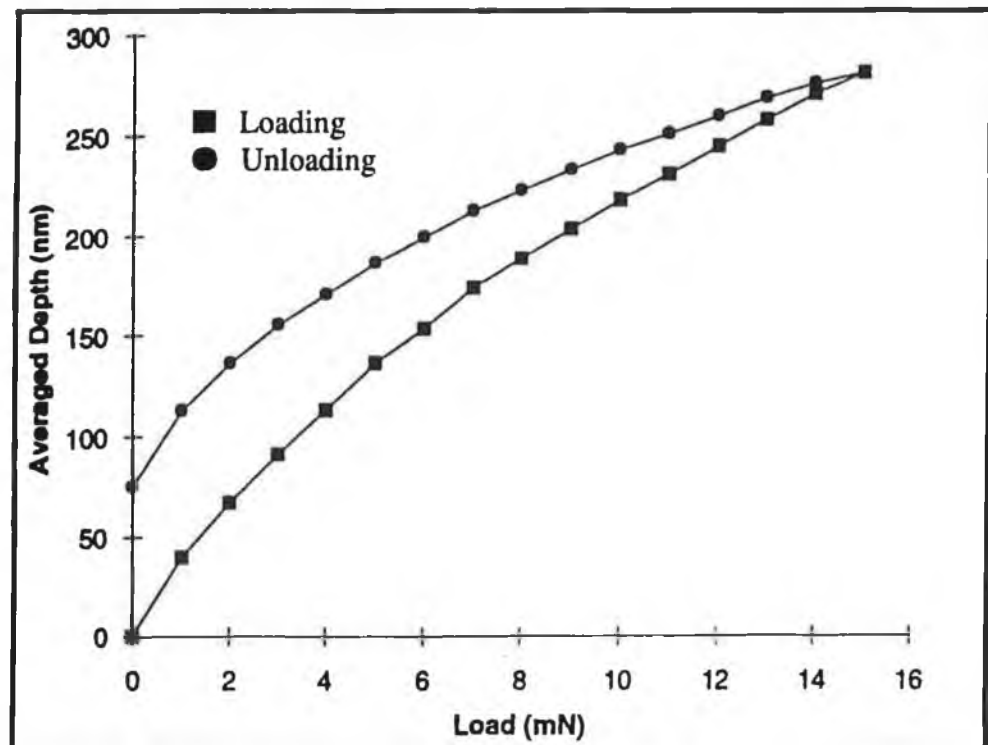
166

Fig. 4.24:   A typical Nano Indentation hysteresis curve.
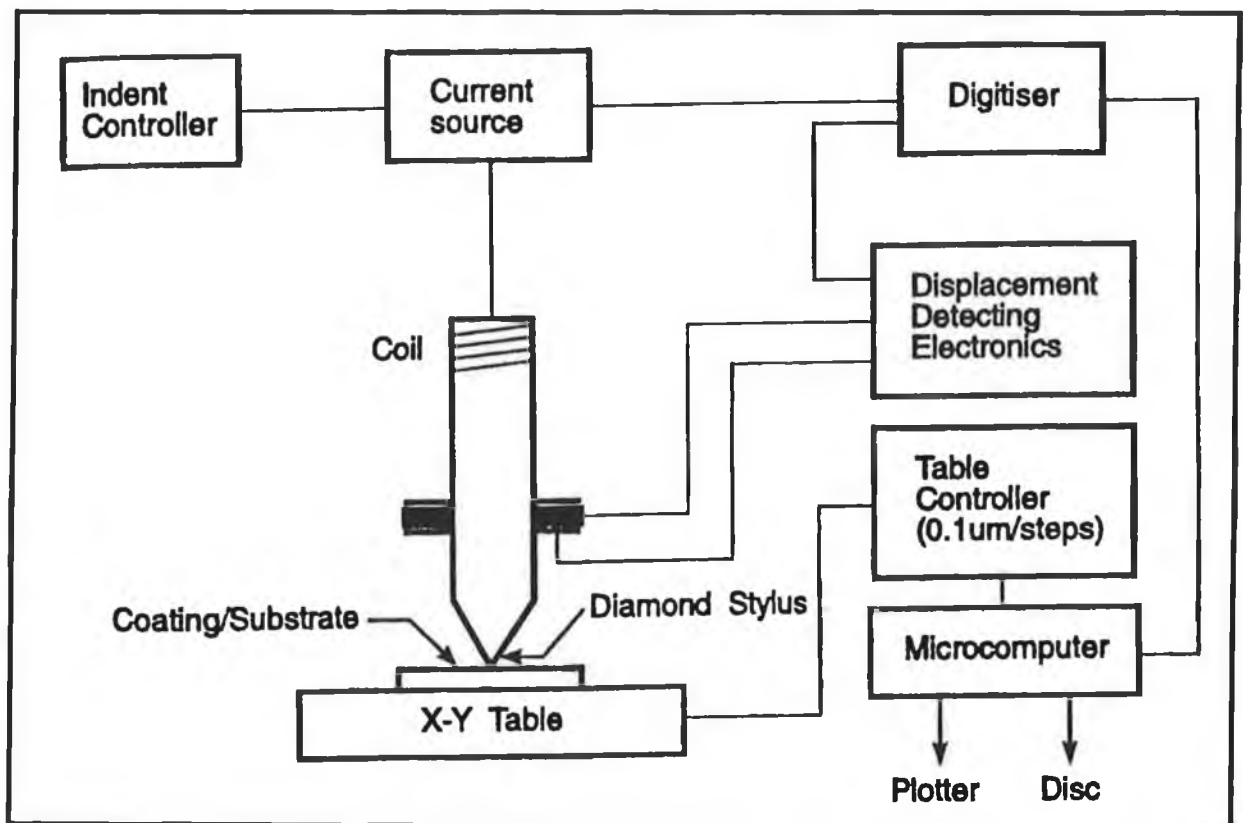
Fig. 4.25:   A schematic representation of the Nano Indentor.

4.8.2 OPERATION OF NANOTESTER

During operation of the NanoTest, the specimens were mounted on an aluminium stub using a cyanoacrylate adhesive. As a test of consistency, measurements were performed periodically on an etched silicon standard. Depth calibration and load calibration were carried out before every batch of sample. The environment during the measurements was suitably controlled and measurements were made usually at night to avoid vibrations in the building.

In the Nano-Test, specimen-diamond contact is detected when a change in capacitance occurs. For each run, the load was increased to a predetermined level and then automatically reversed. The loading and unloading curve were obtained and the resulting hysteresis curve produced.

The depth values therefore contain both plastic and elastic contributions. In order to eliminate the elastic contributions, the elastic recovery parameter ERP [180,181] was determined for each run. This is found from the unloading branch of the hysteresis curve where the intercept at zero load represents the plastic depth.

A two dimensional array of indentation points were produced using an X-Y-Z translatory stage upon which the specimens were supported during the experiment. The instrument has been reported to possess a depth resolution of 0.2 nm, a load resolution of 0.5 μN and an X-Y-Z positioning accuracy of 0.5 μm.

4.8.3 HARDNESS OF THE FILMS

The load was varied for each sample from 20 mN to 0.2 mN and at each load, a hysteresis plot of load vs. depth was obtained. The resulting hardness values for each run were plotted against plastic depth.

Fig 4.26 shows the hardness vs depth curve for sample no. 1 grown at 400 W rf power with a substrate temperature of 350°C and filament temperature of 1600°C. In the same figure, curve for uncoated and etched silicon is also shown for a comparison of composite hardness and substrate hardness. Fig. 4.27 shows the same curves for sample no. 2 grown at 300 W rf power under the same conditions together with the curve for Si. For higher indentation load, the films begin to display a trend in hardness values which approaches that of the underlying material (Si). There is a slight improvement in the hardness of the coated substrate. All the films are approximately 300 nm thick.

It is often most practical to simply compare specimens by normalising one set of data to another. This approach effectively eliminates questions of the diamond geometry. Fig. 4.28 shows the hardness data from sample 1 normalised to the hardness data obtained from the substrate material. An improvement of approximately 1.5 times is apparent from the figure.
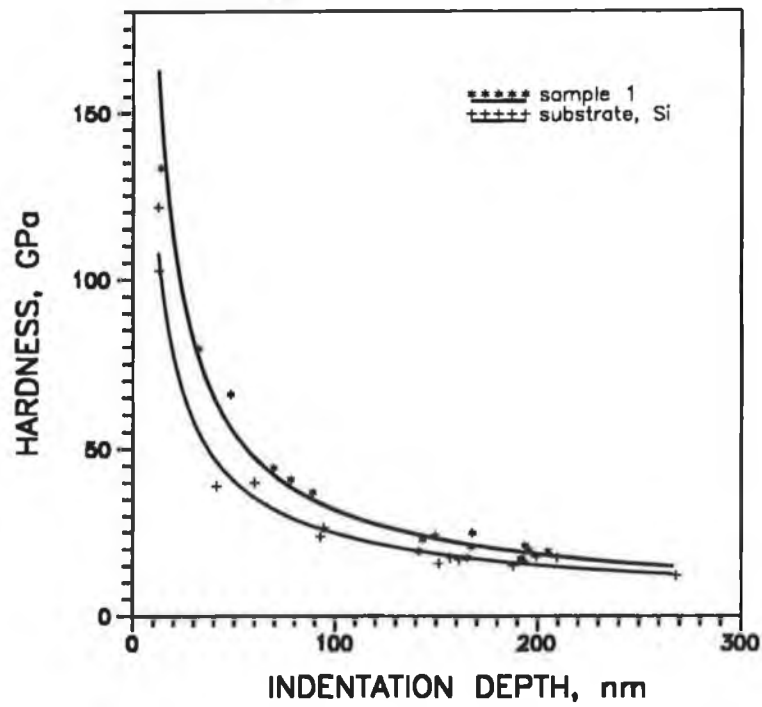
Fig. 4.26: Apparent Hardness vs. depth curves
for sample 1 and substrate Si. Sample 1:
Mixed—phase BN films grown at rf power
of 400 W, T_s=350°C, T_f=1600°C.
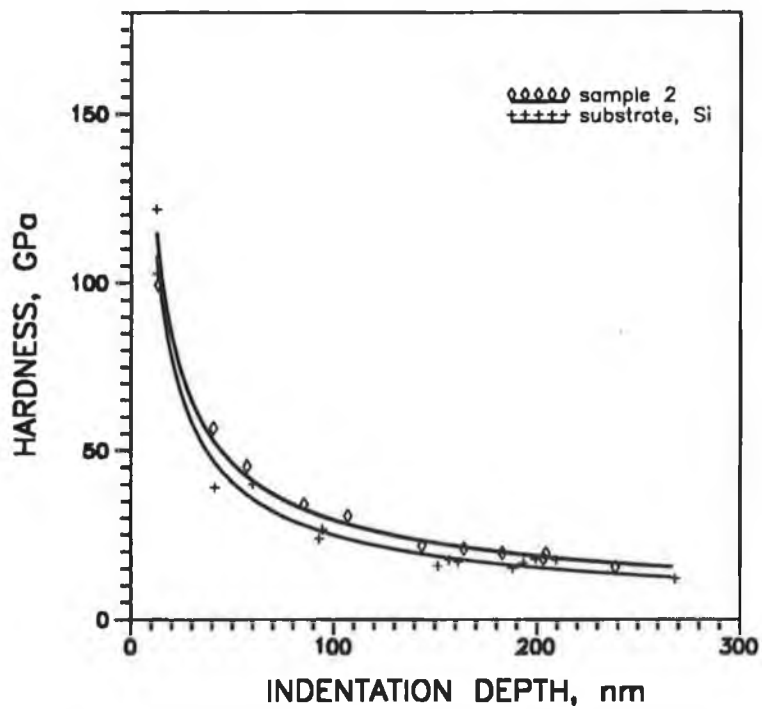
Fig. 4.27: Apparent Hardness vs. depth curves
for sample 2 and substrate Si. Sample 2:
Mixed—phase BN films grown at rf power
of 300 W, T_s=350°C, T_f=1600°C.
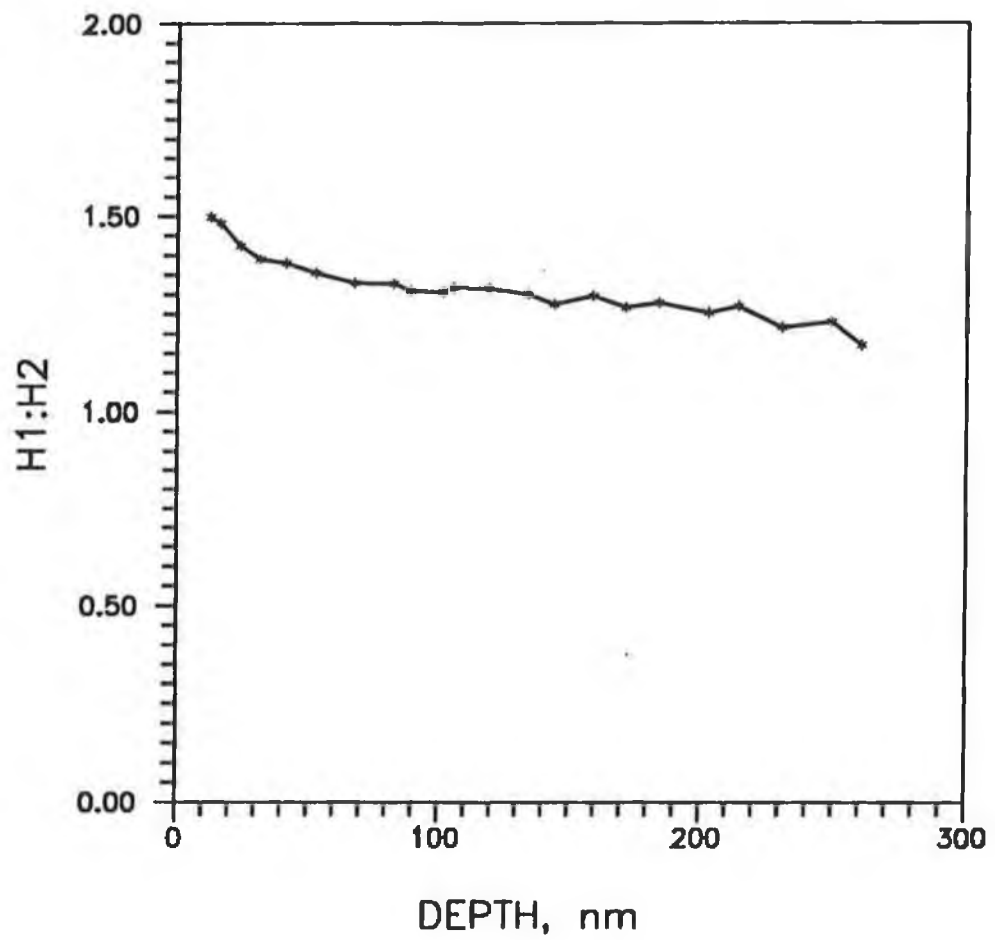
Fig. 4.28:   Normalised hardness data
(Sample 1:substrate Si)

The hexagonal film coated substrate did not show any improvement of the hardness compared to silicon substrate.

4.8.4 DISCUSSIONS

No absolute value of hardness was estimated from the nanoindenter measurements. Several effects tend to complicate the interpretation of submicroscopic test results in addition to experimental limitations such as vibrations, surface roughness and contamination, and imperfect indenter geometry. First, the value of hardness depends on the strain rate at the time when the measurement is made: even at ambient temperature, time-dependent effects can be significant at submicron depths and at low loads. Also surface roughness affects the measurements. The quantity of scatter associated with each set of data was noticeable at low loads, this may be due to the result of slightly poorer surface roughness of the BN films.

Films were also too thin to have a reliable absolute hardness. In addition, vibration effects were significant during the measurement sometime giving spurious results. However the majority of the measurements were consistent.

4.9 CONCLUSIONS

The properties of mixed-phase BN films containing cubic phase grown by PACVD from borane-ammonia were investigated as a function of deposition parameters. There is an excellent correlation between the cubic content of the films and the properties of the films. The threshold value for obtaining the cubic phase was found to be 160 W of rf power and more than 300°C of substrate temperature.

The films are thought to be amorphous in structure, containing crystallites of the cubic phase embedded in a hexagonal matrix. Structural characterization was also done by Siemens D-500 X-ray diffractometry. Other than a big peak due to Si, no peaks due to BN phases could be found. As B and N are poor X-ray scatterers and the films are thin (100-300 nm), this was not unexpected. It would appear that the films do not contain any long-range crystallographic order, and are amorphous or nano-crystalline in structure.

A correlation between plasma parameters and film properties was also obtained by plasma diagnostics and film characterization.

171

CHAPTER 5

ELECTRONIC PROPERTIES

OF

MIXED-PHASE BN THIN FILMS

5.1 INTRODUCTION

The metal-insulator-semiconductor (MIS) diode is the most useful device in the study of semiconductor surfaces. In MIS structure, as the thin insulating films are sandwiched between metal and semiconductor, we are concerned with conduction through, rather then along, the plane of the film.

Since our films are generally less than 500 nm thick, it will also be apparent that we will be concerned primarily with the high field electrical properties of the films, since applied biases as low as even a few volts will induce fields of the order of some KV per cm in the films.

Having studied the structural property of mixed-phase BN films on semiconductor (Si) substrates, investigation of the insulating properties can give valuable information about the potentiality of these films for electronic applications. Measurement of the current-voltage and capacitance-voltage characteristics can specify the insulating properties of the films and can show the deviation of the actual MIS structure from the ideal model.

5.2 CONSIDERATIONS IN INSULATING THIN FILMS

An insulator is a material which contains very few volume-generated carriers, and thus has virtually no conductivity. The electrical properties of thin film insulators are determined not by the intrinsic properties of the insulator but by other properties, such as the nature of the metal-insulator and insulator-semiconductor contact.

The observed conductivity in thin film insulators is often believed to be due to extrinsically rather than intrinsically bulk-generated carriers. The source of the extrinsic conductivity is thought to be the inherent defect nature of vacuum deposited films. A further problem arises is due to the contamination of the films by deposits arising from residual gases like oxygen and carbon. In addition to that, insulating films are usually polycrystalline, and in many cases are amorphous. This induces traps because of grain-boundary defects alone. Furthermore, vacuum-deposited films contain large stresses which induce further trapping centres.

It follows then that thin film vacuum-deposited insulators can contain a large density of both impurity and trapping centres. A judicious study of electrical conduction in vacuum deposited thin films cannot be accomplished without considerations of these possibilities.

The energy diagrams for an ideal MIS structures of fig. 5.1(a) is shown in fig. 5.1(b). In this energy diagram, the forbidden gap separating the conduction and valence bands for the insulator is not shown as the insulator band gap is big. However, this gap is usually shown with well-defined boundaries. Strictly, a well-defined energy gap is a

172
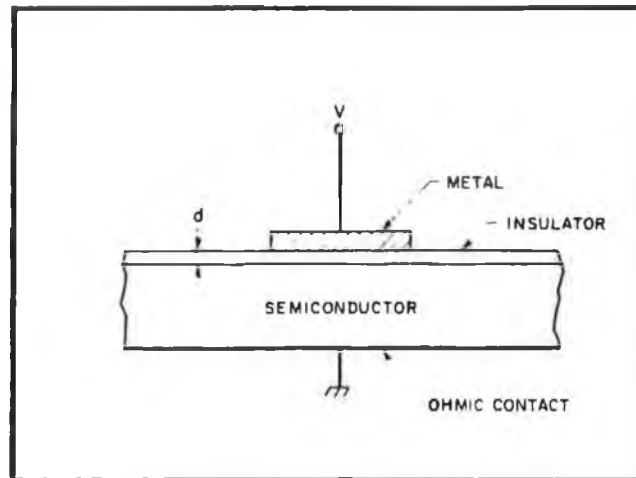
Fig. 5.1(a): Metal-insulator-semiconductor (MIS) structure.
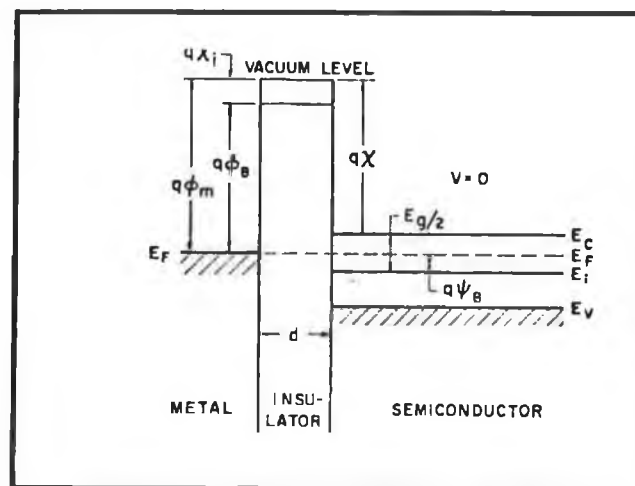
Fig. 5.1(b): Energy band diagram for ideal MIS structure (n-type semiconductor) [183].

property of a crystalline solid, and in general we are not dealing with such materials; rather we are concerned with polycrystalline, or even amorphous, insulators. The lack of the long range order in a non-crystalline solid causes smearing of the conduction and valence band edges so the energy gap is no longer well defined. What is normally done in the study of thin insulating films is to assume that this smeared-out energy gap, to a first order approximation, can be represented by a well-defined energy gap which is representative of perhaps an average value of the actual non-discrete energy gap.

5.3 PRACTICAL MIS STRUCTURES

In appendix C1, a detailed description of an ideal MIS structure has been given.

Now, in the practical case, the transition from ordered semiconductor crystal lattice to the insulator layer represents a major discontinuity which will result in dangling and unsaturated bonds. In an energy band diagram, the effect of unsaturated bonds as well as of impurities incorporated on the surface will appear as localized allowed energy levels in an otherwise forbidden band at the semiconductor/insulator interface. These allowed energy levels are possible sources of charge at the semiconductor surface, and thus may strongly affect the ideal MIS characteristics.

Surface states or interface states are known to introduce energy levels in the band gap of the semiconductor and to be spatially localized in the interface. They can exchange charges with the semiconductor in a short time. Together with the interface states, there are fixed surface charges which are located near or at the semiconductor surface and are immobile under applied electric fields. Some workers have also considered the possible existence of interface traps, spatially localized in the insulator, near the interface, and exchanging charges with the silicon by tunnel effect. Defects or impurities which are present in the semiconductor substrate introduces deep level centres in the semiconductor band gap.

States at the semiconductor interface can be either slow or fast even at normal temperature. Slow states may be in the insulator but still near to the semiconductor. States at the air-insulator interface will give 'fixed' charges (which may drift very slowly) but are not interface states. The fast states exchange charge with the conduction or valence band rapidly, and are assumed to lie close to the interface between the semiconductor and the insulator.

When a voltage is applied, the surface levels will move up or down with the valence and conduction bands while the Fermi level remains fixed. A change of charge in the surface state occurs when it crosses the Fermi level. This change of charge will contribute to the MIS capacitance and alter the ideal MIS curve.

5.3.1 MEASUREMENT OF SURFACE STATES

The most widely used tool to determine the surface state properties is the MIS capacitor. The presence of surface states will alter the shape of a C-V curve even if the measurements are made at a frequency high enough that the states do not contribute their charge to the capacitance measurements.

At a given bias, the surface states lying above the Fermi level will give rise to an additional field in the insulator. This will result in larger voltage drop across the insulator than would be experienced if no states were present. The C-V curve will consequently be shifted horizontally by the amount of the increased drop in the insulator. The amount of this shift will depend of the density and location of the states . So a comparison between the actual and theoretical high frequency C-V curve may be used to determine the density and location of states. This method was proposed by Terman [182].

Comparison of actual and theoretical MIS curves gives a curve of ΔV versus V where ΔV is the voltage shift. The total charge in the surface states (Q_{ss}) in Coul/cm^2 at a given surface potential is then given by

$$Q_{ss} = C_i(\Delta V) \tag{5.1}$$

The surface state density per unit energy (N_{ss}) in states/cm^2/eV is then obtained by graphical differentiation:

$$N_{ss} = \frac{1}{q}\left(\frac{\delta Q_{ss}}{\delta \psi_s}\right)_v \tag{5.2}$$

As we do not expect a value of N_{ss} less than a few times of 10^{10}, Terman's method could be useful to determine interface state density of BN insulator.

5.3.2 EFFECTS OF METAL WORK FUNCTION

For an ideal MIS diode, the work function difference given by equation (C1.1) in appendix C1, is assumed to be zero. If the value of ϕ_{ms} is not zero, and if a fixed surface charge density Q_{fc} exists at the insulator-semiconductor interface, the experimental C-V curve will be displaced from the ideal theoretical curve by an amount

$$V_{fc} = \frac{Q_{fc}}{C_i} - \phi_{ms} \tag{5.3}$$

where V_{fb} is the shift of voltage corresponding to the flat-band capacitance. The fixed charges density is obtained from (6.3):

$$Q_{fc} = \frac{C_i}{q}(V_{fb} + \phi_{ms}) \ coul/cm^2 \tag{5.4}$$

5.4 CARRIER TRANSPORT IN INSULATING FILMS

In an ideal MIS structure, it is assumed that the conductance of the insulating film is zero. Real insulators, however, show carrier conduction at a field of 10^6 V/cm or lower. Clearly, the conductivity of the insulator per se will determine the conductivity of the MIS system, since it is much lower than that of the metal or semiconductor.

The basic conduction processes in insulators fall into mainly six categories. In Schottky emission process, thermionic emission across the metal-insulator interface or the insulator-semiconductor interface are responsible for the carrier transport. The voltage and temperature dependence can be written as

$$I \propto T^2 \exp[\frac{1}{T}(a\sqrt{V} - b]\tag{5.5}$$

The Frenkel-Pool emission is due to field-enhanced thermal excitation of trapped electrons into the conduction band. This can be shown as

$$I \propto V \exp[\frac{1}{T}(2a\sqrt{V} - b)]\tag{5.6}$$

The tunnel emission is due to field ionization of trapped electrons into the conduction band or due to electrons tunnelling from the metal Fermi energy into the insulator conduction band. The tunnel emission has the strongest dependence on the applied voltage but is essentially independent of temperature given by,

$$I \propto V^2 \exp(-\frac{c}{V})\tag{5.7}$$

The space-charge-limited (SCL) current results from carrier injected into the insulator where there is no compensating charge present. The current for the trap-free case is proportional to the square of the applied voltage,

$$I \propto V^2 \tag{5.8}$$

At low voltage, the characteristic is ohmic, because the bulk generated current exceeds the SCL current and current is carried by thermally excited electrons hopping from one isolated state to the next. This can be written as,

$$I \propto V \exp(-\frac{\acute{c}}{T}) \qquad\qquad (5.9)$$

The ionic conduction is similar to a diffusion process. Generally, the dc ionic conductivity decreases during the time the electric field is applied, since ions cannot be readily injected into or extracted from the insulator. The ionic conduction is given by

$$I \propto \frac{V}{T} \exp(-\frac{\acute{d}}{T}) \qquad\qquad (5.10)$$

In the above equations from (5.5) to (5.9), a, b, c, $\acute{c}$ and $\acute{d}$ are constants.

After an initial current flow, positive and negative space charges will build up near the metal insulator and the semiconductor-insulator interfaces. This causes a distortion of potential distribution. When the applied field is removed, large internal fields remain which causes some, but not all, of the ions to flow back toward their equilibrium position and hysteresis effects result.

For a given insulator, each conduction process may dominate in certain temperature and voltage ranges depending also on intrinsic and extrinsic properties of the insulator. We will discuss the conduction process of BN insulator with respect to the above processes.

5.5   EXPERIMENTAL

In order to examine the insulating properties and stabilities of BN films, Al/BN/Si MIS structures were fabricated on <100> n-type Si substrates. An ohmic contact was formed on the back surface of the Si wafers by vacuum evaporation of Al. Some of the wafers had back contacts formed by sputtered Au before film deposition. During deposition, these layers of Au underwent annealing at the deposition temperature in a predominantly N_2 environment. 2 and 3 mm square Al dots were evaporated on the BN insulator through a metallic mask. The structure is shown in fig. 5.2.

Measurement and analysis of the current-voltage (I-V) characteristics were carried out using a Keithley 614 electrometer to measure the current. This characteristic of the structures were measured point by point. Measurements were always made by scanning the I-V curve several times with both increasing and decreasing voltages. The first application of high field caused a permanent decrease in resistance, thereafter the samples were quite stable. For this reason, each sample was aged for a few minutes at a certain field before the measurements were begun. All measurements were carried out at room temperature.
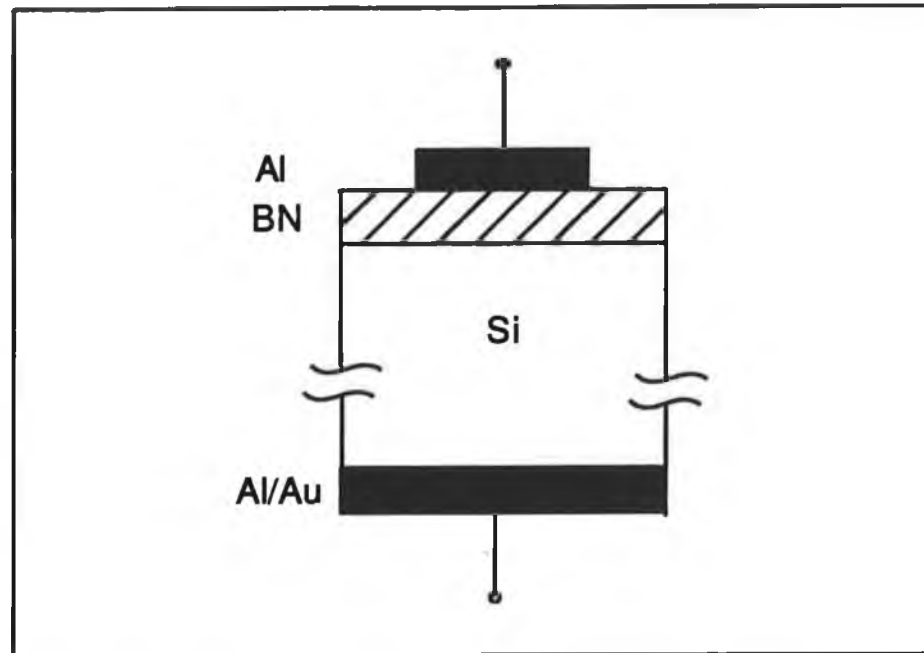
Fig. 5.2: Al/BN/Si MIS structure.

The capacitance-voltage (C-V) curves were measured with a Boonton capacitance meter at a frequency of 1 MHz. The initial trace was obtained for voltages varying from negative to positive. The retrace was obtained for voltage varying from positive to negative and was measured immediately following the completion of the initial trace.

5.6   CHARACTERISTICS OF MIS STRUCTURES

5.6.1   C-V CHARACTERISTICS

The typical MIS diode capacitance-voltage (C-V) characteristics of an Al/BN/n-Si measured at 1 MHz are shown in fig. 5.3, using a top surface contact with an area of 4 mm^2. The silicon doping was 1.45×10^{16} cm^{-3} and the film thickness was 936 Å. Th ideal curve, drawn using a computer program given in appendix C2 which is based on the equations in appendix C1, is shown in the same figure.

In the C-V characteristics obtained for voltages corresponding to the deep depletion state up to those corresponding to the accumulation state and back, a highly reproducible
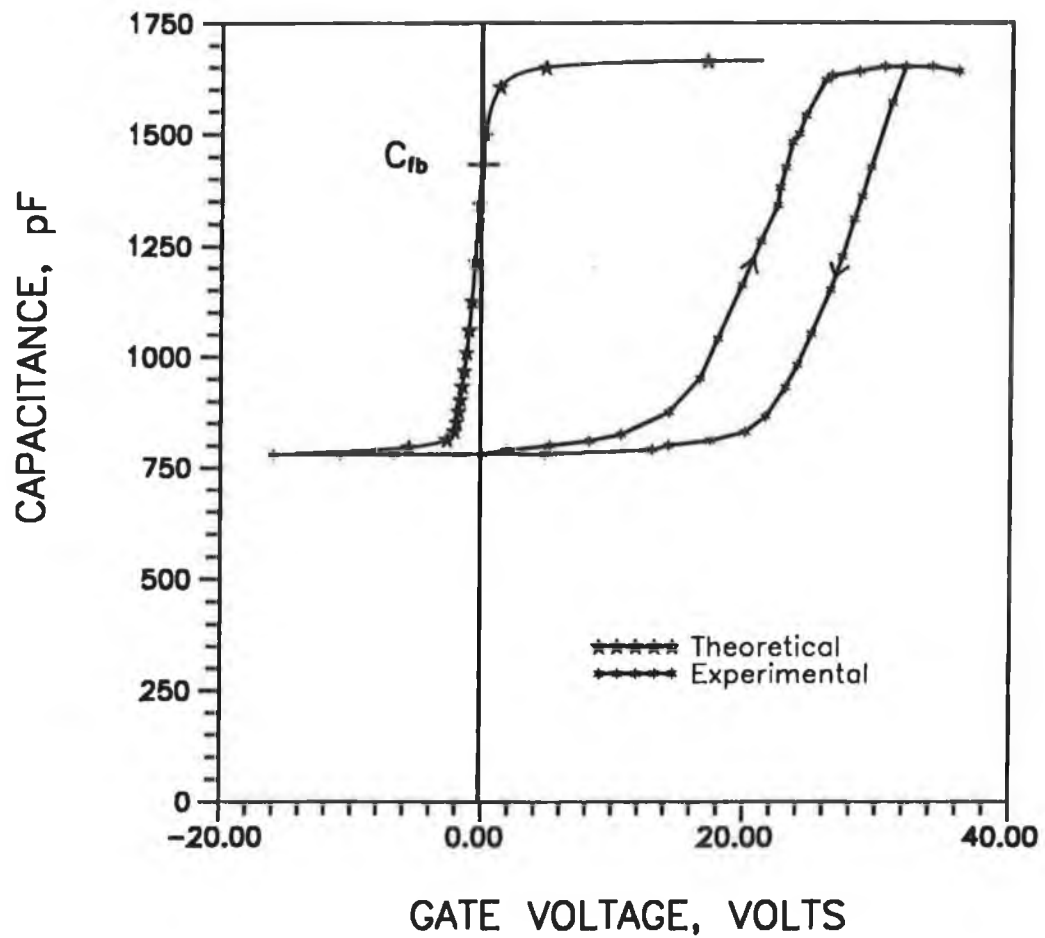
Fig. 5.3: High frequency C-V characteristics of Al/BN/Si MIS structure (n-type 100 Si;f_{meas}=1 MHz; C_{max}=1663 pF; dielectric thickness 93.6 nm, gate surface area 4 mm^2).

hysteresis loop appeared. The hysteresis displayed was in the clockwise direction. The arrows on the curve indicate the direction in which the voltage was varied. The initial trace was obtained for voltage varying from positive to negative and was measured immediately following the completion of the initial trace. The curves shifted towards rather a big positive voltage, as compared with the ideal curve.

The MIS structure was used as the vehicle by which the interfacial properties could be analyzed. These included the dielectric constant ε_i of the BN insulator, the flat band voltage V_{fb}, the surface-state density N_{ss} and its distribution and the fixed charge density Q_{fc} in the insulator.

As from the C-V curves, in the voltage range to the accumulation state near the semiconductor surface, the capacitance increases to saturation, attaining the value C_{max}. From the assumption that $C_{max}=C_i$ and the thickness of the BN films obtained by ellipsometry, the dielectric constant of mixed-phase BN films were in the range 2.2-4.41. These values are close to the reported values for BN films in ref. 145 where they have a value of greater than 4.2 for cBN films.

The flat-band voltage, V_{fb} was determined from standard analysis of the C-V characteristics. Depending on the equation (C1.6) and (C1.8), V_{fb} was determined on the basis of theoretical calculations of the flat-band capacitance C_{fb}, which in turn was calculated from the known dopant concentration in the substrate and C_{max}. Using the program in appendix C2, the flat band capacitance for fig. 5.3 was 1467 pF and corresponding voltage was approximately 26 V. The hysteresis voltage, which is the flat band voltage difference between the two trace, was no greater than 5 V. Fig. 5.4 shows the dependence of surface potential on applied voltage for the same system as of fig. 5.3.

Using Terman's method, a computer program using equations (5.1) and (5.2) was developed to determine the distribution of surface state density. This distribution was approximated by U-shaped curve given in fig. 5.5. The minimum interface state density was found to be 1.75×10^{12} states/cm^2/eV.

5.6.2 DISCUSSIONS

It can be seen that the surface is in an inverted state with zero applied gate bias. The depletion width W of the BN-Si junction was calculated from the capacitance at zero bias assuming an abrupt approximation and was found to be 0.278 μm. There may be a slight effect due to the fringing fields at the edges of the top contact since the substrate has much larger area, but the length of the top contact is about 1000 times larger than the films thickness so this is not thought to be significance.

The overall shift of the curves towards positive voltage, as compared with the ideal C-V curve, corresponds mainly to fixed negative charges located in the bulk of the BN insulator or at the BN/SI interface. Using equation (5.4), this fixed charge density was found to be 6.67×10^{12} states/cm^2 from the known metal work function, ϕ_{ms} [183].
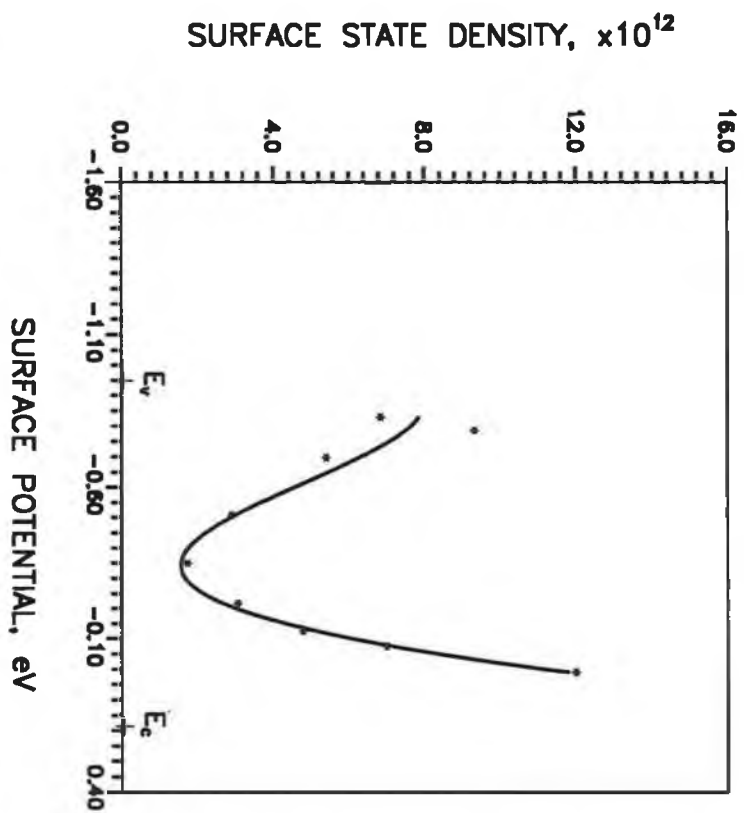
Fig. 5.5 Variation of surface state density with surface potential for Al/BN/Si MIS structure.
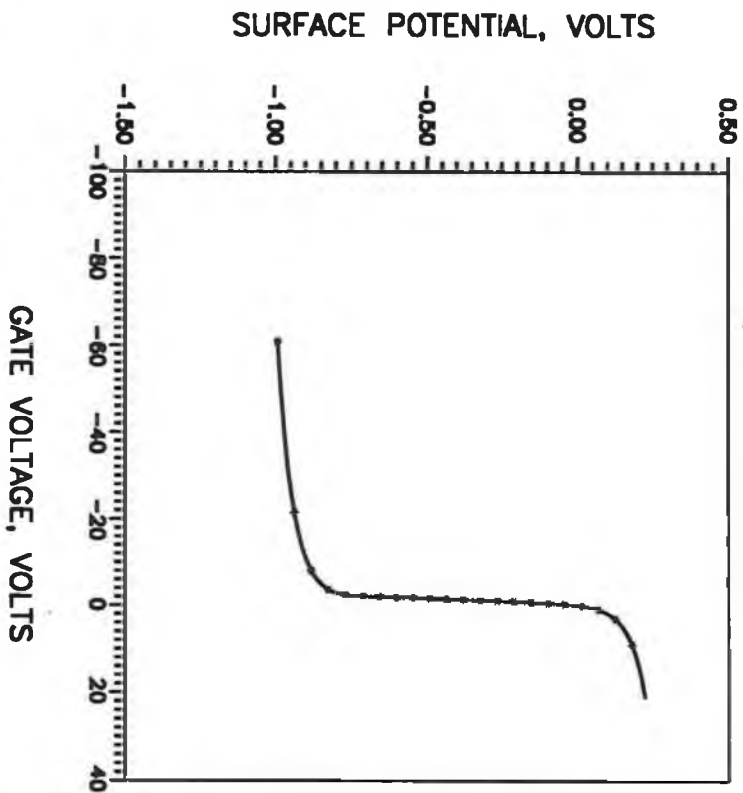
Fig. 5.4: Surface potential vs applied voltage for Al/BN/Si MIS structure (n-type (100) Si; $f_{meas}=1$ MHz, $C_{max}=1663$ pF; dielectric thickness 93.6 nm, gate surface area 4 mm^2).

The overall shape of the curve show a satisfactory capacitance modulation, and a clockwise hysteresis displayed by the C-V curve was probably due to electron injection from the silicon into the BN films.

Fast interface state density values can be comparable to the value for plasma deposited SiN (2×10^{11} - 7×10^{12} cm^{-2}) and SiO$_2$ (2×10^{11} cm^{-2}). A high interface state density could be due to the amorphous nature of the films.

On the other hand, Terman's method's precision is rather poor and it only gives information on the same restricted part of the gap. The facts that only the integral of N$_{ss}$ is measured and there is uncertainty about the magnitude of the semiconductor depletion-layer capacitance makes the method somewhat unreliable.

5.6.3 I-V CHARACTERISTICS OF MIS

The I-V characteristics shown in fig. 5.6 were essentially linear in the low voltage region. Changing from Al to Au electrodes had no effect on the characteristics. Reversing direction or polarity had little or no effect; with some samples a few percentage difference was observed.

From the measured I-V characteristics, the resistivity of the films was measured and varied between 3.24×10^{12} to 3.3×10^{13} Ω cm. Most of the films showed consistent resistivity of a value not less than 3.24×10^{12} Ω cm.

The dielectric breakdown strength of our films was ranging from 8×10^5 V/cm to 4×10^6 V/cm.

5.6.4 DISCUSSIONS

The metal/BN contact and the Si/metal contact resistances are neglected, due to the high value of the resistance of BN insulator. The resistivity of the layers are better than 10^{12} Ω cm, indicating a good insulating properties.

The transport properties probably agrees with the equation (5.9) at this low voltage range, showing ohmic behavior. At low voltage, there will normally be a sufficient supply of carriers available to enter the insulator from the cathode to replenish the carriers drawn out of the bulk of the insulator. A number of authors reported Frenkel-Poole mechanism for the current transport of the BN insulator on Si or InP [104,107], such a process was not involved due to low fileds.

Again, as the films are amorphous, impurity conduction is possible which is usually ohmic in nature.
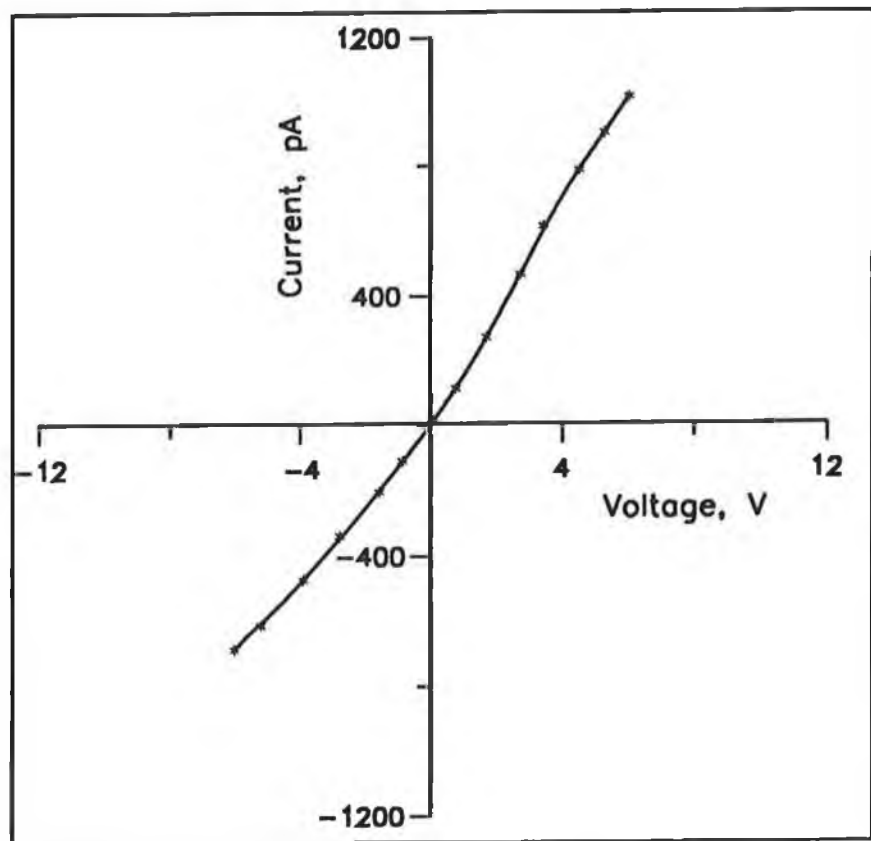
182

Fig. 5.6: I—V characteristics of Al/BN/Si MIS structure.

An excellent correlation was found between the refractive index (n) and delectric constants (ε_i) of the films. Fig. 5.7 showed a approximately linear relationship between n^2 and ε_i.

The real and imaginary parts of the dielectric constant, ε_1 and ε_2 are related to n and k, extinction coefficients by the following equations:

$$\varepsilon_1 = n^2 - k^2 \quad \text{and}$$
$$\varepsilon_2 = 2nk$$

The difference in the fig. 5.7 could be due to non-inclusion of extinction coefficient which is usually small. This interdependence, then, could be related to the cubic content of the films and rf power of the system. But this curve is drawn depending on only 5 films, so the conclusions are not reliable.

5.7   CONCLUSIONS

Our mixed-phase boron nitride films showed a high resistivity and a high breakdown field and MIS capacitors on silicon substrates using these films showed normal behavior with a rather high negative charge density in the insulator and a relatively low level of fast interface states. Table 5.1 lists some of the electro-physical properties of our films.

Based on these results, cBN containing films show potential for use in electronic circuits. The value for the dielectric constant, the high breakdown field, the high chemical resistance, the good adhesion, the amorphous structure and the high melting point of the BN films are favourable properties for semiconductor device applications, Neverthless, the exploitation of these advantages requires improvement in the quality of the dielectric and in the state of the boundary region between the dielectric and the semiconductor.
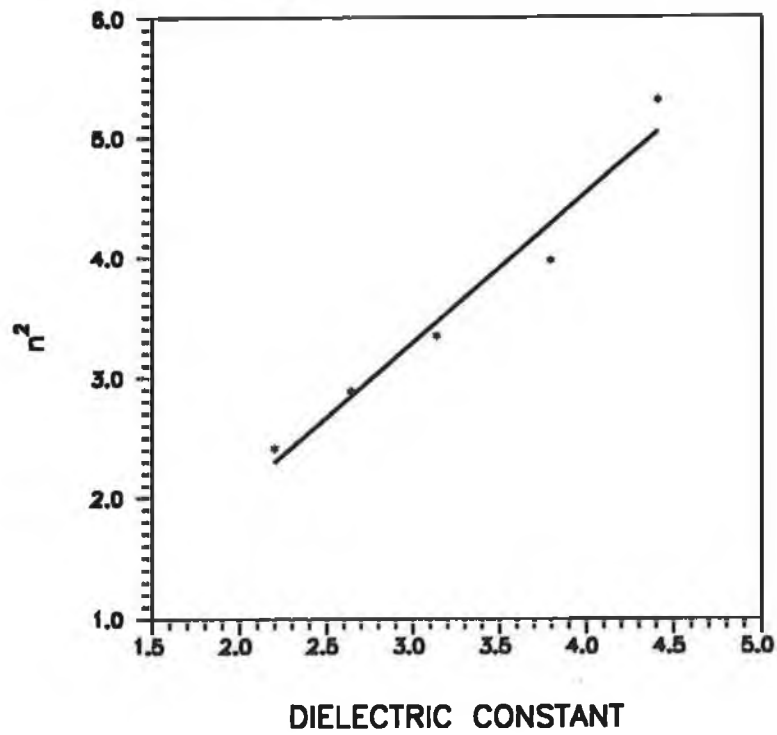
Fig. 5.7: Refractive index as a function of dielectric constant for BN films.

Table 5.1 Electro-physical parameters for MIS structure

Properties	Al/BN/n-Si
n	1.55-2.3
ε_i	2.2-4.41
V_{fb}	26 V (for ε_i=4.41)
N_{ss} (states cm^{-2} eV^{-1})	(1.75-7)x10^{12}
ρ (Ω-cm)	(3.24-33)x10^{12}
Q_{fc}	7x10^{12}
Breakdown voltage (V cm^{-1})	(8-40)x10^5

185

CHAPTER 6

CONCLUSIONS

6.1 INTRODUCTION

The formation of the metastable cubic phase was obtained using a filament activated PACVD process. In this section, the growth mechanism leading to the formation of BN films will be discussed, and the directions in which future research in this area should take place will be outlined.

6.2 GROWTH MECHANISM OF BN FILMS

Although considerable research has been done over the last few years to understand deposition of cBN films, the mechanisms involved during nucleation and growth of cBN are not yet well understood. Only recently, Komatsu et al. [147] presented a growth mechanism of their BN films deposited on laser-irradiated substrates. Probably at this stage, the only concern is to grow well-crystallized cBN; the investigation of growth mechanism will succeed this stage. Yet a central issue for the foreseeable future lies with the question of why presence of cBN should be observed in the films grown by many PACVD techniques, including this work. In this section, a probable growth mechanism will be presented backed by OES study of the plasma and applicable chemistry.

After understanding the crystal structures of BN from chapter 2, we will try in this section to explain a predicted model by which BN films with their metastable phases are actually growing on the substrates.

In sections 2.4, the growth mechanism under high temperature high pressure conditions and under shock compression was explained. In that section, it was claimed that though hBN is thermodynamically stable and cBN is metastable, cBN could be more stable than the layered phases - once it is formed.

In section 2.5, it was also explained that the preparation of relatively defect-free cBN is not thermodynamically inconsistent and there is no reason to suppose any fundamental theoretical limitations on either the amount or the quality of the metastable phase of cBN might be grown using low pressure vapour phase methods. Bearing all these in mind, we will explain the mechanism of the PACVD and the influence of plasma species in the growth of cBN films.

6.2.1 COMPARISON WITH DIAMOND FILM GROWTH

Despite the analogy to carbon shown in chapter 2, the growth mechanism, growth chemistry, and thermodynamic situation of cBN are totally different from what is today believed to the diamond growth mechanism. Diamond can be grown near thermal equilibrium if the system is provided with a sufficient amount of atomic hydrogen and

methyl radicals achieved by using plasmas or hot filament activated CVD processes. Atomic hydrogen probably reacts as a specific etching agent for graphite and stabilizes the sp^3 configuration of carbon. On the other hand, experimental conditions, which typically produce very well-crystallized diamond in the hydrogen carbon system produce, at best, only poorly crystallized cBN in the hydrogen/boron-nitrogen system. Although some researchers claimed of a role of atomic hydrogen in their poorly crystallized cBN growth from $BF_3/H_2/N_2$ system, but the claim was not based on any firm experimental achievement as the roles of other process parameters are ignored and they were discounting the roles of fluorine and nitrogen ions [136]. This result can be rationalized by studying the thermochemistry of analogous compounds in both the carbon and BN systems and also with a simple comparison of their descriptive chemistries.

The relative stabilities of analogous saturated and unsaturated compounds in the two chemistries can be compared by examining the enthalpies of formation for these compounds. For example, comparing ethane (C_2H_6) and diborane (B_2H_6), their respective enthalpies of formation are found to be - 20.2 kcal/mol and +7.53 to +9.8 kcal/mol, suggesting that the fully hydrogenated boranes are significantly less stable than their fully hydrogenated carbon analogues. On the other hand, the enthalpies of formation of the unsaturated analogs, borazine ($B_3N_3H_6$) and benzene (C_6H_6) are found to be -129 kcal/mol and +19.8 kcal/mol, respectively, strongly suggesting that although unsaturated carbon compounds are relatively unstable with respect to hydrogen saturation, their boron-nitrogen analogs are relatively stable. This suggests, consistent with the experimental data, that although atomic hydrogen can stabilize sp^3 hybridized carbon at the growth surface of diamond, an analogous stabilization of the BN growth surface by atomic hydrogen is more difficult if not impossible.

6.2.2 BACKGROUND OF PROCESS MECHANISM

In PACVD of thin films, several reaction paths can contribute to the dissociation of parent molecules or to the formation of precursors to the growth: (1) electron-impact dissociation, (2) pyrolytic decomposition, (3) hydrogen-abstraction reaction by atomic hydrogen in a plasma containing hydrogen, (4) photolysis for some cases; (5) rare-gas sensitized dissociations for the process using rare gas, and (6) dissociative attachment of an electron. Although the contribution ratio of them to the dissociation depends on experimental conditions, we may believe that the dissociation is dominantly initiated by collisions with electrons in an ordinary low-pressure PACVD, as is established in PACVD of a-Si: H [184]; the electronic excitations of the parent molecules to those low-lying states which lead to their spontaneous dissociations take place owing to the relatively high-electron temperature (T_e), amounting to a few eV.

However, especially in the experiments where T_e is low in the deposition region set apart from the plasma generating port, the dominance of these dissociative reactions can be partially taken over by the regeneration of the thermodynamically stable parent molecules. In this case, if the substrate temperature (T_s) is kept high enough with an auxiliary substrate heater or if the filament temperature (T_f) is kept high very near to the substrate, the pyrolysis of the molecules on the film surface or in its vicinity must play

an important role in the deposition process. In this work, these thermal- and electron-impact decomposition of the source material, borane-ammonia, will be attributed to the growth of BN films.

Again, the relatively low substrate temperature (T_s), needed for crystal growth in PACVD compared with pyrolytic CVD may be attributed to two factors. First, in the PACVD environment, many of the source-gas molecules are dissociated into radicals ready to react with surface sites, therefore T_s need to provide the thermal energy only for the surface growth reaction (a chemical reaction which results in the incorporation of the material atom into the film structure) and surface migration. Second, these surface processes are assisted by ion-bombardment and/or other effects attendant with a low-pressure plasma, which effectively lowers their activation energies. This effect also plays an important role in the formation of cBN films in this work.

We can thus presume that the structure of the deposit in PACVD synthesis is kinetically rather then thermodynamically determined; the type of reaction mechanism occurring at the surface is more influential than the thermodynamical stability of a structure under given conditions in determining the resultant film structure. In other words, the "growth structure" may be different from the "equilibrium structure" in PACVD. For instance, we may site the PACVD of diamond films at reduced pressure [22], under which conditions the graphite structure must be thermodynamically stable.

In the PACVD growth of mixed-phase BN films in this work, all the parameters discussed above, e.g. plasma power which in turn produces atomic species in the plasma, substrate temperature and filament temperature played an important but predicted role in the deposition which will be correlated in the following section.

6.2.3 GROWTH MECHANISM OF FILMS

We already explained the growth mechanism of cBN under high temperature and high pressure conditions and under shock compression in section 2.4. After confirming the possibility of growing cBN films under metastable condition in section 2.5 and understanding the pyrolysis mechanism of the reactant, borane-ammonia $(BH_3\text{-}NH_3)$, in section 3.3.5, a growth mechanism will be presented here.

6.2.3.1 Deposition of BN layer

As explained in previous section (6.2.2), a thermal- and electron-impact dissociation of the precursor is expected inside the reaction chamber. As shown in equation (3.1) through (3.3), the product after thermal pyrolysis from borane-ammonia is a material with BNH composition. With the carrier nitrogen gas, the evaporated ammonia-borane or the intermediate species was brought into the plasma chamber. The electron energy in the nitrogen plasma was sufficient to dissociate the incoming evaporated precursor. So this electron-impact dissociation of borane-ammonia or its intermediate species is an important

188

phenomenon in this deposition. In addition to that, by the substrate temperature and the high filament temperature the pyrolysis of the molecules on the film surface or in its vicinity was greatly enhanced.

Moreover, filament inclusion was shown to be favourable in the growth of the cBN films as shown in the IR study of section 4.5, which is consistent with the other study [134].

As the plasma species are difficult to identify due to the presence of numerous dominant peaks of N_2 species, the atomistic level of the decomposition of the precursor in the plasma volume was not clear to us. As mentioned in section 4.2, no emission due to boron species was detected, but an increase of all the nitrogen peaks with ammonia-borane evaporation has been seen with the same N_2 flow. This is thought to be an increase in ionic species in the plasma which proves that reactant material might have decomposed in ionic level.

So the deposition of BN layers could be from plasma species or it may even be partially of the deposition of BNH species.

6.2.3.2   Role of substrate temperature and ion bombardment

As mentioned in section 4.4, without substrate temperature and at low rf power (<100 W), the film is hexagonal BN with high hydrogen content. At greater than 300°C, hydrogen elimination reaction from the surface migrating species occurs, though the temperature is so low compared to the melting point of BN that it does not play an important role in the structural growth of BN.

However, in the present case, ion-bombardment plays a very important role in the growth of sp^3 bonded BN. From IR study, the TO mode of sp^3-bonded BN absorption was found to increase with r.f. power. From OES study, the emission intensity due to N_2^+ was increased considerably with r.f. power. Ions accelerated by self-bias to the substrate contributed in increasing the volume fraction of sp^3-bonded BN in the film. The key role of the ions during the cBN growth implies that sp^3-bonded BN is only accessible under conditions far from thermal equilibrium.

Thus, aside from the substrate temperature, the flux and energy of ions bombarding the precursor molecules and the substrate surface are determining the sp^3 microstructure of BN. Also, ion bombardment may be responsible for eliminating hydrogen (bonded to N and B) from the films or from the deposited BNH species.

6.2.3.3   Designation of sp^3-bonded BN

As mentioned in section 2.4 and 4.5, under conditions not appropriate for cBN growth, the wBN could be formed. Our film showed the IR peak at 1054 cm^{-1} due to cBN. This could be explained as follows:

189

It was evident from section 2.4 that only wBN was produced from hBN and only cBN was produced from rBN under shock compression [26]. This was attributed to the fact that the hBN → cBN and the rBN → wBN transitions would have required a rearrangement of the BN layers. The hBN → wBN transition has a lower activation barrier than the hBN → cBN transition [26,185a].

The sp^3-modifications wBN and cBN can be described as stacks consisting of sp^3 hexagons in 'boat' and 'chair' forms (shown in figs. 2.4 and 2.7). The wBN structure contains 'boat' and 'chair' configurations whereas cBN is exclusively constructed from 'chair' forms. As pointed out by Bundy and Kasper [185b], in order to achieve the observed epitaxial relationship between the parent and the daughter phases, the graphite layers must deform into the 'boat' instead of the 'chair' configuration to get hexagonal diamond phase. The possibility of a similar mechanism, 'boat' rather than 'chair' deformation, being operative in the layered BN to wBN transition was raised [185b,186] in HPHT condition.

Supposing an arrangement of sp^2 hybrids of B and N atoms as preform on a silicon substrate generated from the sp^2 precursor molecules, only the formation of wBN is possible without the rearrangement of the rings (see fig. 6.1). The formation of cBN occurs only at r.f. power more than 160 W with a substrate temperature of more than 300°C. The transition wBN → cBN is only possible by cleaving the wBN bonds and reorganizing them into a cBN structure as illustrated in fig 6.1. That explained why a shift of TO mode band of BN occurred and why our films contain cBN contents. But the supplied activation energy from ion and substrate temperature were probably not enough to overcome a complete transition thereby getting pure cBN films. For that, we probably need a recently reported growth condition (r.f. power 3 kW, substrate temperature 900°C with laser irradiation of the film) [147].

The active species forming the sp^3-BN modifications in PACVD and PVD processes are unknown and therefore any conclusions concerning growth mechanism and chemistry have only deductive character or more carefully expressed are speculations. But the mechanism probably resemble a close relation with that of HPHT condition described in section 2.4.
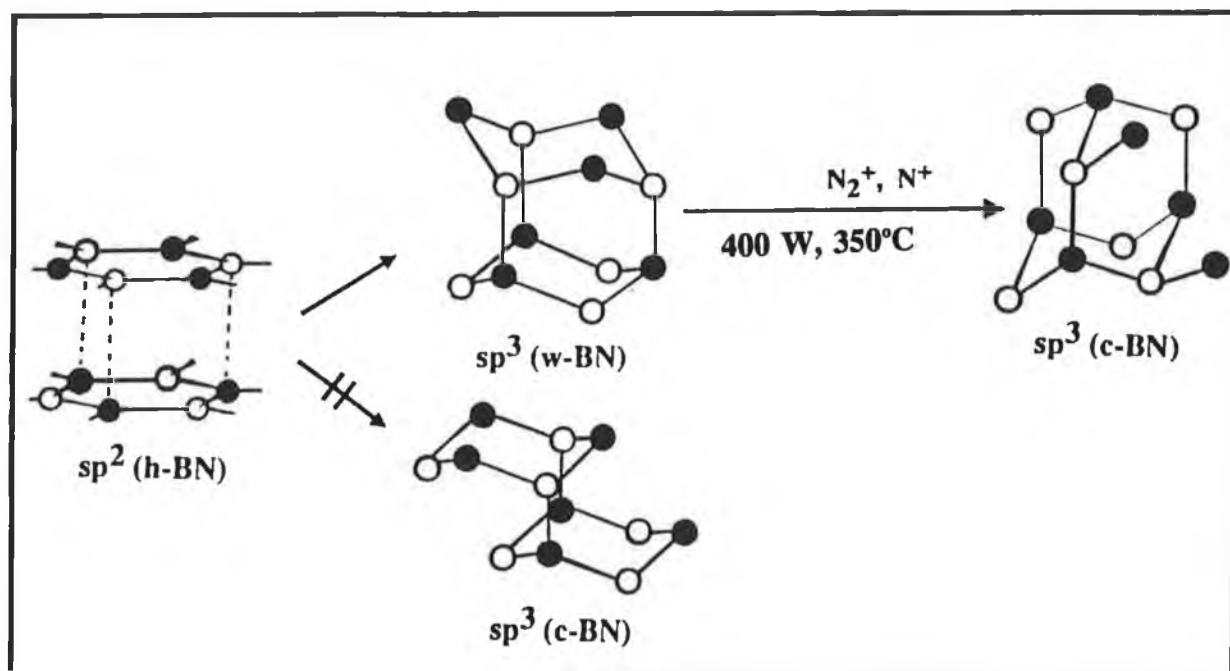
Fig. 6.1: **Formation path of wBN and cBN starting from a sp² BN preform.**

6.3 CONCLUSIONS

The deposition of BN films containing cubic phases was achieved by a filament activated PACVD system deposited from non-toxic material, borane-ammonia. With a moderate substrate temperature, the amount of cBN in the film was maximized, varying the deposition parameters. An excellent correlation between the plasma diagnostics and deposition parameters with the properties of cubic phase containing film were obtained.

6.3.1 GROWTH OF MIXED-PHASE FILM

This is one of the first reports of growing mixed-phase BN films grown from a non-toxic material, borane-ammonia by a rf PACVD system as mentioned in the literature survey of ref. 139. Borane-ammonia is considerably easier to handle and safer than diborane, boric acid, boron trichloride, boron triflouride, borazine etc. and free of impurities like oxygen and carbon.

A rf PACVD system incorporating a hot filament and substrate heating was developed with good stability in radio frequency environments and excellent potentiality of growing different thin films. In producing metastable films like cubic boron nitride, it was found that a capacitively coupled system is more efficient in producing metastable phases than an inductively coupled system or inductively coupled system with dc substrate bias.

Mixed phase BN films were deposited by the above technique under a wide range of conditions. Depending on deposition conditions, both hexagonal and mixed-phase BN films could be deposited by this PACVD system. But only under certain conditions, a mixed-phase characteristics of BN films obtained. In the growth and phase stabilization of cubic phase, it was found that ion-bombardment plays an important and unique role in forming the sp^3-microstructure of BN films. It was evident from this work that for a specific substrate and filament temperature, if the deposition conditions are measured in terms of ion-bombardment, a sharp threshold value exists where the phase of the films starts to go from being hexagonal to being cubic. At a substrate temperature of 350°C, this threshold value was found to be 160 W of rf power where the volume fraction of N_2^+ species in the plasma is considerable with respect to N_2 species. The ion density and thus ion flux to the more negatively biased substrate was increased with r.f. power and contributed in increasing the volume fraction of cubic phase.

In addition to bombardment, substrate and filament temperature can be important factors in the films growth. It was found that a substrate temperature of 300°C was necessary for enhancing the growth of cubic phase in the films. A filament temperature of more than 1400°C was contributing in the film growth in a form of thermal- and electron-impact dissociation of the precursor and perhaps also by electron contribution in the plasma. This is a temperature level, however, that is low enough to allow for deposition on a wide range of materials, without damage to those materials.

192

Moreover, the ion bombardment and substrate temperature contributed in hydrogen elimination from the film. Thus the favourable growth condition were determined as 400 W of rf power under a substrate temperature of 350°C and filament temperature of 1600°C at 0.3 torr.

6.3.2 PROPERTIES OF FILMS

As determined by IR spectra of the films, the volume fraction of cubic phase was increasing with the rf power coupled to the substrate. Films grown less then 100 W were hexagonal determined by IR peaks. With increasing rf power, the peak height of cubic phase increased with a shift towards lower wave number. This was predicted to be a transition to the cubic phase from the wurtzite phase of BN which was grown under less activated condition, similarly to HPHT growth. It should be noted that on the basis of the quite distinct IR absorption spectra for cBN and hBN, useful microstructural conclusions can be drawn. Hydrogen content of the films was found to be decreasing with rf power and substrate temperature and hydrogen free film was deposited in this work.

Most of the mixed-phase films showed a smooth and featureless surface and a compact structure. This mixed-phase films, containing crystallites of the cubic phase embedded in a hexagonal matrix, are thought to be amorphous in structure with no long range crystallographic order.

The films showed a wide range of refractive indices between 1.8 to 2.3 for the mixed phase films. The refractive index of the films increased with rf power, which correlates with the increasing cBN content of the films. The indices of the films with cBN content are substantially higher than those of hBN (1.553-1.77). Moreover, a predicted linear relationship was also found between n^2 and the dielectric constant of the films.

There was a significant improvement in the adhesion of the films on silicon and steel substrates and films grown above 300°C with rf power more then 200 W were adherent to the substrate even after exposure to the atmospheric environments and showed little deterioration after months. Films grown on not appropriately cleaned substrates showed delamination with a stress relief pattern.

The state of stress was examined, and it was observed that the stress crossed over from tensile to compressive at from 100 W to 200 W and remained compressive up to 400 W. Thus there is a very close parallel between the film containing increasing cubic phase and a higher level of compressive stress in the film. A high level of stress was found in the mixed-phase films, but the good adhesion may be due to the support the hexagonal region gives to the cubic region for stress relaxation.

Hardness of the mixed-phase film measured by near-surface ultra-low load indentation testing, showed an improvement compared to the substrate.

Mixed-phase BN films showed a high resistivity and a high breakdown field and MIS capacitors on silicon substrates using these films showed normal behaviour with a rather high negative charge density in the insulator and a relatively low level of fast interface states. A clockwise hysteresis curve was obtained with a large flat-band voltage of 26 volts. The dielectric constant of these films were in the range of 2.2-4.4. The distribution of surface state density showed a U-shape variation with a minimum density of 1.75×10^{12} states/cm^2/eV.

The I-V characteristics were essentially linear in the low-voltage region. The films showed consistent resistivity of a value not less than 3.2×10^{12} Ω-cm.

Thus these mixed-phase BN films showed potential for use in electronic circuits.

6.4 RECOMMENDATIONS FOR FUTURE WORK

Pure cubic boron nitride films were not achieved in this work. But the growth mechanism and the growth region derived suggests a possibility of depositing cBN films. It is believed that at a higher temperature (>600°C) and at a high level of ionisation, films containing purely cubic phase may be deposited. For this purpose, a modification may have to be done to the existing system to improve the heating arrangement of the substrate, as the tantalum wires are not susceptible to go to a high current flow and break very easily after a short use. The current supply system should be improved to provide a high level of current. Instead, a halogen bulb heating system could be introduced for a high substrate temperature.

In that case, the system should be capable of handing high rf power, incorporating probably an automatic matching network. A computer control of the different parameters would be very convenient for the operator to work in rf environments and to avoid unnecessary turning off the rf for checking different variables: this will also improve film quality. A high filament temperature, measured by some accurate techniques, is also recommended. With high bias and high substrate and filament temperature, cubic boron nitride thin films can be deposited with the necessary modification to the present system. The only problem in that case is that high temperature is not suitable for most of the electronic substrates.

As OES showed interesting plasma diagnostics, a Langmuir probe can be developed and introduced to the present system to get the knowledge about electron density distribution function and plasma parameters. To improve the ionisation of the plasma species and to get good quality cBN films, a low pressure system might be useful in which case high rf power or microwave techniques need to be used.

In terms of the reactant material, the evaporation technique of borane-ammonia need to be improved. It was found difficult to evaporate the reactant material evenly and with good control. Besides, the sublimation of the reactant on the flow-path posed a problem. An electron beam evaporation of borane-ammonia inside the reactor could be useful in controlling the evaporation and in obtaining high growth rate. Other non-toxic material, such as borane-diethylamine, borane-triethylamine or even N-trimethyl borazine $[(CH_3-N-B-H)_3]$ could be used. These materials contain carbon and carbon can be prevented from incorporating in the films by high substrate temperature. Obviously, at high substrate temperature, the choice of substrate will be limited. However, a carbon containing BN film might have desirable properties like high hardness and high thermal conductivity etc.

The obvious, and planned, extension to this work is to obtain a higher thickness of the film for the ease of characterization. Thinness of the film imposed difficulties to characterize by XRD, nano-indentation and other techniques. But it is suspected that a thicker film may contain high stress resulting delamination and cracking. In that case, an intermediate layer or a graded BN inter-layer might be useful to stabilize the film.

Though infra-red is a reliable technique to characterize different phases of BN in thin films, other characterization techniques, such a X-ray diffraction, electron diffraction and TEM should be used to confirm cubic phase authentically if a predominantly cubic phase containing film is produced. In addition, stoichiometry of the film should be determined by Auger or X-ray photoelectron spectroscopy if they are available. Adhesion of the film should be determined by some technique in the case of a thick film.

As the film showed good potentiality in electronic applications, defect free smooth BN films should be employed for this purpose. In that case, the inductively coupled system could be introduced for the low level of the ion bombardment. Future work involving doping of cBN films for electronic application is also suggested.

The scaling up of laboratory equipment to production unit which will allow viable and economical production is already in progress for the case of diamond coating. In that respect, cBN film deposition is at embryonic stage, but needs to be developed with a long range outlook. Though different from diamond, there is no principle obstacle known yet which would prevent the synthetic creation of superhard BN at low pressure similar to those in the diamond synthesis. This is an exciting challenge for the near future specially in view of the considerable market potential of cBN coatings.

APPENDIX A

NOMENCLATURE IN EMISSION SPECTROSCOPY

Theory and notation used for electronic transition are out of the scope of this study, but a brief note will be given here to identify the emission of N_2 plasma. A detailed discussion can be found elsewhere [160].

The quantum number Λ corresponding to the component of the electronic orbital angular momentum along the internuclear axis can take the values

$$\Lambda = 0,1,2... ... ...$$

According as $\Lambda = 0$, 1, 2, ..., the corresponding molecular state is designated a Σ, Π, Δ, Φ, ... state. The multiplet structure of atoms due to electron spin is added as a left superscript. Thus the singlet, doublet, and triplet states of Π state are written as $^1\Pi$, $^2\Pi$, $^3\Pi$ respectively. In a diatomic molecule, any plane through the internuclear axis is a plane of symmetry. Therefore the electronic eigenfunction [160] of a Σ state either remains unchanged or changes sign when reflected at any plane passing through both nuclei. In the first case, the state is called a Σ^+ state, and in the second case, it is called a Σ^- state. Even electronic states are designated by g and odd states by u in right subscript of a state (i.e. Σ_g or Σ_u).

If several electronic states of a molecule are known, they are distinguished by a letter X, A, B,......., a,b,...., in front of the term symbol. X is frequently used for the ground state of the molecule. The upper state is always written first and then the lower in designating a given electronic transition, e.g. $A^1\Pi$-$X^1\Sigma$.

A1

APPENDIX B

NOMENCLATURE IN VIBRATIONAL SPECTROSCOPY

Normal vibrational modes are defined by their symmetry properties. In group theory, the symmetry or point group to which a molecule belongs is described by its irreducible representations and each vibrational mode has a symmetry corresponding to one of these representations. Before studying vibrations due to B-N bonds, the notation used will be cited. Irreducible representations and vibrations are distinguished according to Mulliken's notation. Those which are symmetric with respect to a particular n-fold symmetry axis, C_n are designated A. If antisymmetric with respect to this axis, they are labelled B. The symbols E and T are used to designate respectively two and three fold degenerate irreducible representations. Subscripts 1 and 2 refer respectively to symmetric and antisymmetric irreducible representations relation to a C_2 axis perpendicular to the principal axis. The superscripts ´ and ″ refer to irreducible representations which are respectively symmetric or antisymmetric with reference to a horizontal plane of symmetry. Where there is a centre of inversion, the subscript g designates irreducible representations which are symmetric with respect to inversion and the subscript u is used for those which are antisymmetric.

APPENDIX C1

CHARACTERISTICS OF IDEAL MIS DIODE

In the MIS structure shown in fig. 5.1(a), V is the applied voltage on the metal field plate. The energy band diagram of an ideal MIS structure for V = 0 is shown in fig. 5.1(b) for n-type semiconductors. An ideal MIS diode is defined as follows:

(1) at zero applied bias, there is no energy difference between the metal work function ϕ_m and the semiconductor work function, or the work function difference ϕ_{ms} is zero:

$$\phi_{ms} = \phi_m - (\chi + E_g - \psi_B) = 0 \tag{C1.1}$$

where, χ is the semiconductor electron affinity, E_g is the band gap, ψ_B is the potential difference between the Fermi level E_F and the intrinsic Fermi level E_i and ϕ_B is the potential barrier. In other words, the band is flat when there is no applied voltage.

(2) the only charges which can exist in the structure under any biasing conditions are those in the semiconductor and those with the equal but opposite sign on the metal surface adjacent to the insulator; and

(3) there is no carrier transport through the insulator under dc biasing conditions, or the resistivity of the insulator is infinity.

When an ideal MIS is biased with positive or negative voltages, there are basically three cases which may exist at the semiconductor surface. These cases are illustrated in fig. C1.1 for a n-type semiconductor. The potential ψ is defined as zero in the bulk of the semiconductor, and is measured with respect to the intrinsic Fermi level E_i as shown in fig. C1.1. At the semiconductor surface, $\psi = \psi_s$, surface potential. When a positive voltage ($\psi_s > 0$) is applied to the metal plate, the top of the conduction band bends downward and is closed to the Fermi level. This band bending causes an accumulation of majority carriers (electrons) near the semiconductor surface. This is the case of accumulation. When a small negative voltage is applied, ($\psi_B < \psi_s < 0$), the bands bend upward, and the majority carriers are depleted. This is the case of depletion. When a large negative voltage is applied the bands bend even more upward, such that E_i at the surface closes E_F where the number of minority carriers (holes) at the surface is larger than that of the electrons and this is the case of inversion.

In the absence of any work function differences as given in equation (C1.1), the applied voltage will partly appear across the insulator and partly across the silicon. Thus,

$$V = V_i + \psi_s \tag{C1.2}$$

where V_i is the potential across the insulator. For a given voltage drop across the silicon there will be a known net surface charge (Q_s) in silicon. Since no charge

A3
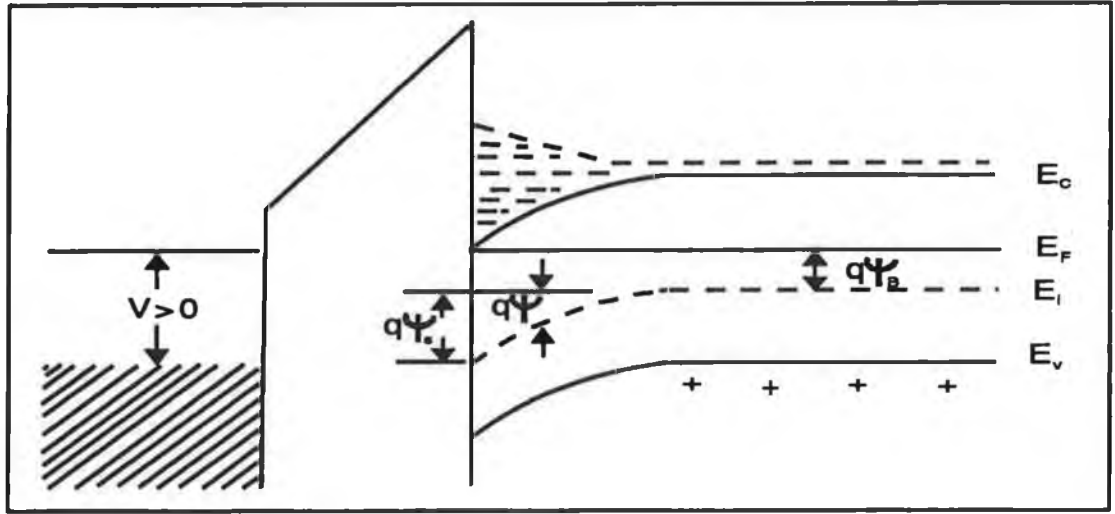
Fig. C1.1: Energy band diagram for ideal MIS structures when V >0 of n-type semiconductor.

is present in the insulator, the field will be uniform and V_i will be

$$V_i = \frac{Q_s}{C_i}$$ (C1.3)

where C_i is the insulator capacitance.

The total capacitance C of the MIS system, arising from two conducting regions (the metal and silicon) separating by an insulating region (the insulator and any depletion region existing at the silicon surface) is a series combination of the insulator capacitance C_i and the silicon space-charge capacitance C_D.

$$C = \frac{C_i C_D}{C_i + C_D}$$ (C1.4)

The insulator capacitance per unit area may be determined solely from geometry and is given by,

$$C_i = \frac{\varepsilon_i}{d}$$ (C1.5)

which corresponds to the maximum capacitance of the system.

The capacitance of the silicon surface cannot be expressed in as simple a manner. It depends upon the distribution of net charge at the silicon surface as a function of the voltage drop across the silicon. C_D can be derived [183]

A4

$$C_D = \frac{\sqrt{\beta \varepsilon_s \frac{q}{2} [n(e^{\beta \psi_s} - 1) - p(e^{-\beta \psi_s} - 1]}}{[n(e^{\beta \psi_s} - \beta \psi_s - 1) + p(e^{-\beta \psi_s} + \beta \psi_s - 1)]^{1/2}} \qquad (C1.6)$$

for n or p type where $\beta = q/kT$.

The space charge per unit area required can be derived as

$$Q_s = \mp \sqrt{2 \varepsilon_s \frac{q}{\beta} [n(e^{\beta \psi_s} - \beta \psi_s - 1) + p(e^{-\beta \psi_s} + \beta \psi_s - 1)]} \qquad (C1.7)$$

The flat-band capacitance, C_{fb} can be derived from equations (C1.4) and (C1.6) at $\psi_s = 0$,

$$C_{fb} = \frac{\varepsilon_i}{d + \frac{1}{\sqrt{2}}(\frac{\varepsilon_i}{\varepsilon_s})L_D} \qquad (C1.8)$$

where, extrinsic Debye length, L_D is given by,

$$L_D = \sqrt{\frac{2\varepsilon_s}{qn\beta}} \qquad (C1.9)$$

The silicon capacitance C_D depends on the voltage. This ideal capacitance vs voltage curve of MIS can be drawn from equations (C1.4) through (C1.6).

In the following appendix, we will use a program on these equations to derive the ideal C-V curve for our BN insulator.

APPENDIX C2

PROGRAM FOR C-V PLOT

```
C        APPENDIX C2
C        PROG NAME : IDEAL C-V PLOT
C
C        THIS PROGRAM CALCULATES INSULTOR CAPACITANCE (CI) FROM
C        EQU. (C1.5), SILICON SPACE CHARGE CAPACITANCE (CD) FROM EQU.
C        (C1.6), SPACE CHARGE (QS) FROM EQU. (C1.7), FLAT BAND
C        CAPACITANCE (CFB) FROM EQU. (C1.8) AND TOTAL CAPACITANCE
C        (C) FROM EQU. (C1.4). CORRESPONDING VOLTAGE IS CALCULATED
C        FROM EQU. (C1.2). ALL THESE EQUATIONS ARE GIVEN IN APPENDIX C1.


        CHARACTER TYPE*(1),FREQ*(2),SEMI*(4)
        DIMENSION PSI(112),CAP(112),V(112),VI(112),QS(112)
        REAL NC,NV,NI,N0,P0,P01,K0,K01,K1,K0A,K0B,K0B1,LD
        INTEGER D
        PI=3.14159
C        DATA ARE TAKEN TO GRAPHER FOR PLOTTING
C
        open(unit=7,status='unknown',file='e:\fv\bin\cv1.dat')
        open(unit=5,status='unknown',file='cvplot.out')
        open(unit=8,status='unknown',file='c:\grapher\cv3.dat')
        open(unit=9,status='unknown',file='c:\grapher\cv4.dat')
        open(unit=10,status='unknown',file='c:\grapher\cv2.dat')
10      FORMAT(' CHOOSE SEMICONDUCTOR',/,' SI   =1',/,' GAAS =2')
20      FORMAT(' INP  =3',/,' INAS =4',/,' OTHER=5')
        WRITE(5,10)
        WRITE(5,20)
C
C        SEMICONDUCTOR DATA FOLLOWS
        WRITE(*,*) 'ENTER THE VALUE OF M'
        READ(*,*) M
        GOTO(100,200,300,400,500),M
100     EG=1.12
        NI=1.6E10
        NC=2.8E19
        NV=1.02E19
        ER=11.8
        SEMI='SI'
        GOTO 1000
200     EG=1.43
        NI=1.1E7
        NC=4.7E17
        NV=7.0E18
        ER=10.9
        SEMI='GAAS'
        GOTO 1000
300     EG=1.29
        NI=2.9E7
        NC=4.6E17
        NV=6.3E18
        ER=14.0
        SEMI='INP'
        GOTO 1000
400     CONTINUE
C..............
C...........
C..............
C..............
        SEMI='INAS'
```

```
            GOTO 1000
500         CONTINUE
C......
C..........
C..........
C...........
            SEMI='XXXX'
1000        CONTINUE
C
C           TYPE AND DOPING OF THE SEMICONDUCTOR
            WRITE(*,*) 'ENTER TYPE,DOPING'
1010        FORMAT(A1,E7.2)
            READ(*,1010) TYPE,DOP
1015        FORMAT(1X,A1,',',E7.2)
            WRITE(5,1015)TYPE,DOP
C
C           THICKNESS OF THE INSULATOR IN ANGSTROMS
            WRITE(*,*) 'INSULATOR THICKNESS(ANGS) D'
            READ(*,*) D
            TH=FLOAT(D)
1035        FORMAT(1X,I6)
            WRITE(5,1035)D
C
C           DIELECTRIC CONSTANT OF THE INSULATOR
            WRITE(*,*) 'ENTER DIELECTRIC CONSTANT EI'
            READ(*,*) EI
1038        FORMAT(F4.1)
            WRITE(5,1038)EI
            GOTO 2010
C
C           HIGH OR LOW FREQUENCY MEASUREMENT
2025        FORMAT(A2)
2010        WRITE(*,*) 'ENTER LF OR HF'
            READ (*,2025) FREQ
2030        FORMAT(1X,A2)
            WRITE(5,2030)FREQ
C
C           CALCULATING CI FROM DIELECTRIC CONSTANT
            E0=8.85E-14
            CI=E0*EI/TH/1E-8
C           CI=CAPACITANCE/CM2 OF INSULATOR................................
C
            BETA=1/.026
C           BETA=Q/KT (ROOM TEMP)......................................
C
            WRITE(*,*) 'ENTER AREA (CM2) AREA'
            READ(*,*) AREA
            CIA=CI*AREA
            WRITE(5,*) AREA,CIA
C           ACTUAL VALUE OF MIS CAP............................
C
C           CALCULATING BAND EC, EV AND N0
            IF (FREQ.EQ.'HF') F0=0
            IF (FREQ.EQ.'LF') F0=1
            IF (TYPE.EQ.'N') GO TO 3000
            EV=-.026*ALOG(NV/DOP)
            EC=EV+EG
            N0=NI**2/DOP*F0

            P0=DOP
            GOTO 3010
3000        EC=.026*ALOG(NV/DOP)
            EV=EC-EG
            N0=DOP
            P0=NI**2/DOP*F0
C
C           CALCULATING CFB FROM CD AT PSI=0
```

A7

```fortran
C       LD IS DEBYE LENGTH OF THE ELECTRON
3010    LD=SQRT(2*E0*ER/(1.6E-19*DOP*BETA))
        CPSI0=SQRT(2.0)*E0*ER/LD
        CFB=AREA*CPSI0*CI/(CPSI0+CI)*1.0E12
        WRITE(5,3020) CFB
3020    FORMAT(1X,'CFB=',E12.6)
C
C       CALCULATES CAP, PSI
        EINC=EG/100
        CMAX=0.
C
        WRITE(5,30)
30      FORMAT(4x,'K0',21x,'QS'18x,'VI',16x,'I')
        A0=AREA
        DO 4020 I=1,110
        P01=NI**2/DOP*(F0+1)
C       CALCULATING SURFACE POTENTIAL PSI AND CD
C
        PSI(I)=EV+I*EINC-5*EINC
        IF(PSI(I).NE.0) GOTO 4000
        CD=CPSI0
        GOTO 4010
4000    K0A=N0*(EXP(BETA*PSI(I))-BETA*PSI(I)-1)
        K0B=P0*(EXP(-(BETA*PSI(I)))+BETA*PSI(I)-1)
C       WRITE(*,*) BETA,PSI(I)
        K0B1=P01*(EXP(-(BETA*PSI(I)))+BETA*PSI(I)-1)
C       WRITE(*,*) K0B,K0B1
        K0=ABS(K0A+K0B)
        K01=ABS(K0A+K0B1)
C       WRITE (*,*) K0,K01
        K1=ABS(N0*(EXP(BETA*PSI(I))-1)-P0*(EXP(-(BETA*PSI(I)))-1))
        CD=SQRT(BETA*E0*ER*1.6E-19/2)*K1/SQRT(K0)
        IF (K0.LT.1.0E-3) THEN
                QS(I)=0.
        ELSE
                QS(I)=SQRT(2*1.6E-19*ER*E0*K01/BETA)
        END IF
        IF (PSI(I).LT.0.) THEN
                VI(I)=-QS(I)/CI
        ELSE
                VI(I)=QS(I)/CI
        END IF
        V(I)=VI(I)+PSI(I)

4015    FORMAT(1X,E8.3,15X,E9.3,10X,E9.3,10X,I3)
        WRITE(5,4015)K0,QS(I),VI(I),I
4010    CAP(I)=A0*CD*CI/(CD+CI)*1.0E12
        IF (CAP(I).GT.CMAX) CMAX=CAP(I)
4020    CONTINUE

        WRITE(5,31)
31      FORMAT(4x,'CAP'16x,'PSI',14x,'V1',15x,'VI',16x,'J')
        DO 5010 J=1,110
5002    FORMAT(1X,E12.6,10X,F6.3,10X,E9.3,10X,E9.3,10X,I3)
        WRITE(5,5002)CAP(J),PSI(J),V(J),VI(J),J
        WRITE(7,*) CAP(J),V(J)
        WRITE(10,*) PSI(J),V(J)
        WRITE(8,*) CAP(J),VI(J)
        WRITE(9,*) PSI(J),VI(J)
5010    CONTINUE
        IF (CMAX.GT.100.) GOTO 5020
        CAP(112)=5.
        GOTO 6000
5020    CAP(112)=100*REAL(INT(CMAX/100)+1)/20
6000    CONTINUE
        STOP
        END
```

APPENDIX D

PUBLICATIONS ON THIS WORK

1. M. Z. Karim, D.C. Cameron, M.J. Murphy and M.S.J. Hashmi, *Surface and Coatings Technology*, Vol. 49, No. 1-3, Dec 1991, p 416-421.

2. M. Z. Karim, D.C. Cameron, M.J. Murphy and M.S.J. Hashmi, *Proc. Inst. Mech. Eng., IMechE Conf. (EuroTech Direct '91)*, IMechE, London, 1991, 181-189.

3. M. Z. Karim, D.C. Cameron and M.S.J. Hashmi, *Surface and Coatings Technology*, 54/55, Dec 1992, p 355-359.

4. M. Z. Karim, D.C. Cameron and M.S.J. Hashmi, *Materials and Design*, Vol 13(4), Aug 1992, p 207-214.

5. M. Z. Karim, D.C. Cameron and M.S.J. Hashmi, accepted for publication in *Surface & Coatings Technology*.

6. M. Z. Karim, D.C. Cameron and M.S.J. Hashmi, Paper no. DH-2, to be presented in the *ICMCTF '93*, San Diego, California, April 19-23, 1993 (to be submitted to *Thin Solid Films*).

REFERENCES

1. B. Bhusan and B. K. Gupta, *Handbook of Tribology*, McGraw Hill, New York, 1991.

2. J. L. Shohet, *IEEE Transactions on Plasma Science*, 19(5) (1991) 725-733.

3. H. Kimura, *Fine Ceramic Industry in Japan: Current Developments* (LTCB Res. Special Issue, Japan's High Technol. Industry, Vol. 3), Tokyo: Long Term Credit Bank of Japan, 1984.

4. H. Herman, *Scientific American*, 259 (1988) 112.

5. H. Yasuda, *Plasma Polymerization*, Academic, New York, 1988.

6. S. M Rossnagel, J. J. Cuomo and W. D. Westwood (eds.), *Handbook of Plasma Processing Technology*, Noyes Publication, 1990.

7. J. S. Chapin, *Res. & Dev.*, 25(1) (1974) 37.

8. B. Window and N. Savvides, *J. Vac. Sci. Technol. A*, 4(3) (1986) 453.

9. B. A. Movchan and A. V. Demchishin, *Fiz. Met. Metalloved*, 28 (1969) 653.

10. J. A. Thornton, *J. Vac. Sci. Technol.*, 11 (1974) 666.

11. R. Messier, A. P. Giri and R. A. Roy, *J. Vac. Sci. Technol. A*, 2 (1984) 500.

12. D. S. Rickerby and S. J. Bull, *Surface Coat. Technol.*, 39/40 (1989) 315-328.

13. M. Z. Karim, D. C. Cameron and M. S. J. Hashmi, *Materials and Design*, 13(4) (1992) 207-214.

14. C. Wick, *Manufacturing Engineering*, July 1988, 73-78.

15. G. Watson, *IEEE Spectrum*, 28(1) (1991) 30.

16. K. Miyoshi in J. J. Pouch and S. A. Alterovitz (eds.), *Materials Science Forum*, Vol. 54/55, Trans Tech Publications, Zurich, 1990, p. 375.

17. H. Kuwano in J. J. Pouch and S. A. Alterovitz (eds.), *Materials Science Forum*, Vol. 54/55, Trans Tech Publications, Zurich, 1990, p. 399.

18. S. Ainsberg and R. Chabot, *J. Appl. Phys.*, 42 (1971) 2953.

19. E. G. Spencer, P.H. Schmidt, D.C. Joy and F.J. Sansalone, *Appl. Phys. Lett.*, 29 (1976) 118.

20. C. Weissmantel, *Thin Solid Films*, 58 (1979) 101.

21. B. V. Spitsyn, B. V. Derjaguin, L. L. Builov, A. A. Klochkov, A. E. Gorodetslei and

A. V. Smoiyanihov, *Sov. Phys. Dokl.*, 21 (1976) 767.

22. S. Matsumotuo, Y. Sato, M. Kamo and N. Setaka, *Jpn. J. Appl. Phys.*, 21 (1982) 219.

23. L. Holland and S. M. Ojha, *Thin Solid Films*, 38 (1979) 117.

24. *Handout for the Business and Technical Outlook for CVD Diamond and DLC*, Gorham Advanced Materials Res. Ins., Maine, USA.

25. C. R. Aita in J. J. Pouch and S. A. Alterovitz (eds.), *Materials Science Forum*, Vol. 54/55, Trans Tech Publications, Zurich, 1990, p. 1.

26. P. K. Lam, R. M. Wentzcovitch and M. L. Cohen in J. J. Pouch and S. A. Alterovitz (eds.), *Materials Science Forum*, Vol. 54/55, Trans Tech Publications, Zurich, 1990, p. 165.

27. W. Grigoriew and J. Leciejewicz, *Thin Solid Films*, 172 (1989) L75-L79.

28. L. Vel, G. Demazeau and J. Etourneau, *Materials Sci. Eng.*, B10 (1991) 149-164.

29. Y.-N. Xu and W. Y. Ching, *Phys. Rev. B*, 44(15) (1991) 7787-7798.

30. O. Madelung et al. (eds.), *Landolt-Börnstein*, Vol. 17 and 22, Springer-Verlag, 1982

31. J. C. Angus and C. C. Hayman, *Science*, 241 (1988) 913.

32. W. A. Yarbrough and R. Messier, *Science*, 241 (1988) 913.

33. N. Tanabe, T. Hayashi and M. Iwaki, *Diamond and Related Materials*, 1991.

34. (a) T. Ikeda, Y. Kawate and Y. Hirai, *J. Vac. Sci. Technol. A*, 8(4) (1990) 3168-3174.

    (b) T. Ikeda, Y. Kawate and Y. Hirai, *KOBELCO Technol. Rev.*, 6 (1989) 1-4.

    (c) T. Ikeda, *Appl. Phys. Lett.*, 61(7) (1992) 786-788.

35. (a) M. Mieno and T. Yoshida, *Jap. J. Appl. Phys.*, 29(7) (1990) L1175-L1177.

    (b) M. Mieno, T. Yoshida and K. Akashi, *Nippon Kinzoku Gakkaishi*, 52(2) (1988) 199-203.

36. (a) K. Inagawa, K. Watanabe, H. Ohsone, K. Saitoh and A. Itoh, *J. Vac. Sci. Technol.*, A5(4) (1987) 2696-2700.

    (b) K. Inagawa, K. Watanabe, K. Saitoh, Y. Yuchi and A. Itoh, *Surf. Coat. Technol.*, 39-40 (1989) 253-264.

37. (a) M. Murakawa and S. Watanabe, *Surf. Coat. Technol.*, 43/44 (1990) 128-136.

    (b) M. Murakawa and S. Watanabe, *Surf. Coat. Technol.*, 43/44 (1990) 145-153.

    (c) S. Watanabe, S. Miyake and M. Murakawa, *Surf. Coat. Technol.*, 49 (1991)

    (d) S. Miyake, S. Watanabe, M. Murakawa, R. Kaneko and T. Miyamoto, *Thin Solid Films*, 212 (1992) 262-266.

38. (a) H. Saitoh, T. Fujii, T. Ishiguro and Y. Ichinose, *Proc. 5th JIM Intl. Symp. on Non-equilibrium Solid Phases of Metals and Alloys*, The Japan Inst. Metals, Trans. JIM, 29 (1988) 299-302.

(b) Y. Ichinose, T. Fujii, H. Saitoh and T. Ishiguro, in E. Broszeit, W. D. Munz, H. Oechsner, K.-T. Rie, G. K. Wolf (eds.), *Plasma Surface Eng.*, Vol. 2, DGM Informationsge-sellschaft. Verlag, 1988, 793-798.

(c) H. Saitoh, Y. Hirotsu and Y. Ichinose, *Nippon Kinzoku Gakkaishi (J. Japan Inst. Metals)*, 54(2) (1990) 186-192.

39. (a) A. Chayahara, H. Yokoyama, T. Imura and Y. Osaka, *Jap. J. Appl. Phys.*, 26(9) (1987) L1435-L1436.

(b) A. Chayahara, H. Yokoyama, T. Imura, Y. Osaka and M. Fujisawa, *Jap. J. Appl. Phys.*, 27(3) (1988) 440-441.

(c) A. Chayahara, H. Yokoyama, T. Imura, Y. Osaka and M. Fujisawa, *Appl. Surf. Sci.*, 33/34 (1988) 561-566.

(d) H. Yokoyama, M. Okamoto, T. Hamada, T. Imura, Y. Osaka, A. Chayahara and M. Fujisawa, *Jap. J. Appl. Phys.*, 28(3) (1989) 555-556.

(e) M. Okamoto, H. Yokoyama and Y. Osaka, *Jap. J. of Appl. Phys.*, 29(5) (1990) 930.

(f) M. Okamoto, Y. Utsumi and Y. Osaka, *Jap. J. of Appl. Phys.*, 29(6) (1990) L1004.

(g) Y. Osaka, M. Okamoto and Y. Utsumi, *Mat. Res. Soc. Symp. Proc.*, 223 (1991) 81.

(h) H. Yokoyama, M. Okamoto and Y. Osaka, *Jap. J. Appl. Phys.*, 30(2) (1991) 344.

(i) M. Okamoto, Y. Utsumi and Y. Osaka, *Jap. J. of Appl. Phys.*, 31 (1992) 3455-3460.

40. K.S. Forland, T. Forland and S. K. Ratkje, *Irreversible Thermodynamics, Theory and Applications*, John Wiley and Sons, New York, 1988.

41. W. A. Yarbrough, *J. Vac. Sci. Technol. A*, 9(3) (1991) 1145.

42. R. C. DeVries, *Cubic Boron Nitride: Handbook of Properties* in Rep 72 CRD 178, 1972 (GEC).

43. R. T. Paine and C. K. Narula, *Chem. Rev.*, 90 (1990) 73-91.

44. (a) O. Mishima in J. J. Pouch and S. A. Alterovitz (eds.), *Materials Science Forum*, Vol. 54 & 55, 1990, Trans Tech Publications, Zurich, 1990.

(b) O. Mishima, J. Tanaka, S. Yamaoka and O. Fukunaga, *Science*, 238 (1987) 181-183.

(c) O. Mishima, S. Yamaoka and O. Fukunaga, *J. Appl. Phys.*, 61(8) (1987) 2822-2825.

(d) T. Kobayashi, O. Mishima, M. Iwaki, H. Sakairi and M. Aono, *Nuclear Instrum. &*

Meth. in Phys. Res., B45 (1990) 208-211.

45. S. P. S. Arya and A. D'Amico, *Thin Solid Films*, 157 (1988) 267-282.

46. J. J. Pouch and S. A. Alterovitz (eds.), *Materials Science Forum*, Vol. 54 & 55, Trans Tech Publications, Zurich, 1990.

47. M. Z. Karim, D. C. Cameron, M. J. Murphy and M. S. J. Hashmi, *Proc. Inst. Mech. Eng. , IMechE Conf. (EuroTech Direct '91)*, IMechE, London, 1991, 181-189.

48. E.G. Bauer, B.W. Dodson, D.J. Ehrlich, L. C. Feldman, C.P. Flynn, M.W. Geis, J.P. Herbison, R.J. Matyi, P.S. Peercy, P.M. Petroff, J.M. Phillips, G.B. Stringfellow and A. Zangwill, *J. Mat. Res.*, 5 (1990) 852.

49. (a) G. L. Doll, J.A. Sell, C. A. Taylor II and R. Clarke, *Phys. Rev. B*, 43(8) (1991) 6816.

   (b) A. K. Ballal, L. Salamancariba, G. L. Doll, C. A. Taylor II and R. Clarke, *J. Mat. Res.*, 7(7) (1992) 1618-1621.

50. R. H. Wentorf Jr., *J. Chem. Phys.*, 34 (1961) 809-811.

51. P. Bandy, H. T. Hall, H. M. Strong and R. H. Wentorf Jr., *Nature*, 176 (1955) 51.

52. (a) C. Weissmantel, K. Bewilogua, D. Dietrich, H.-J. Erler, H.-J. Hinneberg, S. Klose, W. Norwick and G. Reisse, *Thin Solid Films*, 72 (1980) 19-31.

   (b) C. Weissmantel, *J. Vac. Sci. Technol*, 18(2) (1981) 179-185.

   (c) C. Weissmantel, K. Bewilogua, K. Breuer, D. Dietrich, U. Ebersbach, H.-J. Erler, B. Rau and G. Reisse, *Thin Solid Films*, 96 (1982) 31-44.

   (d) B. Rother, H. D. Zscheile, C. Weissmantel, C. Heiser, G. Holzuter, P. Leonhardt and P. Reich, *Thin Solid Films*, 142 (1986) 83-99.

   (e) C. Weissmantel in K. J. Klabunde (ed.). *Thin Film Formation from Free Atoms and Particles*, Academic Press, New York, 1985, Chapter 4 and *Nuclear Instrum. & Methods in Phys. Res.*, B33 (1988) 905.

   (f) C. Weissmantel, K. Brewer and B. Winde, *Thin Solid Films*, 100(4) (1983) 383-389.

53. S. Shanfield and R. Wolfson, *J. Vac. Sci. Technol.*, A1(2) (1983) 323-325.

54. W. Halverson and D. T. Quinto, *J. Vac. Sci. Technol.*, A3 (1985) 2141-2146.

55. (a) M. Satou and F. Fujimoto, *Jap. J. Appl. Phys.*, 22(3) (1983) L171-L172.

   (b) M. Satou, K. Yamaguchi, Y. Andoh, Y. Suzuki, K. Matsuda, and F. Fujimoto, *Nuclear Instrum. & Methods in Phys. Res.*, B7/8 (1985) 910-914.

   (c) Y. Andoh, K. Ogata, Y. Suzuki, E. Kamijo, M. Satou and F. Fujimoto, *Nuclear Instrum. & Methods in Phys. Res.*, B19/20 (1987) 787-790.

(d) Y. Andoh, K. Ogata and E. Kamijo, *Nuclear Instrum. & Meth. in Phys. Res.*, B33 (1988) 678-680.

(e) F. Fujimoto, *Vacuum*, 39(2-4) (1989) 361-366.

(f) F. Fujimoto, *Vacuum*, 42(1-2) (1991) 67-73.

(g) Y. Andoh, S. Nishiyama, H. Kirimura, T. Mikami, K. Ogata and F. Fujimoto, *Nuclear Instrum. & Meth. in Phys. Res.*, B59/60 (1991) 276-280.

56. (a) M. Sokolowski, *J. Crystal Growth*, 46(1) (1979) 136-138.

(b) M. Sokolowski, A. Sokolowska, A. Rusek, Z. Romanowski and M. Gajawski, *J. Crys. Growth*, 52 (1981) 165-167.

(c) M. Sokolowski, A. Sokolowska, A. Michalski, Z. Romanowski, A. Rusek and M. Wronikowski, *Thin Solid Films*, 80 (1981) 249-254.

57. F. Verinaud, E. Weissmantel, I Grenier, A. Celerier, J. Machet and S. Weissmantel, *Thin Solid Films*, 209 (1992) 59-66.

58. W. G. Sainty, P. J. Martin, R. P. Netter field, D. R. McKenzie, D. J. H. Cockayne and D. M. Dwarte, *J. Appl. Phys.*, 64(8) (1988) 3980-3986.

59. O. Burat, D. Bouchier, V. Stambouli and G. Gautherin, *J. Appl. Phys.*, 68(6) (1990) 2780-2790.

60. C. A. Carosella, G. K. Hubler, D. Van Vechten and E. P. Donovan, *Mater. Res. Soc. Symp. Proc.*, 128 (1989) 79-84.

61. T. G. Tetreault, J. K. Hirvonen, G. Parker and J. P. Hirvonen, *Mater. Res. Soc. Symp. Proc.*, 128 (1989) 439-444.

62. Y. Pacaud, J. P. Riviere, M. F. Denanot, M. Jaouen, A. L. Roy and G. Hug, *Thin Solid Films*, 207 (1992) 131-137.

63. P. Mezentzeff, Y. Lifshitz and J. W. Rabalais, *Nuclear Instrum. Method Phys. Res.*, B44(3) (1990) 289-295.

64. A. Singh, R. A. Lessard and E. Knystautas, *Materials Sci. Eng.*, 90 (1987) 173-176.

65. (a) L. Guzman, F. Marchetti, L. Calliari, I. Scotoni and F. Ferrari, *Thin Solid Films*, 117(1) (1984) L63-L66.

(b) M. Elena, L. Guzman and S. Gialanella, *Surf. Coat. Technol.*, 36 (1988) 199-206.

66. R. J. Bricault, P. Sioshansi and S. N. Bunker, *Nuclear Instr. Meth. Phys. Res.*, B21 (1987) 678-680.

67. Y. Namba, *Seimi Kogaku Kaishi*, 53(10) (1987) 1523-1526.

68.   A. M. Glazova, F. F. Komarov, V. V. Pil'ko, V. S. Solov'ev and V. S. Tishkov, *Akad. Navuk BSSR-Ser. Fiz.-Energ. Navuk,* 4 (1989) 42-46.

69.   P. F. Zhou, T. Mori and Y. Namba, *Shinku,* 28(7) (1985) 581-586.

70.   W. L. Lin, Z. Xia, Y. L. Liu and Y. C. Fen, *Materials Sci. Eng.,* B7 (1990) 107-110.

71. (a) K. Miyoshi, D. H. Buckley, S. A. Alterovitz, J. J. Pouch and D. C. Liu, *NASA tech Memo,* 1987, 88902, p. 15.

    (b) J. J. Pouch, S.A. Alterovitz and J.D. Warner, *NASA Tech. Memo,* 1986, 87258, p. 13.

    (c) K. Miyoshi, D. H. Buckley, J. J. Pouch, S. A. Alterovitz and H. E. Sliney, *Surf. Coat. Technol.,* 33 (1987) 221-233.

72.   D. J. Kester and R. Messier, *J. Appl. Phys.,* 72(2) (1992) 504-513.

73.   T. Wada and N. Yamashita, *J. Vac. Sci. Technol. A,* 10(3) (1992) 515-520.

74.   B. Rother and C. Weissmantel, *Physica Status Solidi,* A87 (1985) K119-K121.

75.   M. D. Wiggins, C. R. Aita and F. S. Hickernell, *J. Vac. Sci. Technol.,* A2(2) (1984) 322-325.

76.   C. Mitterer, P. Rodhammer, H. Stori and F. Jeglitsch, *J. Vac. Sci. Technol.,* A7(4) (1989) 2646-2651.

77. (a) K. H. Seidel, B. Goranchev, K. Reichelt, W. Schaal and H. Dimigen, *6th Int'l Conf. on Ion & Plasma Assisted Techniques,* Brighton, U.K., 1987, p. 222.

    (b) K. H. Seidel, K. Reichelt, W. Schaal and H. Dimigen, *Thin Solid Films,* 151(2) (1987) 243-249.

    (c) B. Goranchev, K. Schmidt and K. Reichelt, *Thin Solid Films,* 149(1) (1987) L77-L80.

78. (a) W. Gissler, J. Haupt, T. A. Crabb, P. N. Gibson and D. G. Rickerby, *Materials Sci. Engg. A,* 139 (1991) 284-290.

    (b) W. Gissler, J. Haupt, A. Hoffmann, P. N. Gibson and D. G. Rickerby, *Thin Solid Films,* 199 (1991) 113-122.

    (c) D. G. Rickerby, P. N. Gibson, W. Gissler and J. Haupt, *Thin Solid Films,* 209 (1992) 155-160.

79.   S. Kikkawa, M. Takahashi, X. Y. Gu, F. Kanamura, S. Katayama and M. Koizumi, *Nuclear Instrum. & Meth. in Phys. Res.,* B59/60 (1991) 341-344.

80.   M. Tosa and K. Yoshihara, *Vacuum,* 41(7-9) (1990) 1873-1875.

81. (a) H. A. Beale, *US Patent 4,297,387,* 1980.

    (b) H. A. Beale, *Industrial Research & Development,* 21(6) (1979) 143-145.

82. (a) R. F. Bunshah, C. Deshpandey, K. L. Chopra and V. D. Vankar, *U.S. Patent Application,* August, 1985.

    (b) K. L. Chopra, V. Agarwal, V. D. Vanker, C. Deshpandey and R. F. Bunshah, *Thin Solid Films,* 126 (1985) 307-312.

    (c) P. Lin, C. Deshpandey, H. J. Doerr, R. F. Bunshah, K. L. Chopra and V. D. Vankar, *Thin Solid Films,* 153 (1987) 487-496.

83. (a) G. Kessler, H.-D. Bauer, W. Pompe and H.-J. Scheibe, *Thin Solid Films,* 147 (1987) L45-L50.

    (b) S. Becker, H.J. Dietze, G. Kessler, H.-D. Bauer and W. Pompe, *Z. Phys. B: Condens. Matter,* 81(1) (1990) 47-51.

84. P. T. Murray, M. S. Donley and N. T. Mcdevitt, *Mater. Res. Soc. Symp. Proc.,* 128 (1989) 469-474.

85. T. K. Paul, P. Bhattacharya and D. N. Bose, *Electron Letter,* 25 (1989) 1602-1603.

86. S. Mineta, M. Kohata, N. Yasunaga and Y. Kikuta, *Thin Solid Films,* 189 (1990) 125-138.

87. T. A. Friedmann, K. F. McCarty, E. J. Klaus, D. Boehme, W. W. Clift, H. A. Johnson, M. J. Mills and D. K. Ottesen, *Appl. Phys. Lett.,* 61(20) (1992) 786-788.

88. E. H. Lee and H. Poppa, *J. Vac. Sci. Technol,* 14(1) (1977) 223-226.

89. M. J. Paisley, Z. Sitar, B. Yan and R. F. Davis, *J. Vac. Sci. Technol.,* 1990, B8(2) (1990) 323-326.

90. B. M. DeKoven, P. L. Hagans, J. J. Leddy and K. K. Kar, *Surf. Coat. Technol.,* 1988, 36, 207-218.

91. G. Clerc and P. Gerlach, *Proc. 5th Int'l Conf. on Chemical Vapor Deposition,* England, 1975, 777-785.

92. (a) A. C. Adams, *J. Electrochem. Soc.,* 128(6) (1981) 1378-1379.

    (b) A. C. Adams and C. D. Capio, *J. Electrochem. Soc.,* 127 (1980) 399-405.

93. H. Wada, K. Nojima, K. Kuroda and C. Kato, *Yogyo Kyokai Shi,* 95(1) (1987) 130-134.

94. A. W. Moore, *J. Crystal Growth,* 106 (1990) 6-15.

95. C. Guimon, D. Gonbeau, G. Pfister-Guillouzo, O. Dugne, A. Guette, R. Naslain and M. Lahaye, *Surf. and Interface Analysis,* 16 (1990) 440-445.

96. H. Hannache, R. Naslain and C. Bernard, *J. Less Common Met.,* 95(2) (1983)

221-246.

97. H. O. Pierson, *J. Composite Materials*, 9 (1975) 228-240.

98. M. Basche and D. Schiff, *Design Engg.*, 59(2) (1964) 78-81. [Also US patent 3,152,006, 1964.]

99. G. Male and D. Salanoubat, *Proc. 7th Int'l Conf. on CVD*, Los Angeles, USA, Oct. 1979, p. 391.

100. (a) T. Matsuda, N. Uno, H. Nakae and T. Hirai, *J. Mater. Sci.*, 21 (1986) 649-658.

    (b) T. Matsuda, *J. Mater. Sci.*, 24(7) (1989) 2353-2357.

101. (a) T. Yogo and S. Naka, *J. Material Sci.*, 25 (1990) 374-378.

    (b) T. Yogo, S. Naka and H. Iwahara, *J. Mater. Sci.*, 1991, 26(14), 3756-3763.

102. (a) K. Nakamura, *J. Electrochem. Soc.*, 132(7) (1985) 1757-1762.

    (b) K. Nakamura, *J. Electrochem. Soc.*, 133(6) (1986) 1121-1123.

103. R. R. Rye, *J. Vac. Sci. Technol.*, A9(3) (1991) 1099-1103.

104. M. J. Rand and J. F. Roberts, *J. Electrochem. Soc.*, 115(4) (1968) 423-429.

105. S. P. Murarka, C. C. Chang, D. N. K. Wang and T. E. Smith, *J. Electrochem. Soc.*, 126(11) (1979) 1951-1957.

106. M. Hirayama and K. Shohno, *J. Electrochem. Soc.*, 122(12) (1975) 1671-1676.

107. E. Yamaguchi and M. Minakata, *J. Appl. Phys.*, 55(8) (1984) 3098-3102.

108. W. Baronian, *Material Research Bullatin*, 7 (1987) 119-124.

109. S. Motojima, Y. Tamura and K. Sugiyama, *Thin Solid Films*, 88(3) (1982) 269-274.

110. M. Sano and M. Aoki, *Thin Solid Films*, 83(2) (1981) 247-251.

111. (a) T. Takahashi, H. Itoh and A. Takeuchi, *J. Crystal Growth*, 47 (1979) 245-250.

    (b) T. Takahashi, H. Itoh and M. Kuroda, *J. Crystal Growth*, 53(2) (1981) 418-422.

112. J. L. Hurd, D. L. Perry, B. T. Lee, K. M. Yu, E. D. Bourret and E. E. Haller, *J. Mater. Res.*, 4(2) (1989) 350-354.

113. (a) Y. G. Kim, P. A. Dowben, J. T. Spencer and G. O. Ramseyer, *J. Vac. Sci. Technol.*, A7(4) (1989) 2796-2799.

    (b) Z. Zhang, Y. G. Kim, P. A. Dowben and J. T. Spencer, *Mater. Res. Soc. Symp. Proc.*, 131 (1989) 407-412.

114. G. Constant and R. Feurer, *J. Less Common Mat.*, 82 (1981) 113-118.

115. L. Maya and H. L. Richards, *J. Am. Ceram. Soc.*, 74(2) (1991) 406-409.

116. J. J. Gebhardt, *4th Int'l Conf. on CVD*, Boston, 1973, 460-472.

117.   S. S. Dana and J. R. Maldonado, *J. Vac. Sci. Technol.*, B4 (1986) 235-239.

118.   D. S. Williams, *J. Appl. Phys.*, 57(6) (1985) 2340-2345.

119.   T. M. Duncan, R. A. Levy, P. K. Gallagher and M. W. Walsh Jr., *J. Appl. Phys.*, 64(6) (1988) 2990-2994.

120.   G. Russo, M. Diana and F. Bereta, *Combustion Sci. Technol.*, 5(5) (1972) 237-242.

121.   S. B. Hyder and T. O. Yep, *J. Electrochem. Soc*, 123(11) (1976) 1721-24.

122.   M. Miyamoto, M. Hirose and Y. Osaka, *Jap. J. Appl. Phys.*, 22(4) (1983) L216.

123.   T. Endo, H. Yamada, T. Sumomogi, K. Kuwahara, T. Fujita and S. Morita, *J. Vac. Sci. Technol. A*, 8 (1990) 468.

124. (a) W. Schmolla and H. L. Hartnagel, *J. Phys. D,* 15(8) (1982) L95-L98.

     (b) W. Schmolla and H. L. Hartnagel, *J. Electrochem. Soc.*, 129(11) (1982) 2636-2637.

     (c) W. Schmolla and H. L. Hartnagel, *Solid State Electronics*, 26(10) (1983) 931-939.

125. (a) A. Bath, P.J. Van Der Put, J. Schoonman and B. Lepley, *Appl. Surf. Sci.*, 39 (1989) 135-140.

     (b) A. Bath, P.J. Van Der Put, J.G.M. Becht, J. Schoonman and B. Lepley, *J. Appl. Phys.*, 70(8) (1991) 4366-4370.

126.   D. M. Schleich, W. Y. F. Lai and A. Lam in M. Highoff (ed.), *Transformation of Organomettalics and Exotic Materials*, Publishers: Dordrecht, 1988, p. 174.

127.   O. Gafri, A. Grill, D. Itzhak, A. Inspektor and R. Avni, *Thin Solid Films*, 72 (1980) 523-527.

128.   A. A. Savel'ev, A. A. Pukhov, B. A. Vishnyakov, A. D. Sulimin and A. P. Ishchenko, *Fiz. Kim. Obrab. Mater.*, 2 (1981) 85-88.

129.   J. Kouvetakis, V. V. Patel, C. W. Miller and D. B. Beach, *J. Vac. Sci. Technol.*, A8(6) (1990) 3929-3933.

130.   K. Montasser, J. Tamano, S. Hattori and S. Morita, *Plasma Chem Plasma Process*, 4(4) (1984) 251-260.

131.   T. H. Yuzuriha and D. W. Hess, *Thin Solid Films*, 140(2) (1986) 199-207.

132.   R. Liepins, B. Jorgensen, R. Jahn, R. A. Geanangel and R. Komm, *Proceedings of 1st Annual Int'l Conf. of Plasma, Chemistry and Technol.*, San Diego CA, USA, 1982, 171-174.

133.   R. Liepins, K. P. Staudhammer, K. A. Johnson and M. Thomson, *Materials Letters,* 7 (1988) 44-46.

134. (a) H. Saitoh, T. Hirose, H. Matsu, Y. Hirotsu and Y. Ichinose, *Surf. Coat. Technol.*, 39-40 (1989) 265-273.

(b) H. Saitoh, Y. Hirotsu and Y. Ichinose, *Nippon Kinzoku Gakkaishi (J. Japan Inst. Metals)*, 54(5) (1990) 562-567.

135. (a) M. Z. Karim, D. C. Cameron, M. J. Murphy and M. S. J. Hashmi, *Surf. Coat. Technol.*, 49 (1991) 416-421.

(b) M. Z. Karim, D. C. Cameron and M. S. J. Hashmi, *Surf. Coat. Technol.*, 54/55 (1992) 355-359.

(c) M. Z. Karim, D. C. Cameron and M. S. J. Hashmi, Paper no. TuWC2, presented in the *Third Int'l Conf. on Plasma Surface Engineering*, Germany, October 25-28, 1992 (accepted in *Surface & Coating Technology*).

136. (a) J. M. Mendez, S. Muhl, M. Farias, G. Soto and L. Cota-Araiza, *Surf. Coat. Technol.*, 49 (1991) 422-426.

(b) J. M. Mendez, S. Muhl and E. Andrade, *Intl. Conf. on Metallurgical Coat. and Thin Films (ICMCTF '91)*, San Diego, CA, April ,1991.

137. L. Maya, J. American Ceramic Soc., 75(7) (1992) 1985-1988.

138. S. Y. Shapoval, V. T. Petrashov, O. A. Popov, A. O. Westner, M. D. Yoder Jr. and C. K. C. Lok, *Appl. Phys. Lett.*, 57(18) (1990) 1885-1886.

139. C. R. Eddy Jr. and B. D. Sartwell, Paper no. TF-TuM9, Presented in the *38th Annual Symposium and Topical Conf. of the American Vacuum Society*, Seattle, Washington, November 11-15, 1991.

140. (a) H. Saitoh and W. A. Yarbrough, *Appl. Phys. Lett.*, 58(20) (1991) 2228-2230.

(b) H. Saitoh and W. A. Yarbrough, *Appl. Phys. Lett.*, 58(22) (1991) 2482-2484.

141. A. Weber, U. Bringmann, C. P. Klages, K. Taube, G. Dollein, H. Meyer and G. Weidenbach, *J. De Physique III*, 2(8) (1992) 1391-1399.

142. R. A. Levy, *Proc.- Electrochemical Soc.*, 89(12) (1989) 182-201.

143. S. Komatsu, T. Yoshida and K. Akashi, *Proc. 9th Symp. on Ion Sources and Ion Assisted Technology (ISIAT) '85*, Tokyo, Kyoto University, Kyoto, Japan, 1985, 421-425.

144. (a) M. Wronikowski and A. Sokolowska, *Proc. of World Congress on High Temperature Ceramics*, Milan, Italy, 1986.

(b) A. Sokolowska and M. Wronikowski, *J. Crystal Growth*, 76 (1986) 511-513.

(c) M. Wronikowski, *Ph.D. Thesis*, Warsaw Technical University, Poland, 1988.

(d) A. Sokolowska and A. Olszyna, *Diamond Films '91*, Nice, France, Sept. 2-6,1991.

145. (a) J. Szmidt, A. Jakubowski, A. Michalski and A. Rusek, *Thin Solid Films*, 110(1) (1983) 7-20.

(b) J. Szmidt, A. Jakubowski and A. Balasinski, *Thin Solid Films*, 142(2) (1986) 269-277.

(c) J. Szmidt, *Diamond Films '91*, Nice, France, Sept 2-6, 1991.

146. D. Sobczynska, W. Torbicz, A. Olszyna and W. Wlosinski, *Analytica Chimica Acta*, 171 (1985) 357-361.

147. (a) S. Komatsu, Y. Moriyoshi, M. Kasamatsu and K. Yamada, *J. Phys. D: Appl. Phys.*, 24 (1991) 1687-1690.

(b) S. Komatsu, Y. Moriyoshi, M. Kasamatsu and K. Yamada, *J. Appl. Phys.*, 70(11) (1991) 7078-7084.

148. D.R. McKenzie, D.J.H. Cockayne, D.A. Muller, M. Murakawa, S. Miyake, S. Watanabe and P. Fallon, *J. Appl. Phys.*, 70(6) (1991) 3007-3012.

149. G. Hanke, M. Kramer and K. Muller, *Mater. Sci. Forum*, 54-55 (1990) 207-227.

150. R. Trehan, Y. Lifshitz and J.W. Rabalais, *J. Vac. Sci. Technol. A*, 8(6) (1990) 4026.

151. M. Murakawa, S. Watanabe and S. Miyake, Paper no. D4-03, Presented in *Intl. Conf. on Metallurgical Coatings and Thin films (ICMCTF '91)*, San Diego, CA, April 22-26,1991.

152. H.A. Jones and I. Langmuir, *General Electric Rev.*, 30(6) (1927) 310.

153. (a) S. G. Shore and R. W. Perry, *J. Am. Chem. Soc.*, 77 (1955) 6084.

(b) S. G. Shore and R. W. Perry, *J. Am. Chem. Soc.*, 80 (1958) 8.

154. G. Socrates, *Infra-red Characteristics Group Frequencies*, Wiley, NY, 1980, p. 45.

155. M. G. Hu, R. A. Geanangel and W. Wendlandt, *Thermochimica Acta*, 23 (1978) 249.

156. K. W. Boeddeker, S. G. Shore and R.K. Bunting, *J. Am. Chem. Soc.*, 88 (1966) 4396.

157. B. N. Chapman, *Glow Discharge Processes*, Wiley, New York, 1980.

158. T. J. Sommerer, W. N. G. Hitcho and J. E. Lawler, *Phys. Rev. Lett.*, 63 (1989) 2361.

159. R. W. Hyland and R. L. Shaffer, *J. Vac. Sci. Technol. A*, 9(6) (1991) 2843.

160. G. Herzberg, *Spectra of Diatomic Molecules*, Van Nostrand Reinhold, Berlin, 1950.

161. R. W. B. Pearse and A. G. Gaydon, *The Identification of Molecular Spectra*, Chapman and Hall, London, 1976.

162. O. Johari and A. V. Samudra in P. F. Kane and G. B. Larrabe (Eds.), *Characterization of Solid Surfaces*, Plenum Press, New York, 1978.

163. G. L. McClure in H. A. Willis, J. H. van der Maas and R. G. J. Miller, *Laboratory Methods in Vibrational Spectroscopy*, John Wiley, Chichester, 1987.

164. R. Geick, C. H. Perry and G. Rupprecht, *Phys. Rev.*, 146(2) (1966) 543-547.

165. P. J. Gielisse, S. S. Mitra, J. N. Plendl, R. D. Griffis, L. C. Mansur, R. Marshall and E. A. Pascoe, *Phys. Rev.*, 155(3) (1967) 1039-1046.

166. D.R. McKenzie, W.G. Sainty and D. Green, *Materials Sci. Forum*, 54-55 (1990) 193.

167. *Gmelin Handbuch der Anorganischen Chemie*, Band 13, Borverbindungen, Springer Verlag, Berlin, 1974, p 65.

168. L. I. Maissel and R. Glang, *Handbook of Thin Film Technology*, McGraw-Hill, New York, 1970.

169. K. Riedling, *Ellipsometry for Industrial Applications*, Springer Verlag, NY, 1988.

170. J. D. Targove and H. A. Macleod, *Appl. Opt.*, 27 (1988) 3779.

171. C. K. Hwangbo, L. J. Lingg, J. P. Lehan, H. A. Macleod, J. L. Makous and S. Y. Kim, *Appl. Opt.*, 28 (1989) 2769.

172. N. Savvides and B. Window, *J. Vac. Sci. Technol. A*, 3 (1985) 2386-2390.

173. J. E. Sundgren and H. T. G. Hentzell, *J. Vac. Sci. Technol. A*, 4 (1986) 2259-2279.

174. R. W. Hoffman in G. Hass and R. E. Thun (eds.), *Physics of Thin Films*, Academic, NY, 1966, Vol. 3, p 211.

175. D. W. Hoffman and M. R. Gaerttner, *J. Vac. Sci. Technol. A*, 17 (1980) 425.

176. M. Itoh, M. Mori and S. Nadahara, *J. Vac. Sci. Technol. B*, 9 (1991) 149.

177. D. W. Hoffman and J. A. Thornton, *Thin Solid Films*, 40 (1977) 334.

178. B. Window, F. Sharples and N. Savvides, *J. Vac. Sci. Technol. A*, 6 (1988) 2333.

179. S. Schiller, G. Beisler, S. Schneider and W. Sieber, *Thin Solid Films*, 83 (1981) 253.

180. H. M. Pollock, D. Maugis and M. Barquins, STP 889, *American Society for Testing and Materials*, 1986.

181. J. D. J. Ross, H. M. Pollock, J. C. Pivin and J. Takadoum, *Thin Solid Films*, 148 (1987) 171-180.

182. L. M. Terman, *Solid State Electron.*, 5 (1962) 285-299.

183. S. M. Sze, *Physics of Semiconductor Devices*, Wiley, New York, 1969.

184. P. A. Longeway, R. D. Ester and H. A. Weakliem, *J. Phys. Chem.*, 88 (1984) 73.

185. (a) F. P. Bundy and R. H. Wentorf Jr., *J. Chem. Phys.*, 38 (1963) 1144.

    (b) F. P. Bundy and J. S. Kesper, *J. Chem. Phys.*, 46 (1967) 3437.

186.   J. R. Riter Jr., *J. Chem. Phys.*, 59 (1973) 1538.

187.   Dr. F. Loffler, University of Aachen, Germany, private communication.

188.   R. F. Bunshah (ed.), *Deposition Technologies for Films and Coatings*, Noyes Publications, New Jersey, 1982.

189.   W. D. Sproul, P. J. Rudnik, M. E. Graham and S. L. Rohde, *Surface and Coatings Technol.*, 43/44 (1990) 270-278.

190.   H. Holleck, *J. Vac. Sci. Technol. A*, 4(6) (1986) 2661-2669.